INAUGURAL-DISSERTATION

zur

Erlangung der Doktorwürde

der Naturwissenschaftlich-Mathematischen

Gesamtfakultät

der Ruprecht-Karls-Universität

Heidelberg

Vorgelegt von

Master of Science Oxana Ciobanu

aus Cluj-Napoca/Romania

Tag der mündlichen Prüfung: 20. *November* 2009

Synthesis and Characterization of New Binuclear Boron Compounds with Bridging Guanidinate Ligands

Gutachter: **Prof. Dr. Dr. Hans-Jörg Himmel**

Prof. Dr. Gerald Linti

Dedicated to my parents and loving boyfriend Martin

Table of contents

Zusammenfassung

Diese Arbeit beschäftigt sich mit der Synthese, chemischen Reaktionsfähigkeit und Charakterisierung neuer zweikerniger Borverbindungen, welche verbrückte Guanidinat Liganden enthalten.

Die Basenaustausch-Reaktion zwischen $H_3B{\cdot}NMe_3$ und den Guanidinen hppH oder $N(H)C(NMe_2)_2$ resultierte in neuen Guanidin-Boran-Addukten $H_3B{\cdot}$hppH und $H_3B{\cdot}N(H)C(NH_2)_2$, welche als Ausgangsubstanzen zur thermischen und katalytischen Dehydrierung verwendet wurden. Der Reaktionsmechanismus wurde mit Hilfe quantenchemischer (DFT) Rechnungen mit der Verwendung des $H_3B{\cdot}N(H)C(NMe_2)_2$ Modells aufgeklärt. Im Gegensatz zu $H_3B{\cdot}$hppH führt die thermische Dehydrierung von $H_3B{\cdot}N(H)C(NMe_2)_2$ zu einer Zersetzung der Ausgangsverbindung und Bildung von polymeren Methyliminoboran $[HBNMe]_n$. Zum näheren Verständnis des Zersetzungsvorgangs wurden quantenchemische (DFT) Rechnungen hinzugezogen. Eine schnellere Dehydrierung konnte durch einen Katalysator erreicht werden. Katalytische Dehydrierung von $H_3B{\cdot}$hppH führte zu einem zweikernigen Borhydrid $[H_2B(\mu\text{-hpp})]_2$, welches zwei Guanidinat (hpp) Liganden enthielt. Weitere (reduktive) katalytische Dehydrierung von $[H_2B(\mu\text{-hpp})]_2$ ergibt ein neues doppelt basenstabilisiertes Diboran(4) $[HB(\mu\text{-hpp})]_2$. Das Diboran(4) $[HB(\mu\text{-hpp})]_2$ reagiert über eine oxidative Addition mit HX ($X = Cl^-$ oder I^-) zu stabilen $B_2H_5^+$ - analogen Verbindungen $[H_3B_2(\mu\text{-hpp})_2]X$. Zur Aufklärung der Bindungseigenschaften im zweikernigen B(III) Hydrid $[H_3B_2(\mu\text{-hpp})_2]^+$-Kation wurden quantenchemische (DFT) Rechnungen hinzugezogen. Die Reaktion zwischen BCl_3 und hppH führte auf direktem Weg zu der Verbindung $[Cl_2B_2(\mu\text{-hpp})_3]BCl_4$, die drei Guanidinat (hpp) Liganden enthält. Dies legt einen weitaus komplizierteren Reaktionsmechanismus als bei der Umsetzung von $H_3B{\cdot}NMe_3$ mit hppH nahe. $B_2Cl_2(NMe_2)_2$ reagiert mit hppH zu $[\{(Me_2(H)N)B(\mu\text{-hpp})\}_2]Cl_2$, dem ersten Vertreter eines binuklearen B(II)-Kations mit einer direkten B-B-Bindung. Die Reaktion zwischen $[\{(Me_2(H)N)B(\mu\text{-hpp})\}_2]Cl_2$ und AgOTf oder $Li[B(C_6F_5)_4]$ führte zu Verbindungen mit schwach koordinierenden Anionen. Die thermische Zersetzung der entstehenden Verbindungen $[\{(Me_2(H)N)B(\mu\text{-hpp})\}_2]X_2$ ($X = Cl^-$, OTf^- und $[B(C_6F_5)_4]^-$) wurde mit Hilfe von NMR-Daten untersucht.

Abstract

This work is concerned with the synthesis, chemical reactivity, and characterization of new binuclear boron compounds containing bridging guanidinate ligands.

The guanidine-borane adducts $H_3B{\cdot}hppH$ and $H_3B{\cdot}N(H)C(NMe_2)_2$, accessed by a base exchange reaction between $H_3B{\cdot}NMe_3$ and the guanidine derivative hppH or $N(H)C(NMe_2)_2$, were targeted as precursors in thermal and catalytic dehydrogenations. The reaction mechanism for these experiments was elucidated by means of quantum chemical (DFT) calculations on the model $H_3B{\cdot}N(H)C(NH_2)_2$. In contrast to $H_3B{\cdot}hppH$, the thermal dehydrogenation of $H_3B{\cdot}N(H)C(NMe_2)_2$ is accompanied by decomposition, leading to methylimino borane oligomers, $[HBNMe]_n$. The decomposition pathway was studied and understood with the aid of quantum chemical calculations. Faster dehydrogenation could be initiated by addition of a catalyst. The dehydrogenation of $H_3B{\cdot}hppH$ in presence of a catalyst leads to the binuclear B(III) hydride $[H_2B(\mu\text{-hpp})]_2$, containing two guanidinate (hpp) ligands. Further (reductive) catalytic dehydrogenation of $[H_2B(\mu\text{-hpp})]_2$ gave the double-base stabilized diborane(4) $[HB(\mu\text{-hpp})]_2$, featuring direct B-B bonding. Besides, $[HB(\mu\text{-hpp})]_2$ undergoes an oxidative addition reaction with HX (X = Cl^- or I^-), respectively which afforded $[H_3B_2(\mu\text{-hpp})_2]X$, representing a stable $B_2H_5^+$ analogues. Quantum chemical (DFT) calculations were carried out to analyse the bond properties in the cationic binuclear B(III) hydride $[H_3B_2(\mu\text{-hpp})_2]^+$. The reaction between BCl_3 and hppH lead to $[Cl_2B_2(\mu\text{-hpp})_3]BCl_4$ containing three guanidinate (hpp) ligands, which suggests that this reaction has a much more difficult mechanism than the $H_3B{\cdot}NMe_3$/hppH reaction. $B_2Cl_2(NMe_2)_2$ reacts with hppH to yield $[\{(Me_2(H)N)B(\mu\text{-hpp})\}_2]Cl_2$, featuring the first representative of two B(II) cations with direct B-B bonding. Further reactions between $[\{(Me_2(H)N)B(\mu\text{-hpp})\}_2]Cl_2$ and AgOTf or $Li[B(C_6F_5)_4]$ yielded new salts with weakly coordinating anions. Additionally, thermal decomposition of $[\{(Me_2(H)N)B(\mu\text{-hpp})\}_2]X_2$ (X = Cl^-, OTf^- and $[B(C_6F_5)_4]^-$) was investigated on the basis of NMR experiments.

Abbreviations

Ac	Acetyl
Bn	Benzyl
Bu	Butyl group
^{t}Bu	*tert*-Butyl group
^{n}BuLi	^{n}Butyllithium
B3LYP	Becke, three-parameter, Lee-Yang-Parr
BSSE	Basis Set Superposition Error
ca.	circa
cat	cathecolato
COD	1,5-Cycloctadiene
Cp	Cyclopentadienyl
CPCM	the Conductor-like Polarizable Continuum Model
Cy	Cyclohexyl
d	doublet
DFT	Density Functional Theory
DMSO	Dimethyl sulfoxide
E	Energy
EA	Elemental Analysis
EI	Electron Ionization
ESI	Electrospray ionization
Et	Ethyl group
g	gram
G	Gibbs free energy
GIAO	Gauge-Including Atomic Orbital
H	Enthalpy
h	hour
hppH	1,3,4,6,7,8-hexahydro-2*H*-pyrimido[1,2-*a*]pyrimidine
HR	High Resolution
HRMAS	High Resolution Magic Angle Spinning
Htbn	2,3,5,6,7,8-hexahydroimidazo[1,2-*a*]pyrimidine
Htbo	2,3,5,6-tetrahydro-1*H*-imidazo[1,2-*a*]imidazole

Hz	Hertz
ip	in phase
IR	Infrared
J	Coupling constant
K	Kelvin
kHz	kilohertz
kJ	kilojoule
LANL2DZ	Los Alamos National Laboratory 2-double-z
m	multiplet (NMR spectroscopy), medium (IR spectroscopy)
M	Mechanism
Me	Methyl
MHz	Megahertz
ml	millilitre
mmol	millimol
MP	Møller-Plesset Perturbation theory
MS	Mass Spectrum, Mass Spectrometry
m/z	mass-to-charge ratio
nm	nanometre
NMR	Nuclear Magnetic Resonance
oop	out of phase
OTf	Trifluoromethanesulfonate, CF_3SO_3-
Ph	Phenyl
pin	pinacolato
pm	picometre
ppm	parts per million
pz	pyrazol
q	quartet
qui	quintet
R	Alkyl or Aryl
[Rh]	$[Rh(1,5\text{-}COD)Cl]_2$
RHF	Restricted Hartree-Fock
RT	Room temperature
s	singlet (NMR spectroscopy), strong (IR spectroscopy)

SVP	Split Valence Polarization basis-set
t	triplet
TMG	1,1,3,3–tetramethylguanidine
TMS	Tetramethylsilane
TS	Transition State
TZVPP	Triple-Zeta Valence double-Polarization basis-set
w	weak
ZPE	zero-point energy
α	Angle
δ	Frequency of the bending vibration (IR spectroscopy), chemical shift (NMR spectroscopy)
λ	Wavelength
υ	Frequency of the stretching vibration
θ	Angle
°	Degree

1. Introduction

1.1 Addition/elimination of H_2 to the E-E bond of binuclear main group element compounds

Up to date, thermal addition of H_2 to the E-E bond of binuclear main group elements compounds is restricted to only a few examples. Nonetheless, a number of studies have shown that vapour phase reactions of H_2 with E_2 (E = Ga or In) can occur (usually with photoactivation) and the products can be trapped in a frozen matrix.[1] It has been shown that the reaction of Ga_2 with H_2 directly or indirectly gives rise to three isomers of Ga_2H_2, namely the bis(μ-hydrido) species Ga(μ-H)$_2$Ga (**a**), the *trans*-bent species HGaGaH (**b**), and GaGaH$_2$ (**c**) with two terminal Ga-H bonds (see Scheme 1.1.1). The barrier for the reaction of Ga_2 with H_2 was estimated experimentally from isotopic measurements and from quantum chemical calculations to be ca. 30-50 kJ mol^{-1}.[2] If the reaction barrier is sufficiently low, the reaction could be driven reversibly.

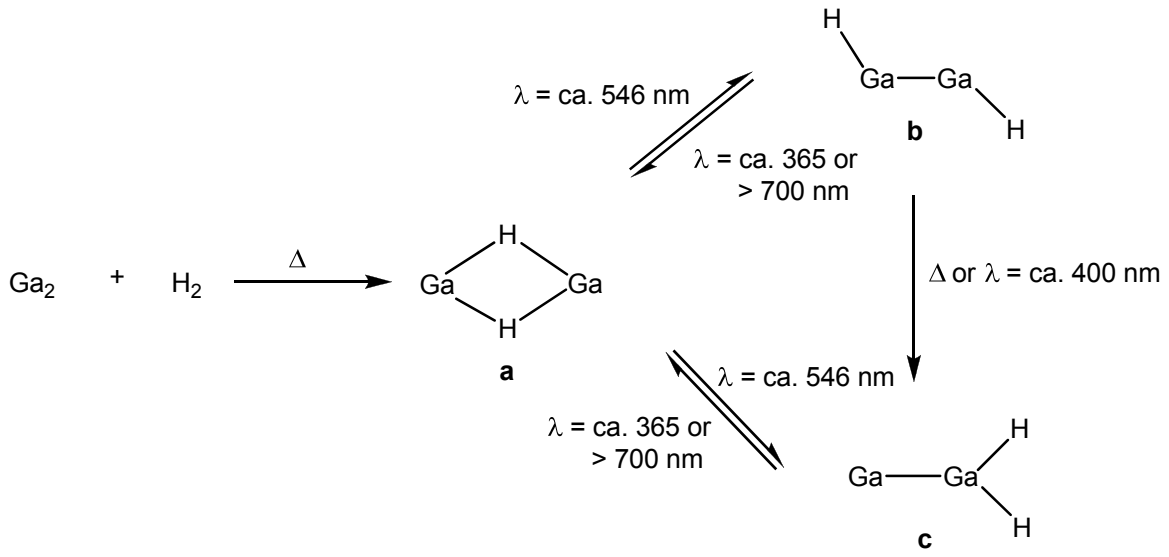

Scheme 1.1.1

In_2 reacts only under photoactivation (λ = ca. 365 nm) with H_2 to give the bis(μ-hydrido) species, In(μ-H)$_2$In. Further irradiation (λ > 450 nm) of this compound leads to the isomer HInInH, together with InH. It was found that the isomers could be interconverted by selective photolysis. All these molecules have been identified and

characterized by IR spectroscopy obtained from experiments and quantum chemical calculations, respectively.

Very recently $[GaAr']_2$ (Ar' = 2,6-(2,6-*i*$Pr_2C_6H_3)_2C_6H_3$) was reacted with H_2 at room temperature and 1 bar to give $[Ar'Ga(\mu\text{-}H)H]_2$.[3]. However, this reaction seems not to involve a binuclear compound since Ar'Ga was shown to be dimeric in the solid state, but monomeric in solution.

In the case of the lightest group 13 element boron, it was reported by Welch and co-workers that the compound $(C_6H_2Me_3)_2PH(C_6F_4)BH(C_6F_5)_2$ cleanly loose H_2 at temperatures above 100°C. It was also shown that the dehydrogenated product $(C_6H_2Me_3)_2P(C_6F_4)B(C_6F_5)_2$ is stable and reacts with 1 atmosphere of H_2 at 25°C to get back the phosphonium borate species which contain an unusual hydride and proton in the same molecule (see Scheme 1.1.2).[4]

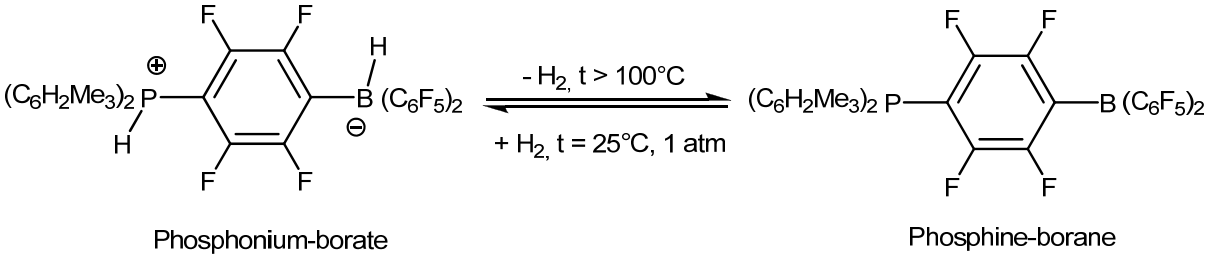

Scheme 1.1.2

The activation of H_2 to the compound reported by Welch *et al.* occurs by a heterolytic cleavage which is likely to proceed via an electrophilic activation mechanism[5] (see Scheme 1.1.3). For comparison, the activation of dihydrogen on transitional metals can proceeds via homolytic or heterolytic cleavage, respectively (see Scheme 1.1.3).[6]

Electrophilic activation according to Welch *et al.*

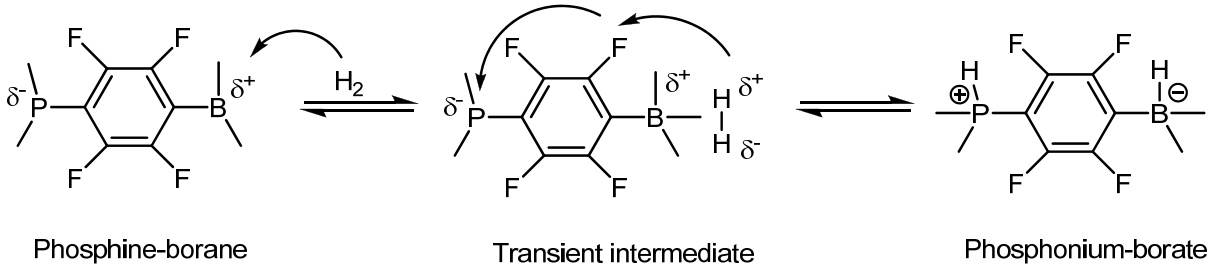

Homolytic and heterolytic cleavage

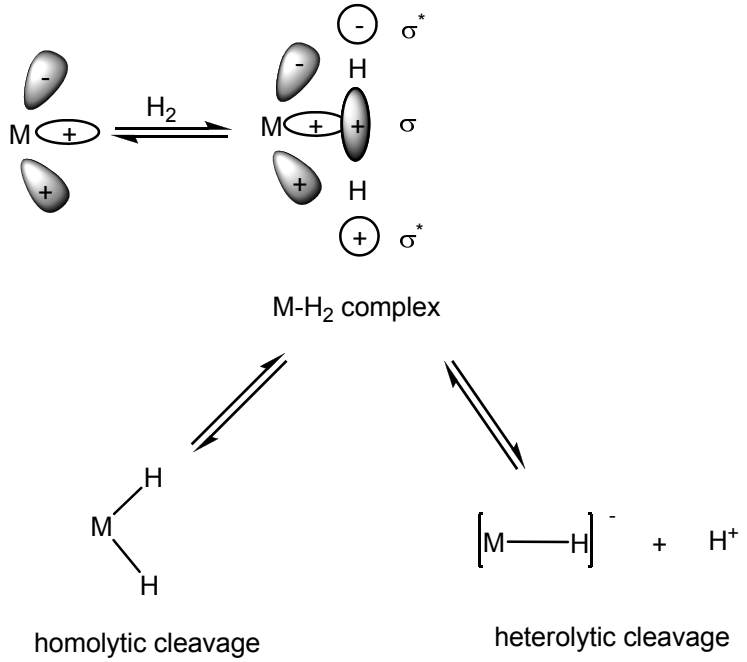

Scheme 1.1.3

The phosphine-borane species synthesised by Welch *et al.* contains a strongly electrophilic (boron) and nucleophilic (phosphorus) centers. For comparison, amine-borane also combines both electrophilic (boron) and nucleophilic (nitrogen) centers. However, these centers are directly bonded, whereas in the phosphine-borane described by Welch *et al.*, they are separated by a linker, increasing the electrophilicity of B and the nucleophilicitiy of P. It should be also noted that catalytic H_2 elimination from amine-borane species has been extensively studied. The first two examples of transition-metal catalyzed dehydrogenation of amine-borane compounds were reported by Roberts et al. in 1989,[7] using 10% palladium or charcoal and then

by Manners et al.[8] and Autrey et al.[9] , respectively. These compounds can certainly be applied for dehydrocoupling reactions and function as a transfer hydrogenation to deliver a stroichiometric amount of H_2 to olefins.[8c] Especially much recent work has focused on catalysing the release of H_2 from ammonia-borane, since the compound was suggested as a hydrogen storage material for mobile applications.[10] It was shown that dehydrogenation of ammonia-borane can also be initiated by acids.[11]

In 2005, Power and co-workers reported that the reaction between the molecular species Ar'GeGeAr' (Ar' = 2,6-(2,6-*i*Pr$_2$C$_6$H$_3$)$_2$C$_6$H$_3$) and H_2 at 1 atmosphere in hexane at 25°C rapidly affords a mixture of Ge_2 and primary germane products (Ar'HGeGeHAr', Ar'H$_2$GeGeH$_2$Ar' and Ar'GeH$_3$), the relative concentration of which could be controlled by the H_2 offer (see Scheme 1.1.4).[12] The addition of H_2 to digermynes is thought to be due in part to the singlet diradical character of the ground state.[13]

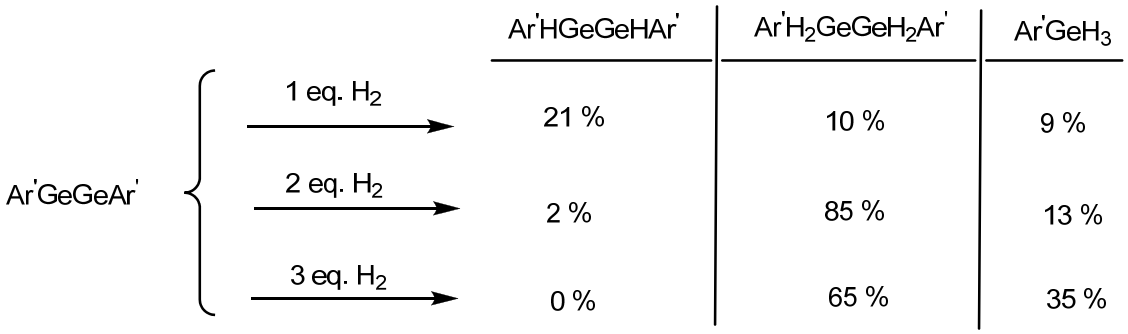

Scheme 1.1.4

Further work in group 14 showed that reaction between distannynes and H_2 at 25°C and 1 atmosphere lead to formation of symmetric hydrogen bridged or unsymmetric stannylstannane products in high yield.[14] In contrast to the reaction of Ar'GeGeAr' with H_2, which yields a mixture of products these reactions cleanly afford a single tin(II) hydride product and the structure of the product is governed by the size of the ligands.[15]

1.2 Diborane(4) compounds

Diborane(4) compounds are important intermediates between simple mono-boron derivatives and the polyhedral electron-deficient compounds of this element. Unlike diborane(6) (B_2H_6) (see Figure 1.2.1) with its electron deficient 2-electron 3-center bonding, the diborane(4) (see Figure 1.2.1) are electron precise compounds $X_2B\text{-}BX_2$ (X = Alkyl, Aryl, Halogen, OR or NR_2) with a boron-boron single bond.

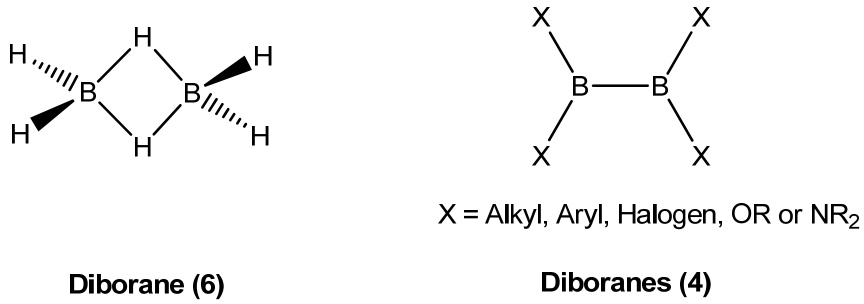

Figure 1.2.1

The first diborane(4) compound B_2Cl_4 was synthesized by Stock[16] in 1925, using an electric discharge between zinc electrodes immersed in liquid BCl_3. Nevertheless an intensive study of diborane(4) derivatives began in the early 1960s, when an easy access to $B_2(NMe_2)_4$ was found.[17] For the synthesis of diborane(4) compounds, two main types of routes have been involved: either *reductive coupling reactions* of monoboron derivatives to form the boron-boron bond, or by *substituent exchange reactions* of compounds possessing performed B_2 fragment[17a], [18] (see Scheme 1.2.1).

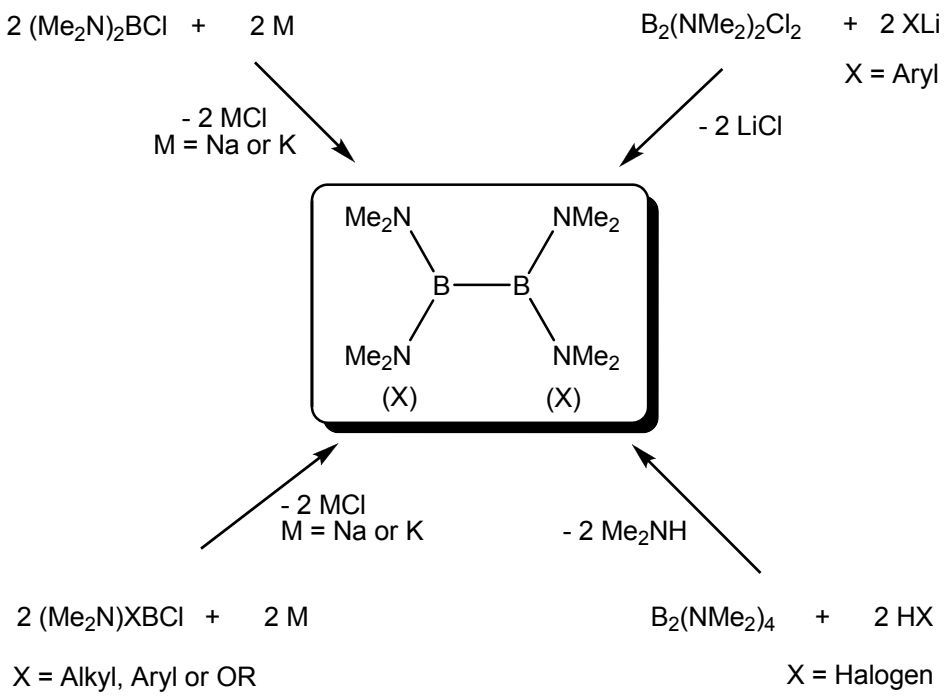

Scheme 1.2.1

The stability of diborane(4) compounds $X_2B\text{-}BX_2$ is strongly dependent on the nature of the substituent X (where X = R_2N > RO > F > Cl ~ Aryl, Alkyl). It was shown that the stability of these species can be improved by increasing the electronic and steric shielding at the boron centers, so as to avoid decomposition into BX_3 and $(BX)_n$.[19] The most stable derivatives are those in which good *π*-donor groups are present such as amido (R_2N) or alkoxy (OR).[20] $R_2B\text{-}BR_2$ are stable only when sterically demanding R groups such as *t*-Bu, CH_2-*t*-Bu and mesityl[21] are present in the molecule. Indeed, the first stable tetraorganyldiborane(4) derivatives, such as $(^t\text{Bu})_2\text{B-B}(^t\text{Bu})\text{Me}$[22] and $(^t\text{Bu})_2\text{B-B}(^t\text{Bu})(\text{CH}_2\text{-}^t\text{Bu})$[23] were synthesised in 1980.

The diborane(4) compounds are involved in many reactions with organic and organometallic systems which make these species very important. For example, addition of diborane(4) compounds to unsaturated organic substrates is one of the most studied of reactions in the synthesis of organoboron compounds and their applications in organic synthesis. It was shown that B_2X_2 (X = F, Cl, Br) can be added in the absence of catalysts to the C=C and C≡C fragment, respectively.[24] Unfortunately, these species suffer from low thermal stability (with exception of B_2F_2) and preparative difficulties. In contrast, the tetraalkoxydiboron compounds, such as bis(pinacolato)diboron (B_2pin_2 - **A**) and bis(catecholato)diboron (B_2cat_2 - **B**) (Figure

1.2.2),[25] are thermally stable and easy to prepare from $B_2(NMe_2)_4$[26] but are inactive toward diboration under conventional reaction conditions.[27]

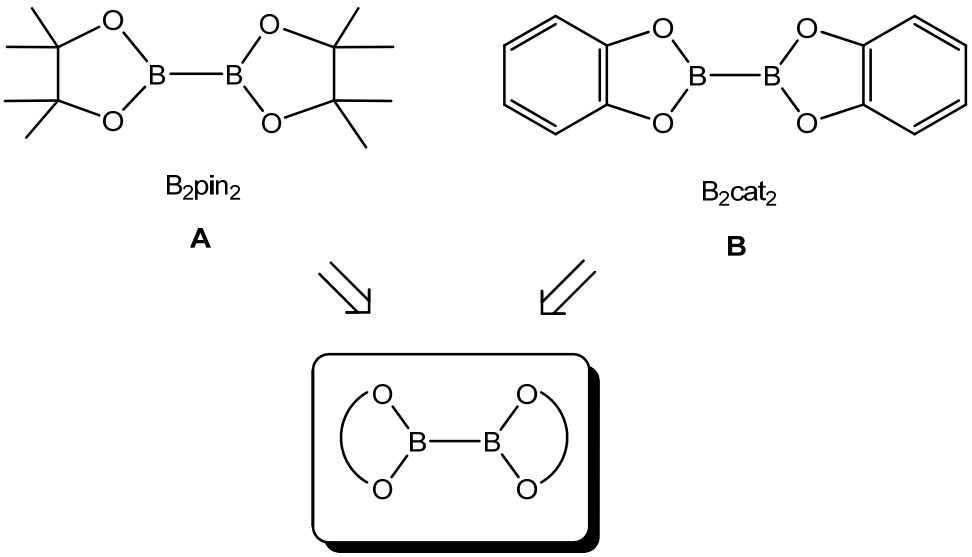

Figure 1.2.2: Bis(pinacolato) diboron (**A**) and bis(catecholato) diboron (**B**).

These compounds can be added to alkenes[28] or alkynes[29] only in presence of a catalyst. The mechanism of catalyzed alkene diboration is illustrated in Scheme 1.2.2, which involves oxidative addition[30] of B_2cat_2 or B_2pin_2 to the platinum complex (**i**), followed by ethylene coordination with simultaneous dissociation of one PPh_3 group (**ii**). Furthermore, insertion of the olefin[31] into the Pt-B bond (**iii**), and the reductive elimination deliver the organoboron product[32] (**iv**).

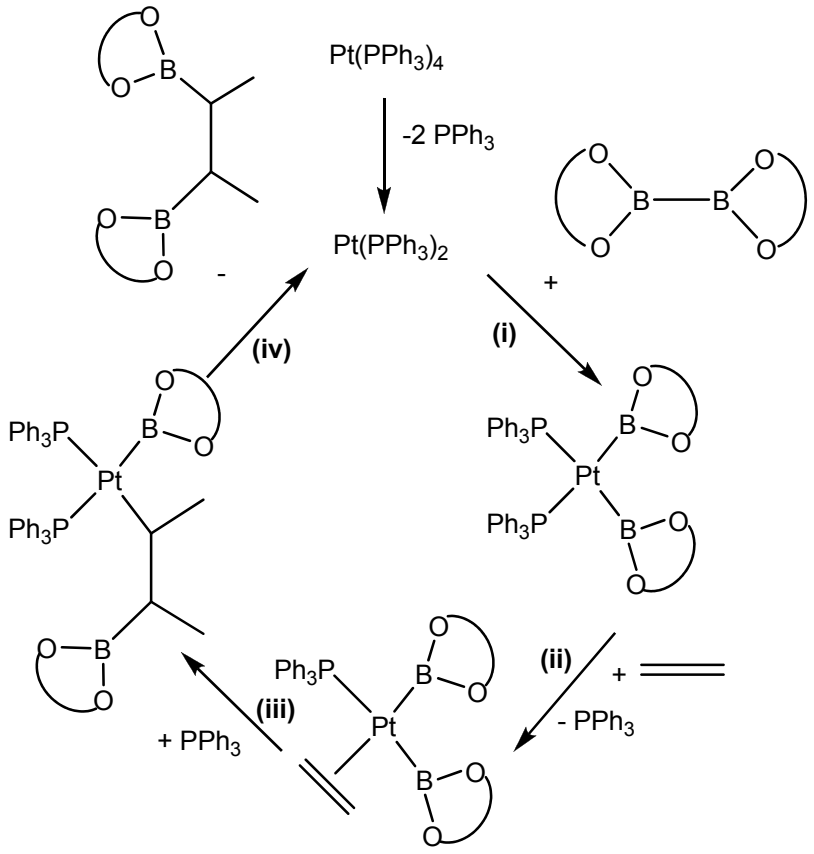

Scheme 1.2.2: The mechanism for the platinum-catalyzed alkene diboration reaction.

As already mentioned, the oxidative addition of diboranes(4) to suitable transition metal complexes leads to corresponding bisboryl compounds,[29a], [32], [33] which are important intermediates in catalytic cycle for diboration of unsaturated substrates (see Scheme 1.2.3).

Marder and Norman observed that the oxidative addition of B_2cat_2 to $(Ph_3P)_2Pt$(ethylene) is faster than the same reaction employing $B_2(pin)_2$[33a] even if the B-B bond length in B_2cat_2 (168 pm) is shorter than the B-B bond length in $B_2(pin)_2$ (171 pm).[33a]

Iverson and Smith indicated that the bis(boryl)species obtained from oxidative addition of B_2cat_2 to Pt-complexes may be more stable than that obtained from $B_2(pin)_2$.[34] It was also shown that the Pt(0) complexes are generally more effective in diboration than Rh(I) and Pd(0) species, respectively. Actually, the increased *d*-electron energy of Pt(0) facilitates oxidative addition referring to Pd(0) and Rh(0).[29b], [35]

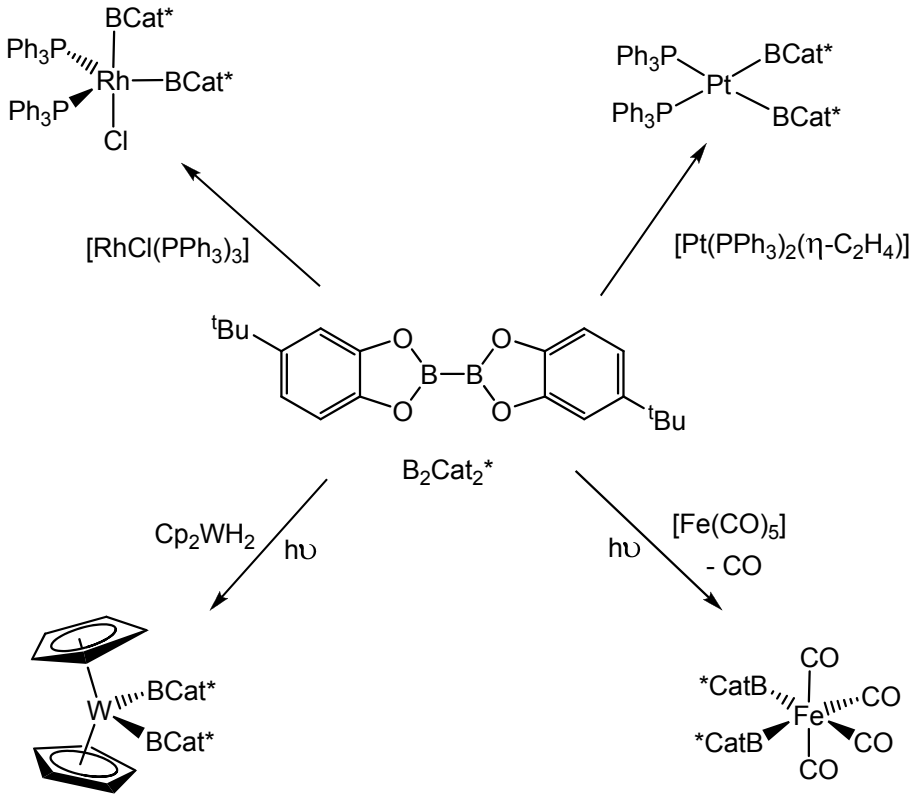

Scheme 1.2.3

Recently, Braunschweig et al.[36] reported the first example of a heterogeneously catalyzed diboration of an alkyne. They used as a catalyst finely dispersed palladium or platinum metals, the last one being the most active. As diboron reagents they used a new class of species namely [2]borametalloarenophanes.[37] For example, 1,2-dibora-[2]ferrocenophane[37b] compound was prepared by the reaction of $Li_2[Fe(Cp)_2]$ with $B_2Cl_2(NMe_2)_2$. (see Scheme 1.2.4, (ii)).

Reaction of $Na[(Cp)Fe(CO)_2]$ and $Na[(Cp)W(CO)_3]$ with diborane(4) derivative $B_2Cl_2(NMe_2)_2$ lead to the formation of diborane(4)yl complexes with retention of the boron-boron linkage[38] (see Scheme 1.2.4 (i)). The same diborane(4) derivative was used to synthesized the first bridge borylene complex $[\mu\text{-}B(NMe_2)\{CpMn(CO)_2\}_2]$[39] (see Scheme 1.2.4, (iii)), which involve the B-B bond cleavage.

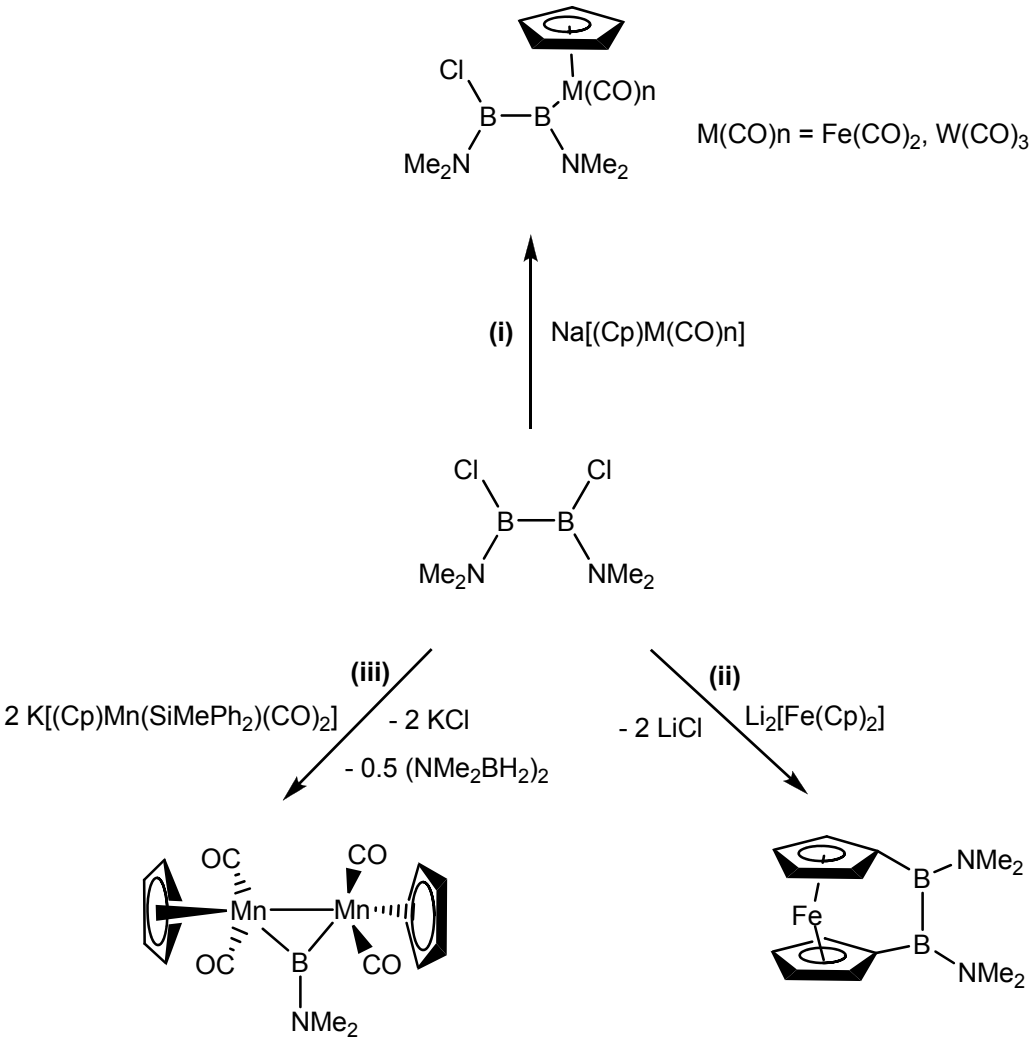

Scheme 1.2.4

Norman et al.[40] reported the use of $B_2Cl_2(NMe_2)_2$ as a diborating reagent in the diboration of alkynes catalyzed by $[Pt(PPh_3)_2(\eta^2\text{-}C_2H_4)]$. The reaction afforded high yields of cyclic 1-azonia-2-borata-5-borole compounds, which were the result of the redistribution of B-Cl and B-NMe_2 bonds (see Scheme 1.2.5).

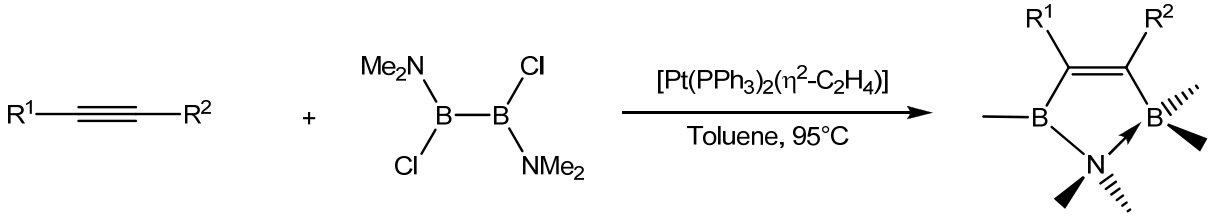

Scheme 1.2.5

1.3 Some aspects of binuclear coordinative compounds with guanidine ligands

The coordination chemistry of guanidine ligands (see Figure 1.3.1) has been well-explored for main-group metals as well as for transition metals.[41] Guanidine derivatives are important compounds, especially due to their large basicity (pK_A = 13.6 for $HN=C(NH_2)_2$)[42] and their role in biological systems.[43] Part of the interest in these compounds stems also from their potential applications in catalytic reactions.[41b] These powerful electron-donating ligands not only coordinate to a remarkably wide range of metal ions from all parts of periodic system, but also show a rich variety of coordination modes.[41], [44] They either bind as neutral ligands and after H^+ abstraction as negatively charged guanidinate ligand or also as guanidinium cation (binding to anions) (see Figure 1.3.1).

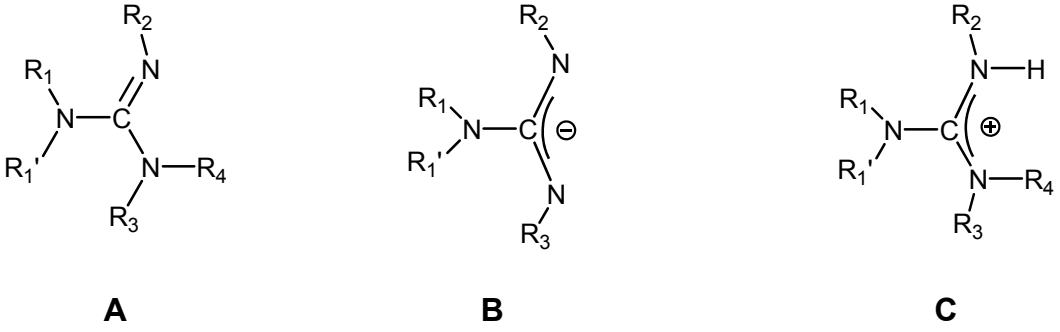

Figure 1.3.1: Representation for guanidines (**A**) and their corresponding guanidinate (**B**) anions and monoprotonated guanidinium (**C**) cations.

The anion of the guanidine hppH (1,3,4,6,7,8-hexahydro-2*H*-pyrimido[1,2-*a*]pyrimidine) was used intensively in the past as complex ligand,[45] which can be converted from neutral guanidine by using organolithium reagents.[44], [45] This hpp^- shows significant differences in its steric and electronic properties when compared with acyclic form (see Figure 1.3.2).[46] For example, the hpp^- has a more trend to bridge rather than bind a single metal (although chelation has been observed in a number of complexes[47]). This ligand has also been proven to be efficient in bringing two transition metals in high oxidation states with direct metal-metal bonding, a feature that was extensively exploited by Cotton and co-workers in the development of bimetallic 'paddle-wheel' compounds.[48] This is attributed to the parallel projection

of the two *N*-donor orbitals (see Figure 1.3.2, **A**) contrasting to the convergence of these orbitals at the 'mouth' of the ligand in the acyclic guanidinate derivatives (see Figure 1.3.2, **B**).[46]

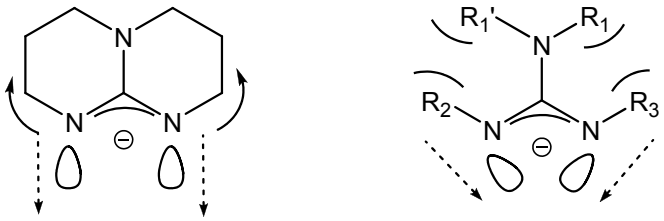

A **B**

Figure 1.3.2: Projection of frontier orbitals for hpp^- compared with an acyclic guanidinate.

Hence a variety of binuclear coordinative compounds were obtained with hpp^- group (see Scheme 1.3.1) where the ligand showed different coordination modes (see Figure 1.3.3).

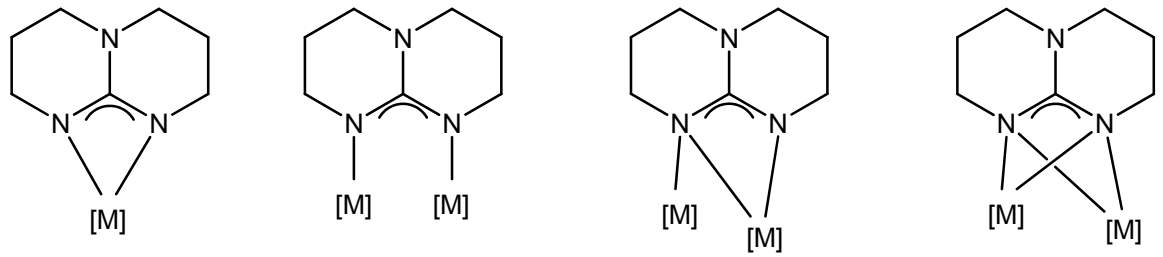

k^1N-k^1N' k^1N-k^2N' k^1N-$k^{1,2}N'$ $k^{1,2}N$-$k^{1,2}N'$

A **B** **C** **D**

Figure 1.3.3: Coordination modes for the hpp^- ligand in binuclear coordinative compounds.

For example, in the dimeric species $[Ti(N^tBu)(hpp)(\mu\text{-hpp})]_2$[47a] (see Scheme 1.3.1, **A**), synthesized by Coles and Hitchcock, one of the hpp^- groups chelates to titanium with k^1N-k^1N'-mode (see Figure 1.3.3, **A**) and the other one bridges two metals (see Figure 1.3.3, **B**), with the coordination sphere completed by a terminal N^tBu ligand (see Scheme 1.3.1, **A**). The bridging hpp^- ligands link the two Ti(NtBu)(hpp) units in

an eight-membered ring with a chair-conformation similar to that previously observed in the dimeric tin and aluminium complexes $[Sn(\mu\text{-hpp})Cl]_2$[49] (see Scheme 1.3.1, **F**) and $[Al(\mu\text{-hpp})Me_2]_2$[50] (see Scheme 1.3.1, **D**).

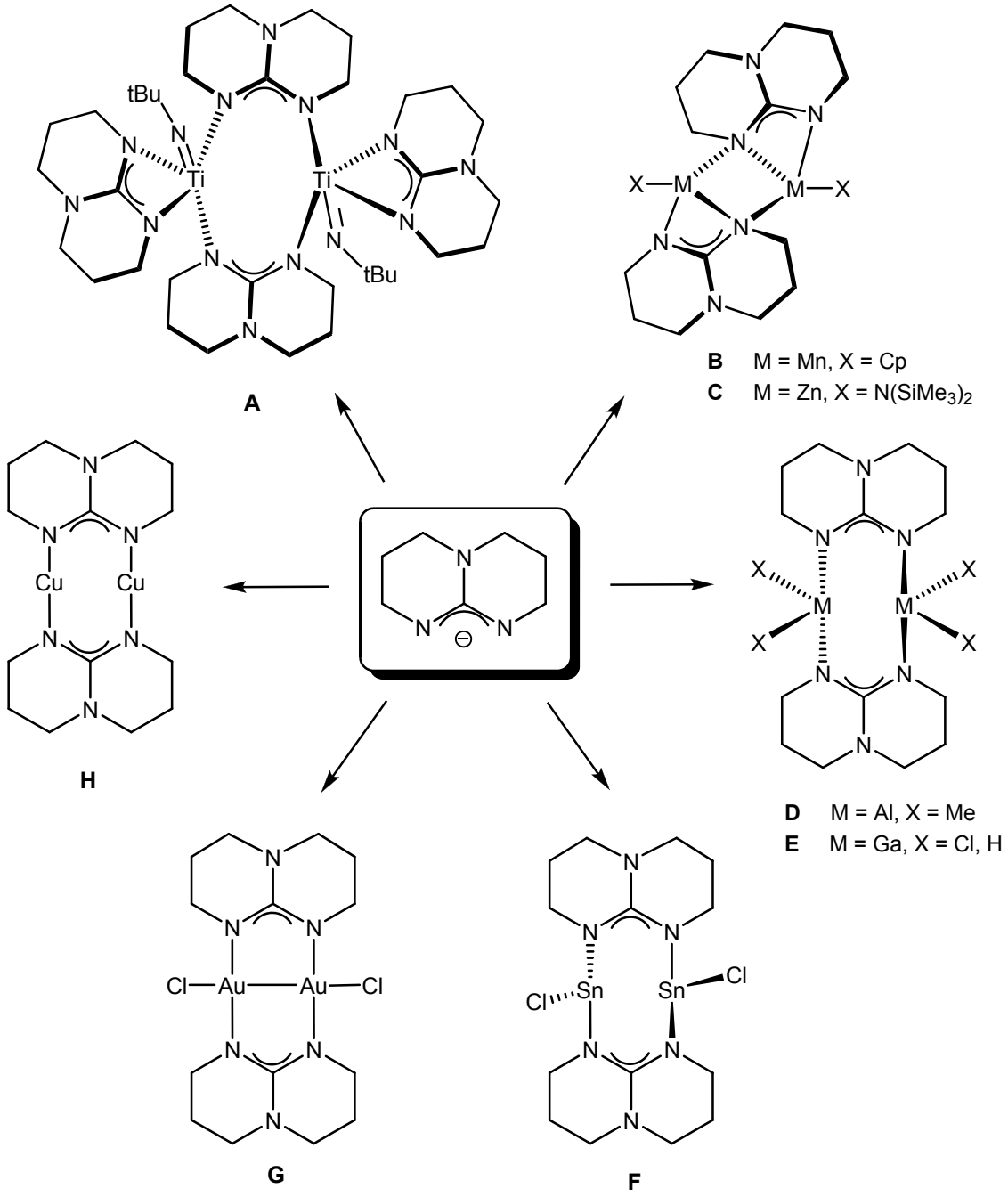

Scheme 1.3.1: Examples of binuclear coordinative compounds with hpp^- ligand.

In case of $[CpMn(hpp)]_2$[51] and $[Zn(hpp)\{N(SiMe_3)_2\}]_2$[52] species (see Scheme 1.3.1, **B** and **C**) which form dimers in the solid state, the guanidinate ligand adopts a

k^1N-$k^{1,2}N'$-coordiantion mode. It was shown that the last compound could be used in the ring-opening polymerisation catalysis of lactide.[52]

We recently reported on the synthesis of the binuclear Ga hydride [H(Cl)Ga(μ-hpp)]$_2$,[53] with two bridging hpp ligands (see Scheme 1.3.1, **E**), which adopt a chair-type conformation in solid state, similar to [Al(μ-hpp)Me$_2$]$_2$.[46]

The coordination chemistry of Cu, Ag and Au with hpp ligand was also explored. Therefore, the Au(II) forms a dinuclear complex, [Au$_2$(μ-hpp)$_2$Cl$_2$][54] (see Scheme 1.3.1, **G** and Scheme 1.3.2) which contain a short Au-Au bond distance (247.52(9) pm). Unfortunately, all attempts to synthesized Au(I) product [Au$_2$(μ-hpp)$_2$] failed.[55] During these studies, Mohamed and co-workers discovered that solvent conditions determined whether oxidation to the dinuclear Au(II) species, [Au$_2$(μ-hpp)$_2$Cl$_2$], occurs or a tetranuclear Au(I) species, [Au(μ-hpp)]$_4$, forms[54] (see Scheme 1.3.2). It appears that the nuclearity of hpp compounds depends upon the solvent used and not upon steric effects, which, with bulky amidinate ligands,[56] are known to block the formation of tetranuclear complexes.

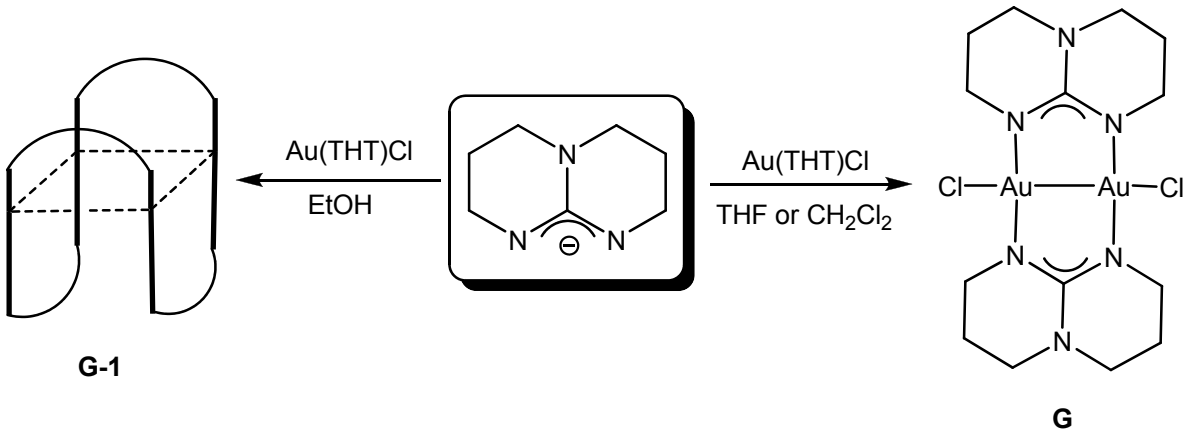

Scheme 1.3.2: Synthesis of [Au(hpp)Cl]$_2$ (**G**) and [Au(hpp)]$_4$ (**G-1**).

The dinuclear species [Cu$_2$(μ-hpp)$_2$][57] (see Scheme 1.3.1, **H**) was also reported where a short internuclear distance (245.3(1) pm) was depicted. Nevertheless, the DFT calculations showed that the close approach of the copper atoms is predictable without involving any significant amount of covalent bonding.[57] In contrast to the copper(I) complex, [Cu$_2$(μ-hpp)$_2$] and the gold(II) complex, [Au$_2$(μ-hpp)$_2$Cl$_2$], the silver (I) forms a tetranuclear complex [Ag$_4$(μ-hpp)$_4$].[54]

As already mentioned, the hpp ligand has been widely used to make paddle-wheel compounds of the type $M_2(hpp)_4X_2$ (see Figure 1.3.4), where the axial ligand (X) may or may not be present. Prominent examples include the paddle-wheel type molecules $[Pd_2(hpp)_4Cl_2]$[58] and $[Pt_2(hpp)_4Cl_2]$.[59] Cotton and co-workers synthesized and analysed also some paddle-wheel $M_2(hpp)_4$ compounds (M = Mo and W) having quadruply bonded units, with very low ionization energies[60] and good reducing ability in solution.[61] The low ionization energies have been attributed to a strong interaction of the guanidinate core with the δ orbitals of the M_2^{4+} units.[60] However, it should be noted that bicyclic guanidinate ligands interact much stronger with dimetal units than non-cyclic guanidinates as shown for example by the oxidation potentials of $Mo_2(hpp)_4$[62] and $Mo_2[(NPh)_2CNHPh]_4$[63] which differ by more than 1.2 V.

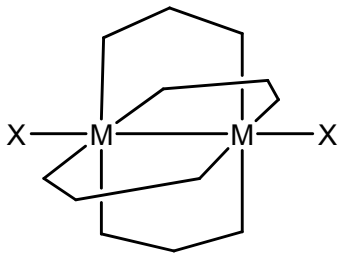

Figure 1.3.4: A schematic sketch of the paddlewheel structural motif.

Reduction of $Ti(hpp)_2Cl_2$[47b] with potassium graphite afforded a compound that analyzed as $[Ti_2(hpp)_4Cl_2]$[64] (see Figure 1.3.5) However, X-ray analysis showed that only two hpp ligands were bridging and that, rather than the expected k^1N-k^2N'-mode (see Figure 1.3.3, **B**), they were oriented perpendicular to the Ti-Ti bond with $k^{1,2}N$-$k^{1,2}N'$-bonding (see Figure 1.3.3, **D**) and the other hpp^- groups chelates to titanium with k^1N-k^1N'-mode (see Figure 1.3.3, **A**).

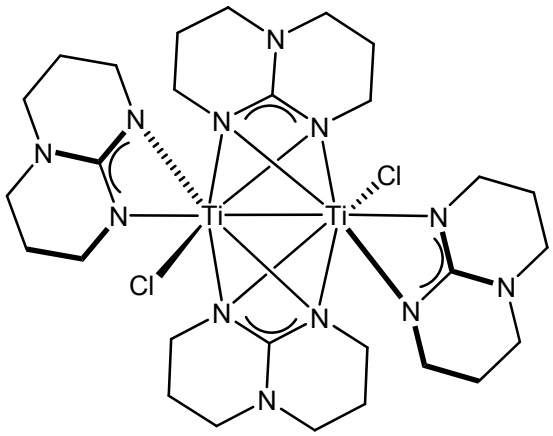

Figure 1.3.5

1.4 Aim of the present research

The main purpose of this dissertation was to synthesize and characterize new binuclear boron hydrides with bridging guanidinate ligands and to explore their chemistry.

A major goal was the preparation of new double-base stabilized diboranes(4) by dehydrogenation of borane adduct $H_3B{\cdot}hppH$ (see Scheme 1) and by reactions between $B_2Cl_2(NMe_2)_2$ and hppH or hppLi (see Scheme 2), featuring guanidinate (hpp) bridges. In following studies the reactivity of these new binuclear B(II) species were investigated. These compounds were especially attractive for oxidative addition reactions to the B-B bond.

The experimental studies were accompanied by quantum chemical (DFT) calculations.

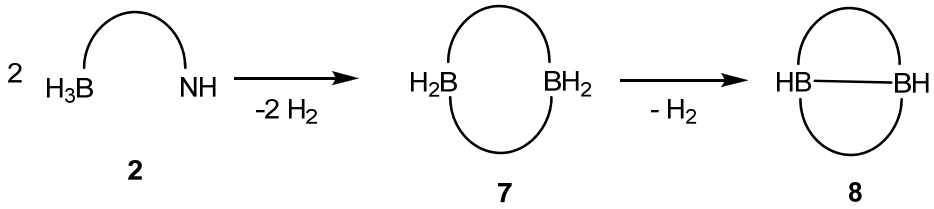

Scheme 1

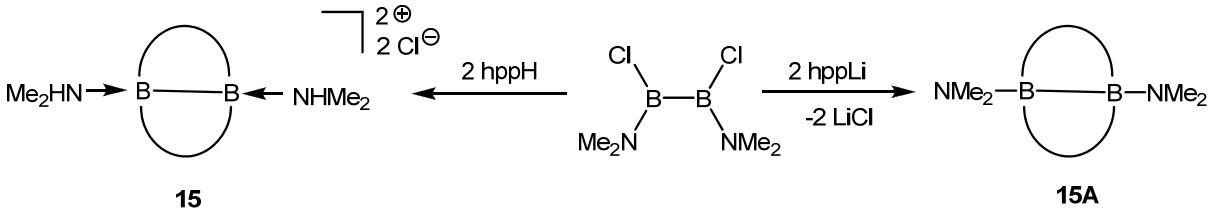

Scheme 2

1.5 References

[1] a) H.-J. Himmel, L. Manceron, A. J. Downs, P. Pullumbi, *Angew. Chem.* **2002**, *114*, 829–832; *Angew. Chem. Int. Ed.* **2002**, *41*, 796–799; b) H.-J. Himmel, L. Manceron, A. J. Downs, P. Pullumbi, *J. Am. Chem. Soc.* **2002**, *124*, 4448–4457.

[2] A. Köhn, H.-J. Himmel, B. Gaertner, *Chem. Eur. J.* **2003**, *9*, 3909–3919.

[3] Z. Zhu, X. Wang, Y. Peng, H. Lei, J. C. Fettinger, E. Rivard, P. P. Power, *Angew. Chem.* **2009**, *121*, 2065–2068.

[4] a) G. C. Welch, R. R. S. Juan, J. D. Masuda, D.W. Stephan, *Science* **2006**, *314*, 1124–1126; b) G. C. Welch, D.W. Stephan, *J. Am. Chem. Soc.* **2007**, *129*, 1880–1881; c) P. A. Chase, G. C.Welch, T. Jurca, D.W. Stephan, *Angew. Chem*. **2007**, *119*, 8196–8199; *Angew. Chem. Int. Ed.* **2007**, *46*, 8050–8053.

[5] G. J. Kubas, *Science*, **2006**, *314*, 1096–1097.

[6] G. J. Kubas, *J. Organometal. Chem.* **2001**, *635*, 37–68.

[7] I. G. Green, K. M. Johnson, B. P. Roberts, *J. Chem. Soc. Perkin Trans. 2* **1989**, 1963–1989.

[8] a) C. A. Jaska, K. Temple, A. J. Lough, I. Manners, *Chem. Commun.* **2001**, 962–963; b) C. A. Jaska, I. Manners, *J. Am. Chem. Soc.* **2004**, *126*, 9776–9785; c) T. J. Clark, C. A. Russell, I. Manners, *J. Am. Chem. Soc.* **2006**, *128*, 9582–9583; d) M. E. Sloan, T. J. Clark, I. Manners, *Inorg. Chem.* **2009**, *48*, 2429–2435.

[9] Y. Chen, J. L. Fulton, J. C. Linehan, T. Autrey, *J. Am. Chem. Soc.* **2005**, *127*, 3254–3255.

[10] See for example: a) F. H. Stephens, V. Pons, R. T. Baker, *Dalton Trans*. **2007**, 2613–2626; b) T. B. Marder, *Angew. Chem.* **2007**, *119*, 8262–8264; *Angew. Chem. Int. Ed.* **2007**, *46*, 8116–8118; and references cited therein.

[11] F. H. Stephens, R. T. Baker, M. H. Matus, D. J. Grant, D. A. Dixon, *Angew. Chem.* **2007**, *119*, 760–763; *Angew. Chem. Int. Ed.* **2007**, *46*, 746–749.

[12] G. H. Spikes, J. C. Fettinger, P. P. Power, *J. Am. Chem. Soc.* **2005**, *127*, 12232–12233.

[13] Y. Yung, M. Brynda, P. P. Power, M. Head-Gordon, *J. Am. Chem. Soc.* **2006**, *128*, 7185–7192.

[14] Y. Peng, M. Brynda, B. D. Ellis, J. C. Fettinger, E. Rivard, P. P. Power, *Chem. Commun.* **2008**, 6042–6044.

[15] E. Rivard, R. C. Fischer, R. Wolf, Y. Peng, W. A. Merrill, N. D. Schley, Z. Zhu, L. Pu, J. C. Fettinger, S. J. Teat, I. Nowik, R. H. Herber, N. Takagi, S. Nagase, P. P. Power, *J. Am. Chem. Soc.* **2007**, *129*, 16197–16208.

[16] A. Stock, A. Brandt, H. Fischer, *Chem Ber*. **1925**, *58*, 643-

[17] a) R. J. Brotherton, A. L. McClosky, L. L. Petterson, H. J. Stein berg, *J. Am. Chem. Soc*. **1960**, *82*, 6242–6245; b) H. Nöth, W. Meister, *Chem. Ber.* **1961**, *94*, 509–514.

[18] a) A. Moezzi, M. M. Olmstead, P. P. Power, *J. Chem. Soc., Dalton Trans.* **1992**, 2429–2434; b) H. Nöth, P. Fritz, *Angew. Chem.* **1961**, *73*, 408–408; c) R. J Brotherton, H. M. Manasevit, A. L. McCloskey, *Inorg. Chem.* **1962**, *1*, 749–754; d) M. J. G. Lesley, N. C. Norman, C. R. Rice, *Inorganic Syntheses*, **2004**, *34*, 3–4.

[19] H. Nöth, P. Fritz, *Z. Anorg. Allg. Chem*. **1963**, *324*, 129–145.

[20] a) R. J. Brotherton, A. L. McCloskey, L. L. Petterson, H.Steinberg, *J. Am. Chem. Soc.* **1960**, *82*, 6242–6245; b) A. H. Abu, I. Goldberg, M. Srebnik, *Eur. J. Inorg. Chem.* **2002**, 73–78.

[21] H. Hommer, H. Nöth, J. knizek, W. Ponikwar, H. Schwenk-Kircher, *Eur. J. Chem.* **1998**, 1519–1527.

[22] W. Biffar, H. Nöth, H. Pommerening, *Angew. Chem.* **1980**, *92*, 63-64; *Angew. Chem. Int. Ed. Engl*. **1980**, *19*, 56–57.

[23] K. Schlüter, A. Berndt, *Angew. Chem.* **1980**, *92*, 64–65; *Angew. Chem. Int. Ed. Engl.* **1980**, *19*, 57–58.

[24] a) J. A. Morrison, *Chem. Rev*. **1991**, *91*, 35–48; b) L. Ahmed, J. Castillo, D.A. Saulys, J. A. Morrison, *Inorg. Chem.* **1992**, *31*, 706–710; c) P. Ceron, A. Finch, J. Frei, J. Kerrigan, T. Parsons, G. Urry, H. I. Schlesinger, *J. Am. Chem. Soc.* **1959**, *81*, 6368–6371.

[25] H. Nöth *Z. Naturforsch*. **1984**, *39b*, 1463–1466.

[26] F. J. Lawlor, N. C. Norman, N. L. Pickett, E. G. Robins, P. Nguyen, G. Lesley, T. B. Marder, J. A. Ashmore, J. C. Green, *Inorg. Chem.* **1998**, *37*, 5282–5288.

[27] W. Clegg, C. Dai, F. J. Lawlor, G. Lesley, T. B. Marder, P. Nguyen, N. C. Norman, N. C. Pickett, C. R. Rice, E. G. Robins, A. J. Scott, N. J. Taylor, *Advances in Boron Chemistry* **1997**, Ed. W. Siebert, R. Soc. Chem. Cambridge.

[28] T. Ishiyama, M. Yamamoto, N. Miyaura, *Chem. Commun.* **1997**, 689–690.

[29] a) G. Lesley, P. Nguyen, N. J. Taylor, T. B. Marder, A. J. Scott, W. Clegg, N. C. Norman, *Organometallics*, **1996**, *15*, 5137–5154; b) T. Ishiyama, N. Matsuda, M. Murata, F. Ozawa, A. Suzuki, N. Miyaura, *Organometallics*, **1996**, *15*, 713–720.

[30] W. Clegg, F. J. Lawlor, T. B. Marder, P. Nguyen, N. C. Norman, A. G. Orpen, M. J. Quayle, C. R. Rice, E. G. Robins, A. J. Scott, F. E. S. Souza, G. Stringer, G. R. Whittell, *J. Chem. Soc. Dalton Trans.* **1998**, 301–310; C. N. Iverson, M. R. Smith, III, *J. Am. Chem. Soc.* **1995**, *117*, 4403–4404.

[31] R. T. Baker, J. C. Calabrese, S. A. Westcott, P. Nguyen, T. B. Marder, *J. Am. Chem. Soc.* **1993**, *115*, 4367–4368.

[32] G. J. Irvine, M. J. G. Lesley, T. B. Marder, N. C. Norman, C. R. Rice, E. G. Robins, W. R. Roper, G. R. Whittell, L. J. Wright, *Chem. Rev.* **1998**, *98*, 2685–2722.

[33] a) P. Nguyen, G. Lesley, N. J. Taylor, T. B. Marder, *Inorg. Chem*, **1994**, *33*, 4623–4624; b) J. F. Hartwig, X. He, *Angew. Chem.* **1996**, *108*, 352–354; c) X. He, J. F. Hartwig, *Organometallics* **1996**, *15*, 400–407.

[34] C. N. Iverson, M. R. Smith, III, *Organometallics* **1996**, *15*, 5155–5165.

[35] Q. Cui, D. G. Musaev, K. Morokuma, *Organometallics*, **1998**, *17*, 742–751.

[36] H. Braunschweig, T. Kupfer, M. Lutz, K. Radacki. F. Seeler, R. Sigritz, *Angew. Chem.* **2006**, *118*, 8217–8220; *Angew. Chem. Int. Ed.* **2006**, *45*, 8048–8051.

[37] a) H. Braunschweig, M. Homberger, C. Hu, X. Zheng, E. Gullo, C. Clentsmith, M. Lutz, *Organometallics* **2004**, *23*, 1968–1970; b) M. Herberhold, U. Doerfler, B. Wrackmeyer, *J. Organomet. Chem.* **1997**, *530*, 117–120.

[38] H. Braunschweig, B. Ganter, M. Koster, T. Wagner, *Chem Ber.* **1996**,*129*, 1099–1101.

[39] H. Braunschweig, T. Wagner, *Angew. Chem.* **1995**, *107*, 904–905; *Angew. Chem. Int. Ed. Engl.* **1995**, *34*, 825–826.

[40] K. M. Anderson, M. J. Gerald Lesley, N. C. Norman, A. G. Orpen, J. Starbuck, *New J. Chem.* **1999**, *23*, 1053–1055.

[41] a) M. P. Coles, *Dalton Trans.* **2006**, 985–1001; and references cited therein; b) M. P. Coles, *Chem. Commun*. **2009**, 3659–3676; and references cited therein.

[42] S. J. Angyal, W. K. Warburton, *J. Chem. Soc.* **1951**, 2492–2494.

[43] Herres-Pawlis, *Nachrichten aus der Chemie* **2009**, *57*, 20–23.

[44] P. J. Bailey, S. Pace, *Coord. Chem. Rev.* **2001**, *214*, 91–141.

[45] See, for example: F. T. Edelmann, *Adv. Organomet. Chem.* **2008**, *57*, 183–352; and references cited therein.

[46] S. L. Aeilts, M. P. Coles, D. C. Swenson, R. F. Jordan, *Organometallics* **1998**, *17*, 3265–3270.

[47] a) M. P. Coles, P. B. Hitchcock, *Organometallics* **2003**, *22*, 5201–5211; b) M. P. Coles, P.B. Hitchcock, *J. Chem. Soc. Dalton Trans.* **2001**, 1169–1171.

[48] *Multiple Bonds between Metal Atoms*, ed. F. A. Cotton, C. A. Murillo, R. A. Walton, Springer Science and Business Media Inc., New York, **2005**.

[49] S. R. Foley, G. P. A. Yap, D. S. Richeson, *Polyhedron* **2002**, *21*, 619–627.

[50] S. L. Aeilts, M. P. Coles, D. C. Swenson, R. F. Jordan, *Organometallics* **1998**, *17*, 3265–3270.

[51] C. Brinkmann, F. García. J. V. Morey, M. McPartlin, S. Singh, A. E. H. Wheatley, D. S. Wright, *Dalton Trans.* **2007**, 1570–1572.

[52] M. P. Coles, P. B. Hitchcock, *Eur. J. Inorg. Chem.* **2004**, 2662–2672.

[53] G. Robinson, C. Y. Tang, R. Köppe, A. R. Cowley, H.-J. Himmel, *Chem. Eur. J.* **2007**, *13*, 2648–2654.

[54] M. D. Irwin, H. E. Abdou, A. A. Mohamed, J. P. Fackler, Jr, *Chem. Commun*. **2003**, 2882–2883.

[55] A. A. Mohamed, A. P. Mayer, H. E. Abdou, M. D. Irwin, L. M. Pérez, J. P. Fackler, Jr, *Inorg. Chem.* **2007**, *46*, 11165–11172.

[56] H. E. Abdou, A. A. Mohamed, J. P. Fackler, Jr, *Inorg. Chem.* **2005**, *44*, 166–168.

[57] F. A. Cotton, X. Feng, D. J. Timmons, *Inorg. Chem.* **1998**, *37*, 4066–4069.

[58] F. A. Cotton, J. Gu, C. A. Murillo, D. J. Timmons, *J. Am. Chem. Soc.* **1998**, *120*, 13280–13281.

[59] a) R. Clérac, F. A. Cotton, L. M. Daniels, J. P. Donahue, C. A. Murillo, D. J. Timmons, *Inorg. Chem.* **2000**, *39*, 2581–2584; b) F. A. Cotton, C. A. Murillo, X. Wang, C. C. Wilkinson, *Inorg. Chim. Acta* **2003**, *351*, 191–200.

[60] a) F. A. Cotton, N. E. Gruhn, J. Gu, P. Huang, D. L. Lichtenberger, C. A. Murillo, L. O. Van Dorn, C. C. Wilkinson, *Science* **2002**, *298*, 1971–1974; b) F. A. Cotton, J. P. Donahue, N. E.Gruhn, D. L. Lichtenberger, C. A. Murillo, D. J. Timmons, L. O. Van Dorn, D. Villagrán, X. Wang, *Inorg. Chem.* **2006**, *45*, 201–213.

[61] a) F. A. Cotton, P. Huang, C. A. Murillo, D. J. Timmons, *Inorg. Chem. Commun.* **2002**, *5*, 501–504; b) F. A. Cotton, P. Huang, C. A. Murillo, X. Wang, *Inorg. Chem. Commun.* **2003**, *6*, 121–126; c) F. A. Cotton, C. A. Murillo, X. Wang, C. C. Wilkinson, *Dalton Trans.* **2007**, 3943–3951.

[62] F. A. Cotton, L. M. Daniels, C. A. Murillo, D. J. Timmons, C. C. Wilkinson, *J. Am. Chem. Soc.* **2002**, *124*, 9249–9256.

[63] a) P. J. Bailey, S. F. Bone, L. A. Mitchell, S. Parsons, K. J. Taylor, L. J. Yellowlees, *Inorg. Chem*. **1997**, *36*, 867-871; b) P. J. Bailey, S. F. Bone, L. A. Mitchell, S. Parsons, K. J. Taylor, L. J. Yellowlees, *Inorg. Chem.* **1997**, *36*, 5420–5420.

[64] F. A. Cotton, S. A. Ibragimov, C. A. Murillo, P. V. Poplaukhin, Q. Zhao, *J. Mol. Struct.* **2008**, *890*, 3–8.

2. Results and discussion

2.1 Synthesis and characterization of new guanidine-borane adducts: $H_3B{\cdot}hppH$ and $H_3B{\cdot}N(H)C(NMe_2)_2$

Section 2.1.1 describes the preparation of two guanidine-borane adducts which later will be used as precursors for dehydrogenation reactions (see chapter 2.2). In section 2.1.2 the compounds are characterized by spectroscopic data (IR, NMR and MS), while section 2.1.3 is devoted to the evaluation of the dimeric assembly through H···H contacts of the molecules in the crystalline phase accompanied by quantum chemical calculations. Section 2.1.4 includes the theoretical comparison of the bonding properties in amine-borane adducts ($H_3B{\cdot}NH_3$, $H_3B{\cdot}NMe_3$ and $H_3B{\cdot}$quinuclidine) (see Scheme 2.1.1) and guanidine-borane adducts ($H_3B{\cdot}N(H)C(NH_2)_2$, $H_3B{\cdot}N(H)C(NMe_2)_2$ and $H_3B{\cdot}hppH$) (see Scheme 2.1.1), as well as the available experimental data for these species.

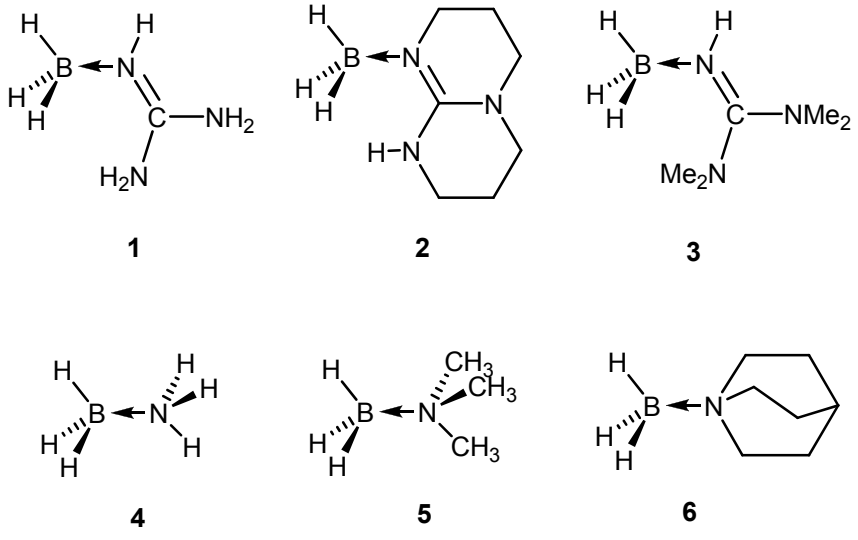

Scheme 2.1.1

All theoretical calculations were carried out with the Gaussian 98 program package[1a] by applying the hybrid DFT functional B3LYP[2] in combination with the 6-311+G* basis set, with exception of calculations to determine whether the inter- or

intramolecular H···H contacts are responsible for the conformation of the BH_3 group in compound **2** (see section 2.1.3).

2.1.1 Synthesis

For the synthesis of base adducts to the EH_3 hydrides (E = B or Ga), two routes have frequently been applied (see Scheme 2.1.2).

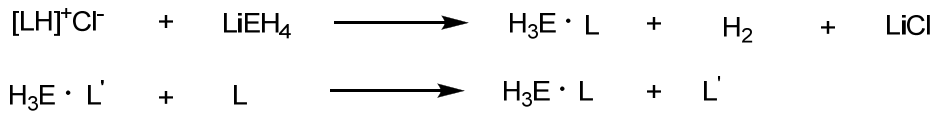

Scheme 2.1.2

In the first reaction the HCl adduct of the guanidine base (L) react with $LiEH_4$ to give guanidine – gallane or – borane adduct. The second represents a base exchange reaction, in which a base L' such as NMe_3 is replaced by a stronger guanidine base L. The last route was used as a method for preparation of $H_3B{\cdot}hppH$ and $H_3B{\cdot}N(H)C(NMe_2)_2$ compounds. As a guanidine base the hppH = 1,3,4,6,7,8-hexahydro-2*H*-pyrimido[1,2-*a*]pirimidine and TMG = 1,1,3,3–tetramethylguanidine were used, respectively (Scheme 2.1.3).

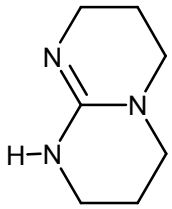

hppH

1,3,4,6,7,8-hexahydro-2*H*-pyrimido [1,2-*a*]pyrimidine

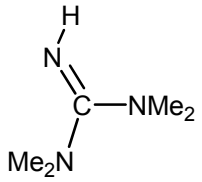

TMG

1,1,3,3–tetramethylguanidine

Scheme 2.1.3

The reaction of $H_3B{\cdot}NMe_3$ with hppH at 60°C allows the preparation of $H_3B{\cdot}$hppH **2** in a good yield (79%) (see Scheme 2.1.4). Crystals suitable for X-ray measurements were grown from hexane/toluene (2:1) mixture at -20°C. This compound is the first example of a structurally characterized 1:1 adduct of hppH to a group 13 element hydride.

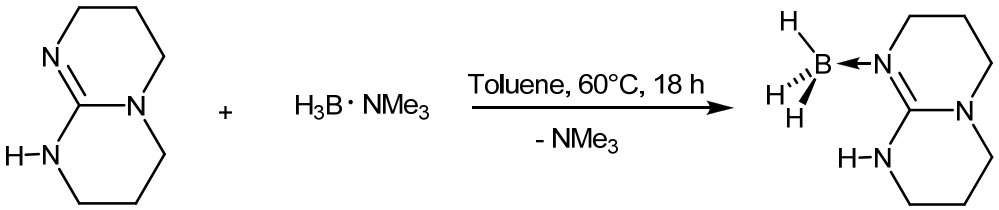

2

Scheme 2.1.4: Synthesis of compound **2**.

The analogues reaction between $H_3Ga{\cdot}NMe_3$ and hppH resulted in the direct formation of the binuclear compound $[H_2Ga(hpp)]_2$,[3] even at 0°C, and it proved impossible to isolate this adduct.

For preparing the $H_3B{\cdot}N(H)C(NMe_2)_2$ adduct we followed the same procedure as for compound **2** but instead of hppH we used $N(H)C(NMe_2)_2$ as a guanidine base (see Scheme 2.1.5). After mixing $H_3B{\cdot}NMe_3$ with $N(H)C(NMe_2)_2$ in toluene solution, the reaction mixture was stirred for 18 h at 80°C. The resulting solution was concentrated and stored at -20 °C to afford colourless crystals of **3**.

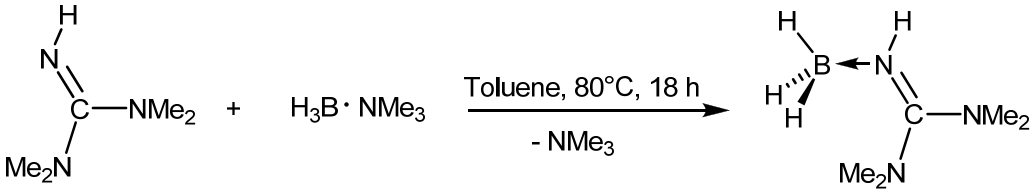

3

Scheme 2.1.5: Synthesis of compound **3**.

2.1.2 Spectroscopic properties

Our experiments have led to the preparation of the 1:1 adducts of BH_3, with the guanidines hppH (**2**) and $N(H)C(NMe_2)_2$ (**3**). The identity of each has been established by using the spectroscopic methods.

Nuclear Magnetic Resonance Spectroscopy

The compounds **2** and **3** were characterized by NMR spectra which are represented in Figure 2.1.1 and 2.1.2, respectively.

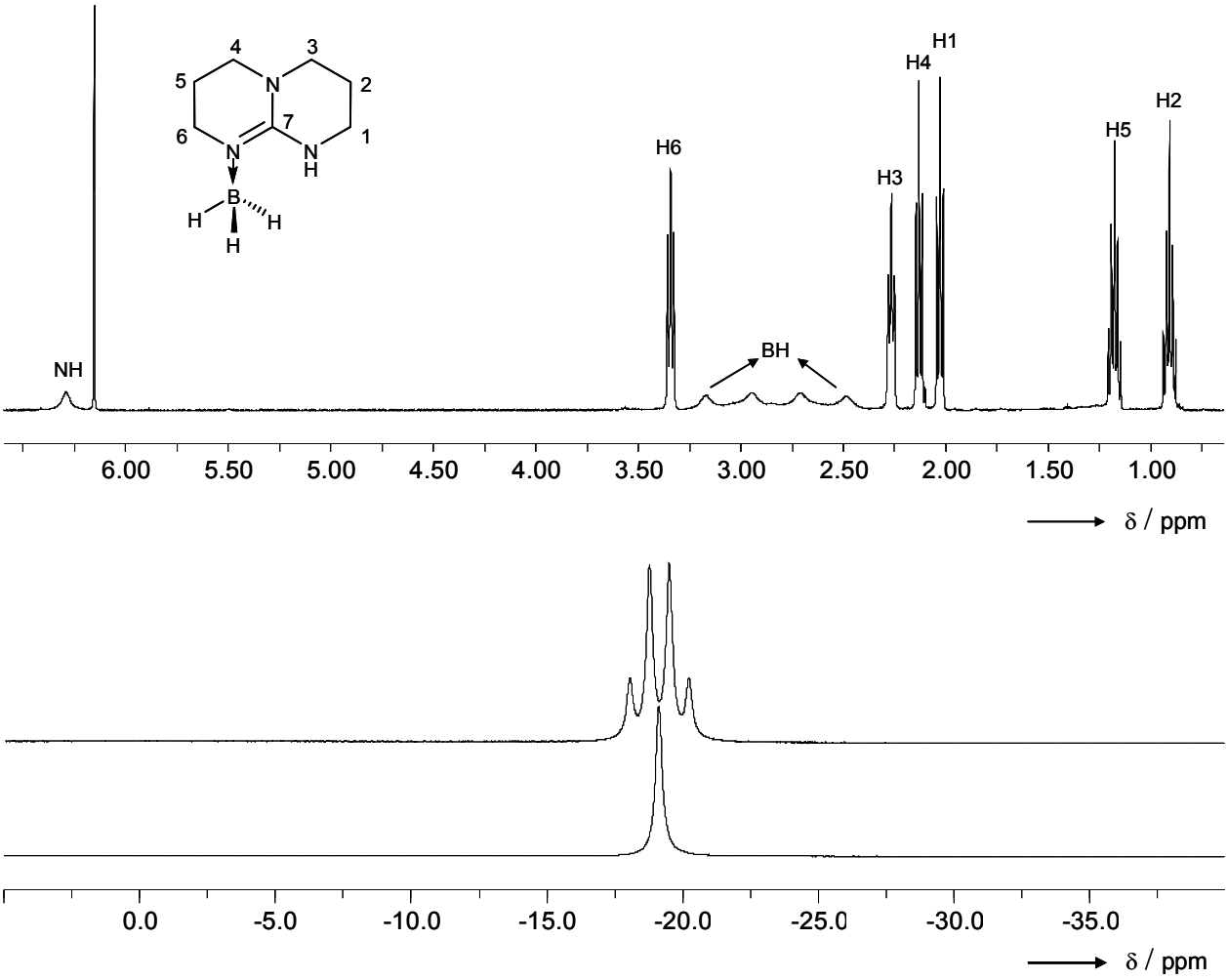

Figure 2.1.1: $^{1}H\{^{11}B\}$ NMR spectrum (400 MHz, C_6D_6); ^{11}B and $^{11}B\{^{1}H\}$ NMR spectra (128.3 MHz, C_6D_6) for **2**.

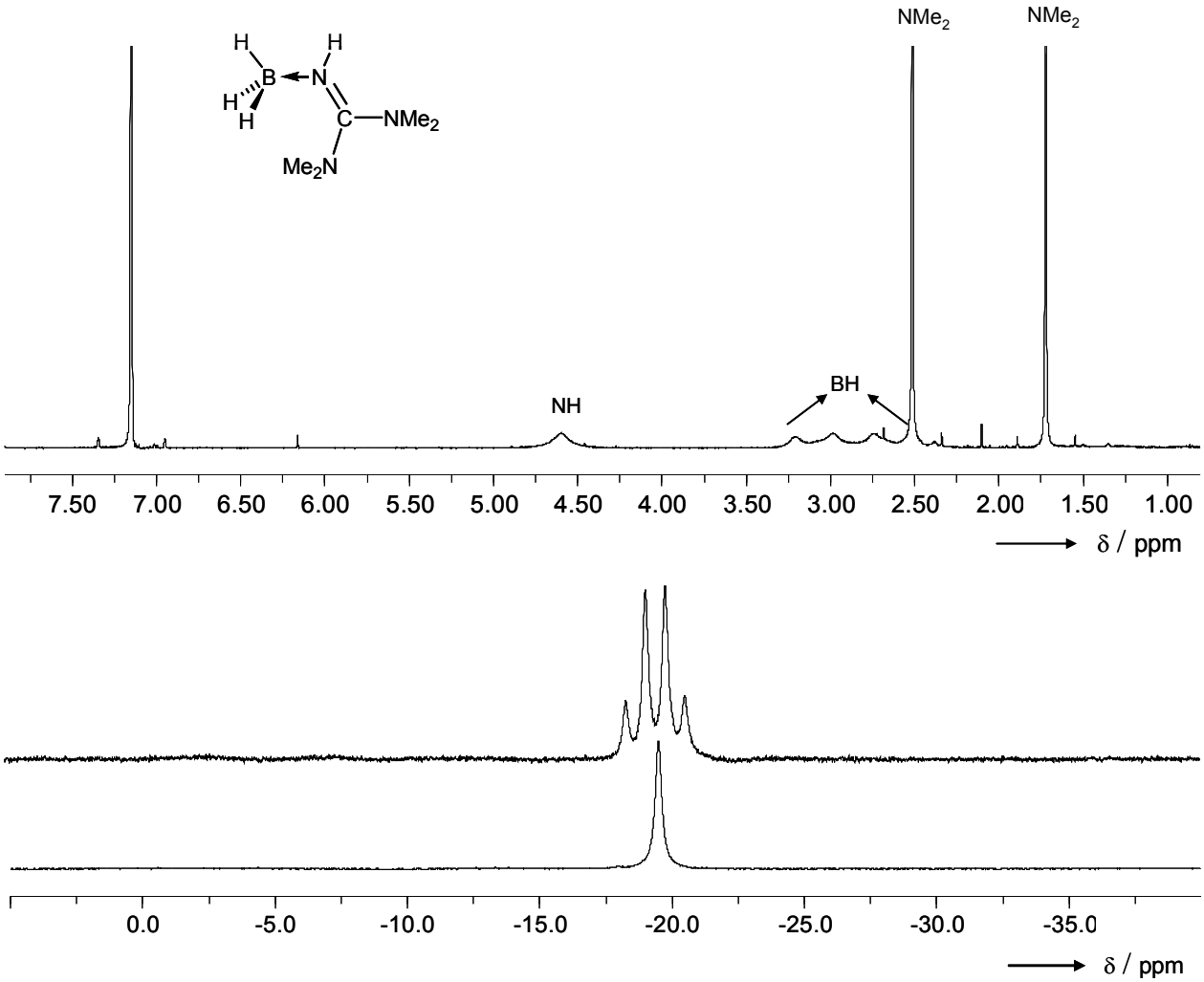

Figure 2.1.2: $^{1}H\{^{11}B\}$ NMR spectrum (400 MHz, C_6D_6); ^{11}B and $^{11}B\{^{1}H\}$ NMR spectra (128.3 MHz, C_6D_6) for **3**.

The resonance at $\delta(^{1}H)$ = 6.29 ppm in the ^{1}H NMR spectrum of **2** (Figure 2.1.1) belongs to the NH proton. It is shifted considerably with respect to the value in free guanidine (hppH), where $\delta(^{1}H)_{NH}$ = 6.77 ppm. In the case of **3** the hydrogen attached to nitrogen resonate at $\delta(^{1}H)$ = 4.61 ppm (Figure 2.1.2) and also is shifted with respect to the value in free base, where $\delta(^{1}H)_{NH}$ = 5.27 ppm. For comparison, in the case of $H_3Ga{\cdot}N(H)C(NMe_2)_2$,[4] $Me_3Al{\cdot}N(H)C(NMe_2)_2$[5] and $Et_3Al{\cdot}N(H)C(NMe_2)_2$[5] values of 4.10, 4.40 and 5.20, respectively, where reported. A broad quartet centered at $\delta(^{1}H)$ = 2.83 ppm (^{1}J(H-B) = 93 Hz) (Figure 2.1.1) can be assigned to the BH_3 protons in compound **2**. For comparison, in $H_3B{\cdot}$Htbo, the BH_3 protons appear at $\delta(^{1}H)$ = 1.63 ppm (^{1}J(H-B) = 88.9 Hz)[6]. In case of compound **3,** the hydrogen atoms attached to boron give rise to a broad quartet centred at $\delta(^{1}H)$ = 2.86 ppm (^{1}J(H-B) =

95 Hz). For comparison, in $H_3B{\cdot}NMe_3$, the BH_3 protons appear at $\delta(^1H)$ = 2.40 ppm (^1J(H-B) = 98 Hz). The protons of the four CH_3 groups in **3** show at $\delta(^1H)$ = 2.51 and 1.72 ppm (see Figure 2.1.2), and these positions are close to the values of 2.50 and 1.91 ppm reported for $H_3Ga{\cdot}N(H)C(NMe_2)_2$[4], but they are shifted to larger values with respect to the free base, for which one obtains $\delta(^1H)$ = 2.64 ppm for CH_3. The compounds **2** and **3** were characterized also by ^{11}B NMR spectrum (see Figure 2.1.1 and 2.1.2). In case of **2** the ^{11}B NMR quartet signal appears at $\delta(^{11}B)$ = -19.15 ppm (^1J(B-H) = 93 Hz) and in **3** at $\delta(^{11}B)$ = -19.50 ppm (^1J(B-H) = 95 Hz). For comparison, in $H_3B{\cdot}$Htbo the ^{11}B NMR spectrum gives evidence for a quartet at $\delta(^{11}B)$ = - 22.92 ppm (^1J(B-H) = 91.3 Hz)[6] and in $H_3B{\cdot}NMe_3$, the signal appears at $\delta(^{11}B)$ = - 7.27 ppm (^1J(B-H) = 98 Hz).

Mass Spectrum

In the HRMS (EI^+) spectrum of **2** appear a strong peak at *m/z* = 152.14 $[C_7H_{15}BN_3]^+$, which can be assigned to ion formed with loss of one hydrogen atom. A small peak at *m/z* = 138.10 $[C_7H_{12}N_3]^+$ belongs to the free guanidine ligand. In case of compound **3**, the spectrum shows strong peaks at *m/z* = 128.2 $[C_5H_{15}BN_3]^+$ and 126.2 $[C_5H_{13}BN_3]^+$, which can be assigned to ions formed with loss of one and three H atoms from the parent molecule, respectively. A small peak at *m/z* = 115.2 $[C_5H_{13}N_3]^+$ belongs to the free guanidine base. Elimination of one methyl group from $[C_5H_{15}BN_3]^+$ is responsible for the peak at *m/z* = 110.2. Loss of two CH_4 groups from the free guanidine base and of the NMe_2 group leads to signals at *m/z* = 85.2 and 71.2, respectively.

IR Spectrum

In Figure 2.1.3 is represented the IR spectrum of solid **2** in CsI. In comparison to **3** and $H_3B{\cdot}$Htbo[6], the wavenumber of the stretching mode ν(N-H) in **2** (3352 cm^{-1}) is larger and lower, respectively, while the modes ν(B-H) (2363, 2301 and 2253 cm^{-1}) are lower and larger in **2**, respectively. These differences reflects the lower basicity of $N(H)C(NMe_2)_2$ and the higher basicity of Htbo.

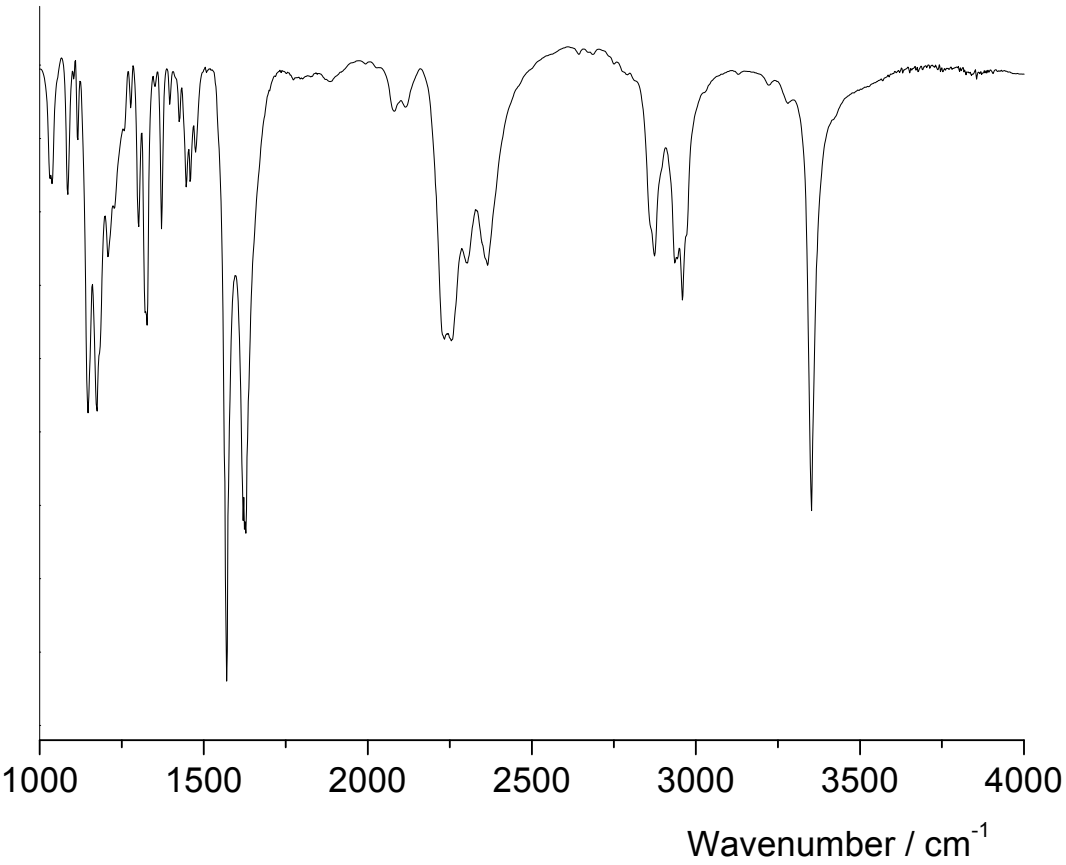

Figure 2.1.3: Measured IR spectrum of solid **2** in CsI.

Compound **3** was also characterized by its vibrational spectra obtained from experiment in addition with the spectra obtained from calculations. Figure 2.1.4 compares (i) the experimentally obtained spectrum of solid **3** in CsI with those calculated for (ii) individual molecules of **3** and (iii) dimeric assemblies of **3**. Table 1 includes the wavenumbers of the strongest bands observed in the IR spectrum of solid **3** in CsI and the calculated wavenumbers of some vibrational modes for which a straightforward description of molecular motion is possible. A sharp band appears at 3337 cm^{-1} and can be assigned to the N-H stretch (see Figure 2.1.4, (i)). For comparison, in the Ga homologue the stretching mode ν(N-H) was observed at 3317 cm^{-1}.[4] As discussed below (see section 2.1.3), the molecules are assembled in dimeric units kept together through B-H···H-N contacts in the solid phase and maybe also in solution. These contacts weaken the N-H bond in addition to the effect of electron donation from the nitrogen base and therefore decrease the wavenumber of the stretching mode ν(N-H). As anticipated, we could observe from calculations that the wavenumber of the ν(N-H) mode calculated for the dimeric assembly is much

lower than that calculated for individual molecules. A broader band with maxima at 2365 and 2291 cm^{-1} can be assigned to B-H stretches of **3**. The wavenumbers of the B-H stretching modes provide useful information about the amount of electron density donated from the base onto the BH_3 fragment. The increased electron density on the BH_3 group with respect to uncoordinated BH_3 leads to a decrease in the ν(B-H) frequencies.

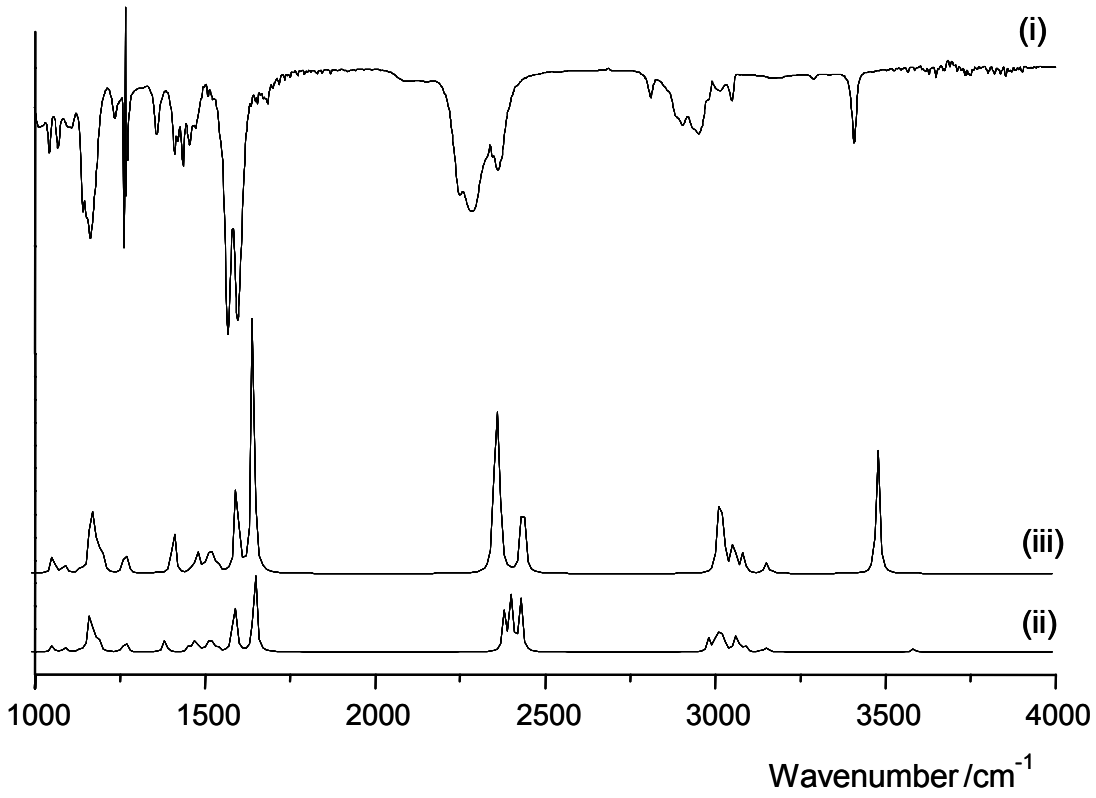

Figure 2.1.4: (i) Measured IR spectrum of solid **3** in CsI; (ii) calculated IR spectrum for individual molecules of **3**; (iii) calculated IR spectrum for dimeric assemblies of molecules of **3** interacting through N-H···H-B contacts. For the visualization of the calculated spectra, Lorenzian-type curves of 10 cm^{-1} half-width were used.

The stretches ν(B-H) of free BH_3 that belong to the irreducible representation e' were reported to occur at 2601.57 cm^{-1} in the gas phase[7] and 2587.3 cm^{-1} in an Ar matrix.[8] In the case of $H_3B{\cdot}NMe_3$, the spectrum of the compound in solution showed bands at 2372 and 2270 cm^{-1} due to antisymmetric and symmetric ν(B-H) stretches,[9] respectively, and the corresponding bands in the spectrum of the molecule in solid Ar appeared at 2393/2275 [$\nu(^{10}$B-H)], 2367/2270 cm^{-1} [$\nu(^{11}$B-H)].[10]

Table 2.1.1: Comparison between experimentally observed and calculated IR properties of compound **3**.

Experimental [cm^{-1}]	Calculated[a] [cm^{-1}] $H_3B{\cdot}N(H)C(NMe_2)_2$	Calculated[a] [cm^{-1}] $[H_3B{\cdot}N(H)C(NMe_2)_2]_2$	Approx. description of molecular motion
3337	3582.9	3478.3/3474.0	ν(N-H)
2949	3175.8 – 2981.7	3171.4 – 3006.7	ν(C-H)
2365, 2291, 2259, 2239	2428.8 – 2381.6	2436.9 – 2341.8	ν(B-H)
1593	1647.8	1650.6/1641.3	ν(C=N)
	1586.2	1598.0/1593.3	δ_{ip}(N-H)
1453, 1433	1540.8 – 1453.3	1540.8 – 1456.5	δ (CH_3)
1159, 1072, 1042	1190.0 – 1176.1	1200.8 – 1193.0	δ(BH_3)
806	718.4	823.4 – 808.2	δ_{oop}(N-H)

[a] Unscaled values.

The calculated wavenumber and the relative intensity for the dimeric assembly are in better agreement with the experimental spectrum. Also, the shapes of the bands and their wavenumbers in the region of the ν(B-H) modes fit better for the dimeric assembly than for individual molecules. This means that the IR spectra are fully consistent with a dimeric assembly of **3** in the solid state.

2.1.3 Structure determinations

The structures of one molecule of $H_3B{\cdot}$hppH **2** and $H_3B{\cdot}N(H)C(NMe_2)_2$ **3**, respectively as derived from X-ray diffraction measurements are illustrated in Figure 2.1.5, together with some selected bond distances (in pm) and angles (in degrees) for every compound.

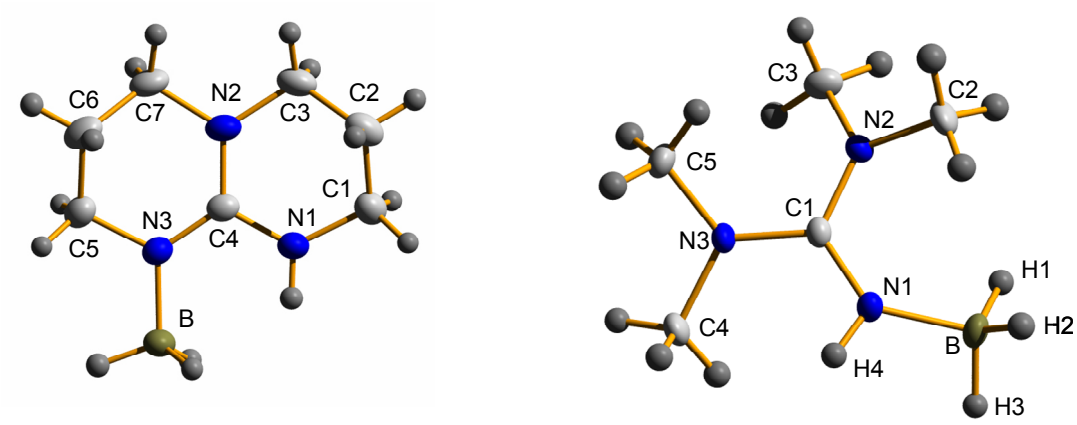

2 **3**

Figure 2.1.5: Molecular structures of $H_3B{\cdot}$hppH **2** and $H_3B{\cdot}N(H)C(NMe_2)_2$ **3** in the crystalline phase as determined by X-ray diffraction. Ellipsoids are drawn at the 50% probability level. Only one of the two independent molecules is shown. Selected bond distances (in pm) and angles (in degrees) for **2**: B-N(3) 157.52(17), B-H(9) 112.3(16), B-H(10) 112.0(15), B-H(11) 110.3(16), N(1)-C(4) 134.79(16), N(1)-C(1) 144.80(17), N(1)-H(8) 89.0(16), N(2)-C(4) 135.48(15), N(2)-C(3) 1.4579(17), N(2)-C(7) 145.93(16), N(3)-C(4) 132.12(16), N(3)-C(5) 146.13(15), N(3)-B-H(9) 109.7(7), N(3)-B-H(10) 109.7(8), N(3)-B-H(11) 108.9(8), B-N(3)-C(4) 122.33(10), B-N(3)-C(5) 117.82(10), N(3)-C(4)-N(1) 117.99(10), N(3)-C(4)-N(2) 123.64(11), N(1)-C(4)-N(2) 118.35(11) and **3**: B-N(1) 157.28(16), B-H(1) 110.2(15), B-H(2) 112.4(17), B-H(3) 112.3(14), N(1)-C(1) 131.54(13), N(1)-H(4) 92.6(16), C(1)-N(2) 134.57(13), C(1)-N(3) 135.82(13), N(2)-C(2) 145.34(14), N(2)-C(3) 144.90(15), N(3)-C(4) 145.33(14), N(3)-C(5) 146.01(14), N(1)-B-H(1) 109.7(7), N(1)-B-H(2) 110.6(8), N(1)-B-H(3) 105.3(7), B-N(1)-C(1) 129.62(9), B-N(1)-H(4) 117.0(9), C(1)-N(1)-H(4) 112.5(9), N(1)-C(1)-N(2) 121.30(9), N(1)-C(1)-N(3) 121.21(9), N(2)-C(1)-N(3) 117.48(9), C(1)-N(2)-C(2) 121.91(10), C(1)-N(2)-C(3) 122.74(9), C(2)-N(2)-C(3) 115.35(10), C(1)-N(3)-C(4) 121.02(9), C(1)-N(3)-C(5) 121.74(9), C(4)-N(3)-C(5) 114.59(9).

In the crystal structure of **2** illustrated in Figure 2.1.6-A are featured two intramolecular as well as two intermolecular H···H contacts that are established between positively and negatively polarized H atoms. These contacts are responsible for the different packing of the molecules in the solid phase. For example, in case of **2** and one isomer of $H_3B{\cdot}$Htbn [with the boron atom attached to the N atom of the six-

membered ring of Htbn] dimeric units are established. Unlike, $H_3B{\cdot}$Htbo and another isomer of $H_3B{\cdot}$Htbn [with the boron atom attached to the five-membered ring of Htbn] are arranged in chains with preference for intermolecular NH···H-B contacts over intramolecular ones.[6]

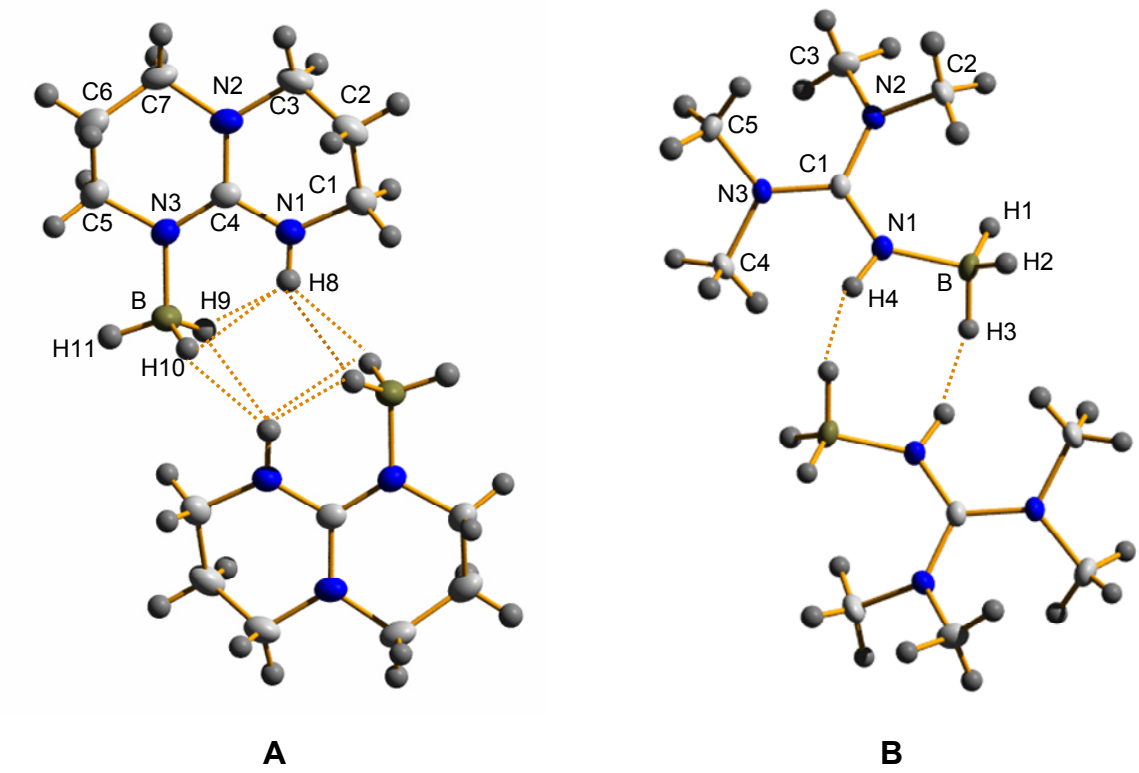

A **B**

Figure 2.1.6: Dimeric assembly of $H_3B{\cdot}$hppH (**A**) and $H_3B{\cdot}N(H)C(NMe_2)_2$ (**B**) through N-H···H-B interactions in the crystalline phase.

These contacts are important, since they lower the barrier for H_2 elimination. The intramolecular H···H contacts between two of the H atoms attached to the B atom and the H atom attached to the N atom of the same molecule are 223 and 224 pm (217 and 218 pm when normalized E-H distances are used[11]), respectively, and the corresponding intermolecular contacts measure 228 and 236 pm (220 and 228 pm). The shortest B···B separations are much shorter in the dimeric arrangements (427.8(2) pm in **2** and 437.7 pm in isomer of $H_3B{\cdot}$Htbn [with the boron atom attached to the N atom of the six-membered ring of Htbn]) than in the chain-type arrangements (481.8(3) pm in $H_3B{\cdot}$Htbo and 524.8(4) pm in isomer of $H_3B{\cdot}$Htbn [with the boron atom attached to the five-membered ring of Htbn]).[6]

The B-N bond length is 157.5 pm, which is slightly larger than the B-N bond distances in $H_3B{\cdot}Htbo$ (155.1(2)/155.2(2))[6] and shorter than the B-N bonds of borane-amine adducts. For comparison, the B-N bond distances in the BH_3 adducts of $PhCH_2N(CH_3)_2$[12] and $HC(CH_2CH_2)_3N$[13] have been determined to be 162.0(2) and 160.8(5) pm, respectively. The distance is also shorter than that reported for imine adducts such as the *N*-benzyl (Bn) imine adduct $Ph_2C{=}N(Bn){\cdot}B(C_6F_5)_3$ featuring a B-N bond length of 164.2(8) pm[14]. The B-N bond length measure 110(2) (no H···H contacts), 112(1) and 112(2) pm, and the N-H bond is 89(2) pm long.

Calculations were carried out to determine whether the inter- or intramolecular H···H contacts are responsible for the conformation of the BH_3 group in compound **2**. Calculations for an isolated molecule returned a conformation very close to that observed, and thus the intramolecular H···H contacts determine the geometry. This is also in line with the smaller observed values for the intramolecular H···H distances. In Figure 2.1.7 the relative energy is plotted as a function of the dihedral angle between the C-N-B and the N-B-H planes as calculated by using MP2/SVP.[15] It can be seen that the barrier for rotation around the B-N axis is no more than 4.5 kJ mol^{-1}.

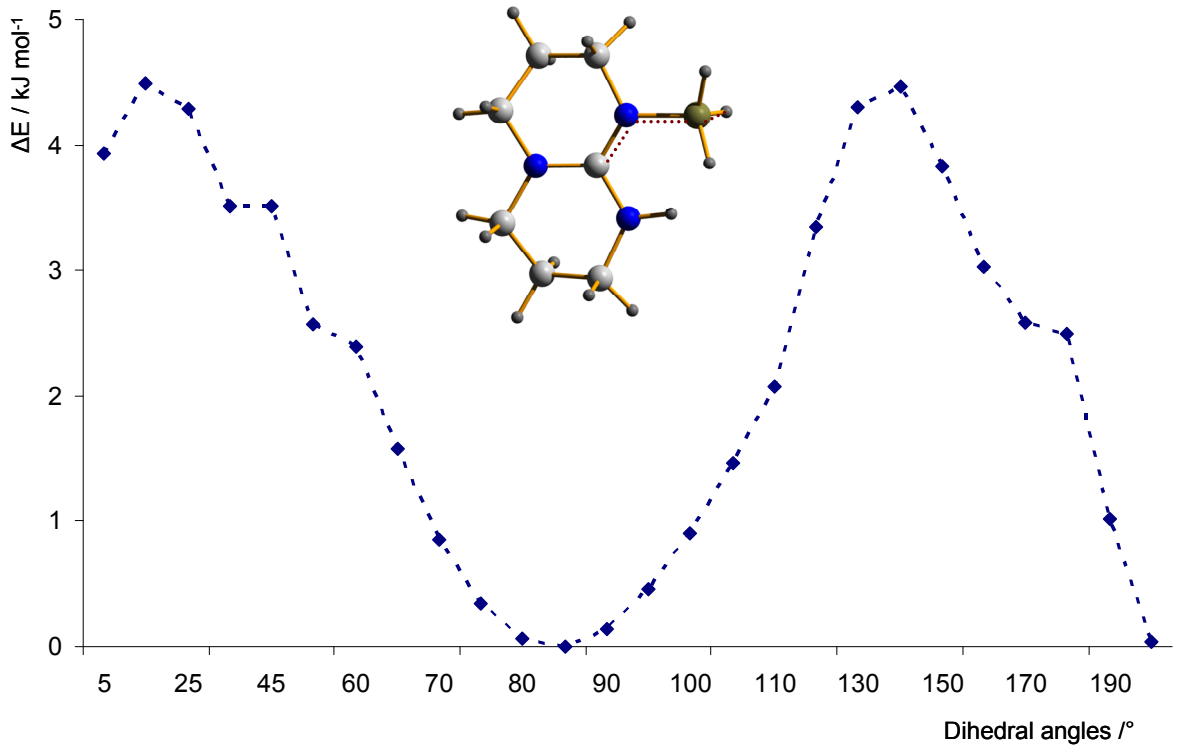

Figure 2.1.7: Relative energy as a function of the dihedral angle C-N-B-H as calculated with MP2/SVP.

As already mentioned, the structure of **3** is represented in Figure 2.1.5. Like the Ga homologue,[4] compound **3** feature a guanidine unit with a planar CN_3 core (the N-C-N angles sum to 360°). The B-N bond length measures 157.3(2) pm, and it is thus almost identical to that measured in crystalline $H_3B{\cdot}hppH$ (see Figure 2.1.5) and significantly shorter than that found in crystalline $H_3B{\cdot}NMe_3$ [161.6(3) pm].[16] With 131.5 pm, the N=C bond is significantly shorter than the N-C bonds (134.6 and 135.8 pm) in the molecule. As in case of **2**, the molecules of **3** are assembled in dimeric units in the crystalline phase, which are connected in this case only through intermolecular B-H···H-N interactions (see Figure 2.1.6-B). These H···H separations amount to 202 pm and are thus well within the range of 200-240 pm normally prescribed for unconventional hydrogen bonding of this sort.[17] By using normalized B/N-H distances, we obtained an even shorter B-H···H-N distance of 195 pm and B-H···H and H···H-N angles of 199.1° and 153.6°, respectively. For comparison, in $[H_2GaNH_2]_3$[18] and $[H_3AlN(H)Me_2]_2$[19] intermolecular H···H contacts of 197(2) and 192.5(1.9) pm, respectively, were measured.

Table 2.1.2 and 2.1.3 include some parameters for **3** and its gallium homologue determined by X-ray measurements which are compared with those obtained from DFT calculations. As expected, the calculated B-N distance is larger than the crystallographically derived one, although the difference is smaller than in the case of the Ga homologue (see Table 2.1.3). Thus, the difference between the calculated and experimental (XRD) E-N distance (E = B or Ga) amounts to 2.7 pm for **3** but to 7.2 pm for $H_3Ga{\cdot}N(H)C(NMe_2)_2$. To test the accuracy for our calculations, we also compared the B-N distances calculated with B3LYP/6-311+G* with those measured for several other related compounds (see Table 2.1.4). As anticipated, the agreement between the calculated distances and those measured for the gas-phase molecules is very pleasing, whereas the values measured by X-ray measurements come out too short. The largest discrepancy occurs for $H_3B{\cdot}NH_3$.

Table 2.1.2: Bond lengths (in pm) and bond angles (in °) as measured and calculated (B3LYP/6-311+G*) for **3**.

	Experimental	Calculated $H_3B{\cdot}N(H)C(NMe_2)_2$	Calculated $[H_3B{\cdot}N(H)C(NMe_2)_2]_2$
B-H1	110.2	121.4	121.2
B-H2	112.4	121.7	122.1
B-H3	112.3	121.9	122.5
B-N1	157.3	160.0	159.0
N1-H	92.6	101.1	101.7
N1=C	131.5	130.9	130.9
N2-C	134.6	136.4	136.8
N3-C	135.8	138.3	137.6
N1-C-N2	121.3	121.9	121.9
N1-C-N3	121.2(1)	121.4	121.5
N2-C-N3	117.5(1)	116.7	116.7
B-N1-C	129.6	130.7	130.0
H···H	202		189.1

Table 2.1.3: Bond lengths (in pm) and bond angles (in °) as measured and calculated (B3LYP/6-311+G*) for $H_3Ga{\cdot}N(H)C(NMe_2)_2$.

	Experimental	Calculated
Ga-H	149(4) / 157(4) / 161(4)	158.6 / 158.9 / 159.2
Ga-N1	198.8(2)	210.6
N1-H	78(3)	101.3
N1=C	131.6(3)	130.9
N2-C	134.7(3)	136.7
N3-C	136.0(3)	138.1
N1-C-N2	120.2(2)	120.9
N1-C-N3	122.2(2)	122.7
N2-C-N3	117.6(2)	116.4
Ga-N1-C	130.6(2)	130.7

Calculations were then carried out for a dimeric assembly of two molecules of **3** in which the molecules are allowed to interact through hydrogen-hydrogen contacts (see Scheme 2.1.6). According to our B3LYP/6-311+G* calculations, the energy gain for formation of this dimeric assembly amounts to 43 kJ mol^{-1}, which implies that each of the N-H···H-B interactions is ca. 21 kJ mol^{-1} strong. This compares with a calculated (head-to-tail) dimerisation energy of –60 kJ mol^{-1} (B3LYP/cc-pVDZ) or –63 kJ mol^{-1} (MP2/cc-pVDZ) for $H_3B{\cdot}NH_3$.[20] However, in the head-to-tail dimer $[H_3B{\cdot}NH_3]_2$, one N-H hydrogen atom interacts with two B-H hydrogen atoms, so that the bonding situation is slightly different. The zero-point corrected energy change for the reaction set out in Scheme 2.1.6 is –39 kJ mol^{-1}, and ΔG^0 = –5 kJ mol^{-1}. As expected, the N1-H and B-H3 bond lengths are slightly elongated in the dimeric assembly with respect to a single molecule of **3** as a result of the H···H interactions.

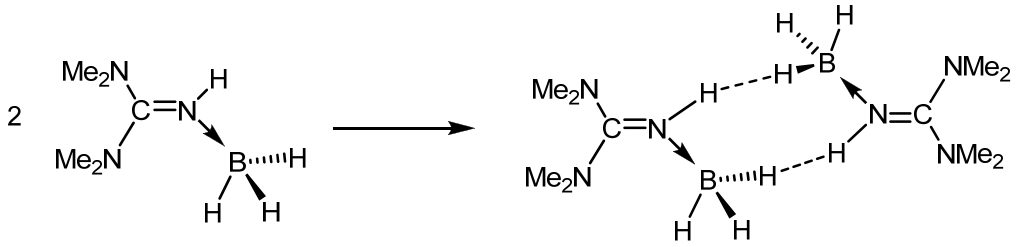

Scheme 2.1.6

2.1.4 Quantum chemical studies of the bonding properties in amine- and guanidine-borane adducts

Calculations were carried out to shed light on the analysis of the bonding properties in amine and guanidine–BH_3 adducts. Here we compare the B-N bond strength in amine–and guanidine–BH_3 adducts. For such a comparison and from the numerous characterized amine-borane adducts, we chose three representatives, $H_3B{\cdot}NH_3$ (**4**), $H_3B{\cdot}NMe_3$ (**5**) and $H_3B{\cdot}$quinuclidine (**6**), because of:

a) extensive structural data is available for these compounds not only in the crystalline phase, but also in the gas phase
b) the strength of the base increase steadily in the order NH_3 < NMe_3 < quinuclidine (quinuclidine is a already a strong amine base[21]).

These amine-borane adducts will be compared with the three guanidine adducts $H_3B{\cdot}N(H)C(NH_2)_2$ (**1**), $H_3B{\cdot}N(H)C(NMe_2)_2$ (**3**) and $H_3B{\cdot}$hppH (**2**). In the case of parent compound **1**, the comparison must exclusively rely on quantum chemical calculations. All attempts to prepare this species failed and only an unknown noncrystalline white precipitate was recovered. For $H_3B{\cdot}N(H)C(NMe_2)_2$ (**3**) and $H_3B{\cdot}$hppH (**2**), X-ray diffraction measurements are available (see Figure 2.1.5). Unfortunately, gas-phase measurements are likely to be hampered by the tendency of these compounds to decompose (in case of **3** (see Section 2.2.2.2)) or to dimerize at elevated temperature (in case of **2**) to give $[H_2B(hpp)_2]_2$ (see Section 2.2.2.1) or $[HB(hpp)_2]_2$ (see Section 2.3.2) dimers. The first observation is that the experimentally determined B-N distances in the crystalline phase do not show any clear trend (see Table 2.1.4).

Table 2.1.4: B-N distances (in pm) as measured (solid and gas phases) and calculated (B3LYP/6-311+G*) for some guanidine ($HNC(NH_2)_2$, $HNC(NMe_2)_2$, hppH) and amine (NH_3, NMe_3, quinuclidine) adducts to BH_3.

	Experimental		Calculated
	Solid phase	Gas phase	
$H_3B{\cdot}N(H)C(NH_2)_2$	–	–	159.9
$H_3B{\cdot}$hppH	157.5(2)	–	160.2
$H_3B{\cdot}N(H)C(NMe_2)_2$	157.28(16)	–	160.7
$H_3B{\cdot}NH_3$	156.4(6)[22]	165.76(16)[23]	166.1
$H_3B{\cdot}NMe_3$	161.6[16]	163.7[24]	165.7
		165.6(2)[25]	
$H_3B{\cdot}$quinuclidine	160.8(5)[13]	162.3(9)[13]	164.2

The distances increase in the order (in pm) **4** (156.5)[22] < **3** (157.3) < **2** (157.5) < **6** (160.9)[13] < **5** (161.6).[16] If $H_3B{\cdot}NH_3$ is treated as an exception, it could be concluded that the bond lengths in guanidine adducts are slightly shorter than those in amine adducts. This trend is supported by the calculated values, which show an increase in

the order (in pm) **1** (159.9) < **2** (160.2) < **3** (160.7) < **6** (164.2) < **5** (165.7) < **4** (166.1). $H_3B{\cdot}NH_3$ now futures the largest distance, which is in line with what is expected on the basis of the basicity order.[21], [26] Because of the generally pleasing agreement between calculated and gas-phase values [165.76(16) pm for **4**,[23] 163.7(4)[24] or 165.6(2) pm[25] for **5** and 162.3(9) pm for **6**],[13] guanidine adducts (in the gas phase) indeed generally exhibit shorter distances than amine adducts.

Next, the B-N dissociation energies as calculated with B3LYP/6-311+G* were inspected (see Table 2.1.5). The values were corrected for basis set superposition errors (BSSE), which are in the range 3–12 kJ mol^{-1}. As expected from the basicities, the dissociation energies for the amine adducts follow the order (in kJ mol^{-1}) **4** (129) < **5** (139) < **6** (151). In the case of the guanidine adducts, the order (in kJ mol^{-1}) comes out to be **3** (138) < **1** (152) < **2** (166). In the case of **2**, the B-H···H-N contacts contribute to the bonding between the two fragments. It might be at first glance surprising that the dissociation energy of **3** is smaller than that of **6** and similar to that of **5**, although the B-N bond length in **3** is shorter in the crystalline phase and also according to the quantum chemical calculations. More importantly, the values do not reflect the basicity order. To obtain a better estimation of the *intrinsic* B-N bond energies, the B-N fragmentation energies have to be considered (see Table 2.1.5). The fragmentation energy differs from the dissociation energy in that relaxation of the fragments after bond cleavage is not included. Therefore, it is a better measure of the actual bond strength than the dissociation energy.[27] From Table 2.1.5 it can be seen that the relaxation energy, ΔE^{BSSE}_{realx}, is the difference between the fragmentation and dissociation energies, and it contributes considerably to the dissociation energy. The relaxation energies of guanidine adducts come out to be larger than those of amine adducts. For example, the relaxation energies of $H_3B{\cdot}$hppH (**2**) and $H_3B{\cdot}$quinuclidine (**6**), amount to 89 and 66 kJ mol^{-1}, respectively. These large values cannot result from relaxation of the base (guanidine or amine) fragments, as the rigid skeleton of the base only allows a small amount of distortion.

Table 2.1.5: Fragmentation and dissociation (both in kJ mol^{-1}) without (ΔE_{frag} and ΔE_{diss}) and with BSSE corrections (ΔE^{BSSE}_{frag} and ΔE^{BSSE}_{diss}) as well as relaxation energy $\Delta E^{BSSE}_{realx}(BH_3)$ and ΔE^{BSSE}_{realx}(base) (summing up to the total relaxation energy ΔE^{BSSE}_{realx}) as calculated for some guanidine ($HNC(NH_2)_2$, $HNC(NMe_2)_2$, hppH) and amine (NH_3, NMe_3, quinuclidine) adducts to BH_3.

Compound	ΔE_{frag}	ΔE_{diss}	ΔE^{BSSE}_{frag}	ΔE^{BSSE}_{diss}	ΔE^{BSSE}_{realx} (BH_3)	ΔE^{BSSE}_{realx} (base)
1	233.47	151.66	238.65	156.84	-73.78	-8.03
2	254.93	165.62	258.24	168.93	-81.36	-7.95
3	226.90	137.73	231.92	142.75	-72.83	-16.34
4	183.96	129.49	195.33	140.86	-54.45	-0.02
5	204.18	138.55	208.9	143.45	-59.11	-6.52
6	216.87	150.57	221.57	155.27	-61.73	-4.57

The largest contribution, therefore, must arise from relaxation of the BH_3 fragment. From Table 2.1.3 it can be seen that indeed for all adducts BH_3 relaxation into its planar D_{3h} symmetric energy minimum is the dominating contribution. The stronger the base, the more the H-B-H bond angles approach the tetrahedral angle of 109.4°. Hence, the average H-B-H bond angle are smaller in the guanidine adducts (111.5, 110.8 and 111.6° for **1**, **2** and **3**, respectively, compared with 113.6, 113.1 and 112.8° for **4**, **5** and **6**, respectively) and consequently the relaxation energy larger. The average H-B-H angle indeed appears to be a more reliable indicator of the B-N bond strength than the B-N bond length. However, the differences between the H-B-H angles are small.

In summary, the base exchange reaction between $H_3B{\cdot}NMe_3$ and the guanidine derivative hppH or $HNC(NMe_2)_2$, affords the new guandine-borane adducts $H_3B{\cdot}$hppH **2** and $H_3B{\cdot}HNC(NMe_2)_2$ **3**, respectively. Both compounds form dimeric units in the solid state, hold together via two intramolecular as well as two intermolecular B-H···H-N contacts in the case of **2** and two intermolecular B-H···H-N

contacts in the case of **3**, respectively. These contacts are responsible for the packing mode of the molecules in the solid state and lower the barrier for H_2 elimination. The strength of the B–N bond in guanidine–borane adducts is accessed and compared to that of amine–borane adducts on the basis of quantum chemical calculations carried out for the compounds $H_3B{\cdot}N(H)C(NH_2)_2$, $H_3B{\cdot}N(H)C(NMe_2)_2$, $H_3B{\cdot}$hppH, $H_3B{\cdot}NH_3$, $H_3B{\cdot}NMe_3$ and $H_3B{\cdot}$quinuclidine, as well as experimental data (X-ray diffraction of the crystalline adducts and gas-phase measurements). Because relaxation of the BH_3 and base fragments is associated with a large energy gain, an adequate comparison has to include not only the dissociation, but also the fragmentation energies. As anticipated from the basicity order, the fragmentation energies are higher for guanidine than for amine adducts of BH_3. The B–N bond lengths turned out to be an unreliable criterion to judge the B–N bond strength. In addition to the large differences between the B–N bond lengths as determined from X-ray diffraction of the molecules in the solid state and gas phase or quantum chemical calculations, there is no direct correlation between the trends in the bond lengths and the fragmentation energies. The H–B–H angles correlate better with the fragmentation energies, although the differences in the angles between adducts are small.

2.2 Experimental and computational studies on the thermal and catalytic dehydrogenation of $H_3B{\cdot}hppH$ and $H_3B{\cdot}N(H)C(NMe_2)_2$

This section will begin with an analysis of the mechanism for thermal (see Section 2.2.1.1) and Cp_2TiCl_2/*n*BuLi catalysed (see Section 2.2.1.2) dehydrogenation of model compound **1** (see chapter 2.1, Scheme 2.1.1) on the basis of quantum chemical calculations. Afterwards, in Section 2.2.2, we discuss the experimental results obtained for the thermal and catalytic dehydrogenation of the guanidine-borane adducts **2** and **3**.

All calculations were carried out with the Gaussian 03 program package.[1b] For the mechanistic calculations on **1** we used the B3LYP density functional[2]. We chose for all guanidine atoms a 6-31++G**, for Ti a LANL2DZ and for the atoms of the Cp rings a 6-31G* basis set. This level has proved its efficiency on a similar systems[28] and allowed us to obtain results in a reasonable time. All the thermodynamic properties calculations were carried on at standard conditions. The solvation effects on electronic energies were estimated on all structures optimised in gas phase by using the CPCM model.[29] The $\Delta_{solv}G^0$ values are based on the gas-phase values to which we added the contribution of the solvation effect on the electronic energies. The energy-minimum structures and the $\delta(^{11}B)$ chemical shifts of all other compounds discussed in section 2.2.2 were calculated at the DFT-GIAO//B3LYP/6-311+G* level (the structure and chemical shifts are represented in Supplementary Material). All calculated $\delta(^{11}B)$ chemical shifts were (like the experimental ones) referenced to $F_3B{\cdot}OEt_2$.

2.2.1 Quantum chemical studies

The catalytic dehydrogenation of $H_3B{\cdot}NMe_2H$ with Cp_2Ti (formed in situ from Cp_2TiCl_2 and *n*BuLi) has been shown to be homogeneous,[30] whereas that with $[Rh(1,5\text{-}COD)\text{-}Cl]_2$ is heterogeneous (or at least involves Rh clusters).[31] Our experimental results argue for a similar situation in the case of the guanidine-boranes. This makes the Cp_2Ti-catalysed reaction a much easier system for calculations. In these calculations we used the same method as in the recently published theoretical work on dehydrogenation of $H_3B{\cdot}NMe_2H$.[28] However, we slightly modified the basis set (see above). The calculations were restricted to a step-

by-step model that does not consider the involvement of a second guanidine molecule in the hydrogen elimination. In the case of $H_3B{\cdot}NMe_2H$, it was shown that such a step-by-step mechanism is favored kinetically over other possibilities. Even with this restriction, we had to consider two possible pathways (in difference to the $H_3B{\cdot}NMe_2H$ case where only one pathway is possible). If the N atom from which H is eliminated is directly bound to B, being thus the imine N atom, the process is named 1,2-dehydrogenation and leads to the allene-type species $H_2BNC(NH_2)_2$. If it is one of the N atoms of the two amido (NH_2) groups, the process is named 1,4-dehydrogenation and results in the diene-type species $H_2BN(H)C(NH_2)(NH)$. In the case of **2** only 1,4-dehydrogenation is possible and for **3** only 1,2-dehydrogenation is possible. Therefore, these two molecules are ideal systems to experimentally verify the theoretical results.

2.2.1.1 Thermal dehydrogenation

We first calculated the possible mechanism for the uncatalysed reactions. An H-H bond is formed at the expense of B-H and N-H bonds in the course of dehydrogenation. To compare the results with catalytic reactions, we assumed a mechanism in which the first H_2 molecule is eliminated in an intramolecular process. The structures of the products and the transition states for all considered pathways are illustrated in Figure 2.2.1. Table 2.2.1 includes calculated thermodynamic properties.

Thermally induced 1,4-dehydrogenation of **1** to give $H_2BN(H)C(NH_2)(NH)$ in its diene-type structure is associated with an energy change of 48.3 kJ mol^{-1}. $\Delta_{solv}G^0$ including solvent effects amounts to not more than +7.0 kJ mol^{-1}. These values are in good agreement to previous calculations.[32] However, a standard Gibbs free energy barrier (including solvent effects) of 109.2 kJ mol^{-1} (at 298 K, 1 bar) opposes dehydrogenation. The H-H bond length in the transition state measures 84.6 pm (compared to 74.4 pm in free H_2). In the diene-type product the B-N bond length (141.1 pm) is significantly shorter than that in adduct (159.9 pm). At the transition state, the B-N bond length measure 149.9 pm and is thus already significantly strengthened. The 1,2-dehydrogenation of **1** is associated with a change in energy and standard Gibbs free energy (including solvent effects) of 43.6 and 4.1 kJ mol^{-1},

respectively. A standard Gibbs free energy barrier as high as 197 kJ mol^{-1} separates the reactant from the product.

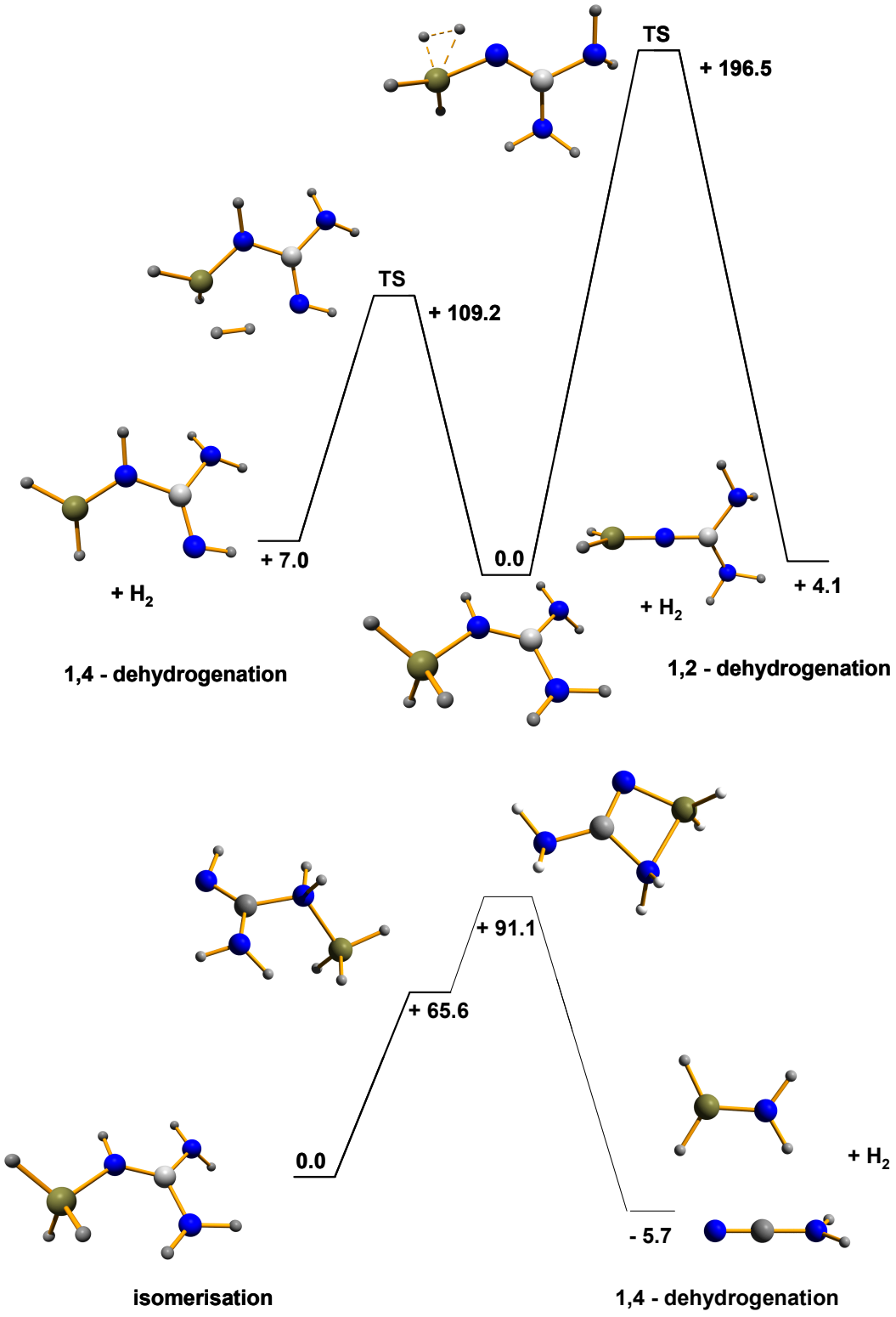

Figure 2.2.1: Calculated structures and $\Delta_{solv}G^0$ for thermal 1,2- or 1,4-dehydrogenation and isomerisation and decomposition under H_2 elimination starting with **1**.

Table 2.2.1: Thermodynamic properties (ΔE, ΔH^0, ΔG^0, $\Delta_{solv}G^0$ all in kJ mol^{-1}) as calculated for thermal 1,4- and 1,2- dehydrogenation starting with the model guanidine-borane adduct $H_3B{\cdot}N(H)C(NH_2)_2$ (TS = transition state).

	ΔE	ΔH^0	ΔG^0	$\Delta_{solv}G^0$
$H_3B{\cdot}N(H)C(NH_2)_2$ **1**	0.0	0.0	0.0	0.0
1,4-dehydrogenation				
TS	100.7	86.1	91.5	109.2
$H_2BN(H)C(NH_2)NH + H_2$	48.3	27.5	-6.3	7.0
1,2-dehydrogenation				
TS	194.1	177.4	179.1	196.5
$H_2BNC(NH_2)_2 + H_2$	43.6	21.6	-15.0	4.1
isomerisation + 1,4-dehydrogenation				
$HNC(NH_2)(NH_2){\cdot}BH_3$ **1A**	56.3	58.7	60.6	65.6
$H_2NC(\mu\text{-}N)(\mu\text{-}NH_2)BH_2 + H_2$	141.6	118.9	86.8	91.1
$H_2BNH_2 + NCNH_2 + H_2$	106.9	72.7	-11.9	-5.7

The transition state features an H–H bond length of 101.2 pm. Again, the B–N bond length in the allene-type product (136.5 pm) is much shorter than that in the starting adduct (159.9 pm). With 156.1 pm, the B-N distance at the transition state is close to that of the reactant. In summary, both 1,4- and 1,2- dehydrogenation are mildly endothermic, with $\Delta_{solv}G^0$ values (including solvent effects) next to zero. However, for both pathways significant barriers were found, in agreement to the experimental results (see Section 2.2.2), showing that **2** and **3** are stable species at room temperature. The significant difference in the barrier height suggests that 1,4-dehydrogenation is clearly kinetically favoured over 1,2-dehydrogenation for **1** if dehydrogenation is carried out thermally.

We also analysed subsequent dimerisation of the diene-type $H_2BN(H)C(NH_2)(NH)$ and the allene-type $H_2BNC(NH_2)_2$ species to give $[H_2B\{\mu\text{-}N(H)C(NH_2)(NH)\}]_2$ and $[H_2B\{\mu\text{-}NC(NH_2)_2\}]_2$, respectively (see Figure 2.2.2 and Table 2.2.2).

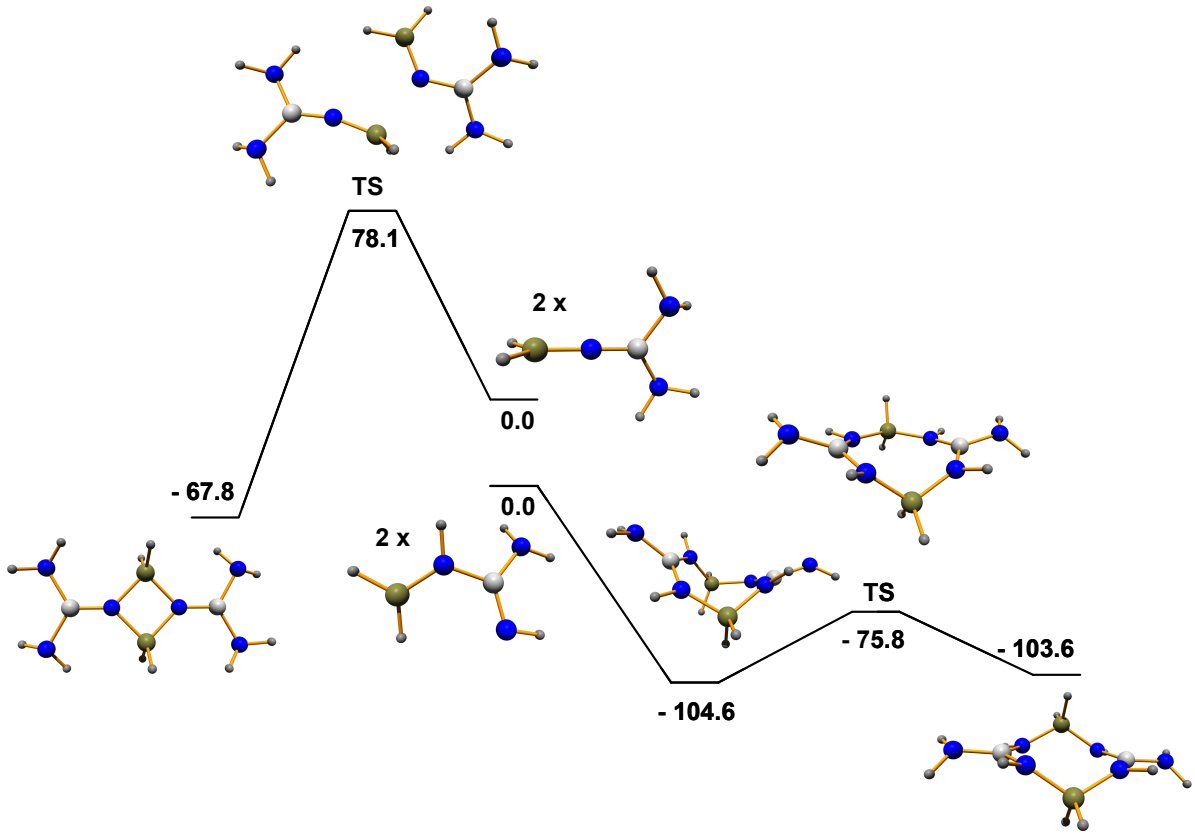

Figure 2.2.2: Quantum chemical calculations on the dimerisation of the diene-type $H_2BN(H)C(NH_2)(NH)$ and the allene-type $H_2BNC(NH_2)_2$ molecules.

As anticipated, dimerisation of $H_2BN(H)C(NH_2)NH$ (to give an eight-member ring) comes out to be more exothermic than that of $H_2BNC(NH_2)_2$ (to give a four-member ring). Interestingly, the calculations predict two conformers of $[H_2B\{\mu\text{-}N(H)C(NH_2)(NH)\}]_2$ ("boat" and "chair") to exhibit almost similar energy. In the solid state, only the chair conformation was found in the case of $[H_2B(\mu\text{-hpp})]_2$ in our experiments, (see Section 2.2.2.1). In the case of pyrazabole molecule $[H_2B(pz)]_2$, a boat conformation is adopted, which is (according to B3LYP/6-311+G**) 21.0 kJ mol^{-1} more stable that the chair conformation.[33] More recently experimental and theoretical studies showed for $[H_2B(\mu\text{-tbo})]_2$ and $[H_2B(\mu\text{-tbn})]_2$ compounds also a boat conformation which was found more stable than the chair conformation.[6] Whereas

dimerisation to the "boat" conformer of $[H_2B\{\mu\text{-}N(H)C(NH_2)(NH)\}]_2$ is barrier-free (concerning the energy), an energy barrier of 25.0 kJ mol^{-1} (barrier of the free Gibbs energy of 78.1 kJ mol^{-1} at 1 bar, 298 K) has to be surpassed to obtain the dimmer of $H_2BNC(NH_2)_2$.

Hydrogen elimination from $[H_2B\{\mu\text{-}N(H)C(NH_2)(NH)\}]_2$ in its "boat" conformer to give the diborane $[HB\{\mu\text{-}N(H)C(NH_2)(NH)\}]_2$ is associated with a change in the standard Gibbs free energy of 25 kJ mol^{-1}. In summary, the calculations on the thermal pathway suggest the first step in the elimination of the first H_2 to be the rate-determining step and predict 1,4-dehydrogenation to be favored over 1,2-dehydrogenation.

Table 2.2.2: Thermodynamic properties (ΔE, ΔH^0, ΔG^0, $\Delta_{solv}G^0$ all in kJ mol^{-1}) as calculated for dimerisation of the diene-type $H_2BN(H)C(NH_2)(NH)$ and the allene-type $H_2BNC(NH_2)_2$ to give $[H_2B\{\mu\text{-}N(H)C(NH_2)(NH)\}]_2$ and $[H_2B\{\mu\text{-}NC(NH_2)_2\}]_2$ (see Figure 2.2.2 for a visualization for the structures).

	ΔE	ΔH^0	ΔG^0	$\Delta_{solv}G^0$
dimerization of $H_2BN(H)C(NH_2)NH$				
x $H_2BN(H)C(NH_2)NH$	0.0	0.0	0.0	0.0
$[H_2B\{\mu\text{-}N(H)C(NH_2)(NH)\}]_2$ ("boat"-conformation)	-183.9	-171.2	-108.9	-104.6
TS	-154.8	-145.1	-81.3	-75.8
$[H_2B(\mu\text{-}N(H)C(NH_2)(NH)]_2$ ("chair"-conformation)	-182.7	-169.9	-109.0	-103.6
dimerization of $H_2BNC(NH_2)_2$				
x $H_2BNC(NH_2)_2$	0.0	0.0	0.0	0.0
TS	25.0	27.6	78.7	78.1
$[H_2B\{\mu\text{-}NC(NH_2)_2\}]_2$	-137.3	-127.4	-68.0	-67.8

All these results are based on the assumption that **1** does not rearrange prior to dehydrogenation. In principal, isomerisation to species **1A** (see Scheme 2.2.1) is possible. However, according to quantum chemical calculations, this isomerisation is associated with a change in energy and standard Gibbs free energy (including solvent effects) of 56.3 and 65.6 kJ mol^{-1}, respectively. On the other hand, **1A** is amenable to 1,4-dehydrogenation, which should be associated with a lower activation barrier than that of 1,2-dehydrogenation. Interestingly, the quantum chemical calculations show that this pathway leads to decomposition (see Scheme 2.2.1) and formation of H_2BNH_2 (which of course oligomerises directly or after loss of an additional H_2 to give oligomeric amino boranes or imino boranes) and cyanamide ($NCNH_2$). A four-membered ring $H_2NC(\mu\text{-}N)(\mu\text{-}NH_2)BH_2$ is a possible intermediate of this decomposition (see Figure 2.2.1). Overall, this pathway is associated with ΔE, ΔH^0, ΔG^0, $\Delta_{solv}G^0$ values of 50.6, 14.0, -72.4 and -71.3 kJ mol^{-1}, respectively. The corresponding values for reaction to the $H_2NC(\mu\text{-}N)(\mu\text{-}NH_2)BH_2$ intermediate are 85.3, 60.2, 26.2 and 25.5 kJ mol^{-1}, respectively. Unfortunately the activation barrier for this process was not found. We will see in the following section that this route indeed is of importance.

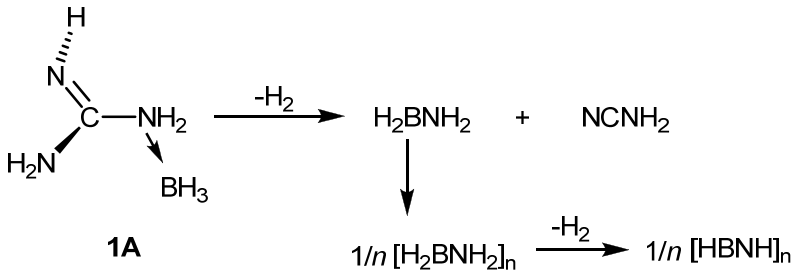

Scheme 2.2.1

2.2.1.2 Catalytic dehydrogenation

The transition states and minima calculated for the Cp_2Ti-catalysed 1,4-dehydrogenation of **1** are illustrated in Figure 2.2.3. Table 2.2.3 contains the calculated thermodynamic properties. In the first step, Cp_2Ti forms a complex with **1** exhibiting a binding energy of -33.4 kJ mol^{-1}. $\Delta_{solv}G^0$ for complex formation amounts to 32.8 kJ mol^{-1}. The second step is the transfer of the first hydrogen atom from N to

Ti and formation of a compound that can in an extreme description be regarded as an ion pair $[Cp_2TiH]^+[H_3B{\cdot}N(H)C(NH)(NH_2)]^-$, but with orbital interactions between the ions and formation of a six-member TiNCNBH ring. The energy and standard Gibbs free energy (including solvent effects) of this species are -128.8 and -39.0 kJ mol^{-1}, respectively, with respect to the noninteracting reactants Cp_2Ti and **1**. A barrier in the standard solvation Gibbs free energy of 83.4 kJ mol^{-1} (values again relative to free Cp_2Ti and **1**) has to be surpassed. The next step is conversion of $[Cp_2TiH]^+[H_3B{\cdot}N(H)C(NH)(NH_2)]^-$ into Cp_2TiH_2 and $H_2BN(H)C(NH_2)NH$. The standard solvation Gibbs free energy barrier of 63.2 kJ mol^{-1} for this step is smaller than that of the previous step. Finally, Cp_2Ti is regenerated and H_2 is released, closing the catalytic cycle. The calculations suggest the rate-determining step to be transfer of the first H atom from the N to the Ti atom, in agreement with the mechanism found for dehydrogenation of $H_3B{\cdot}NHMe_2$.[28]

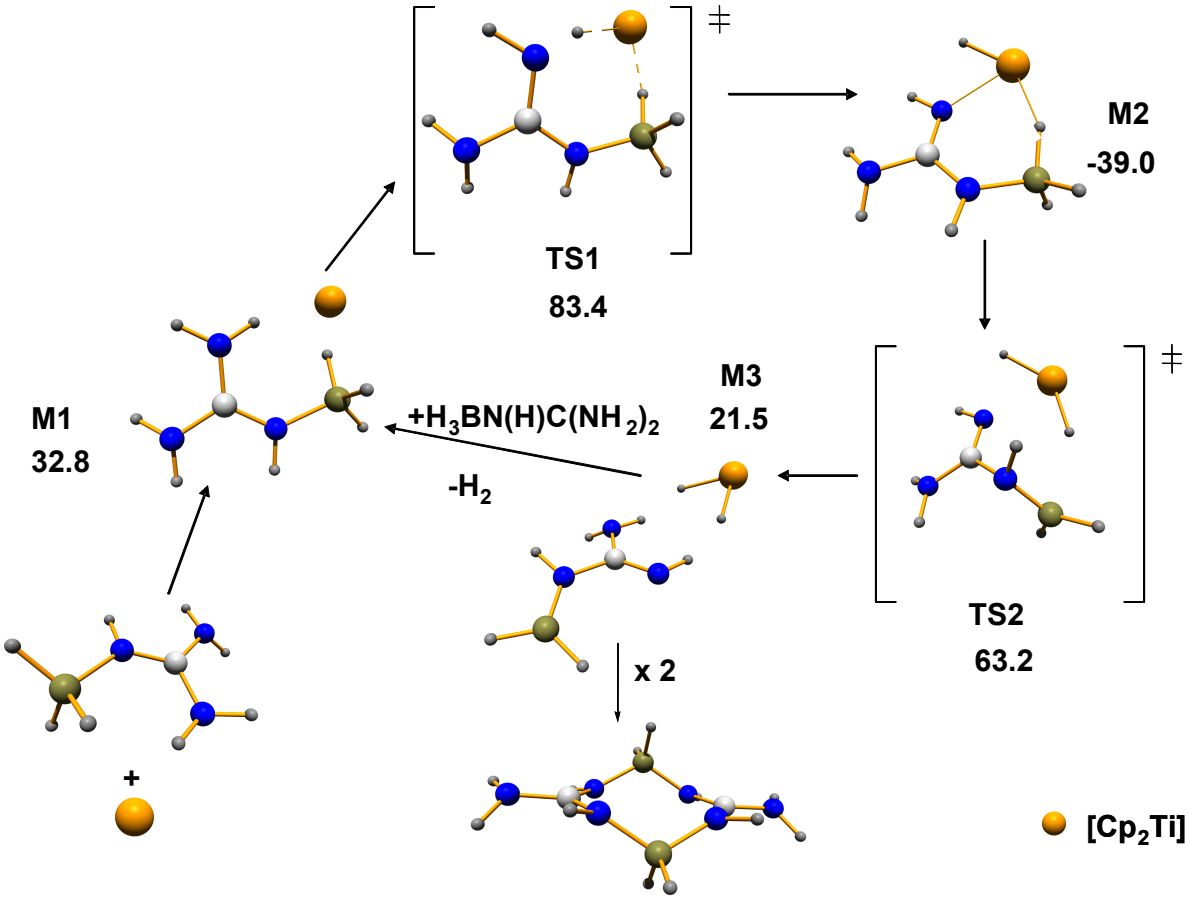

Figure 2.2.3: Calculated structures and thermodynamic properties for Cp_2Ti-catalysed 1,4-dehydrogenation of **1**. The solvation free energies ($\Delta_{solv}G^0$, in kJ mol^{-1}) are relative to $[TiCp_2]$ and **1**. The two Cp rings are omitted for clarity.

The mechanism of Cp_2Ti-catalysed 1,2-dehydrogenation is illustrated in Figure 2.2.4 and the calculated thermodynamic properties are included in Table 2.2.3. Again, the first step is formation of a complex, this time with binding energy and standard Gibbs free energy change (including solvent effects) of -29.2 and 38.4 kJ mol^{-1}, respectively. A first solvation Gibbs free energy barrier of 64.8 kJ mol^{-1} relative to the free reactants separates the complex from the Ti intermediate $[Cp_2TiH]^+[H_3BNC(NH_2)_2]^-$. Then, a second solvation Gibbs free energy barrier of 45.2 kJ mol^{-1} has to be surpassed to yield the allene-type species $H_2BNC(NH_2)_2$ and Cp_2TiH_2.

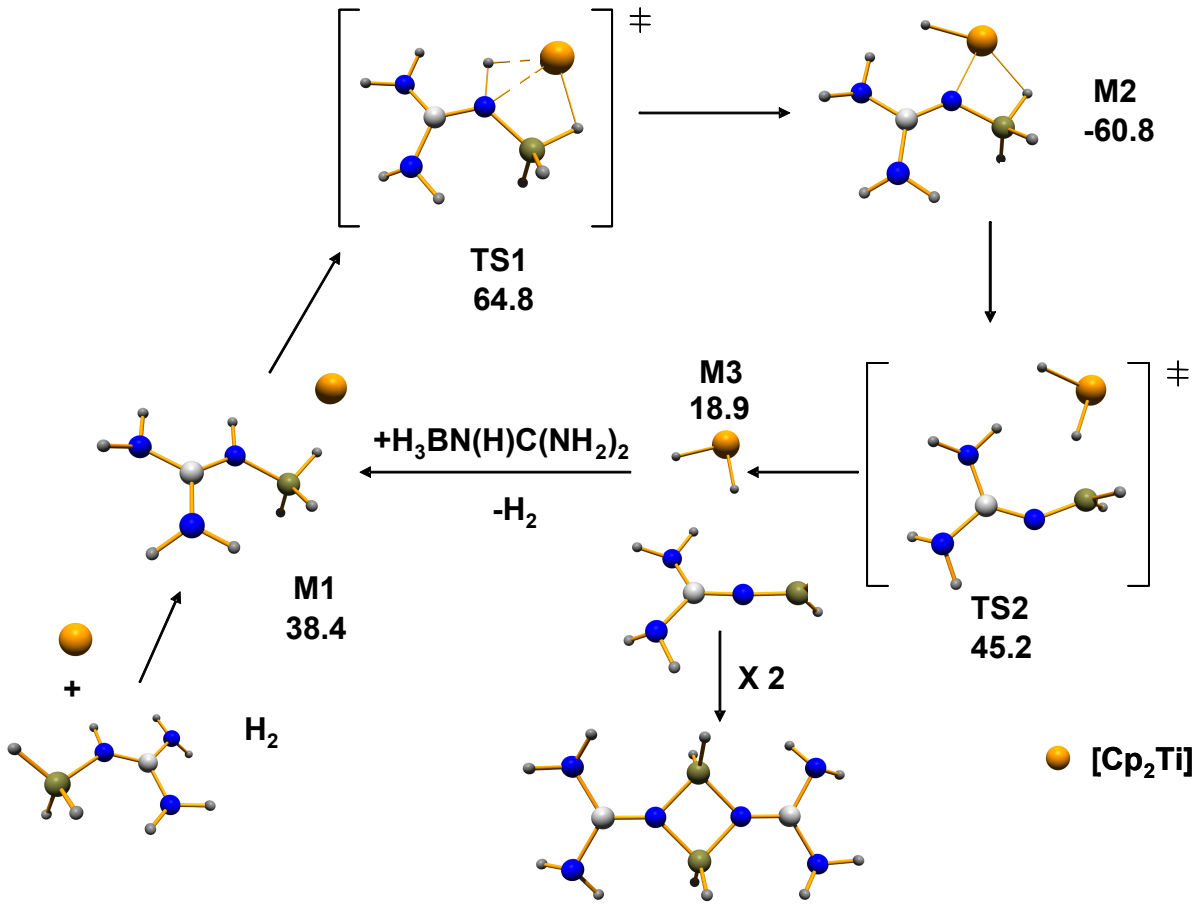

Figure 2.2.4: Calculated structures and thermodynamic properties for Cp_2Ti-catalysed 1,2-dehydrogenation of **1**. The solvation free energies ($\Delta_{solv}G^0$, in kJ mol^{-1}) are relative to $[TiCp_2]$ and **1**. The two Cp rings are omitted for clarity.

Table 2.2.3: Thermodynamic properties (ΔE, ΔH^0, ΔG^0, $\Delta_{solv}G^0$ all in kJ mol^{-1}) as calculated for 1,4- and 1,2-dehydrogenation starting with the model guanidine-borane adduct $H_3B{\cdot}N(H)C(NH_2)_2$ in the presence of $TiCp_2$ as catalyst (See Figures 2.2.3 and 2.2.4 for a visualization of the structures).

	ΔE	ΔH^0	ΔG^0	$\Delta_{solv}G^0$
1,4-dehydrogenation				
$H_3B{\cdot}N(H)C(NH_2)_2 + TiCp_2$	0.0	0.0	0.0	0.0
M1	-33.4	-28.6	24.4	32.8
TS1	14.6	3.0	65.9	83.4
M2	-128.8	-126.1	-59.0	-39.0
TS2	-21.3	-26.3	40.5	63.2
M3	-33.6	-39.0	4.2	21.5
$H_2BN(H)C(NH_2)(NH) + Cp_2TiH_2$	-17.5	-29.2	-20.2	-13.5
$H_2BN(H)C(NH_2)(NH) + Cp_2Ti + H_2$	48.3	27.5	-6.3	7.0
1,2-dehydrogenation				
$H_3B{\cdot}N(H)C(NH_2)_2 + TiCp_2$	0.0	0.0	0.0	0.0
M1	-29.2	-23.1	27.6	38.4
TS1	-16.3	-18.8	47.5	64.8
M2	-154.0	-151.7	-83.8	-60.8
TS2	-20.4	-30.8	26.5	45.2
M3	-31.8	-38.9	-2.3	18.9
$H_2BN(H)C(NH_2)_2 + Cp_2TiH_2$	-22.2	-35.1	-28.9	-16.4
$H_2BN(H)C(NH_2)_2 + Cp_2Ti + H_2$	43.6	21.6	-15.0	4.1

2.2.2 Experimental studies

The theoretical results discussed in section 2.2.1 will be compared in the following to the experimental ones obtained for **2** and **3**. For this purpose, we first prepared the two compounds $H_3B{\cdot}hppH$ and $H_3B{\cdot}N(H)C(NMe_2)_2$ by reaction between $H_3B{\cdot}NMe_3$ and hppH or $HNC(NMe_2)_2$ as reported in section 2.1.1 and started the dehydrogenation experiments with a clean toluene solution of one of the guanidine adducts. As already mentioned, the two compounds are ideal systems to verify the quantum chemical calculations, as **2** is only amenable to 1,4-dehydrogenation and **3** to 1,2-dehydrogenation. However, **3** could isomerise and is then again amenable to 1,4-dehydrogenation (see Scheme 2.2.6).

2.2.2.1 Thermal and catalytic dehydrogenation of $H_3B{\cdot}hppH$

This section is divided into two parts. We start with a study about the thermal dehydrogenation of $H_3B{\cdot}hppH$ **2** followed with an analysis of the catalytic dehydrogenation of this compound. All experiments were monitored by ^{11}B-NMR spectra.

Thermal dehydrogenation of $H_3B{\cdot}hppH$

Figure 2.2.5 shows ^{11}B NMR spectra recorded before (i) and after thermal treatment (ii: 80°C, 23 h, iii: 110°C, 23 h) of a toluene solution of **2**. The ^{11}B NMR spectrum of **2** shows a quartet centred at $\delta(^{11}B)$ = -19.2 ppm (^1J(B-H) = 93 Hz). In both cases of thermal treatment this quartet was extinguished. At the same time, new signals appeared belonging to three different boron products, which are denoted (**7**, **7A** and **7B**) in the following (see Scheme 2.2.2 and 2.2.3 and Figure 2.2.5). The reaction at 80°C led to species **7A** with a doublet signal centered at $\delta(^{11}B)$ = 2.5 ppm (^1J(B-H) = 123 Hz). First, this species was unambiguously identified as $[HB(\mu\text{-hpp})]_2$[34] but further experiments resulted in finding a route to get the $[HB(\mu\text{-hpp})]_2$ species in high purity (see Section 2.3.2). Most likely, the **7A** is $[H_2OB_2(\mu\text{-hpp})_2]$ which probably forms between $[H_2B(\mu\text{-hpp})]_2$ with traces of water from solvents (*vide infra*).

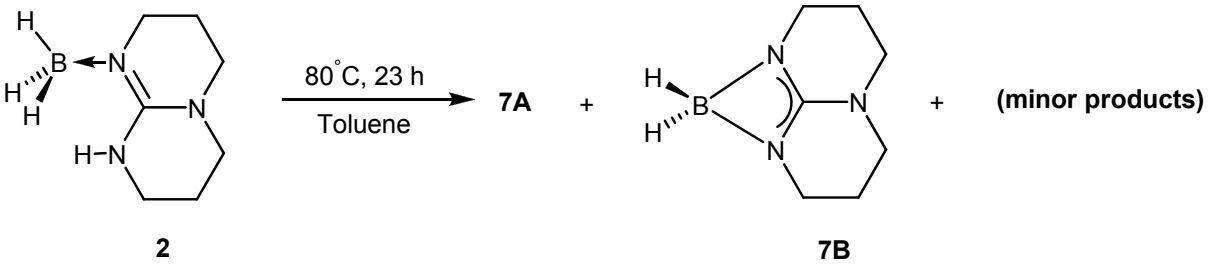

Scheme 2.2.2: Thermal dehydrogenation of **2** at 80°C.

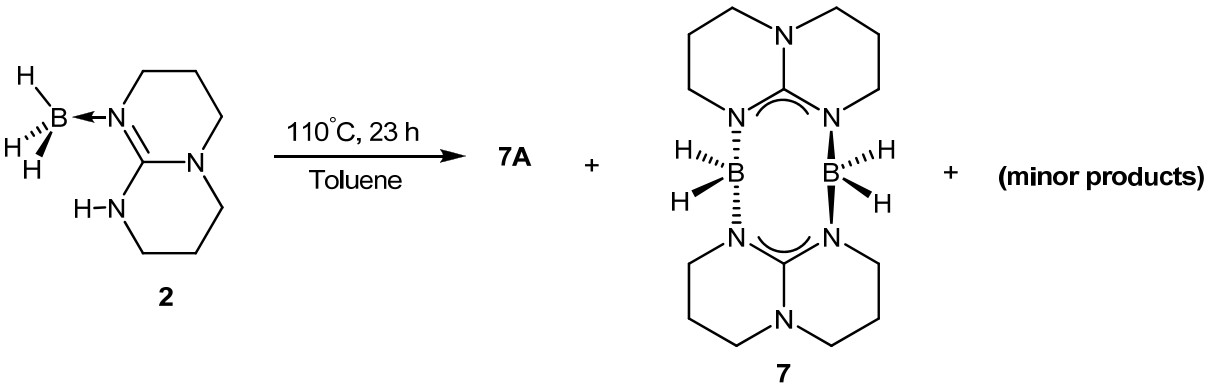

Scheme 2.2.3: Thermal dehydrogenation of **2** at 110°C.

In addition to the doublet from **7A**, a triplet due to a second product **7B** showed at δ(^{11}B) = -6.2 ppm (^{1}J(B-H) = 102 Hz) in the ^{11}B NMR spectrum. The two most likely candidates for this species are [$H_2B(\kappa N,N'$-hpp)] (**7B**, Scheme 2.2.2) and [$H_2B(\mu$-hpp)]$_2$ (**7**, Scheme 2.2.3). The latter will be shown to exhibit a different chemical shift. [$H_2B(\kappa N,N'$-hpp)] was already previously proposed to be involved in the dehydrogenation reaction,[32] so that we tentatively assign the triplet signal to [$H_2B(\kappa N,N'$-hpp)], **7B**. Although the hpp ligand generally prefers a bridging (κ^1N–κ^2N') coordination,[35] the ($\kappa N,N'$) mode is realized in few cases, e.g. recently in the Pt(IV) complex [($\kappa N,N'$-hpp)(hppH)$PtCl_2$(OAc).[36] There are also already some structurally characterized guanidinate boron dichlorides known in which the guanidinate is bound in a $\kappa N,N'$-fashion (e.g. [$Cy_2NC(NCy)_2BCl_2$], [iPrNC$(NCy)_2BCl_2$][37] or [$Ph_2NC(NMes_2)_2BCl_2$ (Mes = 2,4,6-trimethylphenyl) and [$Ph_2NC(NDipp)_2BCl_2$] (Dipp = 2,6-$iPr_2C_6H_3$).[38] A calculated chemical shift δ(^{11}B) of -2.6 ppm for [$H_2B(\kappa N,N'$-hpp)] (see Supplementary Material) compares with an experimentally observed one of -6.2 ppm.

If the reaction is conducted at 110°C, the adduct signal also disappears completely from the ^{11}B NMR spectrum and the doublet signal due to **7A** grows in. The signal due to **7B** was absent, but a different triplet signal due to a new product **7** ($\delta(^{11}B)$ = -2.3 ppm, ^{1}J(B-H) = 96 Hz) appeared instead (see Figure 2.2.5).

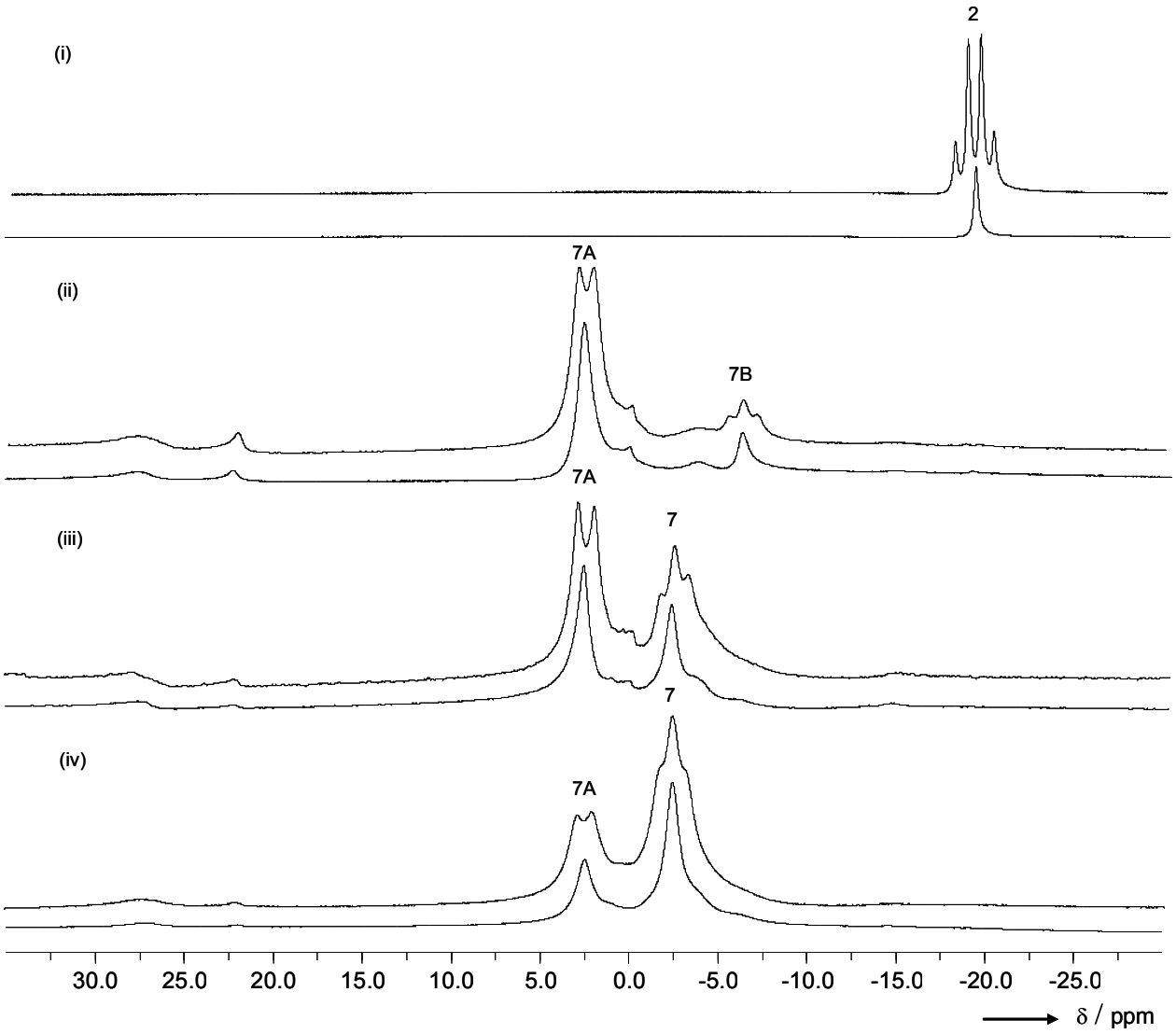

Figure 2.2.5: ^{11}B NMR spectra (128.3 MHz) recorded before (i) and after thermal treatment (trace ii: 80°C, trace iii: 110°C, concentration of **2** in toluene 0.046 mol L^{-1}, trace iv: 110°C, concentration of **2** in toluene 0.123 mol L^{-1}) of a toluene solution of **2** for a period of 23 h. The $^{11}B\{^{1}H\}$ spectra are also shown underneath each spectrum with coupling allowed.

Similar species (**7** and **7A**) were obtained if dehydrogenation of compound **2** was followed in the presence of $[(PPh_3)_3RhCl]$ at 115°C (see Scheme 2.2.4).

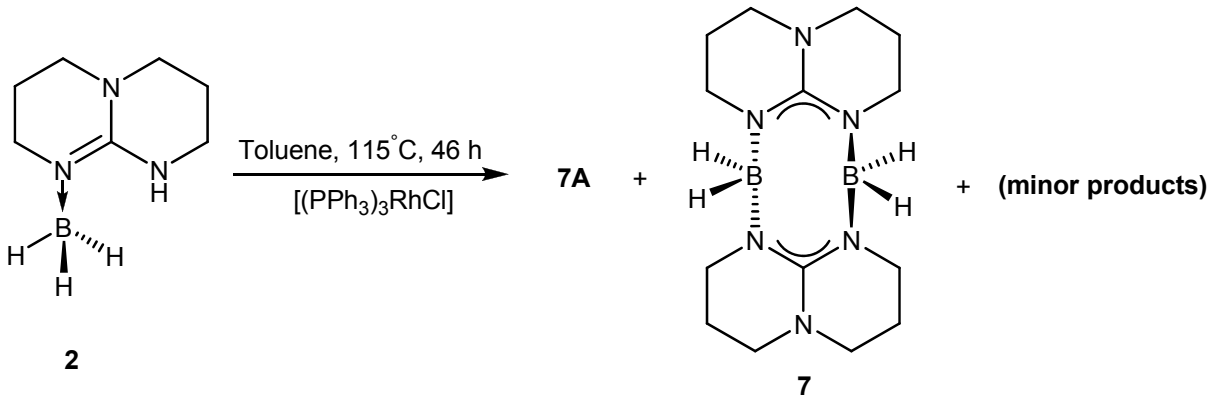

Scheme 2.2.4: Dehydrogenation of compound **2** in presence of $[(PPh_3)_3RhCl]$.

The mixture of compounds was separated by removal of the toluene, addition of hexane and filtration. Compound **7** turned out to be only sparsely soluble in hexane and formed a precipitate which was after filtration easily re-dissolved in toluene. The triplet pattern observed in the ^{11}B NMR spectrum (centered at $\delta(^{11}B)$ = -2.3 ppm, see Figure 2.2.5) proved the presence of H_2B units. This chemical shift agrees with calculated chemical shift $\delta(^{11}B)$ of -3.4 ppm for $[H_2B(\mu\text{-hpp})]_2$ (see Supplementary Material) and with that observed for related molecules. For comparison, $\delta(^{11}B)$ = -10.81 ppm and ^1J(B-H) = 100.9 Hz in the case of compound $[BH_2(\mu\text{-tbo})]_2$[6] and for $[H_2B(pz)]_2$ compound, the $\delta(^{11}B)$ = - 8.8 ppm and ^1J(B-H) = 108 Hz.[39] This compound was also obtained by a reaction of hppH with $H_3B{\cdot}NMe_3$ at 115°C which allowed us to analyse it in more detail (see Section 2.3.1).

From the hexane/toluene solution were possible to grow crystals at 3°C suitable for X-ray diffraction. These crystals turned out to consist of $H_2OB_2(\mu\text{-hpp})_2$ molecules. The ^{11}B NMR spectrum of these crystals showed a chemical shift at $\delta(^{11}B)$ = 2.5 ppm (^1J(B-H) = 123 Hz). In Figure 2.2.6 is represented the X-ray structure for $[H_2OB_2(\mu\text{-hpp})_2]$ **7A**, together with selected bond distances and angles.

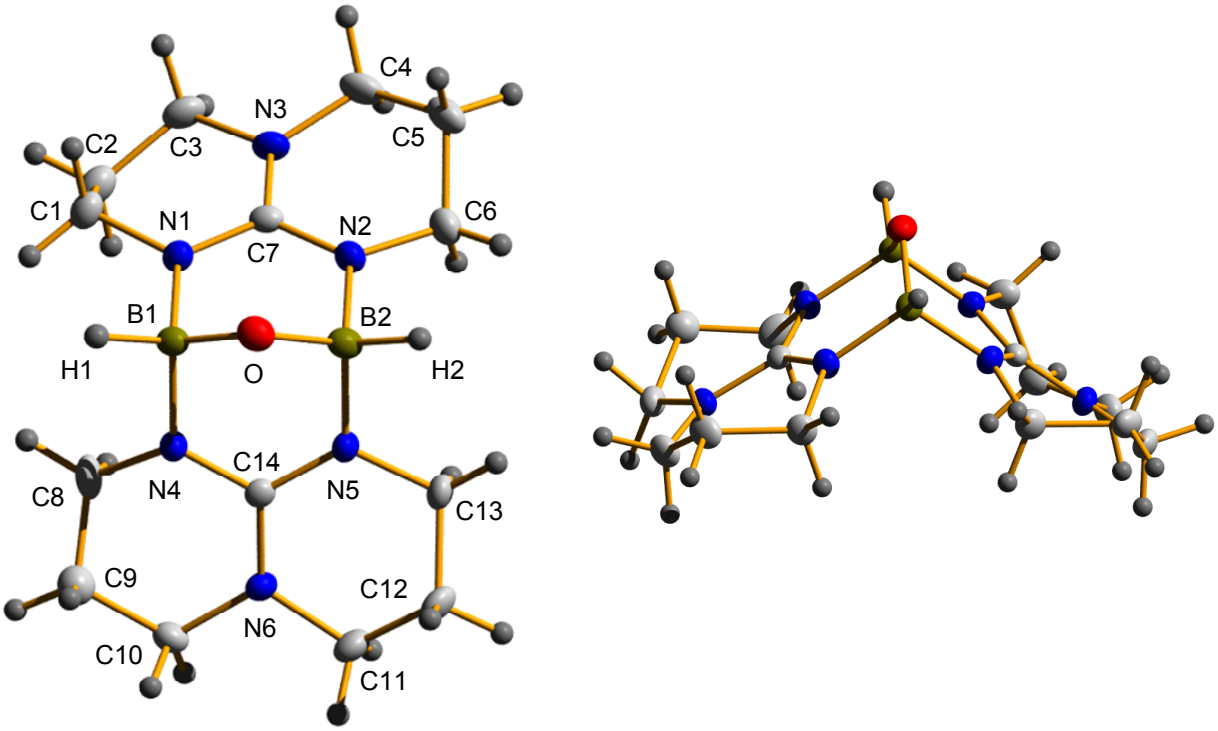

Figure 2.2.6: Molecular structure of $[H_2OB_2(\mu\text{-hpp})_2]$ **7A** derived from X-ray diffraction. Thermal ellipsoids are drawn at the 50% probability level. Selected bond distances (in pm) and angles (in degrees): B(1)-O 142.1(2), B(2)-O 141.7(2), B(1)-N(4) 157.9(2), B(1)-N(1) 158.6(2), B(2)-N(2) 158.2(2), B(2)-N(5) 158.3(2), B(1)-H(1) 113.9(18), B(2)-H(2) 116.4(18), C(7)-N(1) 134.05(19), C(7)-N(2) 134.14(19), C(7)-N(3) 136.00(18), N(4)-B(1)-N(1) 109.14(11), N(1)-C(7)-N(2) 118.57(12), N(2)-B(2)-N(5) 108.54(12), N(4)-C(14)-N(5) 118.14(13).

Catalytic dehydrogenation of $H_3B{\cdot}hppH$

In further experiment dehydrogenation of compound **2** was followed in the presence of the potential pre-catalysts $[Rh(1,5\text{-}COD)Cl]_2$ and Cp_2TiCl_2/*n*BuLi. As mentioned before, these precatalysts were shown to initiate the room-temperature dehydrogenation of amine boranes;[40] the reaction involving the [Rh] complex is an example of heterogeneous catalysis and that involving the Ti complex being an example of homogeneous catalysis. We present here the results obtained with the [Rh] catalyst, but the results obtained with Cp_2TiCl_2/*n*BuLi follow a similar pattern. The appearance of a black metal precipitate signals that the [Rh] catalysed reaction represents, like that of $H_3B{\cdot}NMe_2H$, a heterogeneous process. A first important result

of our studies was that experiments at temperatures below 80°C showed little change even for prolonged reaction times. In contrast to $H_3B{\cdot}NMe_2H$, for which catalytic dehydrogenation already occurs at room temperature, dehydrogenation of the guanidine-boranes is obviously subjected to a significantly higher barrier even in the presence of a catalyst. NMR spectra were recorded before and after heating a toluene solution of **2** containing the [Rh] catalyst to a temperature of 80°C. These experiments showed that reaction in the presence of the catalyst leads at 80°C predominantly to **7**, $[H_2B(\mu\text{-hpp})]_2$ (see Scheme 2.2.5). This is in clear contrast to the uncatalysed reaction, for which no significant amount of $[H_2B(\mu\text{-hpp})]_2$ was formed under these conditions. The ^1H NMR spectrum gave in addition evidence for the formation of smaller amounts of a minor product (see Scheme 2.2.5), which was not observed in the absence of a catalyst.

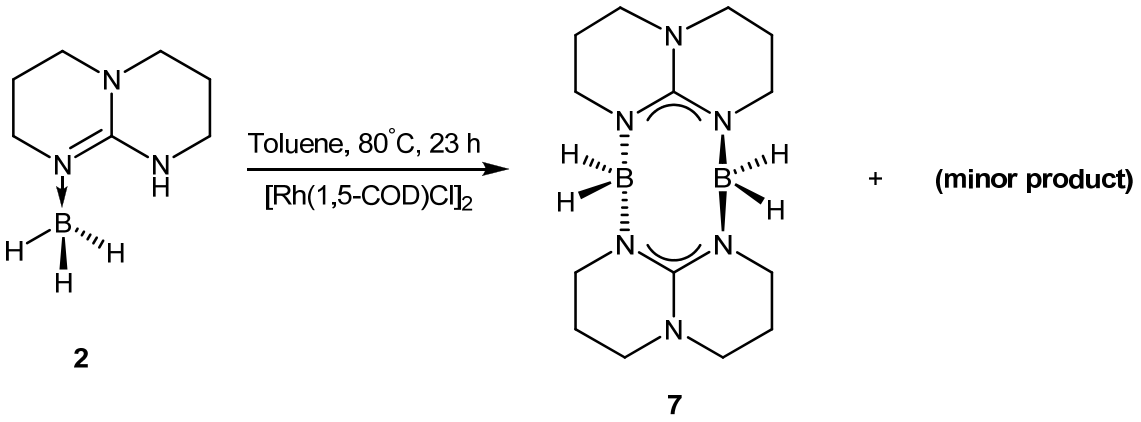

Scheme 2.2.5: Catalysed dehydrogenation of compound **2**.

2.2.2.2 Thermal and catalytic dehydrogenation of $H_3B{\cdot}N(H)C(NMe_2)_2$

Thermal dehydrogenation of $H_3B{\cdot}N(H)C(NMe_2)_2$

Figure 2.2.8 displays the ^{11}B NMR spectra recorded before (i) and after stirring a solution of $H_3B{\cdot}N(H)C(NMe_2)_2$ in toluene for 20 h at 80°C (ii) and for 6 h to 110°C (iii). A new species **3A** was formed in small amounts (q, $\delta(^{11}B)$ = -12.6 ppm, ^1J(B-H) = 98 Hz) in these experiments, but the starting adduct at $\delta(^{11}B)$ = -19.50 ppm (^1J(B-H) = 95 Hz) was still the main component in the solution. From the quartet structure of the ^{11}B signal and its position **3A** can be assigned to a base adduct of BH_3. One

possible author of this signal is the isomer of $H_3B{\cdot}N(H)C(NMe_2)_2$, in which one of the N atoms of the amido (NMe_2) groups is bound to boron. Quantum chemical calculations (see Supplementary Material) predict this isomer to be less stable by 74.19 kJ mol^{-1} (isomerisation is associated with a change in the Gibbs free energy of 81.76 kJ mol^{-1}) with respect to **3**. As already mentioned, this isomer is amenable to 1,4-elimination. ΔG^0 for this process leading first to H_2BNMe_2 and $NCNMe_2$ (see Scheme 2.2.6) is calculated to be -151.41 kJ mol^{-1}. However, we cannot estimate the barrier for this process. It is worth mentioning in this context that the Ga analogue of **3**, $H_3Ga{\cdot}N(H)C(NMe_2)_2$, was observed to decompose to give, besides other products, the cluster $HN\{[HGaNMe][H_2GaNC(NMe_2)_2]\}_3GaH$.[4] The [HGaNMe] group within this cluster should arise from such a decomposition pathway. $[H_2GaNC(NMe_2)_2]$ can either stem from 1,2-dehydrogenation of the Ga analogue of **3** or from reaction between H_2GaNMe_2 and $NCNMe_2$.

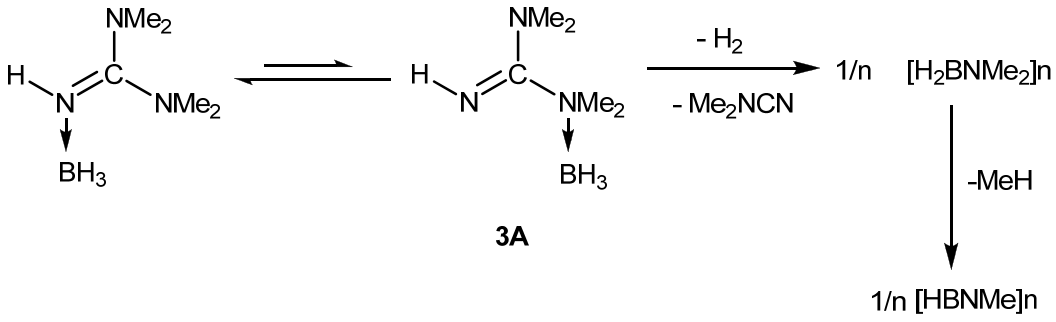

3A

Scheme 2.2.6: Isomerisation and 1,4-dehydrogenation of **3**.

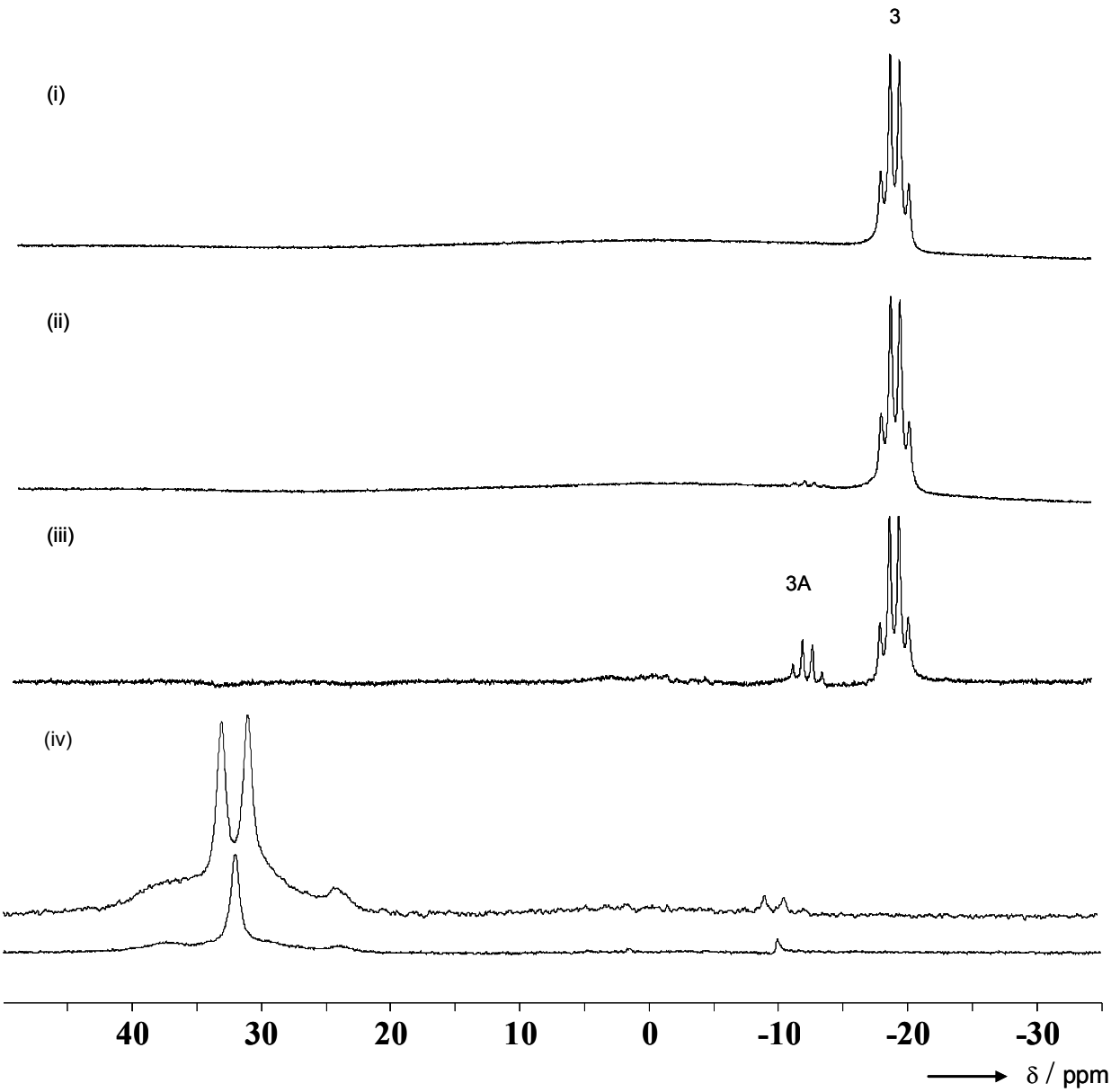

Figure 2.2.7: ^{11}B NMR spectrum (at 128.3 MHz) before (i) and after heating a toluene solution of **3** for 20 h to a temperature of 80°C (ii) and for 6 h to a temperature of 110°C (iii). Trace (iv) shows the spectrum after dehydrogenation at 80°C for 6 d in an NMR tube. For (iv) the ^{11}B{^{1}H} spectrum is additionally shown.

To obtain further information, solutions of **3** were sealed in NMR tubes and heated for 6 d at 80°C. In the ^{11}B NMR spectrum recorded afterwards (see Figure 2.2.7 (iv)) the signals of **3** were absent. The spectrum was dominated by a new intense doublet at δ(^{11}B) = 29.3 ppm with ^{1}J(B-H) = 128.8 Hz. This signal can be assigned to oligomeric

methylimino borane, $[HBNMe]_n$. For comparison, $\delta(^{11}B)$ = 31.7 ppm and ^1J(B-H) = 130 Hz were reported for trimethyl borazine, $[HBNMe]_3$.[41] In the ^1H NMR spectrum, an intense singlet showed at $\delta(^1H)$ = 2.6 ppm, which is close to the reported value in $[HBNMe]_3$ ($\delta(^1H)$ = 3.0 ppm). Thus, under the applied conditions dihydrogen elimination is a very slow process and leads to decomposition and, upon further methane elimination, formation of oligomeric $[HBNMe]_n$ according to Scheme 2.2.6. This result is in full agreement with the quantum chemical calculations.

A sample of the solid product of **3** was also heated for not more then 2 h at 80°C. Afterwards, the NMR spectra were measured and after analyzing them we observed that **3** decomposes relatively fast in solid state. It should be admitted that we were not able to identify any decomposition products. Nevertheless, NMR spectroscopic studies gave useful first information. The ^{11}B NMR spectrum (in C_6D_6) still showed a large quartet signal at $\delta(^{11}B)$ = -19.50 ppm due to **3**, but quartet and triplet signals now appeared in addition at $\delta(^{11}B)$ = -12.75/-11.81 and -3.65 ppm, respectively. In the ^1H NMR spectrum, new equally intense signals were observed at $\delta(^1H)$ = 1.99 (s, CH_3) and 2.26 ppm (s, CH_3), which belong to the same molecule. Furthermore, a signal was detected at $\delta(^1H)$ = 2.6 ppm (s, CH_3). Mass spectra were recorded of the gas-phase over a solid sample while increasing steadily the temperature from 25 °C to 500 °C at a pressure of 10^{-6} Torr. These spectra showed that (in vacuo) **3** partially sublimes without decomposition below 70 °C. However, a substantial fraction of the product decomposes during this process and remains as a solid. Further gas-phase species only occurred at temperatures between 410-500 °C. In the mass spectra recorded in this temperature range, the strongest signal was detected at *m/z* = 207.0 (indicating the presence of dinuclear species in the gas phase), but signals at higher values, *m/z* = 281, 355, 429, 503, were also found. One possible first decomposition product is the dinuclear species $[H_2B\{NHC(NMe_2)(NMe)\}]_2$, which is obtained from **3** upon CH_4 elimination and dimerization (Scheme 2.2.7). The observed value at *m/z* = 107 corresponds to that of this dimmer after removal of one methyl group and all four hydrogen atoms attached to the B atoms.

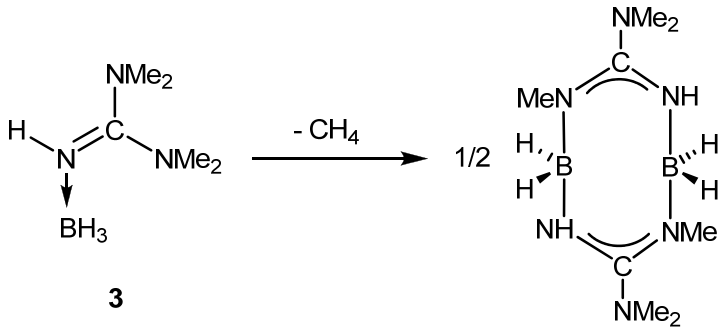

3

Scheme 2.2.7

Calculations were also carried out with Gaussian 98 program[1a] (B3LYP/6-311+G*) to shed light on the first step of the decomposition route of **3**. To this end, the thermodynamic properties of the reaction set out in Scheme 2.2.7 were calculated. Values of -307, -311 and -327 kJ mol^{-1} resulted for the energy change without and with ZPE corrections, respectively, and for ΔG^0. This is as expected, on the basis of the differences between the N–H and N–C bond dissociation energies, much higher than the H_2 elimination and dimerization of $H_3B{\cdot}N(H)C(NMe_2)_2$, for which we obtained ΔE, ΔE_{ZPE} and ΔG^0 values of -89, -128 and -125 kJ mol^{-1}. For comparison, the corresponding reactions of $H_3B{\cdot}N(H)C(NH_2)_2$[32] and the amidine complex $H_3B{\cdot}N(H)C(H)(NH_2)$,[42] in which H_2 is released in place of CH_4, are associated with energy changes of -76 and -84 kJ mol^{-1}, respectively, according to previously calculated BP86/TZVPP estimates.

Catalytic dehydrogenation of $H_3B{\cdot}N(H)C(NMe_2)_2$

The presence of the catalyst has a strong effect on the reaction in the case of the tetramethylguanidine adduct. Dehydrogenation in the absence of a catalyst is an extremely slow at 80°C in solution and leads ultimately to decomposition and formation of oligomeric imino borane. In contrast, the catalyst initiates dehydrogenation at 80°C in much shorter times. This result is in full agreement with the quantum chemical calculations, as now 1,2-dehydrogenation of **3** is possible. Figure 2.2.8 displays the ^{11}B NMR spectra before and after heating a toluene solution of **3** for 20 h to a temperature of 80°C in the presence of $[Rh(1,5\text{-}COD)Cl]_2$ pre-catalyst. The signals due to **3** disappeared completely.

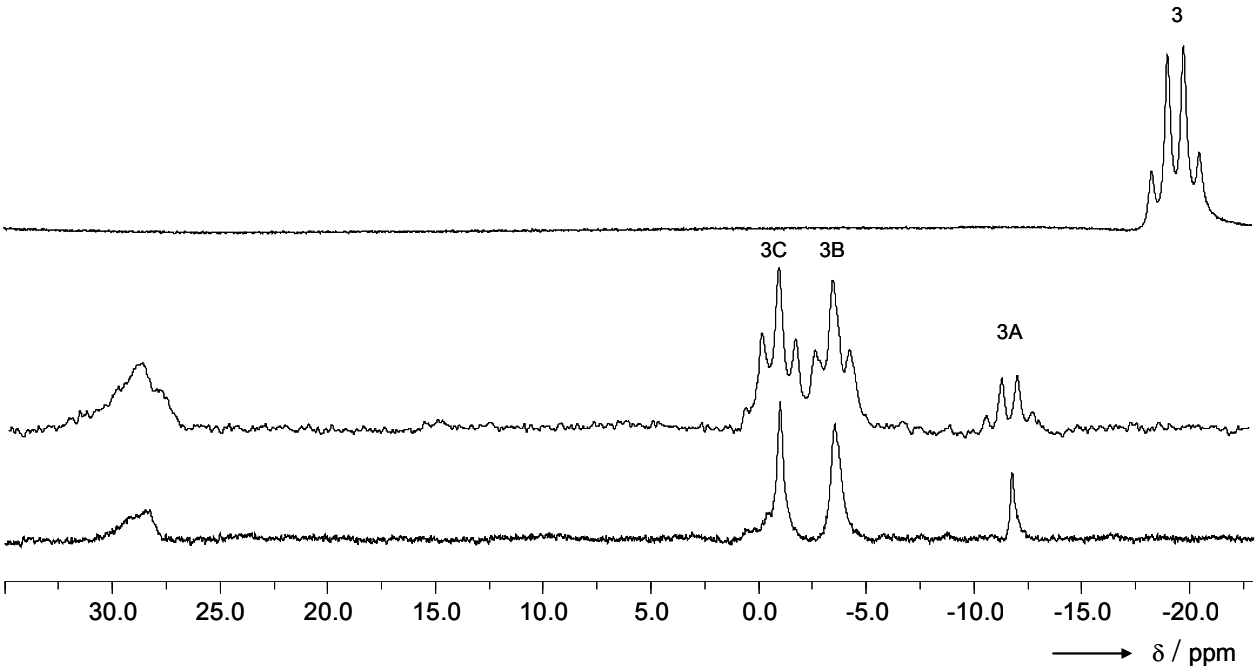

Figure 2.2.8: ^{11}B NMR spectrum (at 128.3 MHz) before (upper trace) and after (lower trace, together with the $^{11}B\{^{1}H\}$ NMR spectrum) heating a toluene solution of **3** for 20 h to a temperature of 80°C in the presence of $[Rh(1,5\text{-}COD)Cl]_2$ pre-catalyst.

The quartet due to species **3A**, which was also visible in the absence of the catalyst, appeared with weak intensity. Most importantly, the spectrum was dominated by two triplets at $\delta(^{11}B)$ = -4.4 ppm (^{1}J(B-H) = 103 Hz) and -1.9 ppm (^{1}J(B-H) = 101 Hz), which were assigned to boron compounds **3B** and **3C** featuring four - coordinate B atoms. The quantum chemical calculations on **1** suggest that 1,2-dehydrogenation is favoured in the presence of a catalyst, and for **3** only 1,2-dehydrogenation is possible. Therefore, we tentatively assigned **3B** to the $HNC(NMe_2)_2$ adduct of $H_2BNC(NMe_2)_2$ and **3C** to the dimer $[H_2B\{\mu\text{-}NC(NMe_2)_2\}]_2$ or the trimer $[H_2B\{\mu\text{-}NC(NMe_2)_2\}]_3$ (see Scheme 2.2.8).

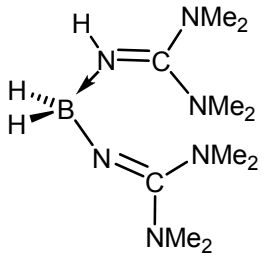

(3B)

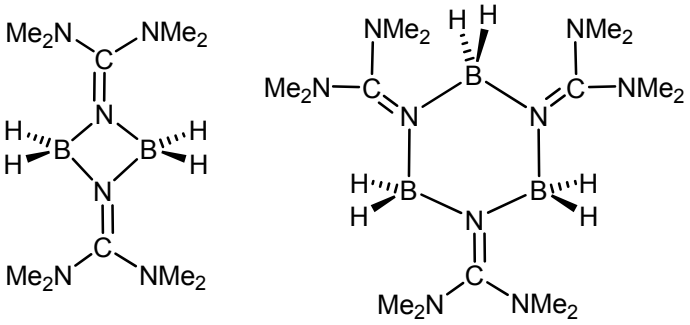

(3C)

Scheme 2.2.8

Dimerisation and trimerisation of $H_2BNC(NMe_2)_2$ according to Scheme 2.2.9 is associated with an energy change of -102.6 and -137.9 kJ mol^{-1}, respectively. The calculated ^{11}B chemical shifts for **3B** and $[H_2B\{\mu\text{-}NC(NMe_2)_2\}]_2$ are -11.9 and -9.2 ppm, respectively.

$$3\ H_2B{=}N{=}C(NMe_2)_2 \longrightarrow 3/2\ [H_2B{=}N{=}C(NMe_2)_2]_2 \longrightarrow [H_2B{=}N{=}C(NMe_2)_2]_3$$

Scheme 2.2.9: Dimerisation and trimerization of $H_2BNC(NMe_2)_2$.

In addition to these two species a broad feature grew in at $\delta(^{11}B)$ = ca. 26-28 ppm, which can be assigned to oligomeric and polymeric methylimino boranes. Thus, in the presence of a catalyst 1,2-dehydrogenation indeed becomes favoured over isomerisation and 1,4-dehydrogenation with decomposition into methylimino borane oligomers, in pleasing agreement with the quantum chemical calculations.

In summary, the thermal and catalytic dehydrogenation of the two guanidine-borane adducts $H_3B{\cdot}$hppH **2** and $H_3B{\cdot}HNC(NMe_2)_2$ **3** were analyzed experimentally. In addition to the experimental work, dehydrogenation was studied computationally for the model complex $H_3B{\cdot}HNC(NH_2)_2$ **1**. The calculations were built on the assumption of a step-by-step mechanism (shown previously to be favored in the case of $H_3B{\cdot}NHMe_2$), in which the first products are either the allene-type $H_2BNC(NH_2)_2$ (1,2-dehydrogenation) or the diene-type $H_2BN(H)C(NH_2)_2(NH)$ (1,4-dehydrogenation), which afterwards dimerise. An alternative route that includes isomerisation of the adduct followed by dehydrogenation and decomposition to give oligomeric amino boranes and imino boranes was also considered.

The calculations clearly showed that the barrier for thermal 1,2-dehydrogenation is much higher than that for 1,4-dehydrogenation arguing for a kinetic preference for 1,4-elimination. Interestingly, the catalyst lowers significantly the barrier for 1,2-dehydrogenation, indicating that the catalyst could alter the preferred reaction channel.

The experimental results show that thermal dehydrogenation of guanidine-boranes is a complex process. In case of $H_3B{\cdot}$hppH **2**, thermal dehydrogenation at 80°C leads to [$H_2B(\kappa N,N'$-hpp)] **7B** and $H_2OB_2(\mu$-hpp$)_2$ **7A** compounds, which were tentatively identified by NMR spectroscopy. Decomposition in boiling toluene (110°C) leads to a mixture of [$H_2B(\mu$-hpp$)]_2$ **7** and $H_2OB_2(\mu$-hpp$)_2$ **7A** , from which **7** could be separated. The $H_2OB_2(\mu$-hpp$)_2$ compound probably was obtained between a reaction of [$H_2B(\mu$-hpp$)]_2$ with traces of water from solvents. In case of $H_3B{\cdot}HNC(NMe_2)_2$ **3**, dehydrogenation is accompanied by decomposition, leading finally to oligomeric methylimino borane. The calculations suggest that such a reaction is generally preferred for guanidines with hydrogen attached to the imine N atom. Decomposition processes of this kind could open up a new, previously unknown route to borazine and imine borane derivatives. The reactions in the presence of a catalyst are in line with the simple “step-by-step” model analysed in the quantum chemical calculations. $H_3B{\cdot}$hppH undergoes catalytic 1,4-dehydrogenation leading to [$H_2B(\mu$-hpp$)]_2$ **7**, and $H_3B{\cdot}HNC(NMe_2)_2$ undergoes 1,2-dehydrogenation to give [$H_2BNC(NMe_2)]_n$ (n = 1, 2 or 3).

2.3 Synthesis and characterization of new binuclear boron hydrides containing two bridging guanidinate (hpp) ligands

Section 2.3.1 and 2.3.2 describe the synthesis of the binuclear B(III) $[H_2B(\mu\text{-hpp})]_2$ and B(II) $[HB(\mu\text{-hpp})]_2$ hydrides. The spectroscopic and X-ray data characteristic for these compounds are included in the same sections in addition with theoretical calculations.[15] Section 2.3.3 is devoted to the synthesis and characterization of $[B_2H_3(\mu\text{-hpp})_2]X$ (X = I^- or Cl^-) compounds. These species include the first cationic binuclear boron hydride $[B_2H_3(\mu\text{-hpp})_2]^+$ which can be assigned as analogue to $B_2H_5^+$. The experimental studies characteristic for $[B_2H_3(\mu\text{-hpp})_2]^+$ cation are accompanied by quantum chemical calculations.

All calculations were carried out with the Gaussian 03[1] program package by using the B3LYP/6-311++G** level. Vibrational analysis was carried out for all structures, and the absence of any imaginary frequency confirmed that all structures represent minima on the potential energy hypersurface. The topological analyses have been performed on B3LYP/6-311++G** densities, using the AIM 2000 program.[43] The contour maps (see Figure 2.3.12) were plotted by using the same program AIM 2000 where the critical points are represented by points. The $\delta(^{11}B)$ and $\delta(^{1}H)$ chemical shifts were calculated at the DFT-GIAO//B3LYP/6-311+G* level. The $\delta(^{11}B)$ and $\delta(^{1}H)$ chemical shifts were referenced to $F_3B{\cdot}OEt_2$ and TMS, respectively.

2.3.1 Synthesis and characterization of $[H_2B(\mu\text{-hpp})]_2$

In section 2.2.2.1 we showed that thermal and catalytic dehydrogenation of $H_3B{\cdot}$hppH **2** lead to formation of $[H_2B(\mu\text{-hpp})]_2$ **7**. Here we are going to describe the synthesis of **7** by using different route. Therefore, the reaction of hppH and $H_3B{\cdot}NMe_3$ at 115°C afforded the species **7** in a yield (63%) (see Scheme 2.3.1).

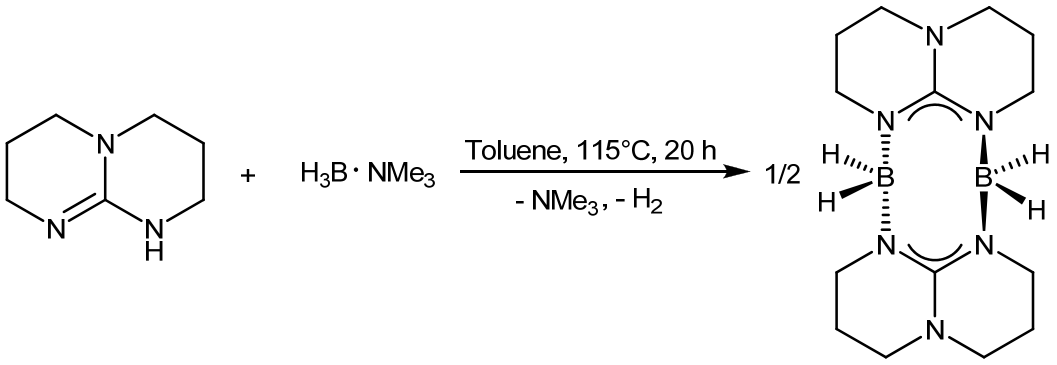

7

Scheme 2.3.1: Synthesis of compound **7**.

This compound was characterized by NMR spectra which are represented in Figure 2.3.1. The resonance at $\delta(^1H)$ = 3.51 ppm in the $^1H\{^{11}B\}$ NMR spectrum (see Figure 2.3.1) confirmed the presence of hydrogen atoms bound to boron. The triplet signal in the ^{11}B NMR spectrum (see Figure 2.3.1) at $\delta(^{11}B)$ = -2.3 ppm (^1J(B-H) = 100 Hz) it is similar to that observed for the product **7** afforded in thermal and catalytic dehydrogenation of **2** (see Section 2.2.2.1).

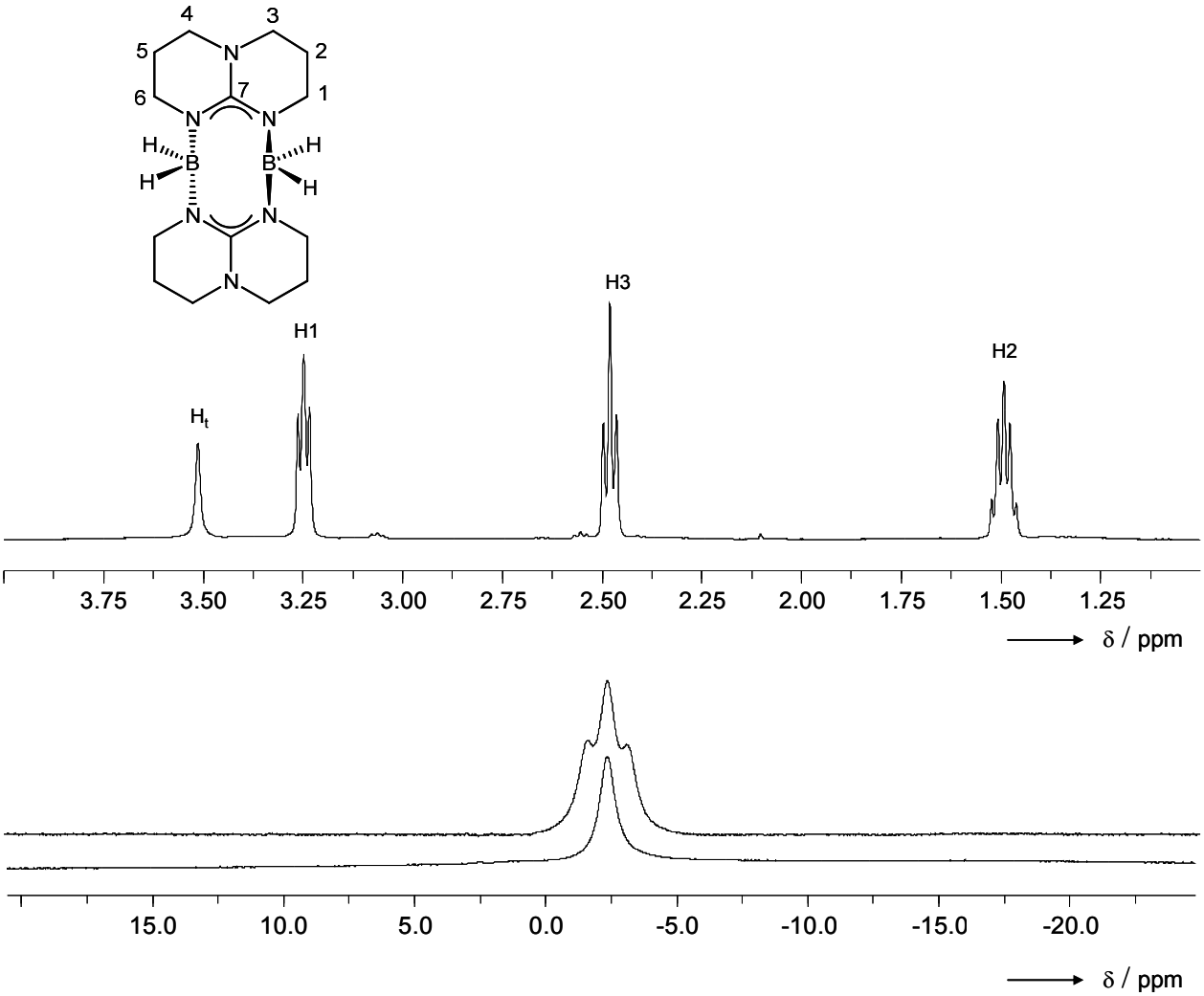

Figure 2.3.1: $^{1}H\{^{11}B\}$ NMR spectrum (400 MHz, C_6D_6); ^{11}B and $^{11}B\{^{1}H\}$ NMR spectra (128.3 MHz, C_6D_6) for **7**.

Compound **7** was crystallized from DMSO solutions and identified unambiguously as the B^{III} hydride $[H_2B(\mu\text{-hpp})]_2$. Figure 2.3.2 shows the molecular structure together with selected structural parameters according to an X-ray diffraction analysis. There are two essentially identical crystallographically independent centrosymmetric half molecules in the asymmetric unit. In agreement with the results of quantum chemical calculations (see Supplementary Material), the two BH_2 groups are located above and below the approximate plane hosting the guanidinate rings thus adopting a chair conformation, and as such, it resembles the structure found previously for $[HClGa(\mu\text{-hpp})]_2$[3] and $[Me_2Al(\mu\text{-hpp})]_2$,[44] respectively. The $[H_2B(\mu\text{-tbo})]_2$ dimer,[6] which was also synthesised in our group, adopted a boat-

type conformation in the solid state, similar to $[Me_2Al(\mu\text{-tbo})]_2$[45] and $[H_2B(pz)]_2$. The B-N bond distances in **7** are 156.2-157.8 pm and compared with 155.7(2) and 156.4(2) pm in $[H_2B(\mu\text{-tbo})]_2$. With 306.5 pm the B1···B1 separation in **7** is significantly smaller than in $[H_2B(\mu\text{-tbo})]_2$ (331.3(2) pm).[6] The X-ray analysis indicates also that the hpp$^-$ anions prefer a bridging κ^1N–κ^2N'-coordination mode.

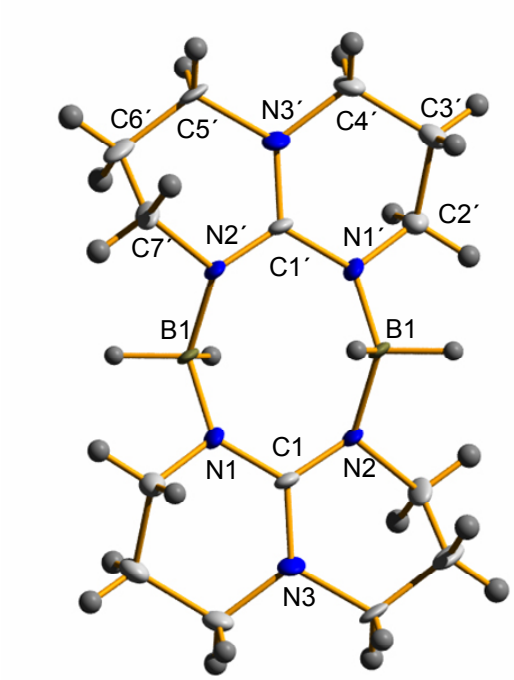

Figure 2.3.2: Molecular structure of $[H_2B(\mu\text{-hpp})]_2$ **7** derived from X-ray diffraction. Ellipsoids are drawn at the 50% probability level. Only one of the two independent molecules is shown. Selected bond distances (in pm) and angles (in degrees): B(1)-N(1) 156.2(4)/157.8(4), B(1)-N(2') 156.5(3)/156.4(4), B(1)-H(1A) 116(2)/114(2), B(1)-H(1B) 111(2)/113(2), C(1)-N(1) 135.4(3)/136.2(4), C(1)-N(2) 132.8(4)/131.8(4), C(1)-N(3) 135.9(3)/135.2(4), N(1)-B(1)-N(2') 115.6(2)/116.1(2), N(1)-B(1)-H(1B) 114(2)/109(2), N(1)-B(1)-H(1A) 107(2)/107(2), N(1)-C(1)-N(3) 119.5(3)/119.0(3), N(1)-C(1)-N(2) 119.5(2)/118.7(3), N(2)-C(1)-N(3) 121.1(2)/122.3(3).

2.3.2 Synthesis and characterization of [HB(μ-hpp)]$_2$

The doubly base-stabilized diborane (4) [HB(μ-hpp)]$_2$ **8** was synthesized by using two methods. The reaction of $H_3B{\cdot}NMe_3$ with hppH at 114°C in presence of [Rh(1,5-COD)Cl]$_2$ precatalyst lead to formation of **8** (see Scheme 2.3.2 (i)). The same species is formed through the dehydrogenation of [H_2B(μ-hpp)]$_2$ **7** in presence of the same precatalyst (see Scheme 2.3.2 (ii)) These two routes were used to obtain **8** in high yield and purity. The thermal or catalytic dehydrogenation of **2** proved to not be the ideal route to **8** (see Scheme 2.3.2 (iii) and Section 2.2.2.1) and also thermal dehydrogenation of **7** turned out to be not a favored route to **8** (see Scheme 2.3.2 (iv)).

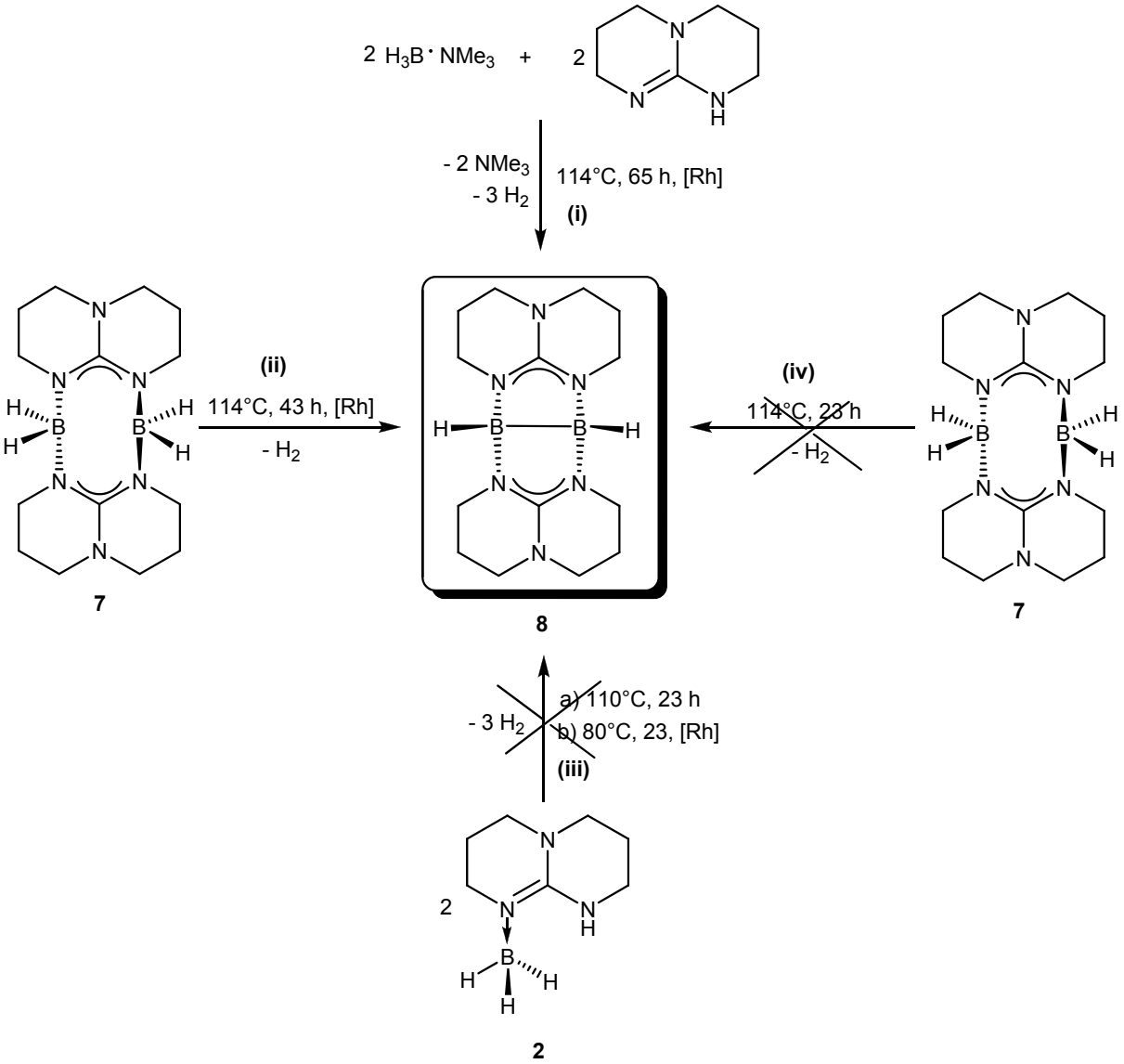

Scheme 2.3.2

Compund **8** is the product of a redox reactions and features two B atoms in the formal oxidation state +2. In the case of $[H_2Ga(\mu\text{-hpp})]_2$, we observed hydrogen elimination even at 25°C, and all signs indicated that $[HGa(\mu\text{-hpp})]_2$ was the product.[3] However, this species could not be structurally characterized. In the case of boron compound $[HB(\mu\text{-hpp})]_2$, we have obtained in few days good-quality crystals from concentrated toluene solution at -20°C.

From the ^1H NMR spectrum (see Figure 2.3.3) we could find out that **8** adopt a "roof-type" conformation.

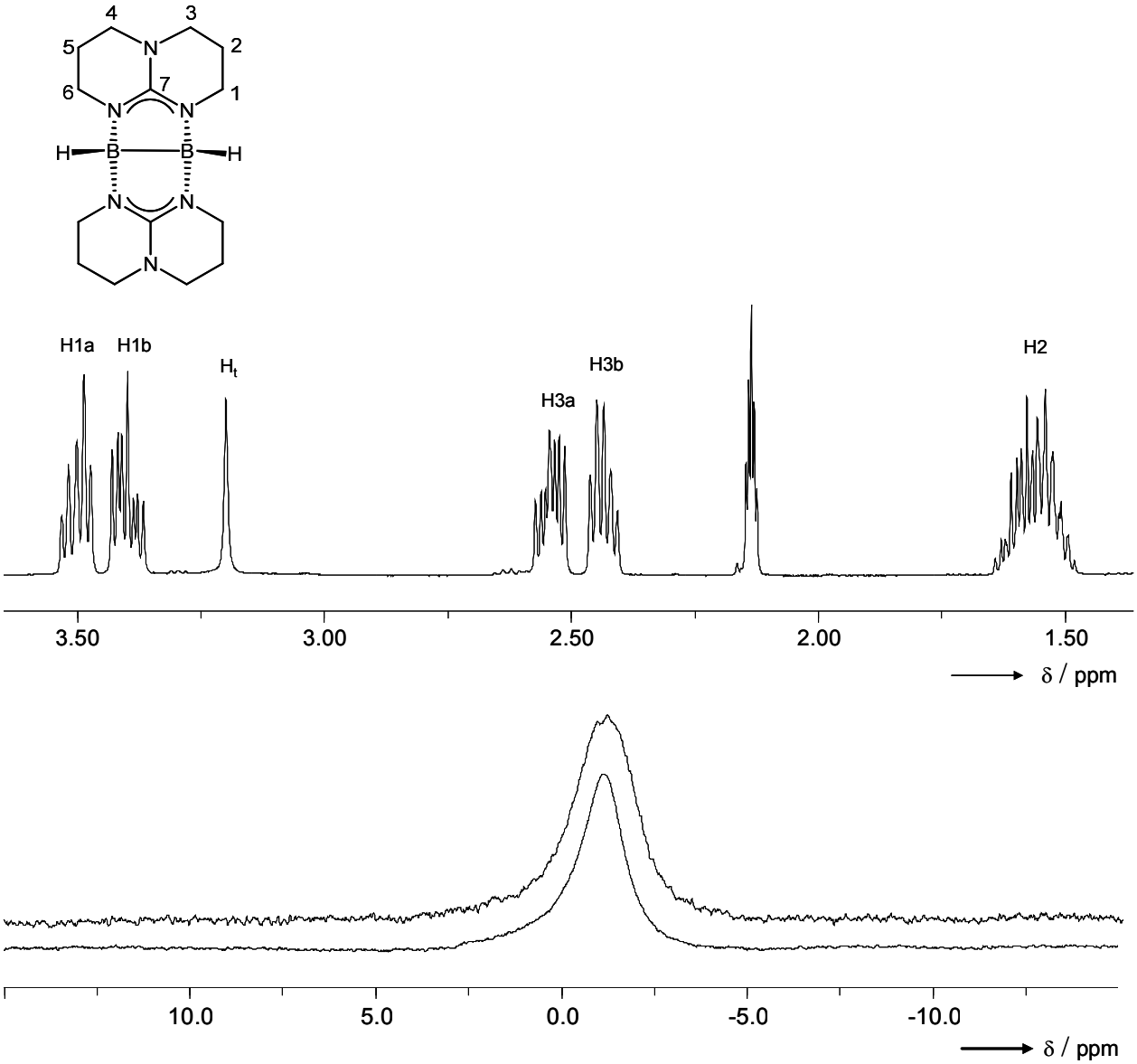

Figure 2.3.3: $^1H\{^{11}B\}$ NMR spectrum (400 MHz, Toluene-d8); ^{11}B and $^{11}B\{^1H\}$ NMR spectra (128.3 MHz, Toluene-d8) for **8**.

Thus the *endo* protons (pointing into the roof) have different chemical shifts than the *exo* protons. The hydrogen atoms attached to boron give rise to a sharp singlet at $\delta(^1H)$ = 3.37 ppm in the $^1H\{^{11}B\}$ NMR spectra (see Figure 2.3.3). The ^{11}B NMR spectrum shows a broad signal at $\delta(^{11}B)$ = - 1.14 ppm (see Figure 2.3.3).

The IR spectrum of **8** futures two overlapping bands, which can be assigned to the in-phase (2272 cm^{-1}) and out-of-phase (2249 cm^{-1}) combination of the two B-H oscillators (see Figure 2.3.4). By applying a simple formula,[46] the angle between the two B-H oscillators can be estimated from the relative intensity of these two modes to be 84°, resulting in an average value of 132° for the two B-B-H angles. The relative intensity of these two modes was obtained by a fit with two Lorentz curves (see Figure 2.3.4, blue line). The value obtained from IR spectrum is in good agreement with the estimates from B3LYP/6-31++G* quantum chemical calculations (128.8° and 128.0°) and from the X-ray diffraction data (B1-B2-H 127°, B2-B1-H 132°) (see Figure 2.3.4).

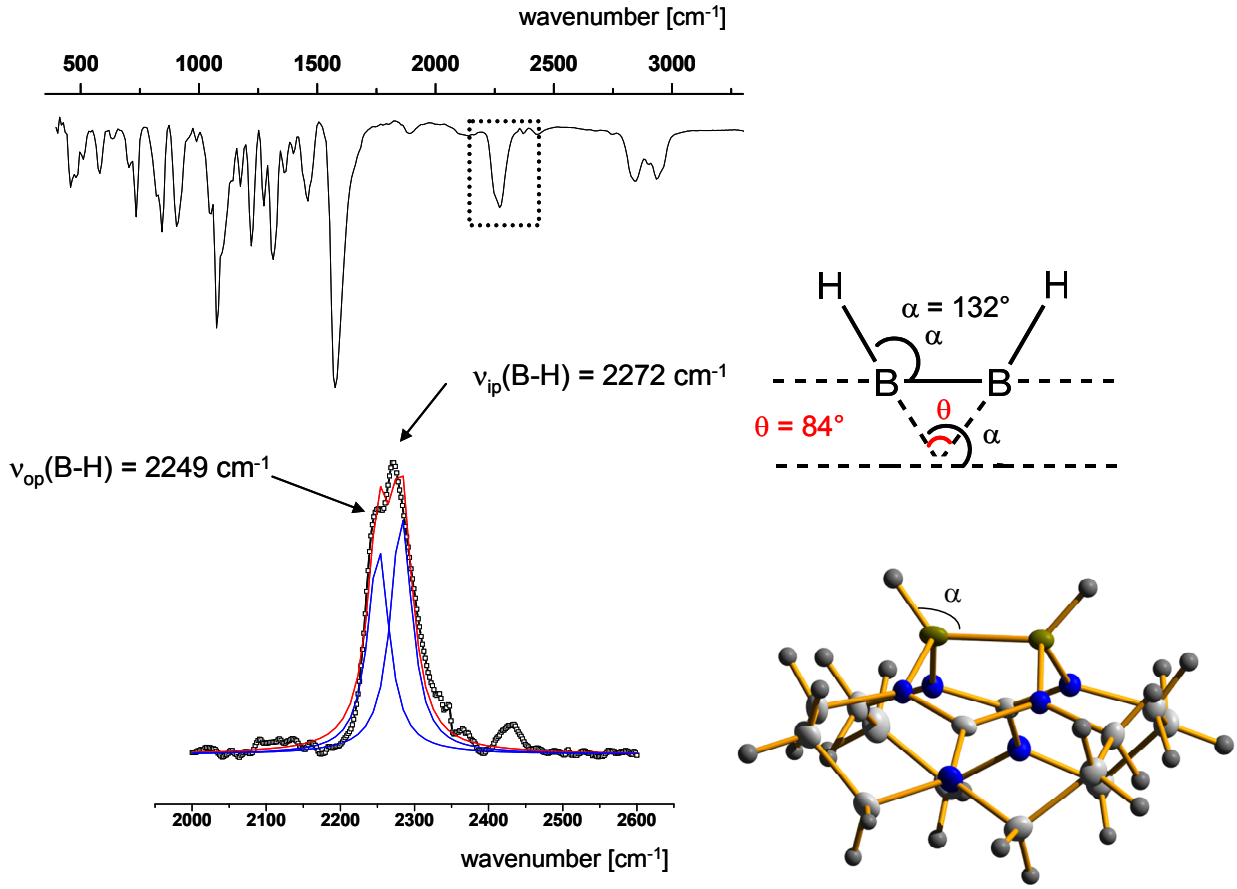

Figure 2.3.4: Determination of the angle α_{BBH} in compound **8**.

Figure 2.3.5 illustrates the crystal structure together with selected bond distances (in pm) and angles (in degrees) for compound **8** derived from our X-ray diffraction measurements. The $[HB(\mu\text{-hpp})]_2$ dimer features a B-B single bond measuring 172.2(3) pm and a *cis*-bent arrangement of the H-B-B-H fragment (with B-H distances of 115.0(3) and 106.0(4) pm). The X-ray analysis indicates also that the hpp^- anions prefer a bridging κ^1N–κ^2N'-coordination mode. The value of the B-B bond length is in a range typical for B-B single bonds. For example, gas-phase electron diffraction measurements of $B_2(NMe_2)_4$ and $B_2(OMe)_4$ indicated B-B bond length of 176.2(1.1) and 172.0(6) pm.[47] The four B-N bond lengths are almost equal: 157.1(2), 157.2(3), 156.3(3) and 158.2(3) pm. The two five-membered BBNCN rings are almost planar, and the dihedral angle between them is 67.80(8)°.

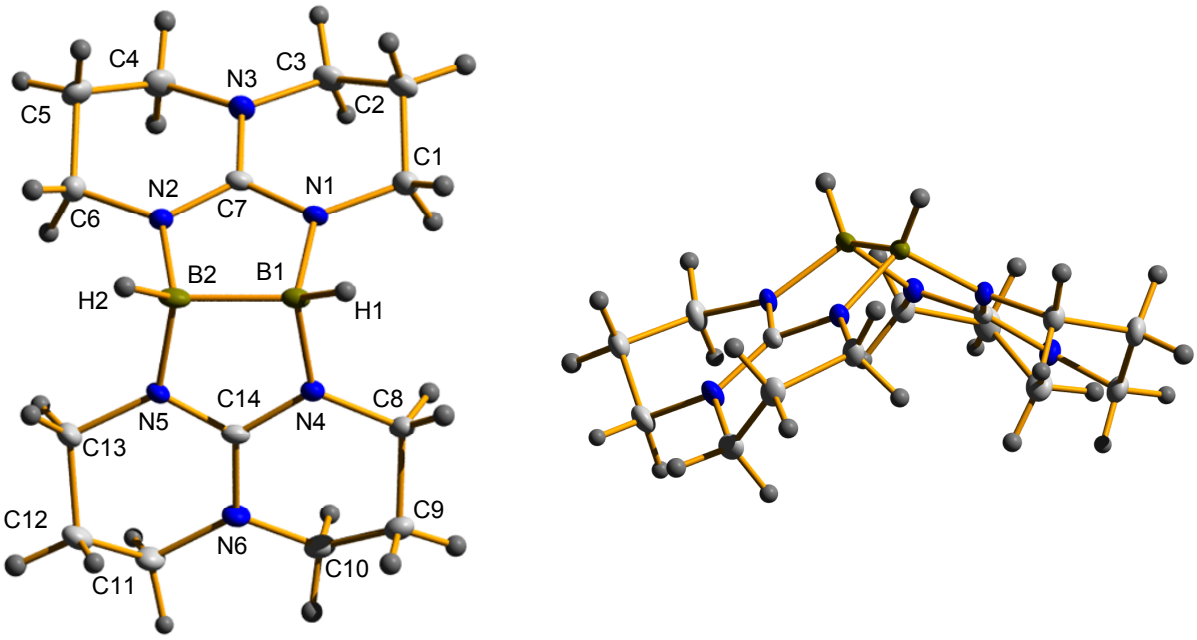

Figure 2.3.5: Molecular structure of $[HB(\mu\text{-hpp})_2]_2$ **8** derived from X-ray diffraction. The thermal ellipsoids are drawn at the 50% probability level. Selected bond distances (in pm) and angles (in degrees): B(1)-N(1) 157.1(2), B(1)-N(4) 157.2(3), B(1)-B(2) 177.2(3), B(1)-H(1) 115.0(3), B(2)-N(5) 156.3(3), B(2)-N(2) 158.2(3), B(2)-H(2) 106.0(4), C(7)-N(1) 134.2(2), C(7)-N(2) 133.1(2), C(7)-N(3) 136.5(2), C(14)-N(5) 133.4(2), C(14)-N(4) 133.8(2), C(14)-N(6) 135.8(2), N(1)-B(1)-N(4) 111.04(15), N(2)-C(7)-N(1) 115.55(16), N(5)-B(2)-N(2) 110.75(15), N(5)-C(14)-N(4) 115.34(16).

2.3.3 Synthesis and characterization of $[H_3B_2(\mu\text{-hpp})_2]X$ (X = I^- or Cl^-)

Section 2.3.3 is divided in three parts. Initially the synthesis and characterization of $[H_3B_2(\mu\text{-hpp})_2]^+X^-$ (where X = I^- or Cl^-) compounds (Section 2.3.3.1 and 2.3.3.2) was performed, followed by a quantum chemical analysis (Section 2.3.3.3).

2.3.3.1 Synthesis and characterization of $[H_3B_2(\mu\text{-hpp})_2]I$

The $[H_3B_2(\mu\text{-hpp})_2]I$ **9** was obtained from a reaction of $[HB(\mu\text{-hpp})]_2$ **8** with I_2 in toluene solutions. Besides of our product, traces of $[hppH_2]I$ were also observed because **9** in toluene solution is not stable for a long time (see Section 2.3.3.2 and Scheme 2.3.7). The possible reaction pathway leading to **9** is shown in Scheme 2.3.3. The HI formed in the first step can react in the second step with **8** to give our product.

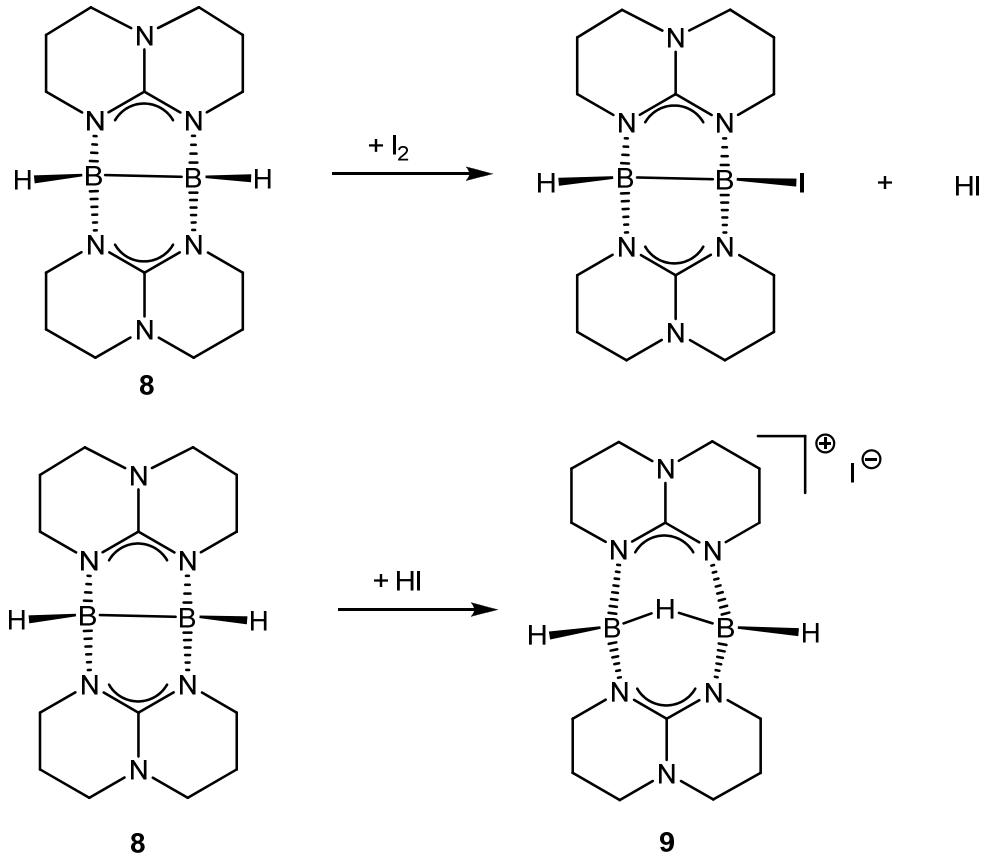

Scheme 2.3.3: Possible reaction pathway to compound **9**.

Normally protonation of a diborane(4) proceeds very differently. For example, tetrakis(dimethylamino)diborane reacts with HX (X = Cl or Br) according to Scheme 2.3.4 to form $X_4B_2(HNMe_2)_2$.[48] Another example is provided by protonation of the doubly base-stabilized diborane(4) $[(Me_2N)B(\mu\text{-hpp})]_2$ **15A** with HCl, producing $[\{(Me_2(H)N)B(\mu\text{-hpp})\}_2]Cl_2$ **15** (see Section 2.5.2, Scheme 2.5.3), again without B(II) oxidation.

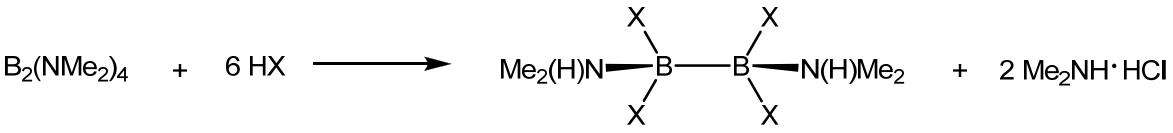

Scheme 2.3.4: Synthesis of $X_4B_2(HNMe_2)_2$[47] (X = Cl or Br).

The $^1H\{^{11}B\}$ NMR spectrum (see Figure 2.3.6) of compound **9** shows that $[H_3B_2(\mu\text{-hpp})_2]^+$ adopt a roof-type conformation and the protons from hpp unit are not equivalent (*endo* and *exo* hydrogen atoms). The $^1H\{^{11}B\}$ NMR spectrum exhibits a triplet and a doublet for the boron-bonded hydrogen atoms at $\delta(^1H_b)$ = 1.97 and $\delta(^1H_t)$ = 3.44 ppm, respectively. These positions are characteristic for bridging and terminal B-H bonds (see Figure 2.3.6). In the ^{11}B NMR spectrum (see Figure 21), a broad doublet is found at $\delta(^{11}B)$ = -2.20 ppm [$^1J(B\text{-}H_t)$ = 125 Hz]. For comparison, in the case of the μ-bis(diisopropylamino)diborane (see Scheme 2.3.5), a broad doublet at $\delta(^{11}B)$ = -10.3 ppm was observed.[49]

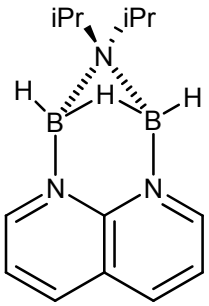

Scheme 2.3.5

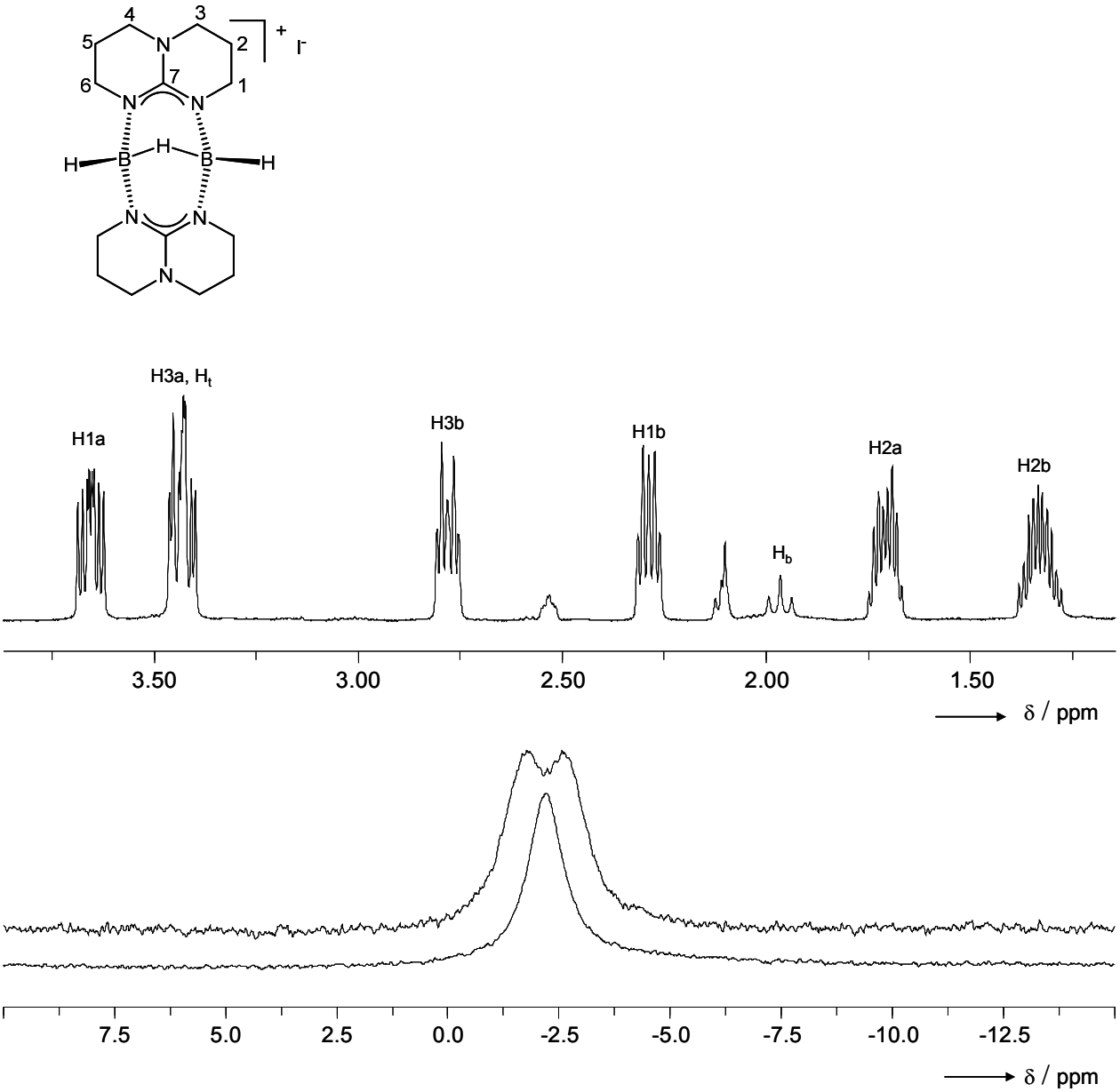

Figure 2.3.6: $^{1}H\{^{11}B\}$ NMR spectra (400 MHz, C_6D_6); ^{11}B and $^{11}B\{^{1}H\}$ NMR spectra (128.3 MHz, C_6D_6) for **9**.

Figure 2.3.7 shows the experimental and simulated ^{11}B NMR spectra (64.1 MHz) of **9** in Toluene-d8 at 80°C, where the doublet is better resolved (see Figure 2.3.7 (i)) and coupling constants $^{1}J(B\text{-}H_t)$ = 125 Hz and $^{1}J(B\text{-}H_b)$ = 40 Hz were obtained from spectrum simulation. ^{11}B NMR spectra (experimental and simulated) with selective decoupling of the bridging hydrogen atom which resonate at 1.97 ppm were also recorded (see Figure 2.3.7 (ii) and (iv)).

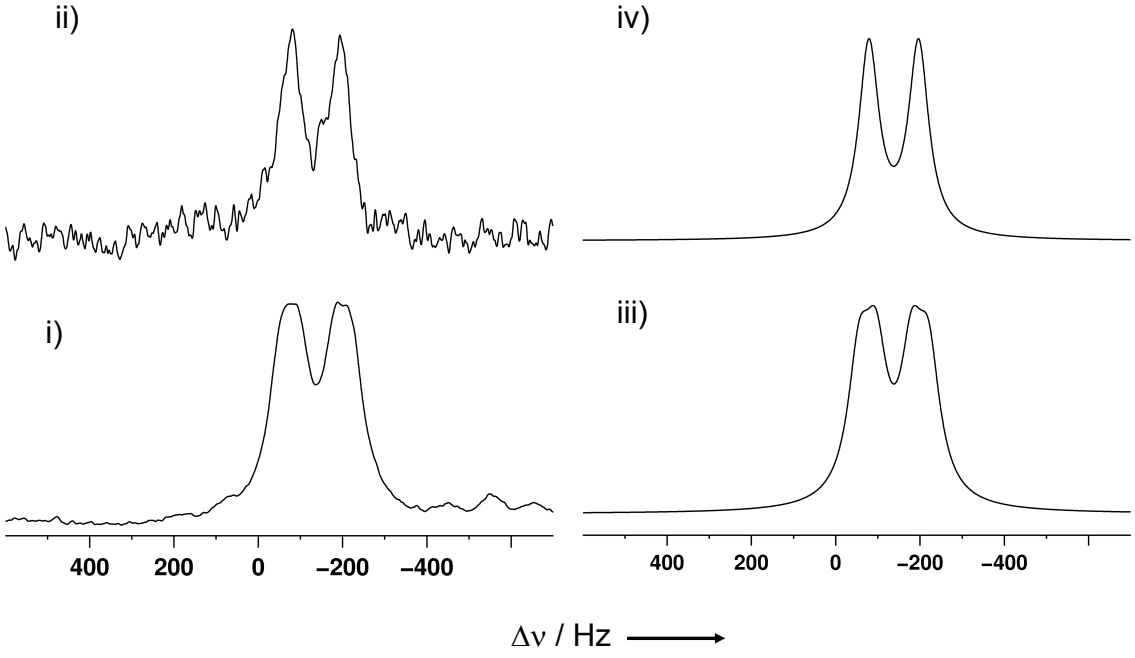

Figure 2.3.7: Experimental and simulated ^{11}B NMR spectra (64. 1 MHz) of **9** in Toluene-d8 at 80°C. i) ^{11}B NMR spectrum without ^{1}H decoupling, ii) ^{11}B NMR spectrum with selective decoupling of the bridging H atom (^{1}H resonance at 1.97 ppm), iii) simulation with the following parameters: ^{1}J(B-H$_t$) = 125, ^{1}J(B-H$_b$) = 40, lineshape = 65 Hz, iv) simulation with coupling to terminal H atoms only.

This species was also characterized by IR spectra (obtained from experiment and calculations) which were compared with the IR spectra characteristic for starting material **8** (Figure 2.3.8). The IR spectrum of **9** has strong bands with absorption maxima at 2425 and 1872 cm^{-1}. These bands can be unambiguously assigned to B-H stretching modes of terminal and bridging hydrogen atoms, respectively. For comparison, in B_2H_6 the IR active stretching modes ν(B-H$_t$) appear at 2613/2518 cm^{-1} and the stretching modes ν(B-H$_b$) at 1924/1615 cm^{-1}.[50]

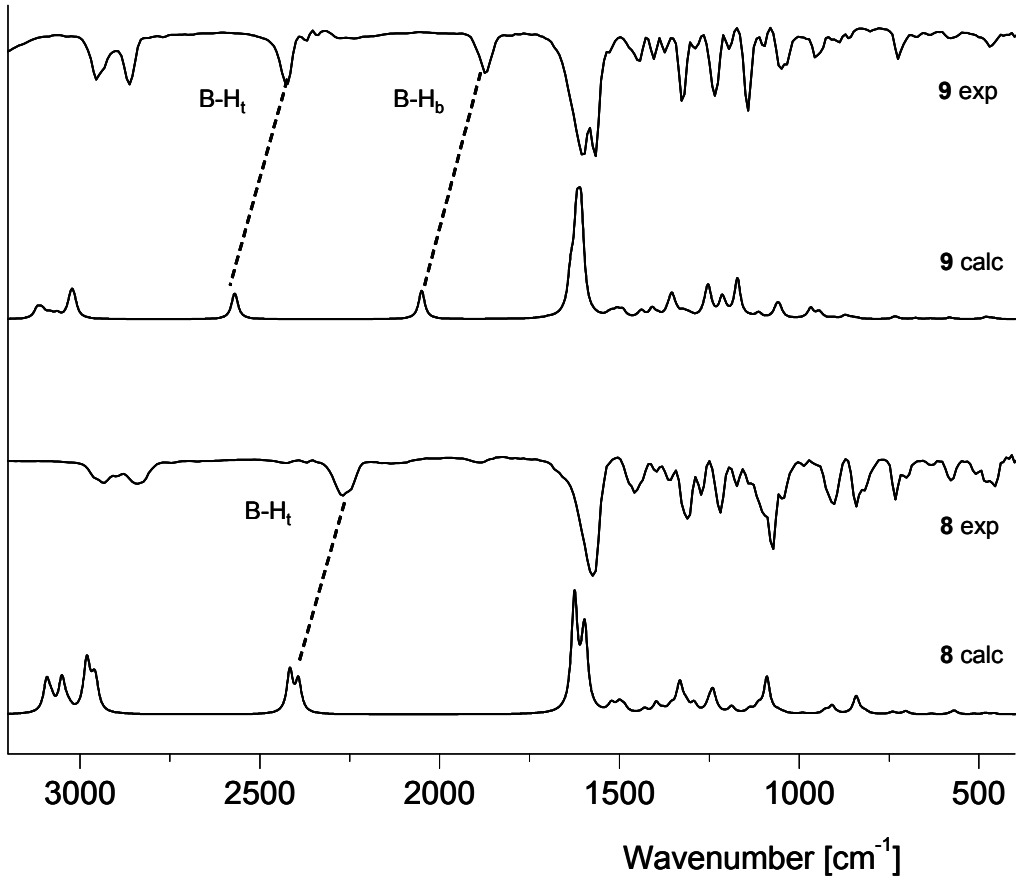

Figure 2.3.8: Comparison of experimental and calculated IR spectra (CsI disks) of solids **8** and **9**. For the simulation of the calculated spectra, Lorentz band profiles were assumed.

The difference between the wavenumbers of ν(B-H$_t$) and ν(B-H$_b$) is thus as expected; however, much larger shifts have also been reported. Thus, in the IR spectrum of [R'B(μ-CCR$_3$)(μ-H)BR'] (R = SiMe$_3$, R' = CMe$_3$), which can be described as a 1,3-diboraalkyl system with a B-H-B bridge, a broad band at 1580 cm^{-1} was assigned to ν(B-H).[51] The spectroscopic measurements thus leave no doubt of the formation of a new binuclear boron hydride featuring terminal and bridging hydrogen atoms.

Crystals of **9** suitable for X-ray diffraction measurements were obtained from toluene/hexane solution. From the X-ray diffraction analysis, **9** can be identified unambiguously as the binuclear B(III) compound [H$_3$B$_2$(μ-hpp)$_2$]I that is formally the product of an oxidative addition of the B(II)B(II) unit. The molecular structure is shown in Figure 2.3.9.

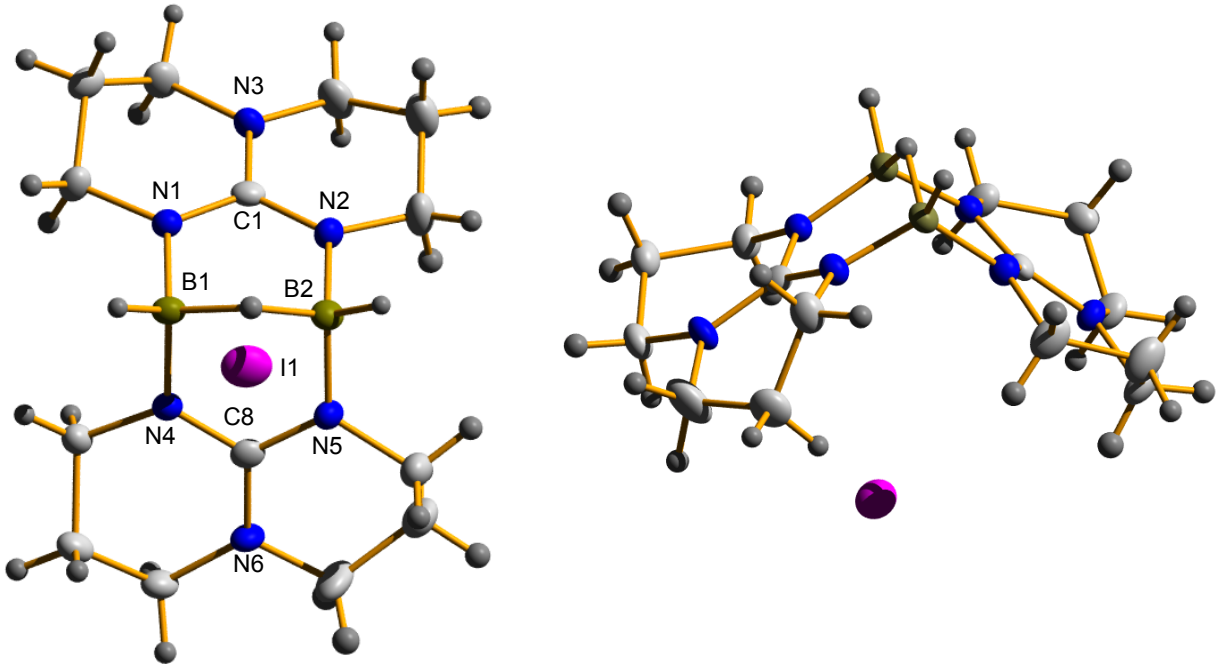

Figure 2.3.9: Molecular structure of $[H_3B_2(\mu\text{-hpp})_2]I$ **9** in the crystalline phase as determined by X-ray diffraction. The thermal ellipsoids are drawn at the 50% probability level. Selected bond distances (in pm) and angles (in degrees): B(1)-N(1) 150.2(4), B(1)-N(4) 152.3(4), B(2)-N(2) 152.1(4), B(2)-N(5) 150.6(4), B(1)···B(2) 222.9(4), N(1)-C(1) 134.3(4), N(2)-C(1) 134.3(3), C(1)-N(3) 134.6(4), N(4)-C(8) 133.9(3), N(5)-C(8) 134.0(3), C(8)-N(6) 133.9(3), B(1)-H_t 108(3), B(1)-H_b 134(3), B(2)-H_t 113(3), B(2)-H_b 128(3), N(1)-B(1)-N(4) 116.6(2), N(1)-C(1)-N(2) 116.3(2), N(2)-B(2)-N(5) 117.4(2), N(4)-C(8)-N(5) 116.3(2).

As already suggested on the basis of the NMR data (the number of *endo* and *exo* signals of the hpp group), the molecule again adopts a “roof-type” conformation. The B···B separation is 222.9(4) pm, and thus is considerably larger than in **8** (177.2(3) pm). It also is significantly larger than the value of 150.2 pm calculated for $B_2H_5^+$ (see Section 2.3.3.3, Table 2.3.1). The B-N bond lengths fall in the region 150.2(4)–152.3(4) pm, and are somewhat shorter that for **7** (156.2(4)–157.8(4) pm) and for **8** (156.3(3)–158.2(3) pm). The N-B-N bond angles (116.6(2)° and 117.4(2)°) are slightly larger than in **8** (111.04(15)° and 110.75(15)°). The separated iodide counterion is positioned below the cationic roof.

Table 2.3.1: Comparison between selected properties of $[B_2H_3(hpp)_2]^+$, $B_2H_5^+$ and B_2H_6.

	$[B_2H_3(hpp)_2]^+$		$B_2H_5^+$	B_2H_6
	exp.	calcd[a]	calcd[a]	calcd[a]
B···B [pm]	222.9(4)	221.9	150.2	176.6
B-H_t [pm]	108(3)/113(3)[b]	120.0	117.1	119.0
B-H_b [pm]	134(3)/128(3) [b]	132.1/131.7	133.5	131.6
ν(B-H_t) [cm^{-1}]	2425	2572[c]	2844[c]	2720/2616[c]
ν(B-H_b) [cm^{-1}]	1872	2050[c]	2220/1420[c]	2008/1718[c]
δ(H_t) [ppm]	3.44	3.89	4.48	4.55
δ(H_b) [ppm]	1.97	1.45	1.77	-0.49
$\delta(^{11}B)$ [ppm]	-2.2	-3.45	-11.26	16.01

[a] The energy-minimum structures were calculated at the B3LYP/6-31++G** level. The $\delta(^{11}B)$ and $\delta(^{1}H)$ chemical shifts were calculated at the DFT-GIAO//B3LYP/6-311+G* level. The $\delta(^{11}B)$ and $\delta(^{1}H)$ chemical shifts were referenced to $F_3B{\cdot}OEt_2$ and TMS, respectively. [b] Estimates from X-ray diffraction. [c] Unscaled values. For comparison, the experimentally observed wavenumbers for B_2H_6 are 2613/2518 cm^{-1} (ν(B-H_t)) and 1924/1615 cm^{-1} (ν(B-H_b)).

2.3.3.2 Synthesis and characterization of $[H_3B_2(\mu\text{-hpp})_2]Cl$

The $[H_3B_2(\mu\text{-hpp})_2]Cl$ **10** was obtained by reaction of **8** with HCl (see Scheme 2.3.6). The spectroscopic data (IR, NMR) confirmed formation of **10**. By realizing this reaction we could also prove the proposed reaction pathway for preparation of **9** (see Section 2.3.3.1, Scheme 2.3.3).

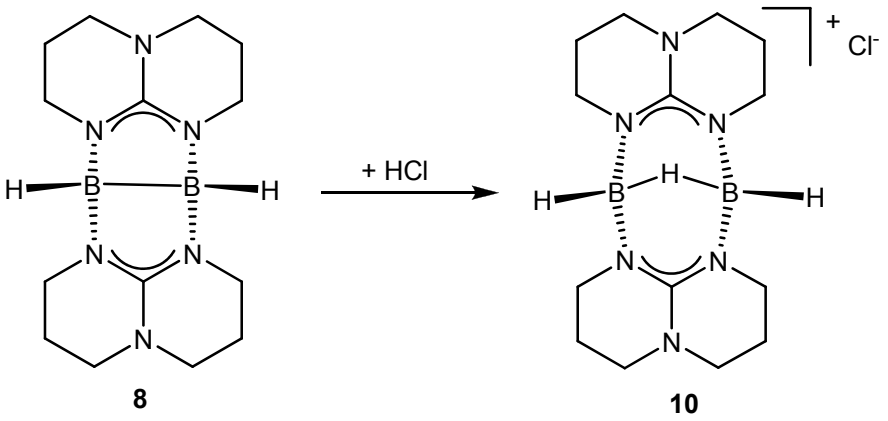

Scheme 2.3.6: Synthesis of compound **10**.

However, in addition to **10**, we obtained the salt [hppH$_2$]Cl **13** as a side product in considerable quantities, which arise from protonation and eliminaton of the hpp ligand in reaction similar to that in Scheme 2.3.7. Indeed, solutions of **9** or **10** in toluene are not stable for prolonged periods of time (several days); slow protonation of the hpp ligand was observed. In solid state, however, both $B_2H_5^+$ analogues are stable compounds.

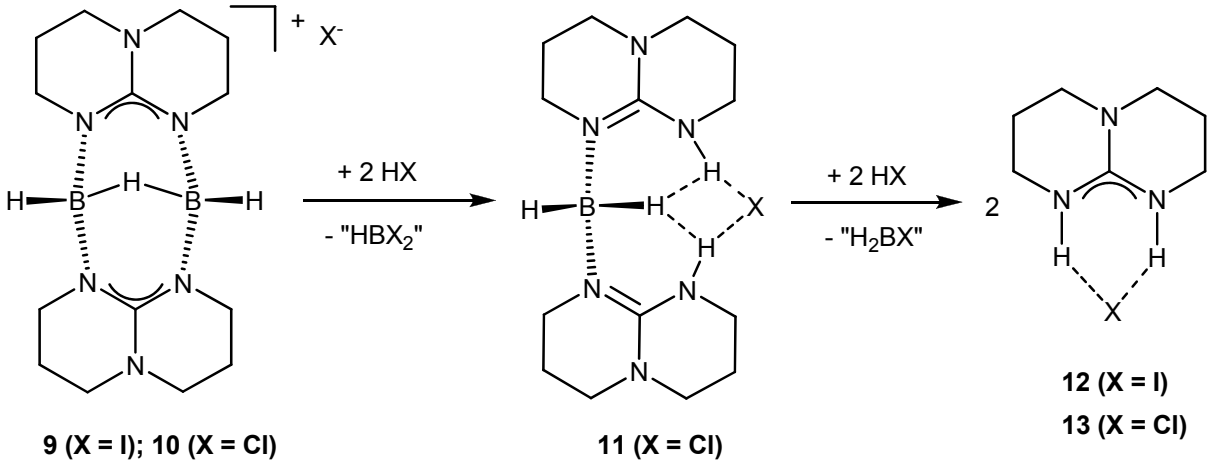

Scheme 2.3.7: Decomposition of compounds **9** and **10**.

We were able to crystallize an intermediate of this decomposition route, namely [$H_2B(hppH)_2$]Cl **11**, which can be described as a boronium cation with extended hydrogen bonding to the chloride ion (Figure 2.3.10). The remaining two B-N bond distances in **11** (156.8(4) and 155.6(4) pm) are considerably elongated with respect

to **9**. Thus decomposition is likely to occur according to Scheme 2.3.7. Both decomposition end-products, [hppH$_2$]I **12** and [hppH$_2$]Cl **13** (see Figure 2.3.11), were also structurally characterized. The hydrogen bonding network between the [hppH$_2$]$^+$ cations and the anions differs depending on the halide counterion.

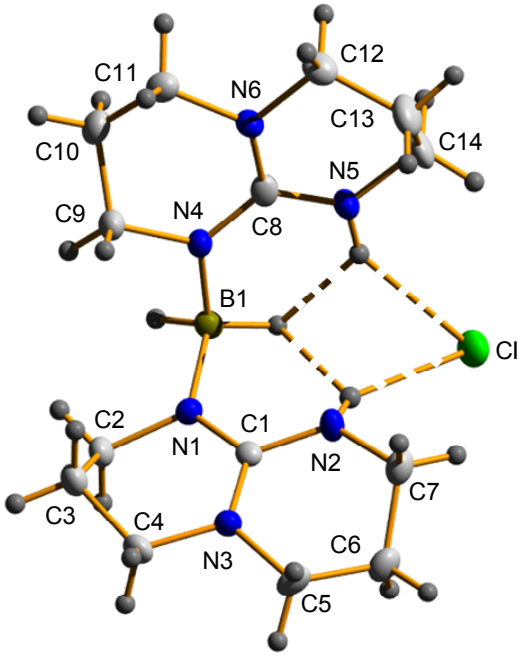

Figure 2.3.10: Molecular structure of [H$_2$B(hppH)$_2$]Cl **11** in the crystalline phase as determined by X-ray diffraction. The thermal ellipsoids are drawn at the 50% probability level. Selected bond distances (in pm) and angles (in degrees): B(1)-N(1) 156.8(4), N(1)-C(1) 134.6(3), N(2)-C(1) 134.7(4), N(3)-C(1) 135.2(4), N(1)-C(2) 147.5(4), B(1)-N(4) 155.6(4), N(4)-C(8) 134.2(4), N(5)-C(8) 134.0(4), N(6)-C(8) 134.9(4), N(4)-C(9) 146.8(4), C(2)-C(3) 151.5(4), C(3)-C(4) 151.4(4), C(9)-C(10) 151.6(4), C(10)-C(11) 149.3(4), C(4)-N(3) 146.0(4), N(3)-C(5) 146.3(4), C(11)-N(6) 146.2(4), N(6)-C(12) 145.9(4), C(5)-C(6) 151.1(4), C(6)-C(7) 150.5(4), C(7)-N(2) 144.9(4), C(12)-C(13) 151.3(4), C(13)-C(14) 150.4(4), C(14)-N(5) 145.9(4), B(1)···Cl(1) 408.7(4), N(5)···Cl(1) 324.7(3), N(2)···Cl(1) 316.8(3), N(1)-B(1)-N(4) 110.6(2), C(8)-N(4)-B(1) 126.8(3), N(4)-C(8)-N(5) 119.8(3), C(1)-N(1)-B(1) 123.6(2), N(2)-C(1)-N(1) 118.9(3).

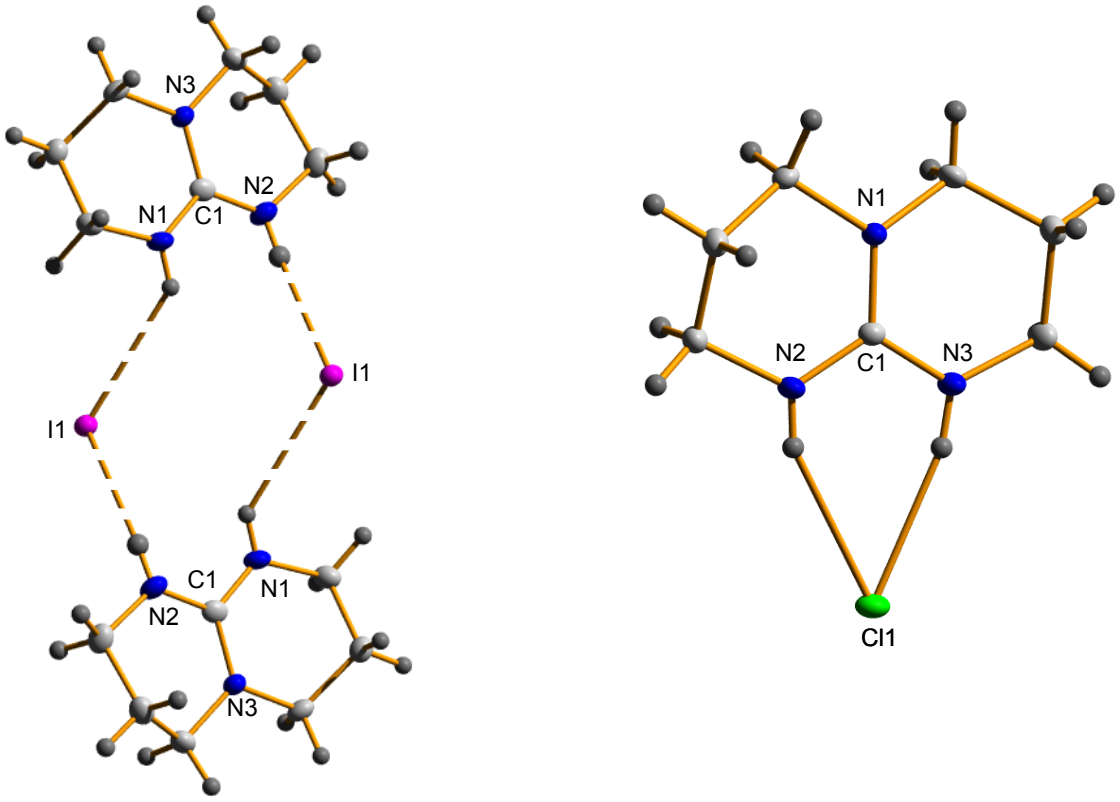

12 **13**

Figure 2.3.11: Molecular structures of $hppH_2I$ **12** and $hppH_2Cl$ **13** in the crystalline phase as determined by X-ray diffraction. The thermal ellipsoids are drawn at the 50% probability level. Selected bond distances (in pm) and angles (in degrees): $hppH_2I$ **12**: N(1)-C(1) 133.7(3), N(2)-C(1) 133.8(3), N(3)-C(1) 133.7(3), N(1)···I(1) 363.5(2), N(2)···I(1) 357.6(2), I(1)···I(1) 465.2(1), N(1)-C(1)-N(2) 118.31(19), N(1)-C(1)-N(3) 120.35(19), N(3)-C(1)-N(2) 121.31(18), I(1)···N(1)-C(1) 133.48(13); $hppH_2Cl$ **13**: N(1)-C(1) 133.40(10), N(2)-C(2) 134.38(10), N(3)-C(1) 133.67(10), N(2)-C(1)-N(3) 117.68(7), N(2)-C(1)-N(1) 121.22(7), N(3)-C(1)-N(1) 120.97(7).

2.3.3.3 Quantum chemical studies

As already mentioned, the protonation of the B-B bond in **8** lead up to the $B_2H_5^+$ analogue $[H_3B_2(\mu\text{-hpp})_2]^+$. Because of the scarceness of experimental information, the $B_2H_5^+$ was the subject of several quantum-chemical calculations.[52] These calculations found a global energy minimum structure with three bridging hydrogen atoms (see Scheme 2.3.8). The geometry of $[H_3B_2(\mu\text{-hpp})_2]^+$ is similar to

that of $B_2H_5^+$ only if two bridging hydrogen atoms are replaced by two hpp units (see Scheme 2.3.8).

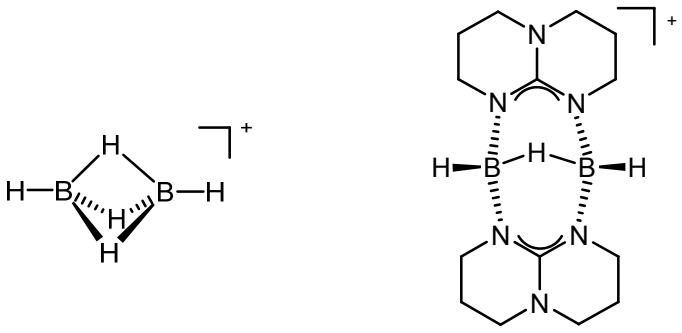

$B_2H_5^+$ $[H_3B_2(\mu\text{-hpp})_2]^+$

Scheme 2.3.8

As already mentioned, the B···B separation in **9** (222.9(4) pm) is significantly larger than the value of 151.8 pm calculated with QCISD(T)/6-311G**,[52c] or 150.2 pm calculated herein for $B_2H_5^+$. The isolation of compound **8** with a short B-B bond shows that the large distance is not necessarily caused by the presence of the hpp ligands. To obtain further information about the bond properties, we calculated the electron density distribution in $[H_3B_2(\mu\text{-hpp})_2]^+$ and compared the results with the parent compound $B_2H_5^+$. An analysis of the topology of the electron distribution has previously been applied successfully for the analysis of other boron hydrides with multicenter bonds, such as B_2H_6.[53] Figure 2.3.12 shows the topology of the electron density for $[H_3B_2(\mu\text{-hpp})_2]^+$, $B_2H_5^+$ and B_2H_6. The bond critical points are also shown. The agreement between the electron densities determined for B_2H_6 at the bond critical points (see Figure 2.3.12) with those obtained previously experimentally[53] is very good, and shows that the applied level theory yields reasonable results.

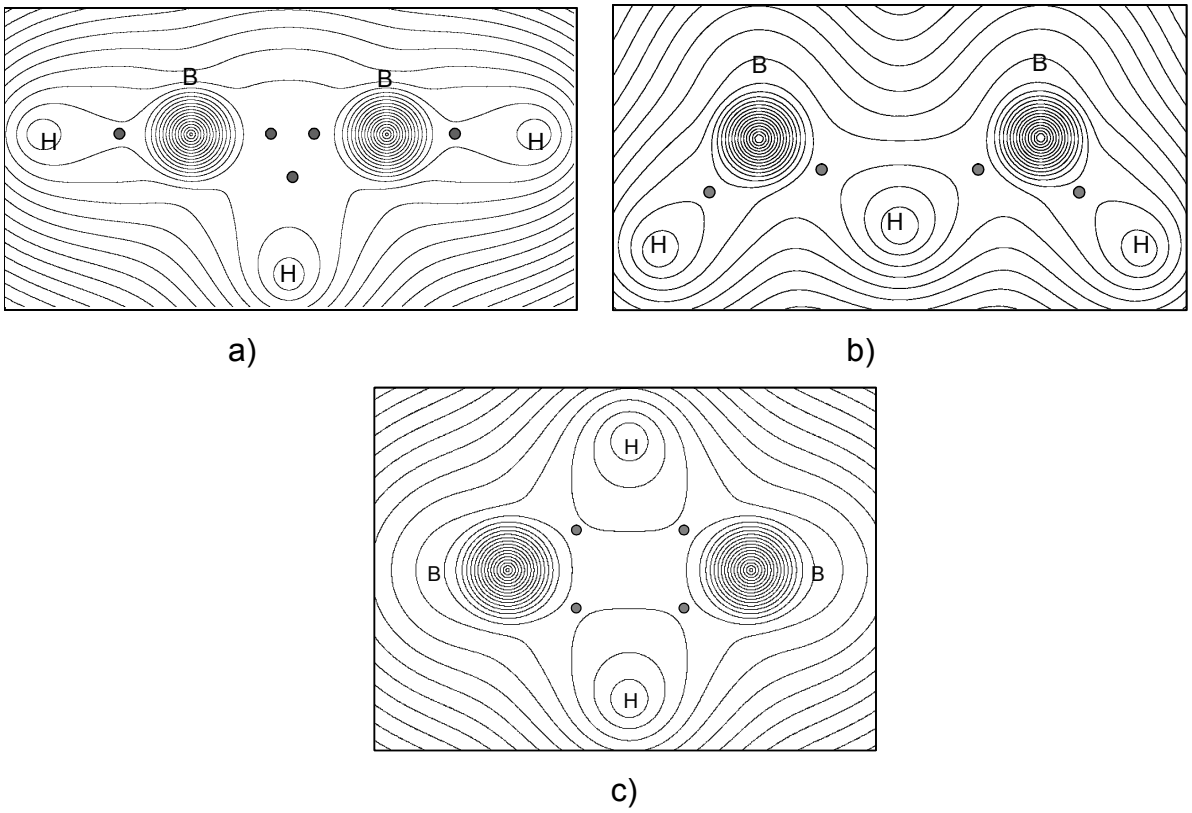

Figure 2.3.12: Topology of the electron density distribution of a) $B_2H_5^+$, b) $[H_3B_2(\mu\text{-hpp})_2]^+$, and c) B_2H_6. Electron density (in e$Å^{-3}$) at the bond critical points: $B_2H_5^+$: B-H_b 1.07, B-H_t 1.36. $[H_3B_2(\mu\text{-hpp})_2]^+$: B-$H_b$ 0.77, B-H_t 1.23. B_2H_6: B-H_b 0.84, B-H_t 1.24.

It can be seen that the B-H-B bonding in B_2H_6 and the $[H_3B_2(\mu\text{-hpp})_2]^+$ cation can be described as three-center two electron bonds, whereas the bonding in $B_2H_5^+$ involves the five centers (both boron atoms and all three bridging hydrogen atoms). Apart from their bonding properties, compounds **9** and **10** could be attractive protonation reagents, and **8** might be an interesting complex ligand. The protonated forms **9** and **10** serve as smallest possible model systems for the bonding situation in such complexes.

In summary, two binuclear boron hydrides $[H_2B(\mu\text{-hpp})]_2$ **7** and $[HB(\mu\text{-hpp})]_2$ **8** have been synthesized by reacting hppH and $H_3B{\cdot}NMe_3$ at 115°C in toluene solution without and in presence of $[Rh(1,5\text{-COD})Cl]_2$ precatalyst, respectively, which were structurally characterized (see Scheme 2.3.9). The X-ray analysis indicates that both species contain two guanidinate (hpp) bridges with a $\kappa^1N\text{-}\kappa^2N'$-coordination mode.

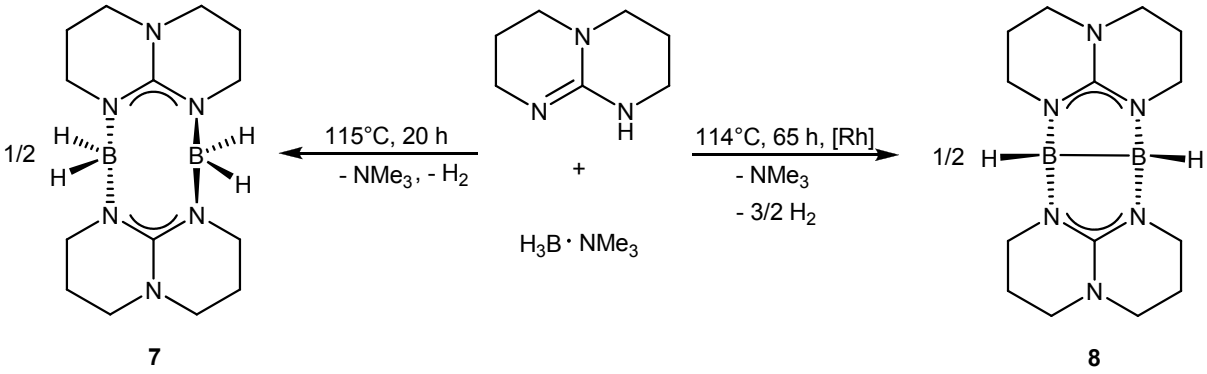

Scheme 2.3.9: Synthesis of compounds **7** and **8**.

Further (reductive) catalytic dehydrogenation of $[H_2B(\mu\text{-hpp})]_2$ **7** leads also to binuclear B(II) hydride $[HB(\mu\text{-hpp})]_2$ **8** which futures a B-B single bond measuring 172.2(3) pm and a *cis*-bent arrangement of the H-B-B-H fragment. Furthermore, $[HB(\mu\text{-hpp})]_2$ undergoes a redox reaction in the course of which the B(II)-B(II) bond is broken and the boron atoms are oxidized to B(III). Thus reaction of $[HB(\mu\text{-hpp})]_2$ **8** with HX (X = I^- or Cl^-) leads to $[H_3B_2(\mu\text{-hpp})_2]^+X^-$ (see Scheme 2.3.10), being an example for a stable $B_2H_5^+$ analogue. Quantum chemical calculations were carried out to analyse the bond properties in the cationic binuclear B(III) hydride $[H_3B_2(\mu\text{-hpp})_2]^+$.

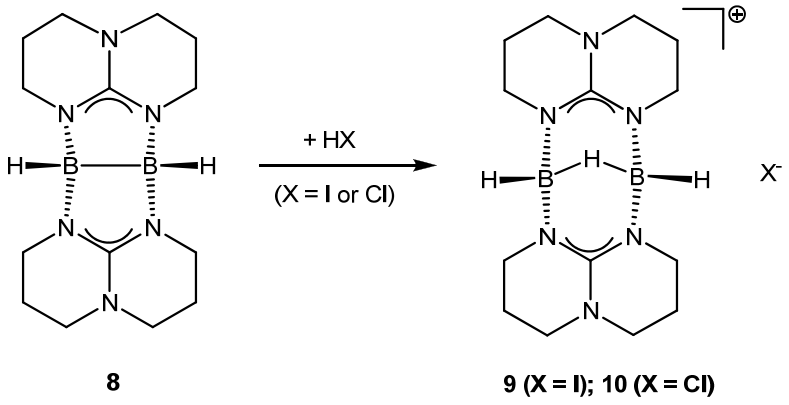

Scheme 2.3.10: Synthesis of compounds **9** and **10**.

2.4 Synthesis and characterization of new binuclear boron monocation containing three bridging guanidinate (hpp) ligands

2.4.1 Synthesis and characterization of $[Cl_2B_2(\mu\text{-hpp})_3]BCl_4$

We showed in Section 2.1.1 that reaction between $H_3B{\cdot}NMe_3$ and hppH afforded $hppH{\cdot}BH_3$, which can be dehydrogenated to give $[H_2B(\mu\text{-hpp})]_2$ (see Section 2.2.2.1) and $[HB(\mu\text{-hpp})]_2$ (see Section 2.3.2). These two species could also be prepared directly from the $H_3B{\cdot}NMe_3$/hppH reactions without and in presence of precatalyst, respectively (see Sections 2.3.1 and 2.3.2, and Scheme 2.3.9).

Here we are going to describe the reaction between BCl_3 and hppH, which at first glance we supposed that will precede similarly as the reaction between $Me_3N{\cdot}BH_3$ and hppH. However, the experiments showed that the product of this reaction is the binuclear species $[(Cl_2B_2(\mu\text{-hpp})_3]BCl_4$ **14**, (see Scheme 2.4.1), with three instead of two bridging hpp units. In addition $[hppH_2]Cl$ is formed as formulated in Scheme 2.4.1. Attempts to separate the boron containing product from this salt were unfortunately only partially successful. The ^1H NMR spectrum of compound **14** shows that the protons from hpp unit are not equivalent. In the ^{11}B NMR spectrum two singlet signals at δ = 4.5 ppm and 6.9 ppm, in a region typical for tetra-coordinated B(III) species, are observed. Of these, the signal at $\delta(^{11}B)$ = 6.9 ppm can be assigned unambiguously to the BCl_4^- anion and $\delta(^{11}B)$ = 4.5 ppm to the boron from the cationic unit.

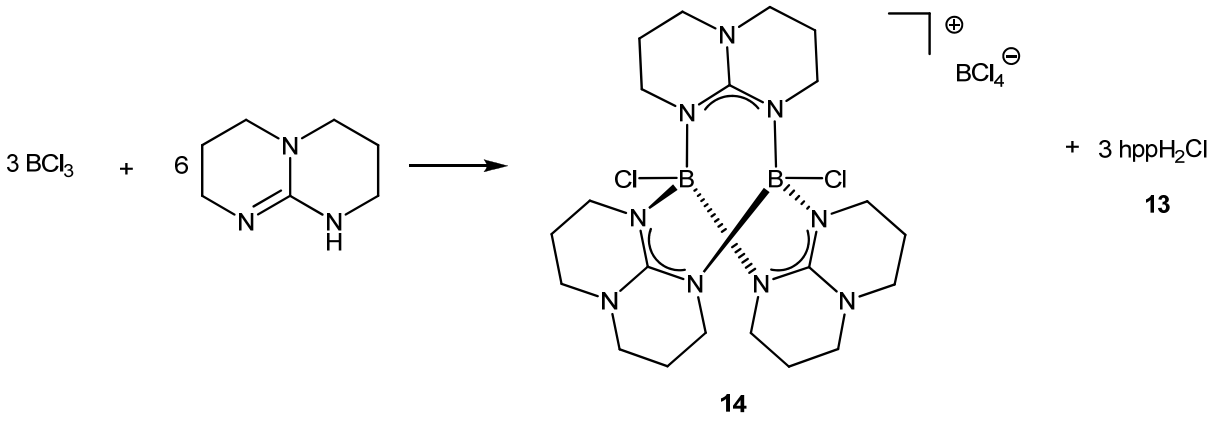

Scheme 2.4.1: Synthesis of compound **14**.

Colourless crystals of **14** suitable for X-ray diffraction measurements were grown from dichloromethane/hexane (2:1) mixture at 3°C. Figure 2.4.1 visualizes the molecular structure as derived from the XRD analysis. The molecule features an almost linear Cl-B···B-Cl unit. An interesting detail is the presence of chiral molecules in the solid state due to the screw-type arrangement of the hpp groups around the Cl-B···B-Cl axis. The B···B separation amounts to 290.1 pm, a value which clearly rules out any significant direct bonding. The B-N bond distances cover the region 152.6(6)-153.9(6) pm, and the N-B-N bond angles were determined to be 111.8(4)-114.3(4)°.

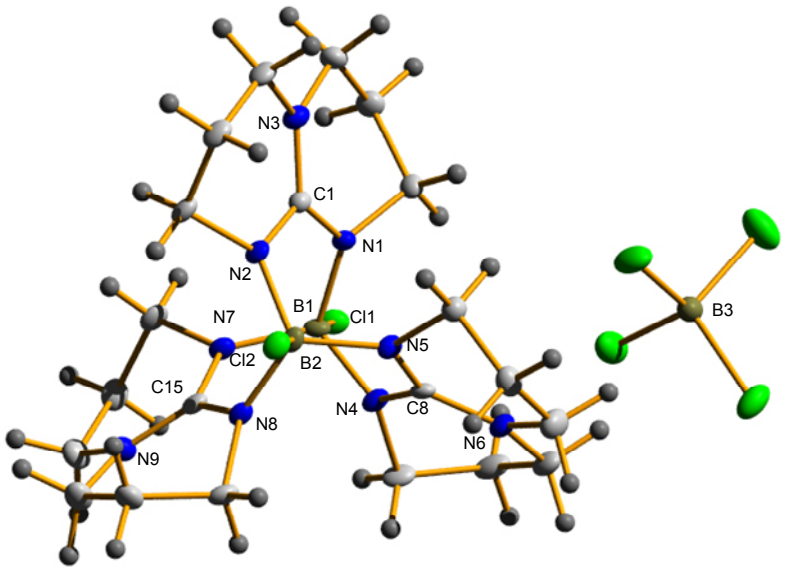

Figure 2.4.1: Molecular structure of $[Cl_2B_2(\mu\text{-hpp})_3]BCl_4$ **14** in the crystalline phase as determined by X-ray diffraction. The thermal ellipsoids are drawn at the 50% probability level. Selected bond distances (in pm) and angles (in degrees): B(1)···B(2) 290.1, B(1)-Cl(1) 192.4(5), B(1)-N(1) 153.6(6), B(1)-N(4) 153.3(6), B(1)-N(7) 153.0(7), B(2)-Cl(2) 194.1(5), B(2)-N(2) 153.9(6), B(2)-N(5) 152.6(6), B(2)-N(8) 153.0(7), N(1)-C(1) 135.4(6), N(2)-C(1) 134.6(6), C(1)-N(3) 133.2(6), N(4)-C(8) 134.0(6), N(5)-C(8) 134.0(6), C(8)-N(6) 134.7(6), N(7)-C(15) 134.4(6), N(8)-C(15) 135.1(6), C(15)-N(9) 147.2(6), Cl(1)-B(1)-N(1) 106.3(3), Cl(1)-B(1)-N(4) 106.5(3), Cl(1)-B(1)-N(7) 105.9(3), Cl(2)-B(2)-N(2) 105.8(3), Cl(2)-B(2)-N(5) 105.9(3), Cl(2)-B(2)-N(8) 105.9(3), N(1)-B(1)-N(4) 112.0(4), N(1)-B(1)-N(7) 113.5(4), N(4)-B(1)-N(7) 111.9(4), N(2)-B(2)-N(5) 112.4(4), N(2)-B(2)-N(8) 111.8(4), N(5)-B(2)-N(8) 114.3(4), N(1)-C(1)-N(2) 118.4(4), N(7)-C(15)-N(8) 119.5(4), N(4)-C(8)-N(5) 118.8(4).

Similar structures were found for pyrazolyl (pz) ligands. Tripyrazolylborate anions $[RB(pz)_3]^-$[39] have been used for a long time as versatile ligands for the synthesis of dinuclear complexes featuring three bridging pz units.[61] Examples which can be directly compared with **14** are provided by the cations of the salts $[HB\{Me_2C_3N_2H\}_3BH]^+[TaCl_6]$[62] and $[EtB(pz)_3BEt]^+[PF_6]^-$.[63] Therein the two B atoms are separated by 267.7(2) and 270.4(1) pm, and the B-N bond distances and N-B-N bond angles are in the range of 145.7(3)-164.8(3) and 155.0(1)-159.6(1) pm, and 98.59(8)-108.56(9)° and 101.13(4)-104.04(4)°, respectively. With 290.1 pm the B···B separation in **14** is significantly lager than in these compounds featuring pz bridges. The B-N bond distances and N-B-N bond angles are in the range of 152.7(5)-153.9(5) and 111.8(3)-114.3(3)° in **14**.

In summary, we showed that the reaction between BCl_3 and hppH proceeds differently to that between $Me_3N{\cdot}BH_3$ and hppH. Although in both cases binuclear complexes are formed, three guanidinate (hpp) bridges are present in the product of the BCl_3/hppH reaction and only two in that of the $Me_3N{\cdot}BH_3$/hppH reaction. While a plausible suggestion for the $Me_3N{\cdot}BH_3$/hppH reaction mechanism was worked out on the basis of the experimental results in alliance with quantum chemical calculations (see chapter 2.2), the BCl_3/hppH reaction mechanism or even pathway is much more difficult to understand, and more experiments are necessary. In addition, the synthesis of $[Cl_2B_2(\mu\text{-hpp})_3]^+$ opens up the question if it is possible to prepare the mononuclear anionic species $[ClB(hpp)_3]^-$, which might be an interesting complex ligand comparable to Trofimenko's $[BR(pz)_3]^-$ (pz = pyrazolyl) anions.

2.5 Synthesis and characterization of new binuclear boron di- and monocations containing two bridging guanidinate (hpp) ligands

Sections 2.5.1–2.5.3 are devoted to the synthesis and characterization of binuclear B(II) di- and monocations with bridging guanidinate hpp ligands. The experimental results are accompanied by theoretical calculations. Afterwards, we show in section 2.5.4 the experimental results obtained for the thermal reactions of binuclear B(II) compounds $[\{Me_2(H)N)B(\mu\text{-hpp})\}_2]_2X_2$ (where X = Cl^-, OTf^- and $[B(C_6F_5)_4]^-$).

2.5.1 Synthesis and characterization of $[\{(Me_2(H)N)B(\mu\text{-hpp})\}_2]Cl_2$

Here is represented the synthesis and characterization of the compound $[\{(Me_2(H)N)B(\mu\text{-hpp})\}_2]Cl_2$ **15** (hpp = 1,3,4,6,7,8-hexahydro-2*H*-pyrimido[1,2-a]pyrimidate), which is the first example for a new class of dimeric cationic B(II) species. The surprisingly simple synthesis of **15** involves treating of diborane(4) $B_2Cl_2(NMe_2)_2$, prepared from $B_2(NMe_2)_4$,[54] with two equivalents of the free base hppH (see Scheme 2.5.1).

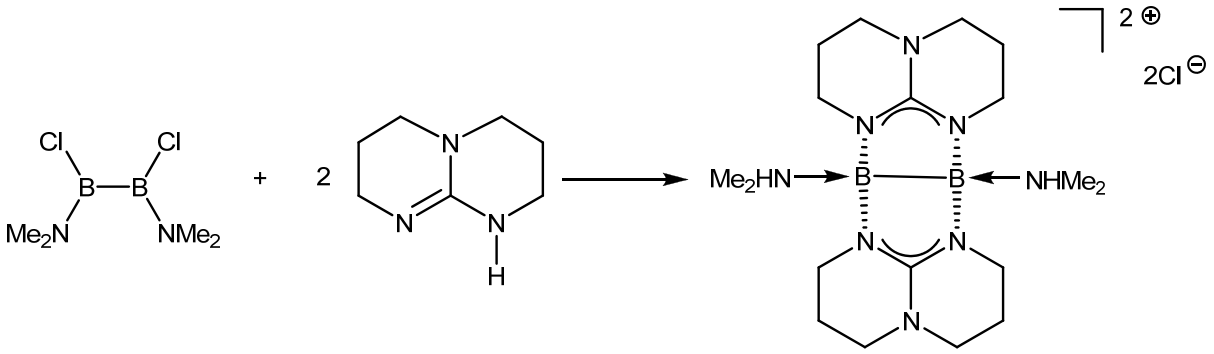

15

Scheme 2.5.1: Synthesis of compound **15**.

Presumably, the doubly base-stabilized diborane(4) species $[(Me_2N)B(\mu\text{-hpp})]_2$ **15A** forms initially, which then reacts with the released HCl to form the salt **15**. The hpp ligands stabilize the dinuclear species and protect it from oxidation or disproportionation. This compound was characterized by various spectroscopic

methods. The ^{1}H NMR spectrum of **15** which is represented in Figure 2.5.1 indicates a “roof-type” conformation of {$B_2(\mu$-hpp$)_2$} group (which contain *endo* and *exo* hydrogen atoms). The large shift for the N-H hydrogen atom of the NMe_2H groups is 8.90 ppm which indicates that the N-H···Cl contacts are present in solution. For comparison, a chemical shift of δ(^{1}H) = 5.5 ppm was obtained for the corresponding signal in the adduct $H_3B{\cdot}NMe_2H$.[55] The ^{11}B NMR spectrum gives evidence for a broad singlet at δ(^{11}B) = 1.43 ppm (see Figure 2.5.1).

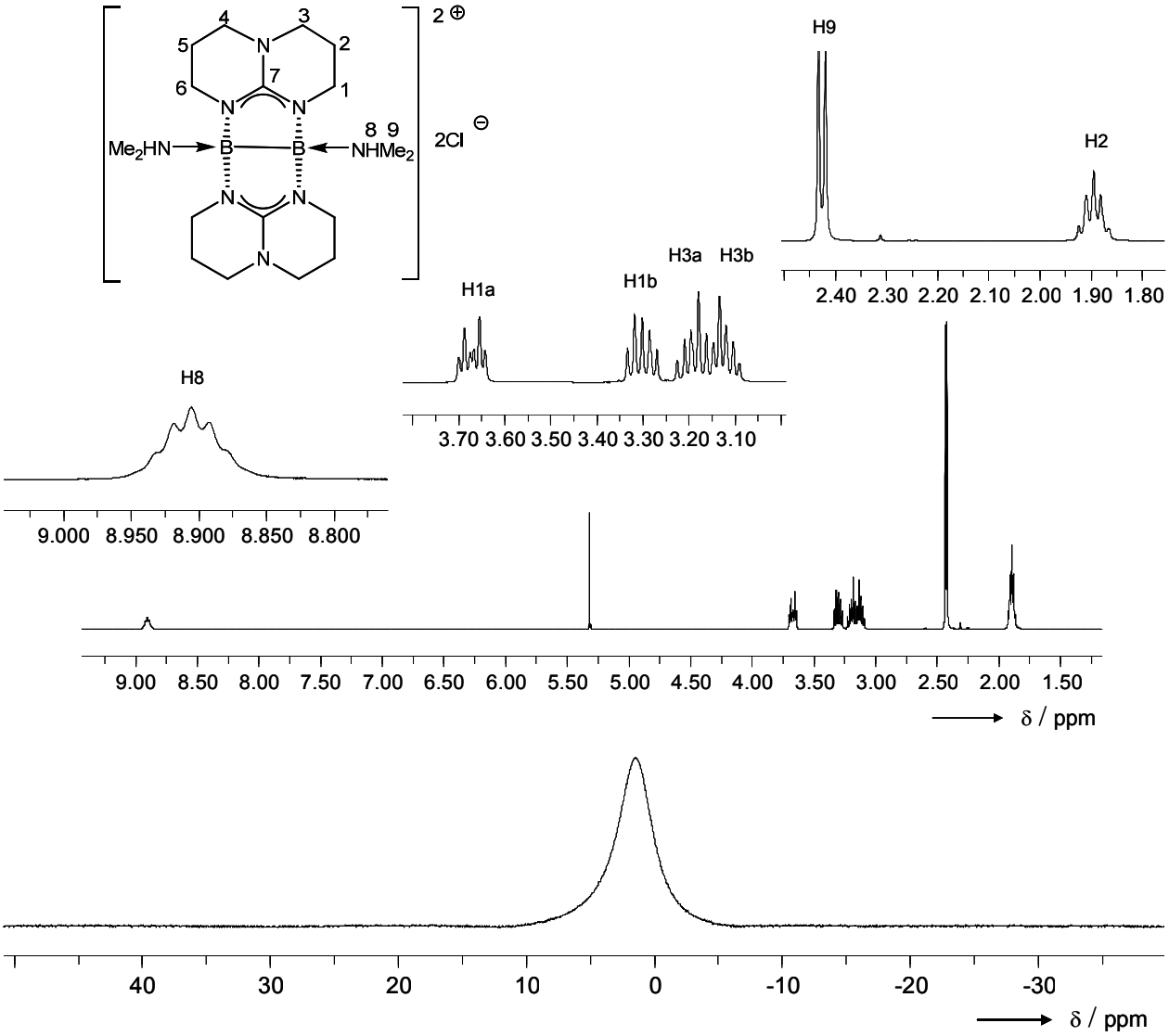

Figure 2.5.1: ^{1}H NMR spectrum (400 MHz, CD_2Cl_2); ^{11}B NMR spectra (128.3 MHz, CD_2Cl_2) for **15**.

Compound **15** was crystallized as a dichloromethane solvate from a mixture of dichloromethane/hexane solution at room temperature. The structure of **15** as determined by X-ray diffraction measurements and some selected bond length and angles are given in Figure 2.5.2. Similar to **8**, the **15** compound contain also the $\{B_2(\mu\text{-hpp})_2\}$ core where the hpp groups adopt a bridging $\kappa^1N\text{–}\kappa^2N'$-coordination mode. The B-B bond (174.6(4) pm) lies well within the range of typical B-B single bonds. For example, gas-phase electron diffraction measurements of $B_2(NMe_2)_4$ and $B_2(OMe)_4$ gave B-B bond lengths of 176.2(1.1) and 172.0(6) pm, respectively.[47] For comparison, in case of **8** and $[\{Me_2(H)N)B(\mu\text{-tbn})\}_2]Cl_2$, the B-B bond distance is slightly larger (177.2(3) pm) (see Figure 2.3.5) and significantly larger (180.1(5) pm)[6] than in **15** (174.6(4) pm), respectively.

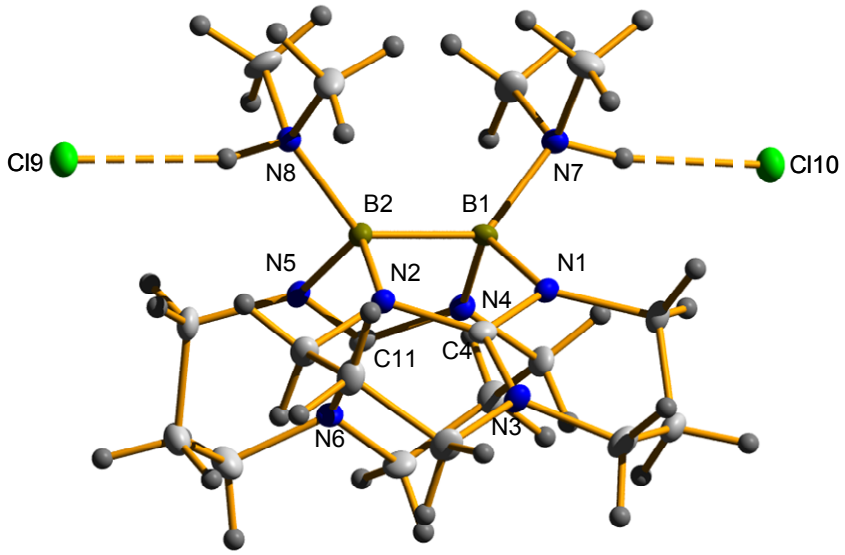

Figure 2.5.2: Molecular structure of $[\{(Me_2(H)N)B(\mu\text{-hpp})\}_2]Cl_2$ **15** derived from X-ray diffraction. The thermal ellipsoids are drawn at the 50% probability level. Selected bond distances (in pm) and angles (in degrees): B(1)-N(1) 155.1(4), B(1)-N(4) 155.2(4), B(1)-N(7) 160.1(4), B(1)-B(2) 174.6(4), B(2)-N(2) 153.9(4), B(2)-N(5) 154.3(4), B(2)-N(8) 160.6(4), C(4)-N(1) 134.4(3), C(4)-N(2) 133.9(3), C(4)-N(3) 134.5(3), C(11)-N(4) 134.5(3), C(11)-N(5) 134.9(3), C(11)-N(6) 133.8(4), N(7)-H(7) 100.08, N(8)-H(8) 89.07, N(1)-B(1)-N(4) 111.8(2), N(2)-B(2)-N(5) 112.2(2), N(2)-C(4)-N(1) 115.2(2), N(4)-C(11)-N(5) 115.0(2), N(7)-B(1)-B(2) 130.7(2), N(8)-B(2)-B(1) 130.1(2).

The B-N bonds to the hpp ligands in **15** are 153.9(4)-155.2(4) pm long, and the bonds to the two NMe_2H groups have lengths of 160.1 and 160.6 pm. For comparison, the B-$N_{guanidine}$ bond distances in **8** and [{$Me_2(H)N)B(\mu$-tbn)}$_2$]Cl_2 fall within the range 156.3(3)-158.2(3) pm (see Figure 2.3.5) and 154.9(4)-155.5(4) pm[6], respectively, and the bonds to two NMe_2H ligands in [{$(Me_2(H)N)B(\mu$-tbn)}$_2$]Cl_2 have lengths of 160.2(4) and 159.8(4).[6] The B-$NHMe_2$ bond lengths are similar to those reported for amine adducts of BH_3. In $H_3B{\cdot}NH_3$,[22] $H_3B{\cdot}NMe_3$[56] and H_3B·quinuclidine,[13] B-N bonds of 156.4, 161.6 and 160.8 pm, respectively, were measured in the solid state. The two boron atoms and the four hpp nitrogen atoms that are directly bound to boron in **15** form the vertices of a trigonal prism with N-B-N angles of approximately 112°. In the solid state, the dications are packed in such a way that large channels form, which are filled with the chloride ions and dichloromethane (five molecules per dication). The chloride ions are involved in hydrogen bonding with the hydrogen atoms of the two $NHMe_2$ groups in **15** (*d*(Cl···H) = 210, 225 pm or 209, 213 pm when normalized N-H bonds (101 pm) are used). Furthermore, somewhat weaker hydrogen bonds are present between the chloride ions and the hydrogen atoms of the dichloromethane molecules (*d*(Cl···H) = 255–268 pm, or 246–260 pm when normalized C-H bonds (108 pm) are used). The observation of a signal in the ESI spectra for **15**+$(CH_2Cl_2)_5$ (*m/z* (%) = 881.8 for $[C_{23}H_{46}B_2N_8Cl_{12}]^+$) shows how significant these interactions are (see Figure 2.5.3).

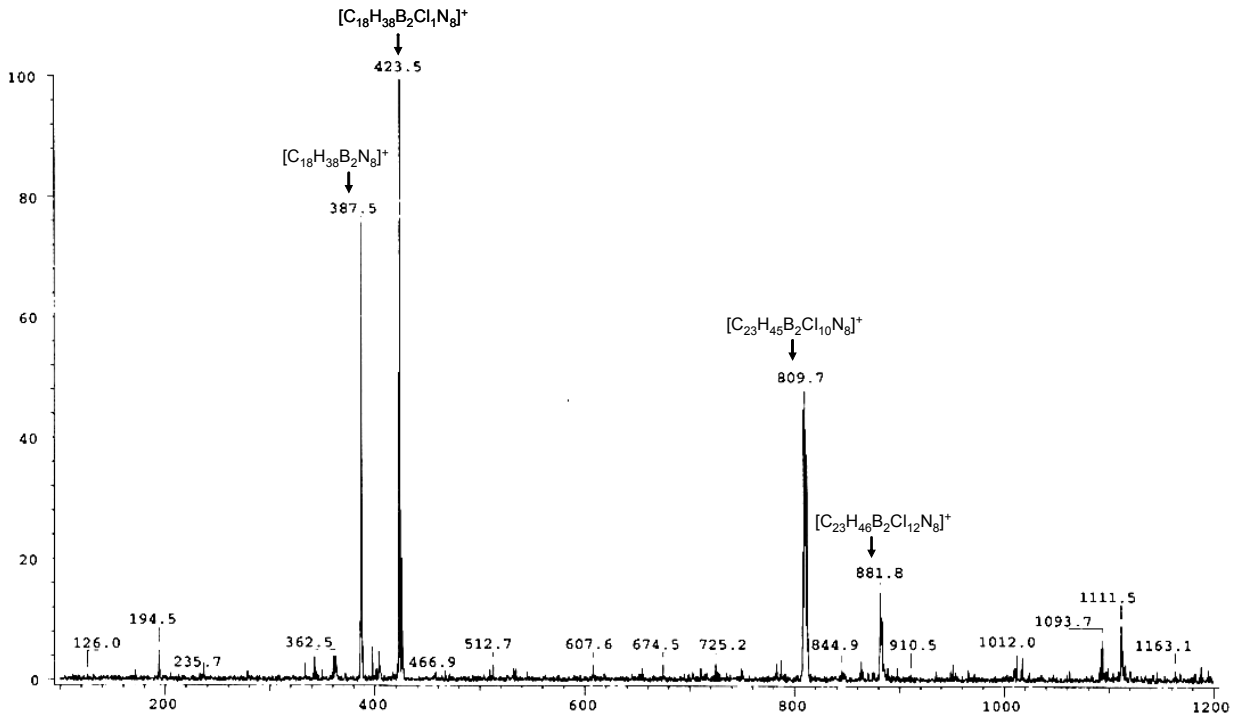

Figure 2.5.3: ESI spectrum of compound **15**.

The compound melts at 226°C, but partial decomposition is observed below this temperature. A thermo-gravimetric analysis showed that **15** (without the co-crystallized CH_2Cl_2) lose in two steps ca. 20 % of its weight. These steps reach their turning points at 138 and 197°C (see Figure 2.5.4).

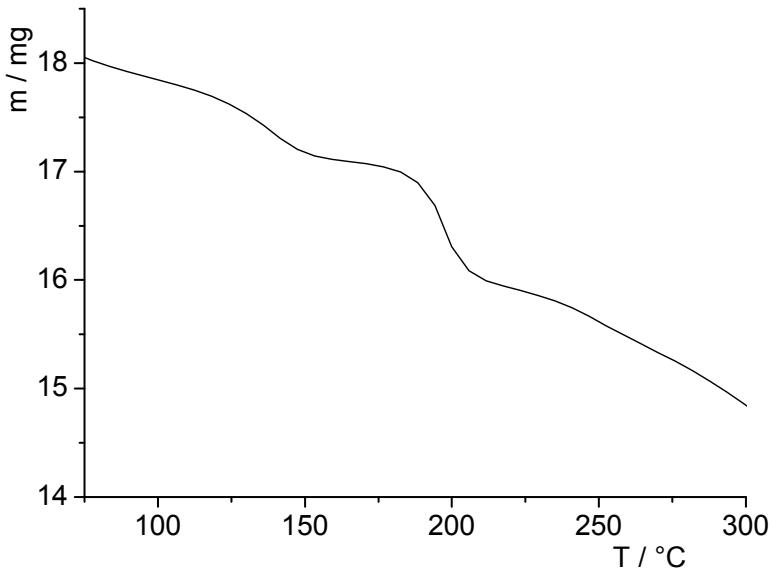

Figure 2.5.4: Thermo-gravimetric curve (10 K / min) for compound **15**.

The mass loss for the combined two steps is in agreement with the expected loss for removal of the two $NHMe_2$ groups from **15**.

The binuclear B(II) dication $[\{B(\mu\text{-hpp})\}_2]^{2+}$ of **15** has been characterized not only by spectroscopic techniques and XRD measurements but also DFT calculations have been carried out.[15] From this calculations a C_2-symmetric energy minimum was found for the $[\{B(\mu\text{-hpp})\}_2]^{2+}$ ion. Two of the canonical frontier orbitals show significant B-B bonding contributions. Localization of the orbitals confirmed the existence of a purely B-B bonding orbital (see Figure 2.5.5).

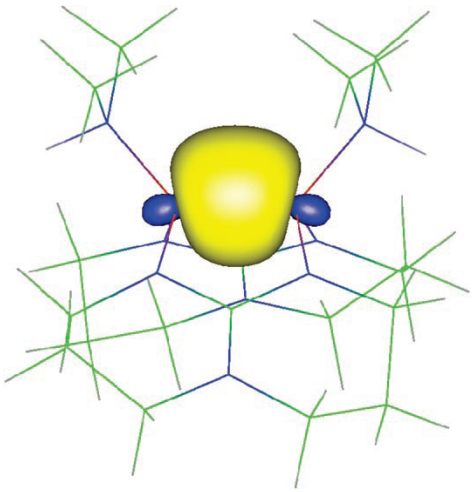

Figure 2.5.5: Illustration of the localized B-B bonding orbital of the $[\{B(\mu\text{-hpp})\}_2]^{2+}$ ion. N blue, C green, H gray.

The calculations also shed light on the B-NMe_2H bond strength. For the removal of both NMe_2H groups from **15** to give the $[\{B(\mu\text{-hpp})\}_2]^{2+}$ ion (see Figure 2.5.6), an energy change without and with zero-point vibrational energy (ZPE) corrections of +248 and + 227 kJ mol^{-1}, respectively, was calculated. The value of ΔG^0 (at 298 K and 1 bar) is +127 kJ mol^{-1}. For comparison, NH_3 elimination from the simple model boronium ion $[B(NH_2)_2(NH_3)_2]^+$ has values of +259, +231, and +153 kJ mol^{-1} for ΔE, ΔE_{ZPE}, and ΔG^0, respectively (see Figure 2.5.6). The dissociation energies for the first and second NH_3 molecules in $[B(NH_2)_2(NH_3)_2]^+$ ion were calculated to be 34 and 225 kJ mol^{-1}, respectively (adding up to 259 kJ mol^{-1}) and are thus very different. In previous restricted Hartree-Fock (RHF) calculations,[57] the dissociation energy of $[B(NH_2)_2(NH_3)]^+$ was estimated to be 231 kJ mol^{-1}, a value which agrees well with our

estimate. Our calculations predict that the $[\{B(\mu\text{-hpp})\}_2]^{2+}$ ion has an almost planar central $N_2B_2N_2$ unit with a B-B bond length of 161.9 pm. As illustrated in Figure 2.5.6, the borinium ion $[B(NH_2)_2]^+$ has a D_{2d} ground-state geometry featuring B-N and N-H bond lengths of 133.7 and 102.2 pm, and H-N-H angles of 113.8°.

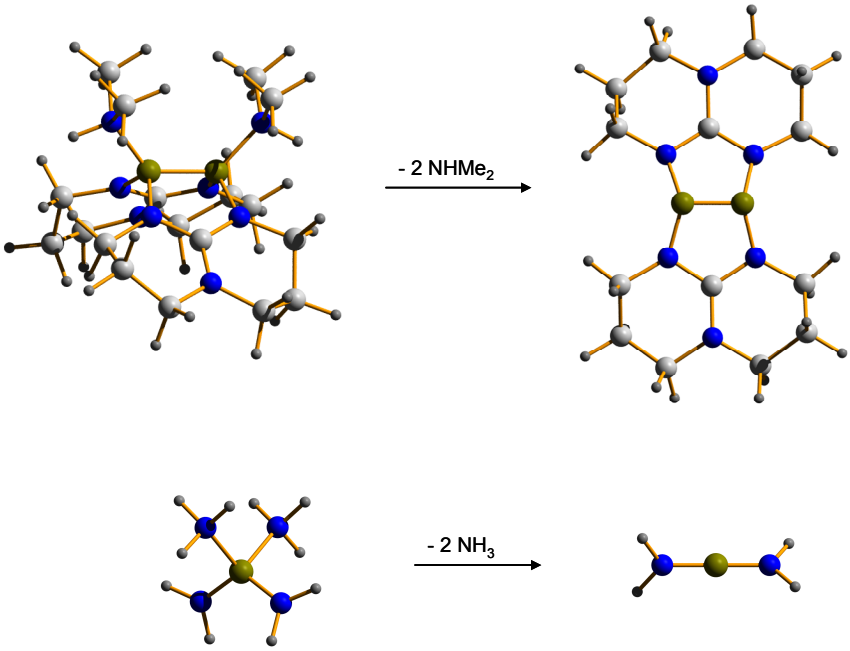

Figure 2.5.6: Calculated structure of $[\{B(\mu\text{-hpp})\}_2]^{2+}$ and $[\{B(NH_2)\}_2]^{2+}$ and the products of their reactions with two equivalents of an amine base.

2.5.2 Synthesis and characterization of $[(Me_2N)B_2(\mu\text{-hpp})_2(NHMe_2)]Cl$ and $[ClB_2(\mu\text{-hpp})_2(NHMe_2)]Cl$

As already we mentioned in section 2.5.1, the synthesis of **15** proceeds in two steps via the bisamide intermediate $[(Me_2N)B(\mu\text{-hpp})]_2$ **15A**. In Scheme 2.5.2 is shown the synthesis of **15A** from a reaction of $B_2Cl_2(NMe_2)_2$ with Li(hpp). This species turned out to be extremely reactive, and we were unfortunately not able to characterize it in detail by spectroscopic methods.

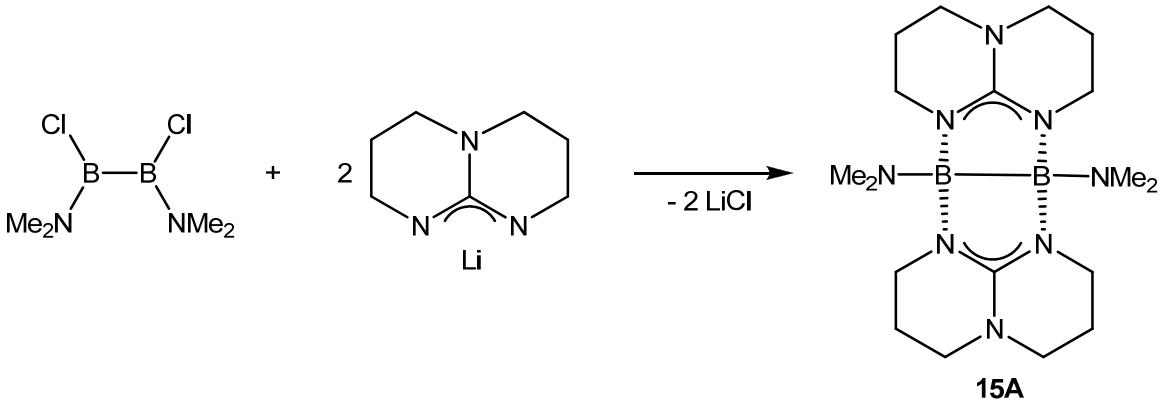

Scheme 2.5.2: Synthesis of compound **15A**.

For this reason, quantum chemical calculations were performed to characterize **15A**.[15] The resulting minimum structure and some selected bond parameters are represented in Figure 2.5.7 and Table 2.5.1, respectively.

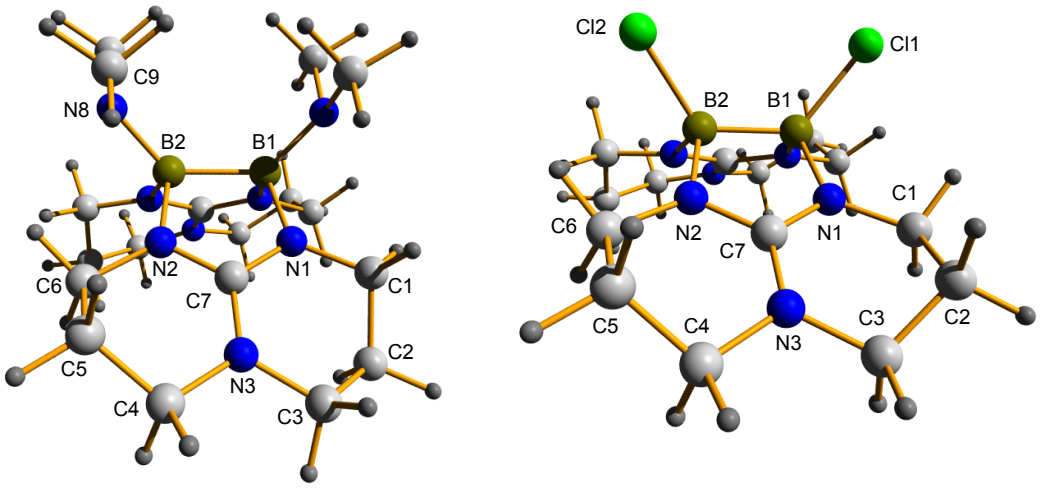

15A **18**

Figure 2.5.7: Illustration of the structures from quantum chemical calculations of **15A** and **18**.

The calculated structure (Figure 2.5.7, **15A**) look like that of the previously characterized [HB(μ-hpp)]$_2$, **8** (see section 2.3.2). Similar to the structure of **15**, the characteristic feature is a slightly distorted trigonal prismatic central B_2N_4 unit. The B-B bond in **8** (177.2(3) pm) and **15** (174.6(4) pm) are in typical region for B-B single

bonds, so that **15A** should also exhibit such a bond, in agreement with the results of the calculations suggesting a B-B bond distance of 179.7 pm.

Table 2.5.1: Selected Bond distances (in pm) and angles (in degrees) as calculated for **15A** and **18**.

	15A	**18**		**15A**	**18**
B1-B2	179.7	173.1	N4-C8	134.3	134.9
B1-N1	159.2	156.2	N5-C8	134.3	134.7
B2-N2	159.6	156.2	C8-N6	137.2	136.5
B1-N4	159.6	156.4	B1-N7	153.4	
B2-N5	159.2	156.0	B1-Cl1		189.6
N1-C1	134.3	134.7	B2-N8	153.4	
N2-C1	134.3	134.8	B2-Cl2		189.8
C1-N3	137.2	136.9			
N1-B1-N4	108.9	113.8	N7-B1-B2	132.2	
N2-B2-N5	108.9	114.0	Cl1-B1-B2		124.9
N1-C1-N2	116.2	115.8	N8-B2-B1	132.2	
N4-C8-N5	116.2	115.8	Cl2-B2-B1		124.9

Addition of $HCl{\cdot}Et_2O$ to **15A** leads to formation of compound **15** (see Scheme 2.5.3). This experiment was monitored by ^1H NMR spectrum (see Figure 2.5.8), showing that the experimental data are consistent with the proposed pathway. The absence of the signal characteristic to NH protons from $NHMe_2$ groups in case of (i) shows most likely the formation of **15A**.

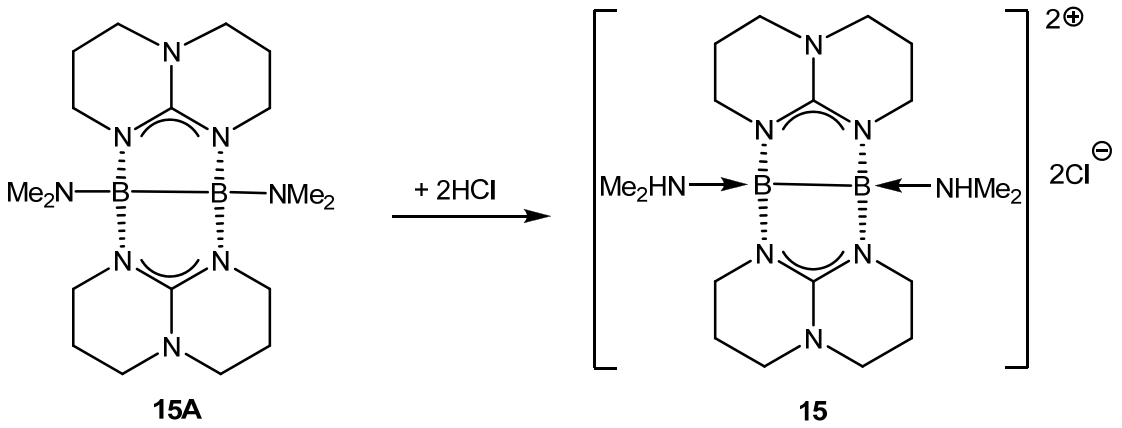

Scheme 2.5.3: Reaction of **15A** with HCl.

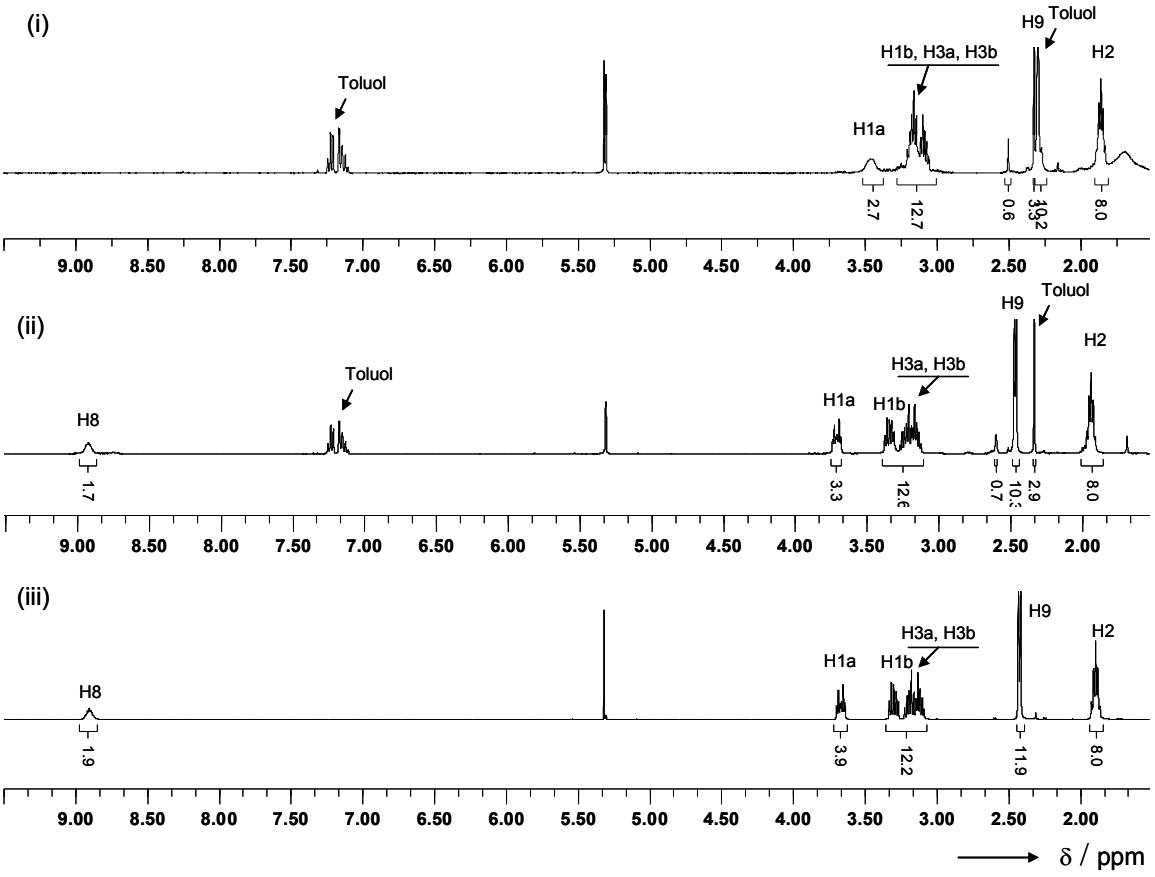

Figure 2.5.8: ^{1}H NMR spectra (400 MHz, CD_2Cl_2) for (i) **15A**, (ii) reaction between **15A** and HCl and (iii) **15**.

Although we were not able to get crystals of **15A**, we managed to isolate a small amount of an intermediate of its reaction with HCl, namely [$(Me_2N)B_2(\mu$-hpp$)_2(NHMe_2)$]Cl, **16**. A few crystals of **16**·CH_2Cl_2 were grown from CH_2Cl_2/hexane. The structure as determined by X-ray diffraction is shown in Figure 2.5.9. The B-B bond distance in **16** was determined to be 175.3(4) pm and is thus slightly larger than that in **15**, where 174.6(4) pm were measured (see Figure 2.5.2). As anticipated, the B-NMe_2 distance (153.7(4) pm) is significantly shorter than the B-NMe_2H distance (160.3(4) pm). For comparison, in **15** the B-NMe_2H distance amount to 160.1(4) and 160.6(4) pm.

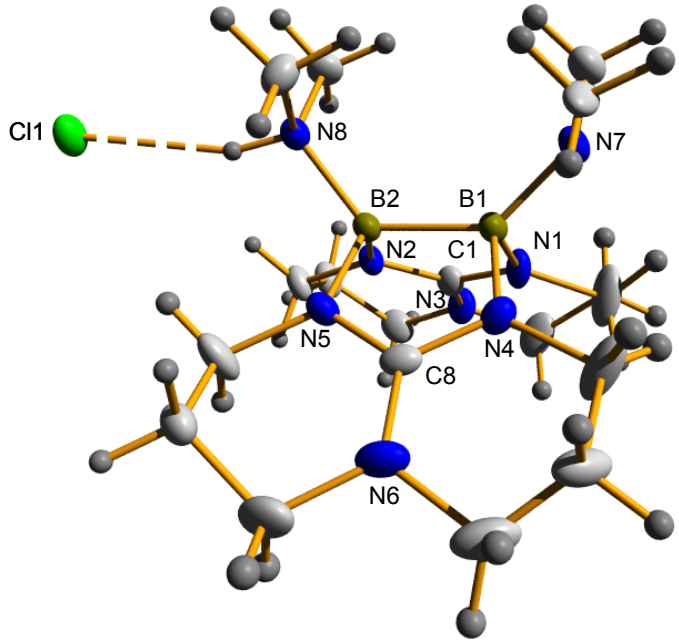

Figure 2.5.9: Molecular structure of [$(Me_2N)B_2(\mu$-hpp$)_2(NHMe_2)$]Cl **16** in the crystalline phase as determined by X-ray diffraction. The thermal ellipsoids are drawn at the 30% probability level. Selected bond distances (in pm) and angles (in degrees): B(1)-N(1) 156.2(4), B(1)-N(4) 156.3(4), B(1)-N(7) 153.7(4), B(1)-B(2) 175.3(4), B(2)-N(2) 153.9(4), B(2)-N(5) 154.8(4), B(2)-N(8) 160.3(4), C(1)-N(1) 133.7(4), C(1)-N(2) 134.4(4), C(1)-N(3) 134.1(4), C(8)-N(4) 132.8(4), C(8)-N(5) 134.5(4), C(8)-N(6) 134.6(4), N(8)-H(8) 92.0(4), N(1)-B(1)-N(4) 110.7(2), N(2)-B(2)-N(5) 113.2(2), N(1)-C(1)-N(2) 114.8(3), N(4)-C(8)-N(5) 115.6(2), N(7)-B(1)-B(2) 134.5(3), N(8)-B(2)-B(1) 125.7(2).

Like **15A**, **16** is a reactive species, and we were not able to separate it from compound **15**. Because the NMR spectra of these compounds are similar, an ambiguous NMR spectroscopic characterisation turned out to be impossible due to lack of enough pure samples.

By keeping a CH_2Cl_2/hexane solution of **15** for several weeks we obtained a new species $[ClB_2(\mu\text{-hpp})_2(NHMe_2)]Cl$ **17**, where the Cl^- counterion replaced the NMe_2H unit to form B-Cl bond instead of B-N bond (see Scheme 2.5.4). Elimination of the second NMe_2H group and substitution with another Cl^- counterion can result in formation of another species $[ClB(\mu\text{-hpp})]_2$ **18** (see Scheme 2.5.4).

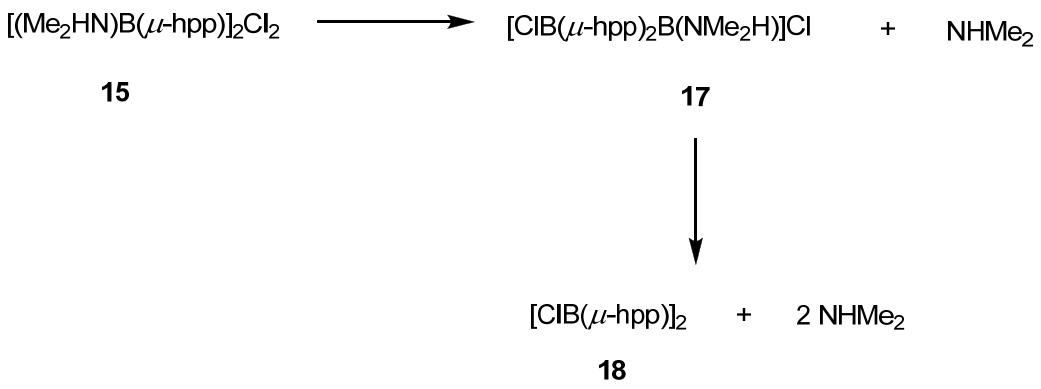

Scheme 2.5.4: Synthesis of compounds **17** and **18**.

Formation of this compound is supported by quantum chemical calculations.[15] Surprisingly further experiments found no evidence for the formation of **18** (see Section 2.5.4). Compound **17** was obtained in larger amounts and could also clearly be characterized by NMR spectra recorded for solutions of the crystalline material (see Figure 2.5.10). The ^{11}B NMR spectrum gives evidence for two broad singlet at $\delta(^{11}B)$ = 3.11 ppm and $\delta(^{11}B)$ = 1.07 ppm, which are characteristic for B-a and B-b, respectively (see Figure 2.5.10). The observed loss of NMe_2H is in full agreement to the thermogravimetric and quantum chemical studies (see Section 2.5.1) which already indicated a relatively weak B–NMe_2H bonding.

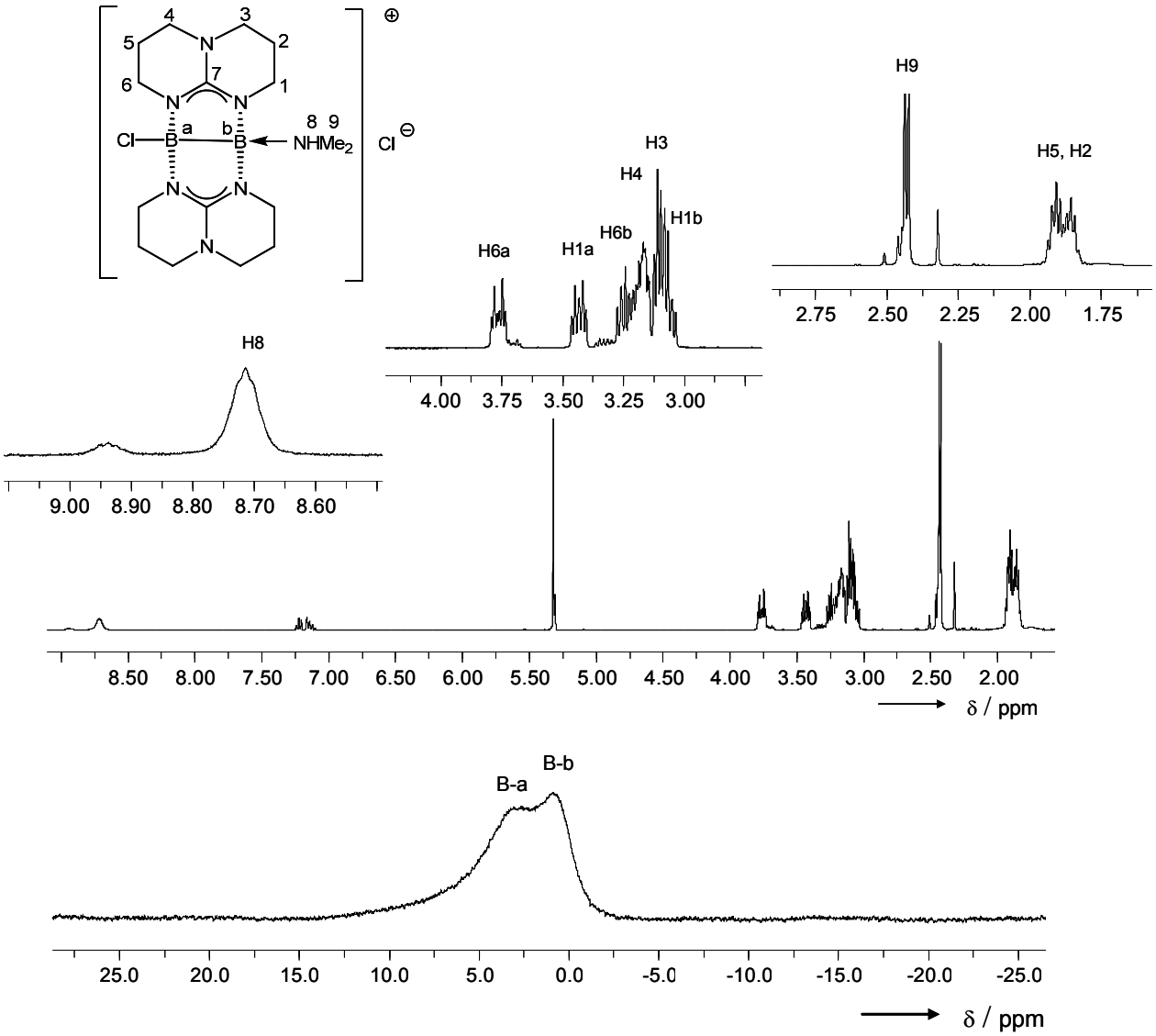

Figure 2.5.10: ^{1}H NMR spectrum (400 MHz, CD_2Cl_2); ^{11}B NMR spectra (128.3 MHz, CD_2Cl_2) for **17**.

Colourless crystals of **17** suitable for X-ray analysis were obtained from the CH_2Cl_2/hexane solution. Figure 2.5.11 illustrates the structure of **17** as determined by X-ray diffraction analysis together with some selected bond distances and angles. With 170.6(7) pm, the B-B bond is significantly shorter than in **15** (174.6(4) pm) or **8** (177.2(3) pm). The B-Cl distance measure 192.2(5) pm and is thus relatively long. For comparison, in $[BCl(NMe_3)]_2$[58] B-Cl bond distances of 186 and 189 pm have been measured. These values are much larger than those adopted in three-coordinated diborane species (e.g., 181.9(4) pm in $[BCl(NH\textit{i}Pr_2)]_2$[59] and

177.0(5)/177.4(4) pm in $[ClB(Mes)]_2$ (Mes = mesityl)).[60] The $B^{\leftarrow}NHMe_2$ donor bond is again more than 5 pm larger than the B-N bonds to the hpp^- ligands.

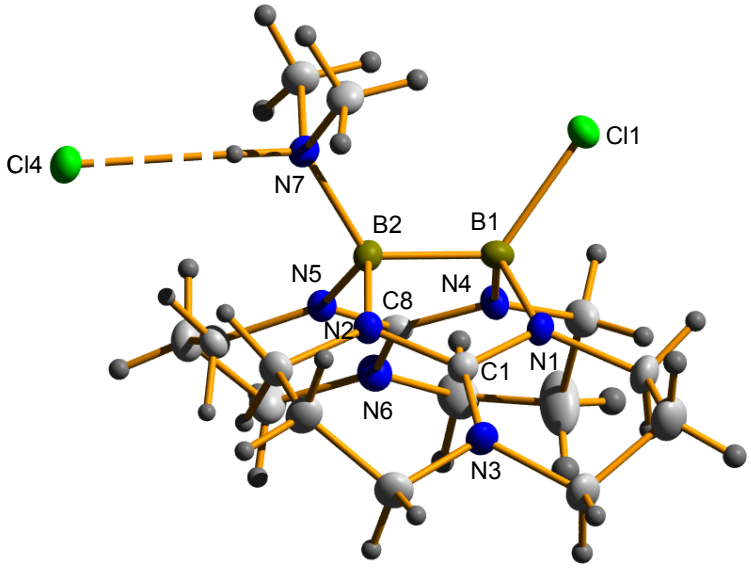

Figure 2.5.11: Molecular structure of $[ClB_2(\mu\text{-hpp})_2(NHMe_2)]Cl$ **17** in the crystalline phase as determined by X-ray diffraction. The thermal ellipsoids are drawn at the 30% probability level. Selected bond distances (in pm) and angles (in degrees): B(1)-N(1) 155.5(6), B(1)-N(4) 152.9(6), B(1)-Cl(1) 192.2(5), B(1)-B(2) 170.6(7), B(2)-N(2) 155.0(6), B(2)-N(5) 153.0(5), B(2)-N(7) 161.0(6), C(1)-N(1) 135.2(5), C(1)-N(2) 133.6(5), C(1)-N(3) 135.6(5), C(8)-N(4) 135.2(5), C(8)-N(5) 134.7(5), C(8)-N(6) 133.9(5), N(7)-H(7) 93.6(19), N(4)-B(1)-N(1) 114.1(4), N(5)-B(2)-N(2) 114.5(3), N(2)-C(1)-N(1) 115.8(4), N(5)-C(8)-N(4) 115.4(3), N(7)-B(2)-B(1) 122.7(4), Cl(1)-B(1)-B(2) 125.1(3).

ESI^+ spectra indicate that **17** dimerizes to give $[B_4Cl_4(hpp)_4(NMe_2H)_2]$ or a salt $[B_4Cl_3(hpp)_4(NMe_2H)_2]Cl$ (see Figure 2.5.12). Thus, in addition to the signals due to $[C_{16}H_{31}B_2Cl_1N_7]^+$ and $[C_{14}H_{24}B_2Cl_1N_6]^+$ at *m/z* = 378 and 333, a large signal appeared in the spectrum of **17** at *m/z* = 791.47 which can be assigned on the basis of the mass and the isotopic pattern to the $[B_4Cl_3(hpp)_4(NMe_2H)_2]^+$. Unfortunately we were so far unable to isolate and crystallize this species.

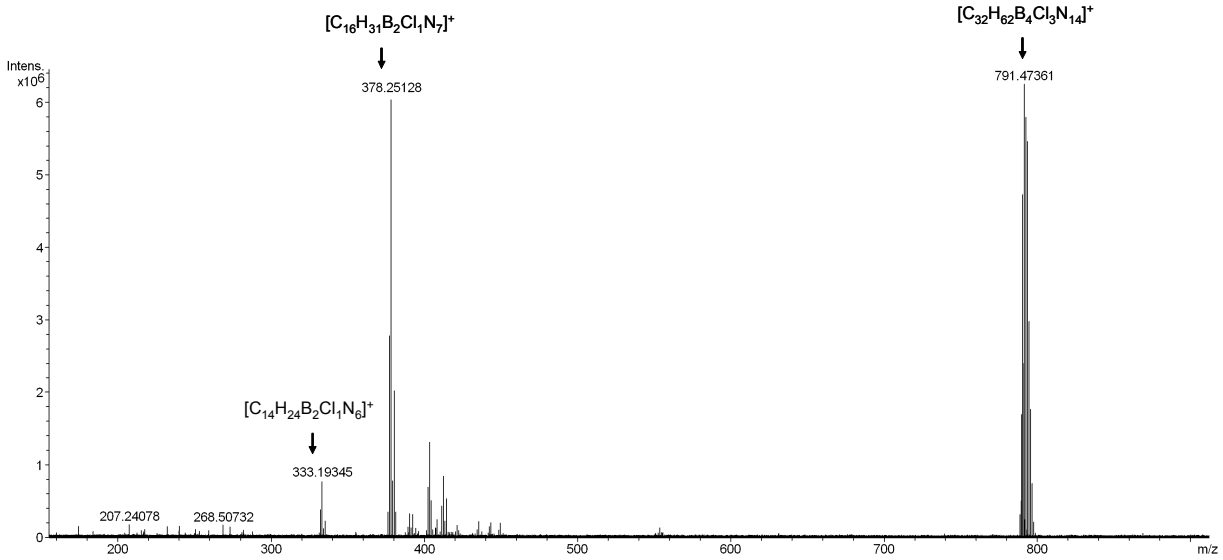

Figure 2.5.12: ESI spectrum of compound **17**.

2.5.3 Synthesis and characterization of $[\{(Me_2(H)N)B(\mu\text{-hpp})\}_2]X_2$ (X = OTf^- and $[B(C_6F_5)_4]^-$)

We reported already in section 2.5.1 the synthesis of the binuclear boron(II) compound $[\{Me_2(H)N)B(\mu\text{-hpp})\}_2]Cl_2$ **15**. In this species, the Cl^- anions interact strongly with the cation via hydrogen bonds through the NMe_2H groups. It was the topic of the subsequent investigations to remove the two NMe_2H units, thereby obtaining a salt of the three-coordinated binuclear boron(II) compound $[B_2(\mu\text{-hpp})_2]^+$, which was predicted by quantum chemical calculations (see Section 2.5.1 and Figure 2.5.6) to exhibit a planar central B_2N_4 unit. Of course, the Cl^- counterions could simply replace the NMe_2H units to form B-Cl bonds instead of B-N bonds, and therefore the right choice of anion might be of crucial importance. We already obtained the product of replacement of one NMe_2H group by Cl^-, namely $[ClB_2(\mu\text{-hpp})_2(NHMe_2)]Cl$ **17** (see Section 2.5.2). By using a weakly coordination of the anion (instead of the Cl^- anion) it should be possible to avoid coordination of the anion to the B atoms. We therefore reacted **15** with AgOTf in the dark (see Scheme 2.5.5) and also with $Li[B(C_6F_5)_4]$ (see Scheme 2.5.6).

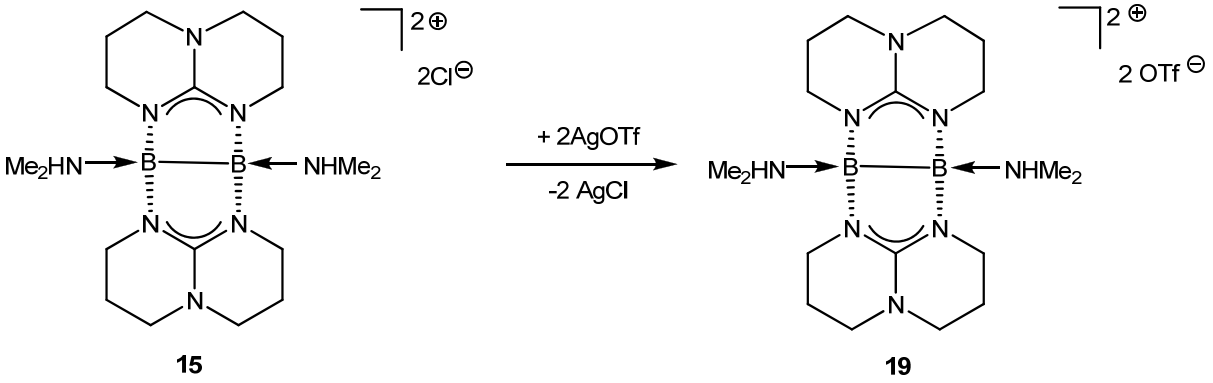

Scheme 2.5.5: Synthesis of compound **19**.

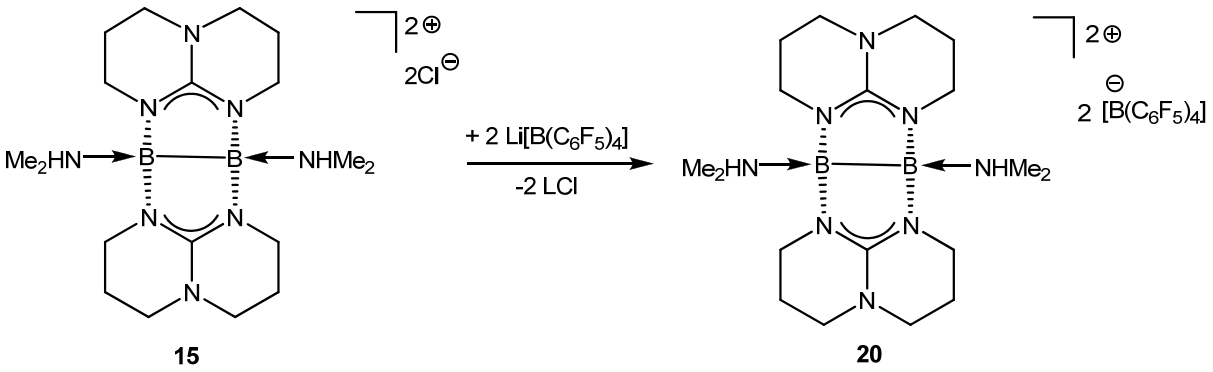

Scheme 2.5.6. Synthesis of compound **20**.

Reaction of **15** with AgOTf yielded the new salt [{Me_2(H)N)B(μ-hpp)}$_2$](OTf)$_2$ **19** and reaction of **15** with Li[$B(C_6F_5)_4$] resulted in formation of another new salt [{Me_2(H)N)B(μ-hpp)}$_2$][$B(C_6F_5)_4$]$_2$ **20**. Both compounds were characterized by NMR spectra (see Figure 2.5.13 and Figure 2.5.14) and only compound **19** could be crystallized from concentrated solution of CH_2Cl_2 at room temperature.

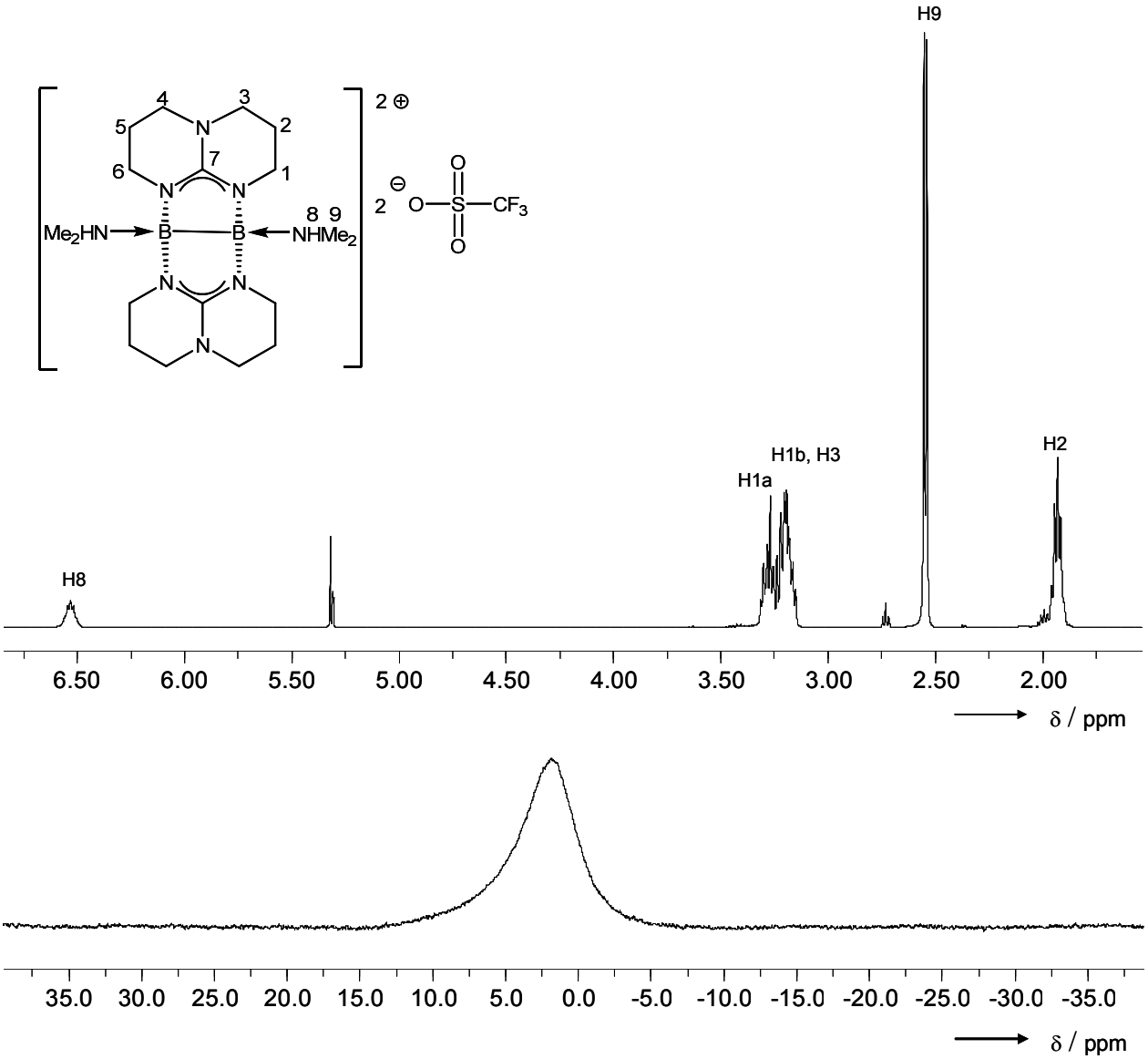

Figure 2.5.13: ^{1}H NMR spectrum (400 MHz, CD_2Cl_2); ^{11}B NMR spectra (128.3 MHz, CD_2Cl_2) for **19**.

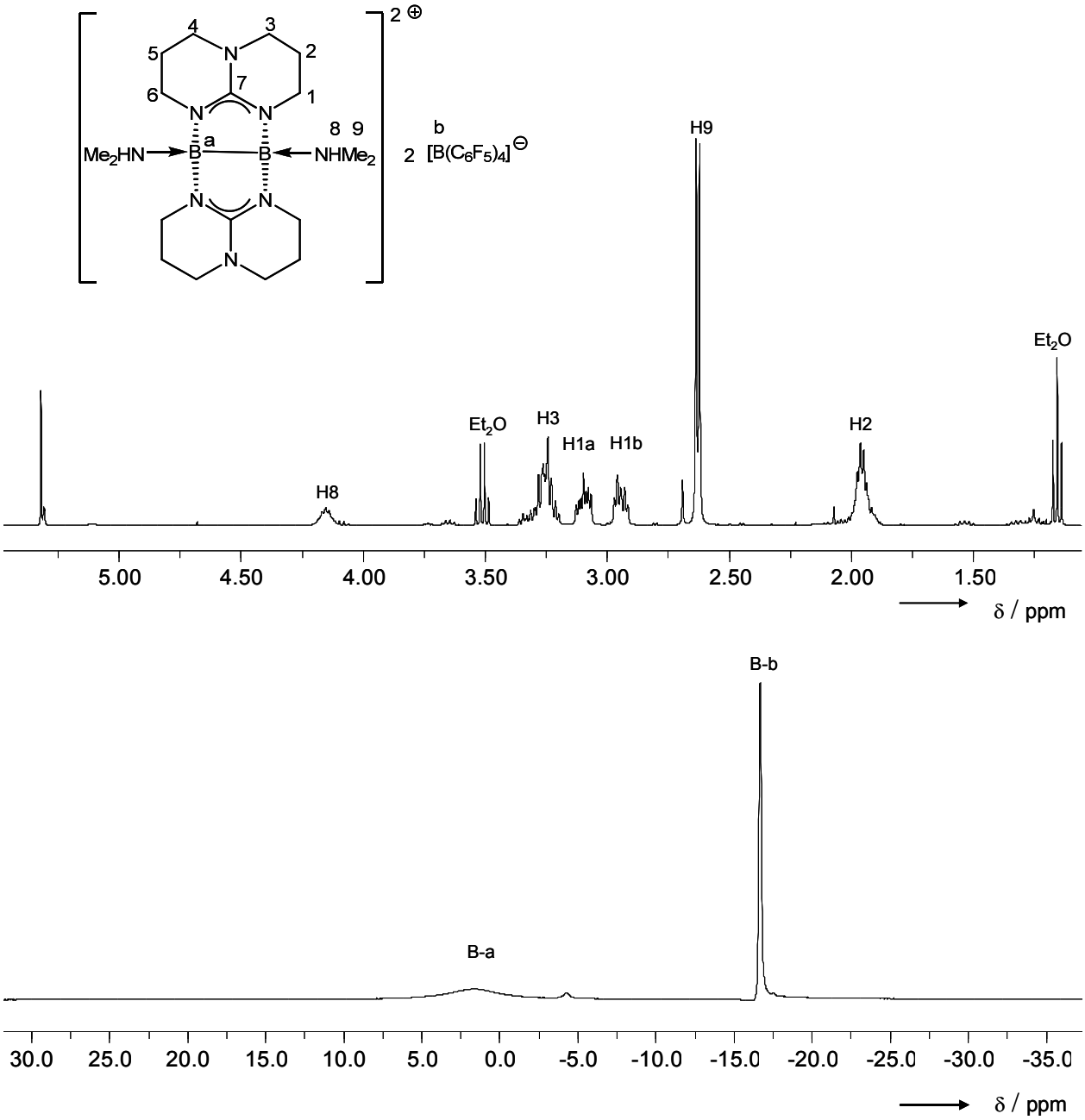

Figure 2.5.14: ^{1}H NMR spectrum (400 MHz, CD_2Cl_2); ^{11}B NMR spectra (128.3 MHz, CD_2Cl_2) for **20**.

Figure 2.5.15 illustrates the molecular structure of **19** as obtained from X-ray diffraction measurements. The B-B distance in **19** was determined to be 172.4(12) pm which is smaller than that in **15**, where 174.6(4) were measured (see Figure 2.5.2). For comparison, in **8** the B-B distance is longer (177.2(3)) and in **18** the B-B distance is shorter (170.6(7)), which it is in line with the electronegativity of the Cl

ligand. The B-NMe_2H distances amount to 163.0(9) and 160.3(10) pm. These values compare with 160.1(4) and 160.6(4) pm in **15** and 161.0(6) pm in **17**.

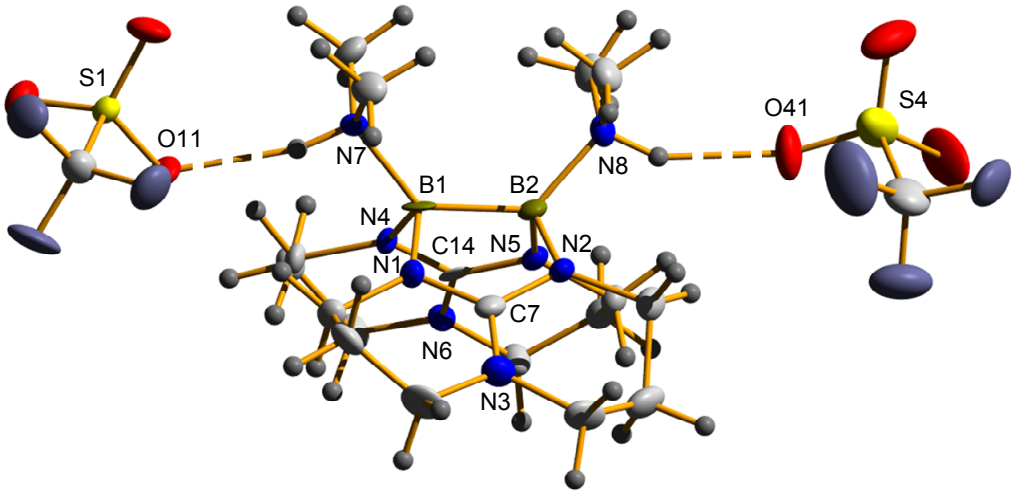

Figure 2.5.15: Molecular structure of [{Me_2(H)N)B(μ-hpp)}$_2$]OTf_2 **19** derived from X-ray diffraction. The thermal ellipsoids are drawn at the 50% probability level. Selected bond distances (in pm) and angles (in degrees): B(1)-N(1) 154.9(10), B(1)-N(4) 152.9(10), B(1)-N(7) 163.0(9), B(1)-B(2) 172.4(12), B(2)-N(2) 154.0(10), B(2)-N(5) 154.6(10), B(2)-N(8) 160.3(10), C(7)-N(1) 133.8(9), C(7)-N(2) 135.8(9), C(7)-N(3) 134.1(9), C(14)-N(4) 136.6(9), C(14)-N(5) 133.9(9), C(14)-N(6) 133.1(8), N(7)-H(7) 93.00, N(8)-H(8) 93.00, N(4)-B(1)-N(1) 114.4(6), N(2)-B(2)-N(5) 112.2(6), N(1)-C(7)-N(2) 114.5(6), N(5)-C(14)-N(4) 113.4(6), N(7)-B(1)-B(2) 130.8(6), N(8)-B(2)-B(1) 129.6(6).

2.5.4 Thermal reactions of [{Me_2(H)N)B(μ-hpp)}$_2$]X_2 (X = Cl^-, OTf^- and [$B(C_6F_5)_4$]$^-$)

Thermal reactions of **15**, **19** and **20** were investigated in solution and in the solid state and followed by NMR spectroscopy. First, compound **15** dissolved in CH_2Cl_2 was heated to a temperature of 40°C for 24 hours. However, the NMR spectra recorded before and after this treatment showed no significant changes. On the other hand, when solid **15** was heated in an Ar atmosphere to 200°C for a period of 5 hours and subsequently to 210°C for another 2 hours the spectra witnessed major changes (see Figure 2.5.16). The ^{1}H NMR spectrum before heating displayed the signals characteristic of **15** marked by empty cycles. Trace (ii) shows the spectrum after heating the compound to 200°C for a period of 5 hours. It can be seen that the signals due to the starting material are still present, but additional signals due to two new species appeared (marked with solid cycles and diamonds). After heating to 210°C (see trace (iii)) the signal of the starting material disappeared completely and only the signals of the two products showed. For comparison, the spectrum of compound **17**, in which one NMe_2H group is substituted by chloride, is also shown in Figure 2.5.16 (trace (iv)). It can be seen immediately that one of the two products is compound **17** (marked with solid cycles) whereas the compound responsible for the signals marked with solid diamonds could easly be identified as the salt [$hppH_2$]Cl arising from ligand protonation and abstraction. Inspection of the corresponding ^{11}B NMR spectra (see Figure 2.5.17) indicated that the compound responsible for the signals marked with filled diamonds does not contain any B atoms. Further thermal treatment at 250°C for 1 hour initiated the decomposition of **15** with formation of larger quantities of [$hppH_2$]Cl. Surprisingly the experiments found no evidence for the formation of [ClB(hpp)]$_2$, even when **15** was heated for prolonged times at 200°C. Thus it proved impossible to substitute both NMe_2H groups thermally by chloride. In further experiments, compound **19** was heated at 200°C for 2 h in an Ar atmosphere. As a result, the solid material turned into a yellow-coloured liquid. The ^{1}H NMR spectrum displayed, in addition to the signals from un-reacted starting material, new signals which can be assigned again to the [$hppH_2$]$^+$ cation arising from decomposition of **19**. Only weak extra signals from an unknown boron-containing product (at δ = 0.2) were visible. Finally, compound **20** was heated to a temperature of 180°C for 2 h.

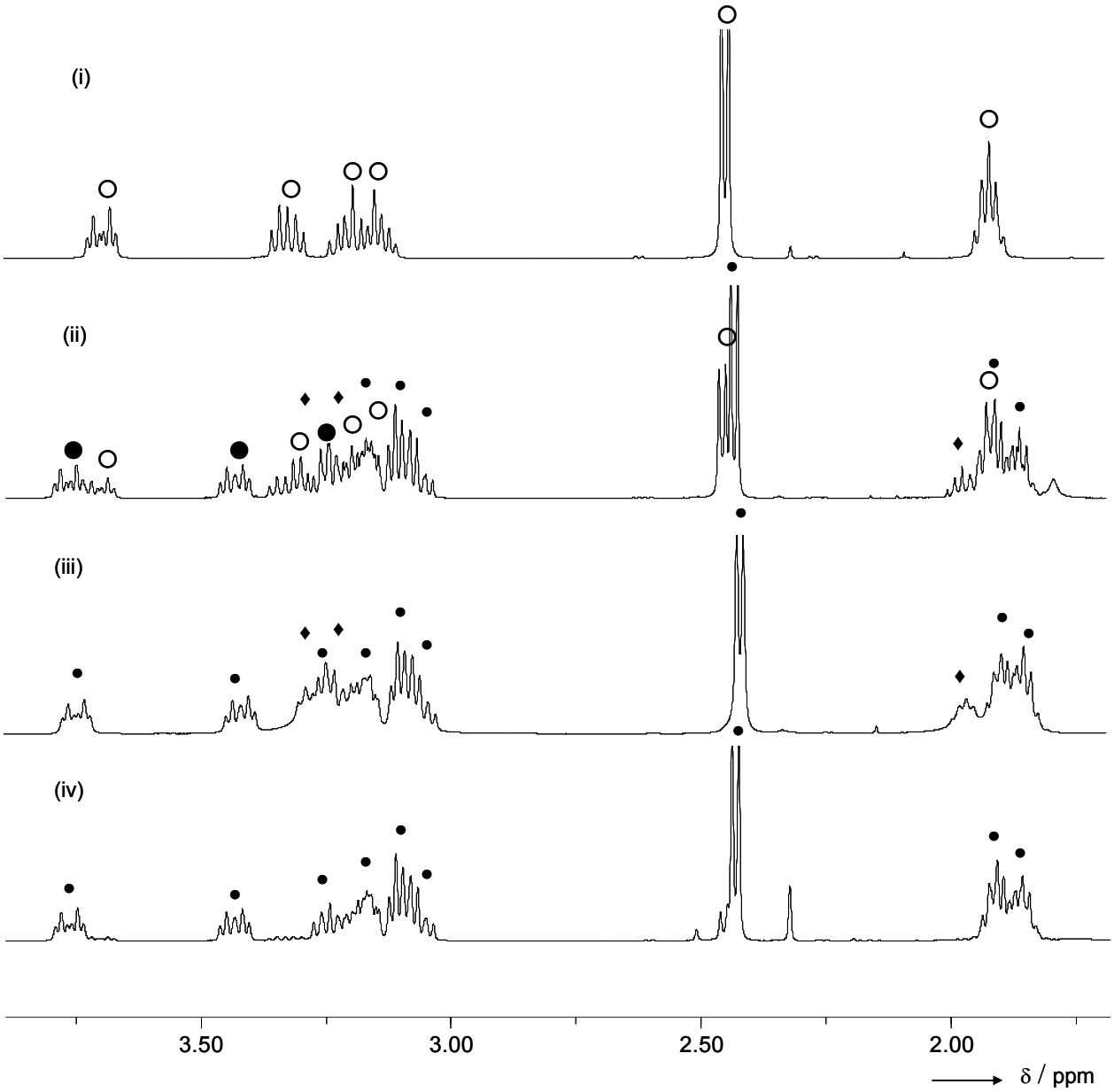

Figure 2.5.16: ^{1}H NMR spectra (at 400 MHz, CD_2Cl_2) for thermal decomposition of compound **15** (marked with ○ cycles). The spectra obtained for compound **17** (marked with ● cycles) are also included for comparison. The signals which are marked with ♦ can be assigned to the $hppH_2^+$.

The ^{1}H NMR spectrum contained signals (at δ = 2,04, 3.33) due to a new compound with shifted N-H proton signals (δ = 4.43, 5.15). In the ^{11}B NMR spectrum a new weak signal appeared (at δ = 0.4) and might be assignable to the same compound. Possibly this compound is formed by elimination of one of the HMe_2N

groups. However, it proved impossible to isolate another binuclear boron species. From these experiments it can be concluded that compounds 1**9** and **20** decompose much faster and at lower temperatures than **15**, but that the formation of a salt of the tri-coordinated binuclear boron(II) compound $[\{B(\mu\text{-hpp})\}_2]^{2+}$, which was predicted by quantum chemical calculations (see Figure 2.5.6) can not be achieved in this way.

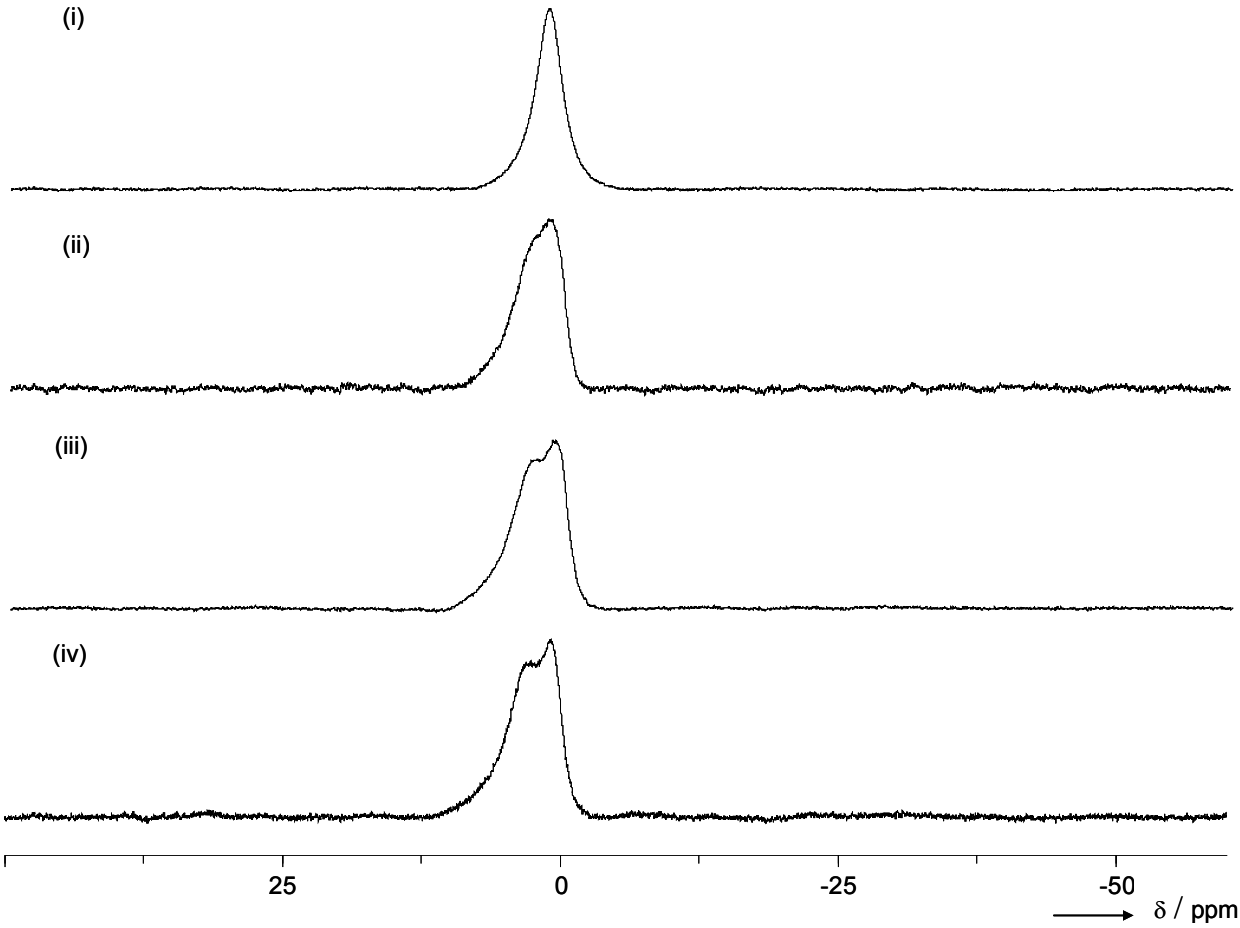

Figure 2.5.17: ^{11}B NMR spectra (at 128.3 MHz, CD_2Cl_2) before (i) and after thermal decomposition (ii): at 200°C for 5 h; (iii): at 210°C for 2 h of compound **15**. For comparison, trace (iv) shows the ^{11}B NMR spectrum for compound **17**.

In summary, the reaction of $B_2Cl_2(NMe_2)_2$ with hppH resulted in the synthesis of the first example of a stable binuclear boron dication $[\{(Me_2(H)N)B(\mu\text{-hpp})\}_2]Cl_2$ **15**, in which the boron centers have the formal oxidation state of II+. This compound was characterized by various spectroscopic techniques and by X-ray diffraction measurements. In addition, quantum chemical calculations were carried out. The

structures of the first B(II) monocations [$(Me_2N)B_2(\mu$-hpp$)_2(NHMe_2)$]Cl, **16**, [$ClB_2(\mu$-hpp$)_2(NHMe_2)$]Cl, **17**, and their reactivity are also described by means of spectroscopic, X-ray, and theoretical data. With 170.6(7), the B-B bond in **17** is the shortest of the compounds for which X-ray data are available (**15**, **8**, **16**, and **18**), in line with the electronegativity of the Cl ligand, and with 177.2(3) pm, the B-B bond in the neutral compound [$HB(\mu$-hpp$)]_2$ **8** is the longest. The B-B bond distance of **15** (174.6(2) pm) and **16** (175.3(4) pm) are in between. In further experiments we synthesized new salts of the dicationic binuclear boron compound $[B_2(hpp)_2(NMe_2H)_2]^{2+}$ by reaction between $B_2Cl_2(NMe_2)_2$ and hppH followed by exchange of the Cl^- anions. Weakly coordinating anions (OTf^- and $[B(C_6F_5)_4]^-$) were used and the thermal decompositions of the obtained new salts were compared on the basis of NMR experiments.

2.6 References

[1] M. J. Frisch, G. W. Trucks, H. B. Schlegel, G. E. Scuseria, M. A. Robb, J. R. Cheeseman, V. G. Zakrzewski, J. A. Montgomery Jr., R. E. Stratmann, J. C. Burant, S. Dapprich, J. M. Millam, A. D. Daniels, K. N. Kudin, M. C. Strain, Ö. Farkas, J. Tomasi, V. Barone, M. Cossi, R. Cammi, B. Mennucci, C. Pomelli, C. Adamo, S. Clifford, J. Ochterski, G. A. Petersson, P. Y. Ayala, Q. Cui, K. Morokuma, P. Salvador, J. J. Dannenberg, D. K. Malick, A. D. Rabuck, K. Raghavachari, J. B. Foresman, J. Cioslowski, J. V. Ortiz, A. G. Baboul, B. B. Stefanov, G. Liu, A. Liashenko, P. Piskorz, I. Komáromi, R. Gomperts, R. L. Martin, D. J. Fox, T. Keith, M. A. Al-Laham, C. Y. Peng, A. Nanayakkara, M. Challacombe, P. M. W. Gill, B. Johnson, W. Chen, M. W. Wong, J. L. Andres, C. Gonzalez, M. Head-Gordon, E. S. Replogle, J. A. Pople, *Gaussian 98*[a] (*Gaussian 03*[b]), Gaussian, Inc., Pittsburgh, **1998**.

[2] a) A. D. Becke, J. Chem. Phys. **1993**, *98*, 5648–5652; b) C. Lee, W. Yang, R. G. Parr, *Phys. Rev. B* **1988**, *37*, 785–789; c) B. Miehlich, A. Savin, H. Stoll, H. Preuss, *Chem. Phys. Lett.* **1989**, *157*, 200–206.

[3] G. Robinson, C.Y. Tang, R. Köppe, A. R. Cowley, H.-J. Himmel, *Chem. Eur. J.* **2007,** *13,* 2648–2654.

[4] A. R. Cowley, A. J. Downs, H.-J. Himmel, S. Marchant, J. A. Yeoman, *Dalton Trans.* **2005,** 1591–1597.

[5] R. Snaith, K. Wade, B. K. Wyatt, *J. Chem. Soc. A* **1970,** 380–383.

[6] N. Schulenberg, M. Jäkel, E. Kaifer, H.-J. Himmel, *Eur. J. Inorg. Chem.* **2009**, accepted for publication.

[7] K. Kawaguchi, *J. Chem. Phys.* **1992,** *96,* 3411–3414.

[8] T. J. Tague Jr., L. Andrews, *J. Am. Chem. Soc.* **1994,** *116,* 4970–4976.

[9] C.F. Lane, *Chem. Rev.* **1976,** *76,* 773–800.

[10] J.D. Carpenter, B. S. Ault, *J. Phys. Chem.* **1991,** *95,* 3507–3511.

[11] Corrections which take into account thermal elongations and the effect of high-electron-density gradients generally leading to too short E-H bond lengths in the X-ray structures.

[12] A. Shibli, H. A. Ali, I. Goldberg, M. Srebnik, *J. Organomet. Chem.* **2005,** *690,* 2180–2185.

[13] F. Blockhuys, D. A. Wann, C. Van Alsenoy, H. E. Robertson, H.-J. Himmel, C. Y. Tang, A. R. Cowley, A. J. Downs, D. W. H. Rankin, *Dalton Trans.* **2007,** 1687–1696.

[14] J. M. Blackwell, W. E. Piers, M. Parvez, R. McDonald, *Organometallics* **2002**, *21,* 1400–1407.

[15] Calculations were carried out with the TURBOMOLE program package. See: a) R. Ahlrichs, M. Bär, M. Häser, H. Horn, C. Kölmel, *Chem. Phys. Lett.* **1989**, *162*, 165–169; b) K. Eichkorn, O. Treutler, H. Öhm, M. Häser, R. Ahlrichs, *Chem. Phys. Lett.* **1995**, *240*, 283–289; c) K. Eichkorn, O. Treutler, H. Öhm, M. Häser, R. Ahlrichs, *Chem. Phys. Lett.* **1995**, *242*, 652–660; d) K. Eichkorn, F. Weigend, O. Treutler, R. Ahlrichs, *Theor. Chem. Acc.* **1997**, *97*, 119–124; e) F. Weigend, M. Häser, *Theor. Chem. Acc.* **1997**, *97*, 331–340; f) F. Weigend, M. Häser, H. Patzelt, R. Ahlrichs, *Chem. Phys. Lett.* **1998**, *294*, 143–152. If not stated otherwise, the BP86 method in combination with a TZVPP basis set has been applied (A. Schäfer, H. Horn, R. Ahlrichs, *J. Chem. Phys.* **1992**, *97*, 2571–2577).

[16] A. Bakac, J. H. Espenson, *Inorg. Chem.* **1989**, *28,* 4319–4322.

[17] a) R. H. Crabtree, P. E. M. Siegbahn, O. Eisenstein, A. L. Rheingold, T. F. Koetzle, *Acc. Chem. Res.* **1966**, *29,* 348–354; b) W. T. Klooster, T. F. Koetzle, P. E.

M. Siegbahn, T. B. Richardson, R. H. Crabtree, *J. Am. Chem. Soc.* **1999**, *121,* 6337–6343.

[18] a) J.-W. Hwang, J. P. Campbell, J. Kozubowski, S. A. Hanson, J. F. Evans, W. L. Gladfelter, *Chem. Mater.* **1995**, *7,* 517–525; b) J. P. Campbell, J.-W. Hwang, V. G. Young Jr., R. B. Von Dreele, C. J. Cramer, W. L. Gladfelter, *J. Am. Chem. Soc.* **1998**, *120,* 521–531.

[19] C. Y. Tang, R. A. Coxall, A. J. Downs, T. M. Greene, S. Parsons, *J. Chem. Soc. Dalton Trans.* **2001**, 2141–2147.

[20] C. J. Cramer, W. L. Gladfelter, *Inorg. Chem.* **1997**, *36*, 5358–5362.

[21] A. J. Hoefnagel, M. A. Hoefnagel, B. M. Wepster, *J. Org. Chem.* **1981**, *46*, 4209–4211.

[22] M. Bühl, T. Steinke, P. v. R. Schleyer, R. Boese, *Angew. Chem.* **1991**, *103,* 1179–1180; *Angew. Chem. Int. Ed. Engl.* **1991**, *30,* 1160–1161.

[23] L. R. Thorne, R. D. Suenram, F. J. Lovas, *J. Chem. Phys.* **1983**, *78*, 167–171.

[24] P. Cassoux, R. L. Kuczkowski, P. S. Bryan, R. C. Taylor, *Inorg. Chem*. **1975**, *14*, 126–129.

[25] K. Iijima, N. Adachi, S. Shibata, *Bull. Chem. Soc. Jpn.* **1984**, *57*, 3269–3273.

[26] R. Schwesinger, *Chimia* **1985**, *39,* 269–272.

[27] H.-J. Himmel, H. Schnöckel, *Chem. Eur. J.* **2003**, *9,* 748–755.

[28] Y. Luo, K. Ohno, *Organometallics* **2007**, *26*, 3597–3600.

[29] a) V. Barone, M. Cossi, *J. Phys. Chem. A* **1998**, *102*, 1995–2001; b) M. Cossi, N. Rega, G. Scalmani, V. Barone, *J. Comput. Chem.* **2003**, *24*, 669–681.

[30] T. J. Clark, C. A. Russell, I. Manners, *J. Am. Chem. Soc.* **2006**, *128*, 9582–9583.

[31] J. L. Fulton, J. C. Linehan, T. Autrey, M. Balasubramanian, Y. Chen, N. K. Szymczak, *J. Am. Chem. Soc.* **2007**, *129*, 11936–11949.

[32] O.Ciobanu, H.-J. Himmel, *Eur. J. Inorg. Chem.* **2007**, 3565–3572.

[33] E. Cavero, R. Giménez, S. Uriel, E. Beltrán, J. L. Serrano, I. Alkorta, J. Elguero, *Cryst. Growth Des.* **2008**, *8*, 838–847.

[34] O. Ciobanu, F. Allouti, P. Roquette, S. Leingang, M. Enders, H. Wadepohl, H.-J. Himmel, *Eur. J. Inorg. Chem.* **2008**, 5482–5493.

[35] M. P. Coles, *Chem. Commun.* **2009**, 3659–3676.

[36] A. Peters, U. Wild, O. Hübner, E. Kaifer, H.-J. Himmel, *Chem. Eur. J.* **2008**, *14*, 7813–7821.

[37] G. A. Pierce, N. D. Coombs, D. J. Willock, J. K. Day, A. Stasch, S. Aldridge, *Dalton Trans.* **2007**, 4405–4412.

[38] M. Findlater, N. J. Hill, A. H. Cowley, *Dalton Trans.* **2008**, 4419–4423.

[39] S. Trofimenko, *J. Am. Chem. Soc.* **1966**, *88*, 1842–1844.

[40] a) C. A. Jaska, K. Temple, A. J. Lough, I. Manners, *J. Am. Chem. Soc.* **2003**, *125*, 9424–9434; b) C. A. Jaska, I. Manners, *J. Am. Chem. Soc.* **2004**, *126*, 9776–9785; c) M. C. Denney, V. Pons, T. J. Hebden, D. M. Heinekey, K. I. Goldberg, *J. Am. Chem. Soc.* **2006**, *128*, 12048–12049.

[41] O. T. Beachley Jr., *Inorg. Chem*. **1969**, *8*, 981–985.

[42] H.-J. Himmel, *Inorg. Chem*. **2007**, *46*, 6585–6593.

[43] F. Biegler-König, J. Schönbohm, *AIM 2000*, version 2.0, University of Applied Science: Bielefeld, Germany, **2000**.

[44] S. L. Aeilts, M. P. Coles, D. C. Swenson, R. F. Jordan, *Organometallics* **1998**, *17*, 3265–3270.

[45] M. S. Khalaf, M. P. Coles, P. B. Hitchock, *Dalton Trans.,* **2008**, 4288–4295.

[46] a) W. M. A. Smit, *J. Mol. Struct.* **1973**, *19*, 789–798; b) I. R. Beattie, J. S. Ogden, D. D. Price, *J. Chem. Soc. Dalton Trans.* **1982**, 505–510; c) H.-J. Himmel, A. J. Downs, T. M. Greene, *J. Am. Chem. Soc.* **2000**, *122*, 922–930.

[47] P. T. Brain, A. J. Downs, P. Maccallum, D. W. H. Rankin, H. E. Robertson, G. A. Forsyth, *J. Chem. Soc. Dalton Trans.* **1991**, 1195–1200.

[48] S. C. Malhotra, *Inorg. Chem.* **1964**, *3*, 862–865.

[49] A. Hergel, H. Pritzkow, W. Siebert, *Angew. Chem.* **1994**, *106*, 1342–1343; *Angew. Chem. Int. Ed. Engl.* **1994**, *33*, 1247–248.

[50] a) C. Liang, R. D. Davy, H. F. Schaefer III, *Chem. Phys. Lett*. **1989**, *159*, 393–398; b) J. L. Duncan, D. C. McKean, I. Torto, *J. Mol. Spectrosc*. **1981**, *85*, 16–39.

[51] R. Wehrmann, H. Meyer, A. Berndt, *Angew. Chem.* **1985**, *97*, 779–781; *Angew. Chem. Int. Ed. Engl.* **1985**, *24*, 788–790.

[52] a) L. A. Curtiss, J. A. Pople, *J. Chem. Phys.* **1988**, *89*, 4875–4879; b) L. A. Curtiss, J. A. Pople, *J. Chem. Phys.* **1989**, *91*, 4189–4192; c) J. F. Dias, G. Rasul, P. R. Seidl, G. K. S. Prakash, G. A. Olah, *J. Phys. Chem. A* **2003**, *107*, 7981–7984; d) L. D. Betowski, M. Enlow, *J. Mol. Struct.* **2003**, *638*, 189–195.

[53] C. B. Hübschle, M. Messerschmidt, D. Lentz, P. Luger, *Z. Anorg. Allg. Chem*. **2004**, *630*, 1313–1316.

[54] M. J. G. Lesley, N. C. Norman, C. R. Rice, *Inorganic Syntheses* **2004**, *34*, 3–4.

[55] C. W. Heitsch, *Inorg. Chem.* **1965**, *4*, 1019–1024.

[56] A. Bakac, J. H. Espenson, *Inorg. Chem.* **1989**, *28*, 4319–4322.

[57] W. F. Schneider, C. K. Narula, H. Nöth, B. E. Bursten, *Inorg. Chem.* **1991**, *30*, 3919–3927. Recently, the dication $[B_2(\text{porphine})]^{2+}$ was synthesized and characterized by ^{1}H NMR spectroscopy and FABMS. B3LYP calculations indicate a

planar B_2N_4 central unit: A. Weiss, M. C.Hodgson, P. D. W. Boyd, W. Siebert, P. J. Brothers, *Chem. Eur. J.* **2007**, *13*, 5982–5993.

[58] Q. Johnson, J. Kane, R. Schaeffer, *J. Am. Chem. Soc.* **1970**, *92*, 7614–7615.

[59] C.-J. Maier, H. Pritzkow, W. Siebert, *Angew. Chem.* **1999**, *11*, 1772–1774; *Angew. Chem. Int. Ed.* **1999**, *38*, 1666–1668.

[60] H. Hommer, H. Nöth, J. Knizek, W. Ponikwar, H. Schwenk-Kircher, *Eur. J. Inorg. Chem.* **1998**, 1519–1527.

[61] See, for example: S. Trofimenko, *Chem. Rev.* **1993**, *93*, 943–980, and references given therein.

[62] D. C. Bradley, M. B. Hursthouse, J. Newton, N. P. C. Walker, *J. Chem. Soc., Chem. Commun.* **1984**, 188–190.

[63] E. M. Holt, S. L. Holt, K. J. Watson, B. Olsen, *Cryst. Struct. Commun.* **1978**, *7*, 613–616.

3. Conclusions

In this work we described the synthesis, characterization and quantum chemical studies of new binuclear boron hydrides and di-, monocations, respectively containing bridging guanidinate ligands.

Two guandine-borane adducts $H_3B{\cdot}hppH$ **2** and $H_3B{\cdot}N(H)C(NMe_2)_2$ **3** were used as precursors to synthesize the new binuclear boron hydrides. Therefore, these compounds were synthesized (see Scheme 1) and fully characterized by spectroscopic, X-ray (see Figure 1) and theoretical data.

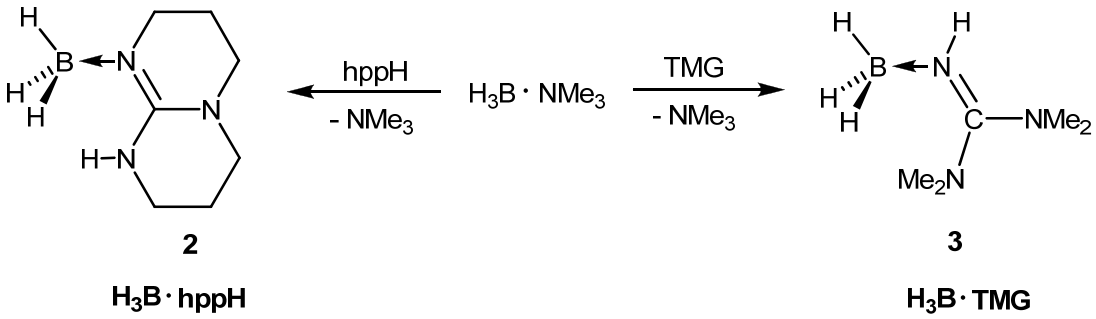

Scheme 1: Synthesis of precursors **2** and **3**.

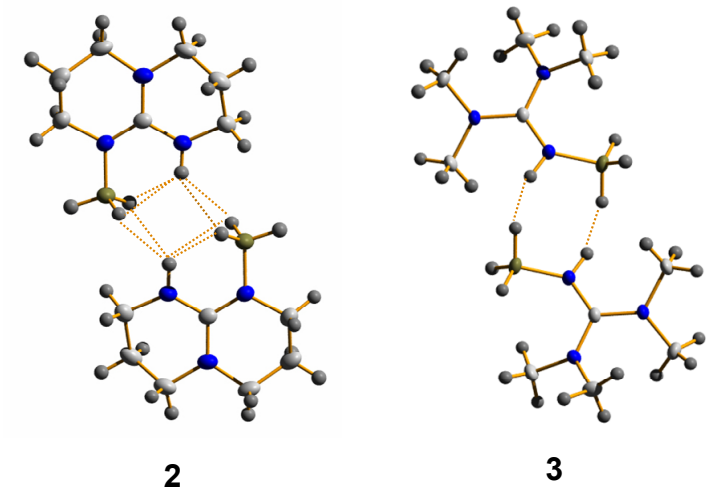

Figure 1: Dimeric assembly of **2** and **3** through N-H···H-B interactions in the crystalline phase. ● C, ● H, ● B, ● N atoms.

Afterwards, the thermal and catalytic dehydrogenations of these two precursors were analyzed experimentally and theoretically. Quantum chemical (DFT) indicated that dehydrogenation can be speeded up by addition of a catalyst. The possible mechanisms for thermal and Cp_2Ti-catalysed dehydrogenation were concentrated on the model compound $H_3B{\cdot}N(H)C(NH_2)_2$ **1**. The experimental results showed that thermal dehydrogenation of $H_3B{\cdot}N(H)C(NMe_2)_2$ **3** is accompanied by decomposition, leading finally to oligomeric methylimino borane, $[HBNMe]_n$. Catalytic dehydrogenation of $H_3B{\cdot}$hppH **2** at elevated temperatures leads to the formation of binuclear boron hydrides with bridging hpp ligands, namely $[H_2B(\mu\text{-hpp})]_2$ **7** and $[HB\mu\text{-hpp})]_2$ **8** (see Scheme 2).

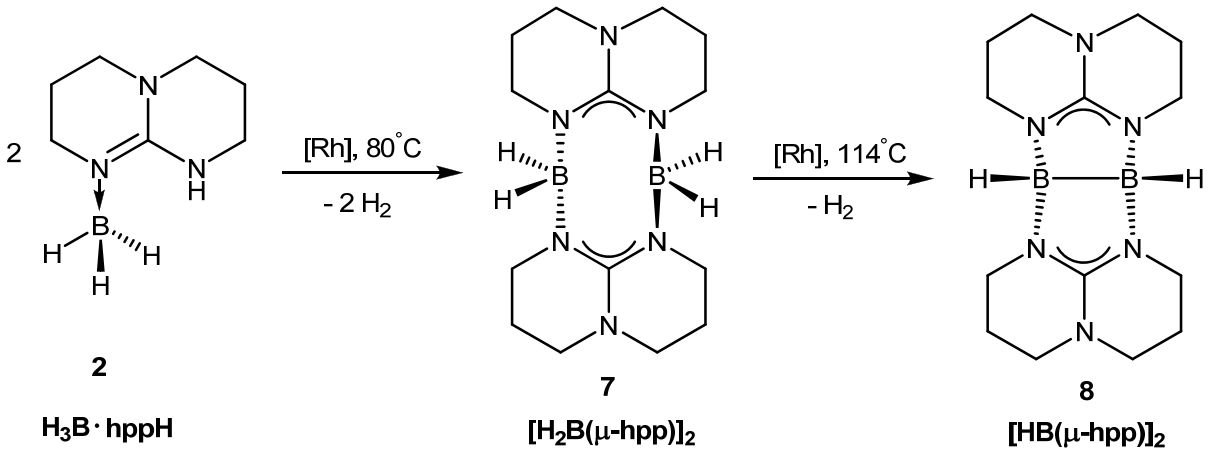

Scheme 2: Synthesis of binuclear boron hydrides **7** and **8**.

The compound **7** and **8** adopt a chair-type (with a B···B separation of 306.5 pm) and a “roof-type” (with a B–B bond distance of 177.2 pm) conformation in the solid state, respectively (see Figure 2). Reaction of **8** with HX (X = Cl, or I) leads to the new boron hydrides $[H_3B_2(\mu\text{-hpp})_2]^+X$, **9** (X = I) and **10** (X = Cl), representing stable $B_2H_5^+$ analogues (see Scheme 3).

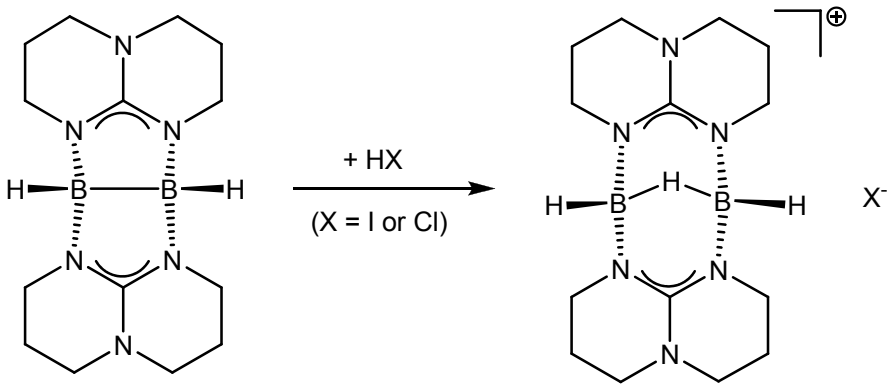

8
[HB(μ-hpp)]$_2$

9 (X = I); 10 (X = Cl)
[H_3B_2(μ-hpp)$_2$]$^+X^-$

Scheme 3: Synthesis of the binuclear boron hydrides **9** and **10**.

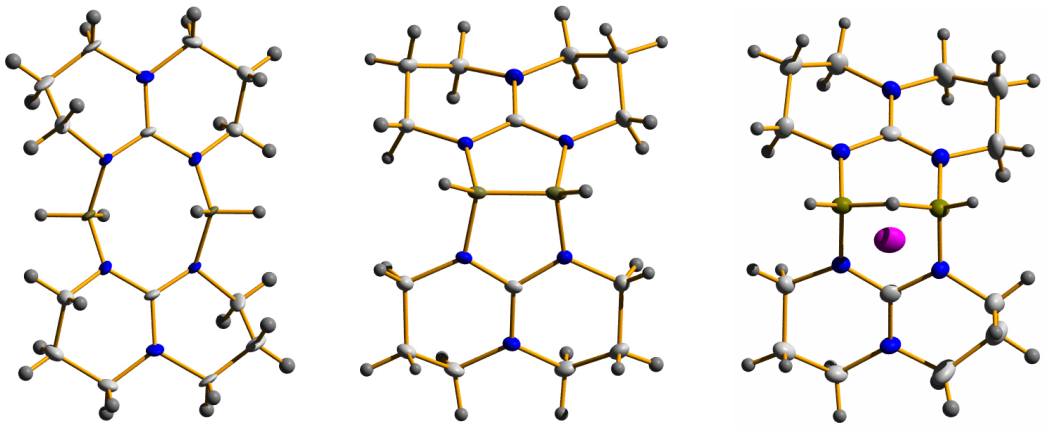

7 **8** **9**

Figure 2: The molecular structures of **7**, **8** and **9** from X-ray diffraction results. ● C, ● H, ● B, ● I, ● N atoms.

These species decompose slowly in toluene solutions with formation of [hppH$_2$]X (X = I$^-$, Cl$^-$) side- products. In the solid state, however, both $B_2H_5^+$ analogues are stable compounds. Compound **9** was characterized by spectroscopic methods, as well as X-ray data (see Figure 2), while **10** was analyzed only by spectroscopic methods. In addition, the topology of the electron distribution in [H_3B_2(hpp)$_2$]$^+$ was calculated and compared with the compounds $B_2H_5^+$ and B_2H_6 to obtain some information about the bond properties in species **9** and **10**.

Reaction of BCl_3 with hppH proceeds differently to that between $Me_3N{\cdot}BH_3$ and hppH, resulting in formation of the compound $[(ClB)_2(\mu\text{-hpp})_3]BCl_4$ **14** (see Scheme 4).

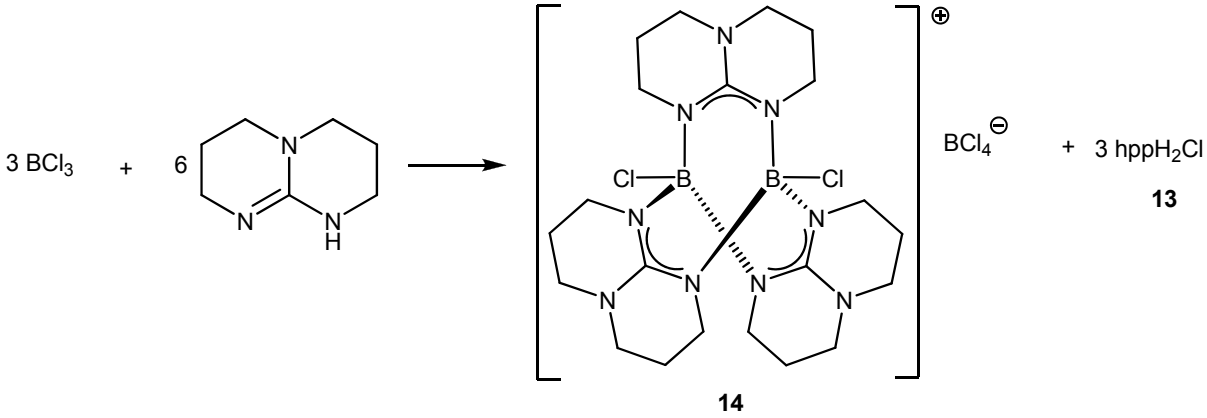

Scheme 4: Synthesis of compound **14**.

This compound was characterized by NMR spectroscopic methods, as well as X-ray analyses. XRD analysis shows that the two boron atoms in **14** are bridge by three guanidinate (hpp) ligands (see Figure 3) instead of two as in case of the complexes **7** – **9**, and **15** – **17, 19** (see Figure 2, 4 and 5).

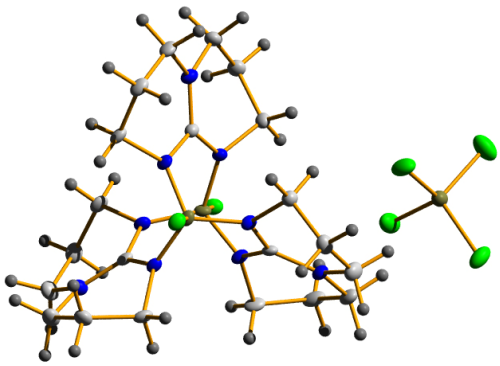

Figure 3: The molecular structures of **14** from X-ray diffraction results. ● C, ● H, ● B, ● Cl, ● N atoms.

In further experiments we synthesized and characterized new binuclear boron di- and monocations with bridging guanidinate hpp ligands. Reaction between the diborane(4) $B_2Cl_2(NMe_2)_2$ and hppH leads to$[\{(Me_2(H)N)B(\mu\text{-hpp})\}_2]Cl_2$. Most likely, the reaction proceeds in two steps via the intermediate $[(Me_2N)B(\mu\text{-hpp})]_2$, **15A**, which reacts with the released HCl to give **15** (see Scheme 5).

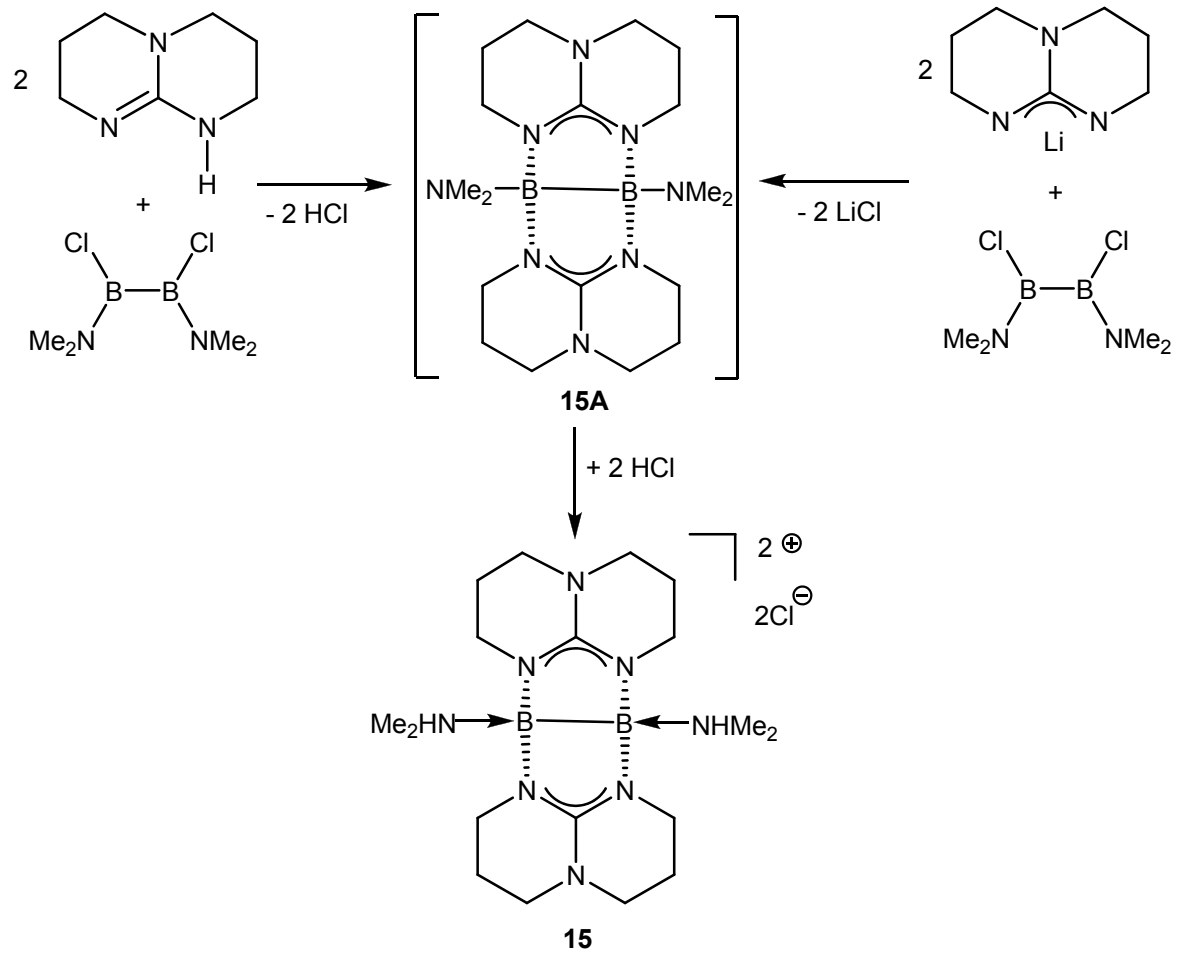

Scheme 5

This compound was characterized by spectroscopic and X-ray data. It was found that **15** adopts a “roof-type” conformation (with a B-B bond distance of 174.6 pm) in the solid state (see Figure 4).

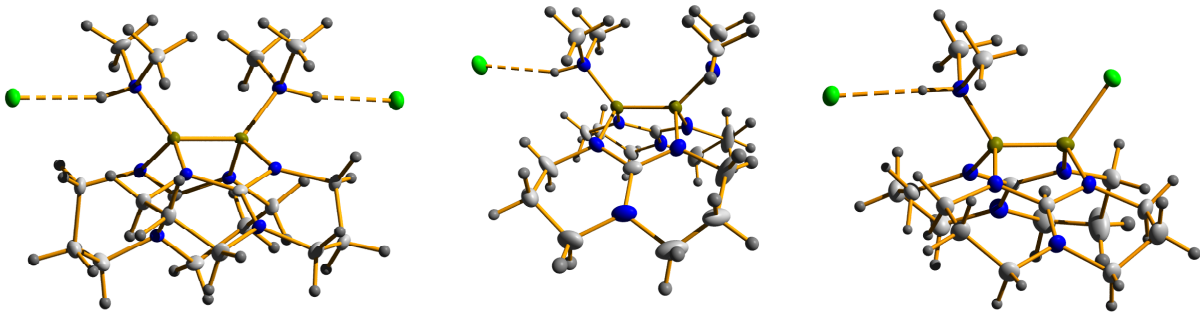

15 **16** **17**

Figure 4: The molecular structures of **15**, **16** and **17** from X-ray diffraction results. ● C, ● H, ● B, ● Cl, ● N atoms.

In addition, thermogravimetric analysis and quantum chemical calculations show the relative weakness of the B-NMe_2H bonds. The removal of the NMe_2H groups right yield a salt of tri-coordinated binuclear boron (II) compound $[B_2(\mu\text{-hpp})_2]^{2+}$ which possibly exhibits interesting for catalytic applications. Reaction between the diborane (4) $B_2Cl_2(NMe_2)_2$ and Li(hpp) leads to $[(Me_2N)B(\mu\text{-hpp})]_2$ **15A** (see Scheme 5). This species can be protonated by $HCl{\cdot}OEt_2$ to give **15** (see Scheme 5). This experiment proved the proposed reaction pathway for the formation of **15**. The unsymmetrical binuclear boron monocation $[(Me_2N)B_2(\mu\text{-hpp})_2(NHMe_2)]^+$ is also obtained. Compound **15** eliminates $NHMe_2$ in a slow reaction leading to $[ClB_2(\mu\text{-hpp})_2(NHMe_2)]Cl$ **17**. We reported the crystal structures of the two binuclear boron monocations $[(Me_2N)B_2(\mu\text{-hpp})_2(NHMe_2)]Cl$ **16** and $[ClB_2(\mu\text{-hpp})_2(NHMe_2)]Cl$ **17** (see Figure 4). The experimental results were accompanied by some quantum chemical (DFT) calculations. Furthermore, the reactions of compound **15** with AgOTf and $Li[B(C_6F_5)_4]$ were studied which lead to $[\{(Me_2(H)N)B(\mu\text{-hpp})\}_2]OTf_2$ **19** and $[\{Me_2(H)N)B(hpp)\}_2][B(C_6F_5)_4]_2$ **20**, containing weakly coordinating anions (see Scheme 6).

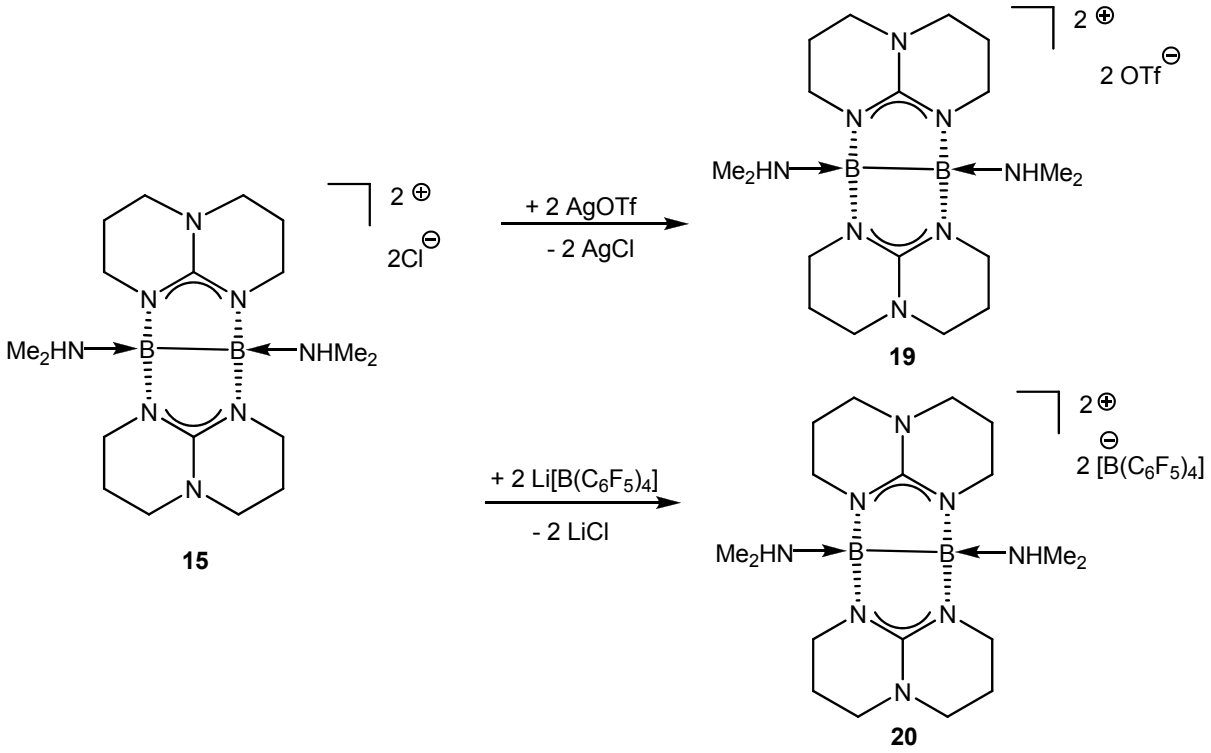

Scheme 6: Synthesis of the compounds **19** and **20**.

The crystal structure of **19** is reported, which shows a “roof-type” conformation (with a B-B bond distance of 172.4 pm) in the solid state (see Figure 5). In addition, thermal decompositions of the obtained new salts of the dicationic binuclear B(II) compound $[\{Me_2(H)N)B(hpp)\}_2]^{2+}$ were compared on the basis of NMR experiments.

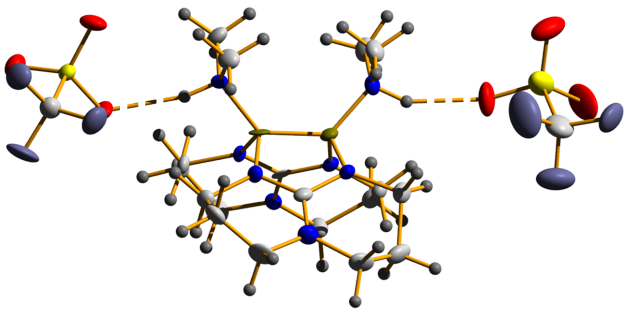

Figure 5: The molecular structures of **19** from X-ray diffraction results. ● C, ● H, ● B, ● F, ● N, ● O, ● S atoms.

4. Experimental Part

4.1 General Comments

Schlenk techniques were applied in all synthetic work. The solvents were dried with the appropriate drying agents and distilled by standard methods, and kept over 4 Å molecular sieves in Schlenk flask under argon atmosphere. A bubbler with paraffin oil served for pressure balance during the reactions. In order to lubricate the ground glass joints, we used the Silicon high-vacuum grease (heavy) from the company Wacker.

IR Spectroscopy

Infrared spectra were recorded with a BIORAD Excalibur FTS 3000. The following terms have been used: w = week, m = medium, s = strong, ip = in phase, oop = out-of-phase.

Melting Points

Melting points were measured with open glass capillaries using a Gallenkamp melting point apparatus.

EA

Elemental analyses were carried out at the Microanalytical Laboratory of the University of Heidelberg.

NMR Spectra

NMR spectra were measured by using the following instruments:

^{1}H-NMR	200 MHz	Bruker Avance DPX AC200
	400 MHz	Bruker Avance II 400
^{13}C-NMR	200 MHz	Bruker Avance DPX AC200
	400 MHz	Bruker Avance II 400

^{11}B-NMR	64 MHZ	Bruker Avance DPX AC200
	128 MHz	Bruker Avance II 400
^{19}F-NMR	376 MHz	Bruker Avance II 400

Benzene-d_6, Toluene-d_8, CD_2Cl_2 and $CDCl_3$ were used as deuterated solvents.

Meaning of the abbreviations in NMR spectra: s = singlet, d = doublet, t = triplet, qui = quintet, ddd = doublet of double-doublets, m = multiplet, br = broad, q = quartet, bq = broad quartet

Mass Spectrometry

Low-resolution mass spectra were recorded on a Finnigan MAT 8230. High-resolution mass spectra and ESI were measured on a Jeol JMS-700 and Bruker ApexQe hybrid 9.4 T FT-ICR spectrometers, respectively.

X-Ray Crystallographic Study

Suitable crystals were taken directly out of the mother liquor, immersed in perfluorinated polyether oil, and fixed on top of a glass capillary. Measurements were made at low temperature (200 and 100 K) on Nonius-Kappa CCD and Bruker AXS Smart 1000 diffractometers (Mo-$K\alpha$ radiation, graphite monochromator, λ = 0.71073 Å). The data collected were processed using the standard Nonius[1] and Bruker software.[2], [3] The structures were solved by the heavy atom method combined with structure expansion by direct methods applied to difference structure factors[4] (**14**), by direct methods with dual-space recycling („Shake-and-Bake")[5] (**19**) or by conventional direct methods (all others), and refined by full-matrix least squares methods based on F^2 against all unique reflections.[6], [7]. Graphical handling of the structural data during solution and refinement was performed with XPMA.[8] The structures have been produced and visualized using Diamond[9] and POVRay[10] programs.

Reagents and Solvents

^{n}Butyllithium, 1.6 M in ^{n}Hexanes	Acros
BCl_3, 1 M in hexane	Aldrich
BCl_3, 1 M in heptane	Aldrich
HCl, 1 M solution in Et_2O	Acros
$B_2(NMe_2)_4$	Boron Molecular Pty Ltd.
Bromopentafluorobenzene	Aldrich
hppH	Acros
$H_3B{\cdot}NMe_3$	Aldrich
$N(H)C(NMe_2)_2$	Aldrich
Cp_2TiCl	Aldrich
$[Rh(1,5\text{-}COD)Cl]_2$	Aldrich
$[(PPh_3)RhCl]$	Aldrich

4.2 Synthesis of new guanidine-borane adducts

4.2.1 Synthesis of $H_3B{\cdot}hppH$

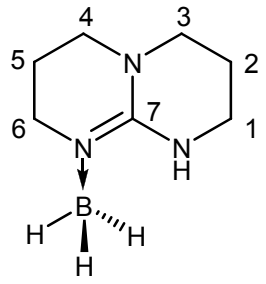

$C_7H_{16}BN_3$

Mol. Wt: 153.03 g/mol

Materials

hppH	0.590 g	4.24 mmol
$H_3B{\cdot}NMe_3$	0.309 g	4.24 mmol
Toluene	40 mL	

Experimental

A solution of $H_3B{\cdot}NMe_3$ (0.309 g, 4.24 mmol) in toluene (20 mL) was added to a solution of hppH (0.590 g, 4.24 mmol) in toluene (20 mL) by syringe, and the reaction was stirred for 18 h at 60°C. The colourless solution was concentrated, and n-pentane (ca. 15 mL) was added to obtain a white precipitate. Crystals suitable for X-ray diffraction were grown from hexane/toluene (2:1) mixture at -20°C.

Yield

0.649 g 4.24 mmol 79 %

^{1}H NMR (400 MHz, C_6D_6):

δ [ppm] = 6.29 (s, NH, 1H), 3.34 (t, H6, 2H, ^3J(H-H) = 5.9 Hz), 2.83 (bq, BH_3, 3H, ^1J(H-B) = 93 Hz), 2.27 (t, H3, 2H, ^3J(H-H) = 5.9 Hz), 2.13 (t, H4, 2H, ^3J(H-H) = 6.0 Hz), 2.03 (t, H1, 2H, ^3J(H-H) = 6.0 Hz), 1.17 (qui, H5, 2H, ^3J(H-H) = 6.0 Hz), 0.9 (qui, H2, 2H, ^3J(H-H) = 6.0 Hz).

^{13}C NMR (100.6 MHz, C_6D_6):

δ [ppm] = 150.69 (C7), 47.47 (C6), 47.27 (C4), 46.82 (C1), 38.38 (C3), 21.80 (C5), 21.57 (C2).

^{11}B NMR (128.3 MHz, C_6D_6):

δ [ppm] = -19.1 (q, BH_3, ^1J(B-H) = 93 Hz).

HRMS (EI$^+$):

m/z (%) = 152.14 (100.0) $[C_7H_{15}BN_3]^+$, 138.10 (28.2) $[C_7H_{13}N_3]^+$, 122.09 (5.6) $[C_6H_{11}BN_2]^+$, 113.00 (5.1) $[C_6H_{13}N_2]^+$, 95.07 (2.8) $[C_5H_7N_2]^+$.

IR (solid CsI):

3352 (s) ν(N-H), 2960 (m) ν(C-H), 2872 (m) ν(C-H), 2363 (m) ν(B-H), 2301 (m) ν(B-H), 2253 (m) ν(B-H), 1625 (s) ν(C=N), 1570 (s) δ(N-H), 1447 (w) δ(C-H), 1322 (m) (B-N), 1174 (m), 1148 (m).

EA:

calcd. C [%] 54.94, H [%] 10.54, N [%] 27.46.

found C [%] 54.36, H [%] 10.38, N [%] 26.91.

Melting point:

65 °C

4.2.2 Synthesis of $H_3B{\cdot}N(H)C(NMe_2)_2$

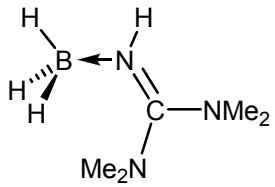

$C_5H_{16}BN_3$

Mol. Wt: 129.01 g/mol

Materials

$N(H)C(NMe_2)_2$	0.644 g	5.6 mmol
$H_3B{\cdot}NMe_3$	0.420 g	5.7 mmol
Toluene	20 mL	

Experimental

A solution of $H_3B{\cdot}NMe_3$ (0.420 g, 5.7 mmol) in toluene (30 mL) was slowly added by syringe to a stirred solution of 1,1,3,3-tetramethylguanidine (0.644 g, 5.6 mmol) in toluene (20 mL). The reaction mixture was stirred for 18 h at 80°C. The resulting solution was concentrated and stored at -20°C to give colourless crystals of $H_3B{\cdot}N(H)C(NMe_2)_2$.

^{1}H NMR (400 MHz, C_6D_6):

δ [ppm] = 4.61 (s, NH, 1H), 2.80 (bq, BH_3, 3H, ^1J(H-B) = 95 Hz), 2.51 (s, Me_2N, 6H), 1.72 (s, Me_2N, 6H).

^{13}C NMR (100.6 MHz, C_6D_6):

δ [ppm] = 37.83 (CH_3), 39.63 (CH_3).

^{11}B NMR (128.3 MHz, C_6D_6):

δ [ppm] = -19.5 (q, *B*H_3, ^1J(B-H) = 95 Hz,).

HRMS (EI$^+$):

m/z (%) = 128.2 (78) $[C_5H_{15}BN_3]^+$, 126.2 (100) $[C_5H_{13}BN_3]^+$, 115.2 (2) $[C_5H_{13}N_3]^+$, 110.2 (8) $[C_4H_9BN_3]^+$, 85.2 (24) $[C_3H_7N_3]^+$, 71.2 (31) $[C_3H_7N_2]^+$.

IR (solid CsI):

3337 (m) ν(N-H), 2949 (m) ν(C-H), 2365 (m) ν(B-H), 2291 (m) ν(B-H), 2259 (m) ν(B-H), 2239 (m) ν(B-H), 1593 (s) ν(C=N), 1453 (m) δ(C-H), 1433 (m) δ(C-H), 1159 (m) δ (B-H), 1072 (m) δ (B-H), 1042 (m) δ (B-H), 806 (w) δ (N-H, oop).

EA :

calcd. C [%] 46.55, H [%] 12.50, N [%] 32.57.

found C [%] 45.54, H [%] 11.87, N [%] 31.06.

4.3 Thermal and catalytic dehydrogenation of guanidine-borane adducts

4.3.1 Thermal dehydrogenation of H_3B·hppH at 80°C

A solution of H_3B·hppH (0.15 g, 0.98 mmol) in toluene (10 mL) was stirred for 23 h at 80°C. Removal of the solvent resulted in an oil, the ^{11}B NMR spectrum of which showed the presence of species: **7A** [δ = 2.5 ppm (d, ^1J(B-H) = 123 Hz)], **7B** [δ = -6.2 ppm (t, ^1J(B-H) = 102 Hz)], **(minor products)** [δ = 22.4 ppm (s) and δ = 28.1 ppm (s)].

4.3.2 Thermal dehydrogenation of H_3B·hppH at 110°C

A solution of H_3B·hppH (0.071 g, 0.46 mmol) in toluene (10 mL) was stirred for 23 h at 110°C. Removal of the solvent resulted in an oil, the ^{11}B NMR spectrum of which showed the presence of species: **7A** [δ = 2.5 ppm (d, ^1J(B-H) = 123 Hz)], **7** [δ = -2.3 (t, ^1J(B-H) = 100 Hz)], **(minor products)** [δ = 22.4 ppm (s) and δ = 28.1 ppm (s)].

4.3.3 Thermal dehydrogenation of $H_3B{\cdot}N(H)C(NMe_2)_2$ at 80°C and 110°C

A solution of $H_3B{\cdot}N(H)C(NMe_2)_2$ (0.15 g, 1.16 mmol) in toluene (12 mL) was stirred for 20 h at 80°C. The ^{11}B NMR spectrum recorded afterwards showed the presence of unreacted $H_3B{\cdot}N(H)C(NMe_2)_2$. In addition, a new weak quartet signal appeared belonging to species **3A** [δ = -12.6 ppm (q, *J*(B-H) = 98 Hz)].

4.3.4 Catalysed dehydrogenation of $H_3B{\cdot}$hppH at 80°C in the presence of $[Rh(1,5\text{-}COD)Cl]_2$

$H_3B{\cdot}$hppH (0.13 g, 0.80 mmol) was dissolved in toluene (10 mL) and $[Rh(1,5\text{-}COD)Cl]_2$ (0.0079 g, 0.016 mmol, ca. 2 mol-% [Rh]) was added. After stirring the reaction mixture for 23 h at 80°C, the solution was filtered. The NMR spectra provided evidence for the presence of two species: **7** [δ = -2.3 (t, ^1J(B-H) = 100 Hz)] and **(minor product)**: ^{1}H NMR (400 MHz, C_6D_6): δ [ppm] = 2.95 (t, H'2, 2H, ^3J(H-H) = 5.8 Hz), 2.42 (t, H'4, 2H, ^3J(H-H) = 5.8 Hz), 1.36 (qui, H'3, 2H, ^3J(H-H) = 5.8 Hz). ^{13} C NMR (100.6 MHz, C_6D_6): δ [ppm] = 47.2 (C'4), 41.0 (C'2), 23.0 (C'3).

4.3.5 Catalysed dehydrogenation of $H_3B{\cdot}N(H)C(NMe_2)_2$ at 80°C in the presence of $[Rh(1,5\text{-}COD)Cl]_2$

$H_3B{\cdot}N(H)C(NMe_2)_2$ (0.075 g, 0.58 mmol) was dissolved in toluene (10 mL). $[Rh(1,5\text{-}COD)Cl]_2$ (0.0057 g, ca. 2 mol-% [Rh]) was added as a solid, and the reaction mixture was stirred for 20 h at 80°C. The solution was filtered, and the pale-yellow solution was concentrated and stored for several weeks at -20 °C. The ^{11}B NMR spectrum provided evidence for the presence of different products: **3A** [δ = -12.6 ppm (q, ^1J(B-H) = 98 Hz)], **3B** [δ = -4.4 ppm (t, ^1J(B-H) = 103 Hz)], **3C** [δ = -1.9 (t, ^1J(B-H) = 101 Hz)]. In addition, weak and broader features showed at δ = 26.9 and 28.2 ppm.

4.3.6 Dehydrogenation of $H_3B{\cdot}$hppH at 115°C in the presence of $[(PPh_3)_3RhCl]$

$H_3B{\cdot}$hppH (0.265 g, 1.73 mmol) was dissolved in toluene (20 mL) and $[(PPh_3)_3RhCl]$ (0.0083 g, ca. 0.5 mol-%) was added. After stirring the reaction mixture for 46 h at 115°C, the solution was filtered. The ^{11}B NMR spectrum provided evidence for the presence of different products: **7A** [δ = 2.5 ppm (d, ^1J(B-H) = 123 Hz)] and **7** [δ = -2.3 (t, ^1J(B-H) = 100 Hz)].

4.3.7 Dehydrogenation of $H_3B{\cdot}N(H)C(NMe_2)_2$ at 80°C in the presence of Cp_2TiCl_2/*n*BuLi

Reaction of Cp_2TiCl_2 (0.0017 g) in d_8-toluene (0.4 mL) with *n*BuLi (0.009 mL, 1.6 M in hexane) at -10°C in an NMR tube resulted in the formation of a red-brown solution in 3 min. After being warmed to room temperature, $H_3B{\cdot}N(H)C(NMe_2)_2$ (0.04 g, 0.31 mmol) in d_8-toluene (0.6 mL) was added, and the reaction mixture was mixed for 3 min in an ultrasonic bath, which resulted in a change of colour from red-brown to grey. After flame sealing the NMR tube, the reaction was heated for ca. 6 d at 80°C. The reaction was monitored by NMR spectroscopy by providing evidence for the formation of **3B** [δ = -4.4 ppm (t, ^1J(B-H) = 103 Hz)] and **3C** [δ = -1.9 (t, ^1J(B-H) = 100 Hz)] as well as two further products with ^{11}B signals at δ = 26.9 and 28.2 ppm.

4.4 Synthesis of new binuclear boron hydrides containing two bridging guanidinate (hpp) ligands

4.4.1 Synthesis of $[H_2B(\mu\text{-hpp})]_2$

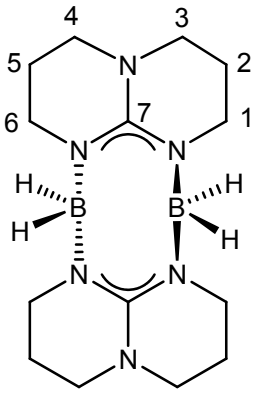

$C_{14}H_{28}B_2N_6$

Mol. Wt: 302.03 g/mol

Materials

hppH	1.720 g	12.36 mmol
$H_3B{\cdot}NMe_3$	0.902 g	12.36 mmol
Toluene	120 ml	

Experimental

A solution of $H_3B{\cdot}NMe_3$ (0.902 g, 12.36 mmol) in toluene (60 ml) was slowly added by syringe to a solution of hppH (1.720 g, 12.36 mmol) in toluene (60 ml). The reaction mixture was heated under reflux for 20 h. The colourless solution was concentrated, and hexane (ca. 50 ml) was added to obtain a white precipitate. Crystals suitable for X-ray diffraction were grown from DMSO at room temperature.

Yield

1.176 g 3.89 mmol 63%

^{1}H NMR (400 MHz, C_6D_6):

δ [ppm] = 3.25 (t, H1, 8H, ^3J(H-H) = 5.8 Hz), 2.47 (t, H3, 8H, ^3J(H-H) = 6.6 Hz), 1.49 (qui, H2, 8H, ^3J(H-H) = 5.8 Hz, ^3J(H-H) = 6.6 Hz).

^{13}C NMR (100.56 MHz, C_6D_6):

δ [ppm] = 47.88 (C3), 47.66 (C1), 24.11 (C2).

^{11}B NMR (128.3 MHz, C_6D_6):

δ [ppm] = -2.3 ppm (t, BH_2, ^1J(B-H) = 100 Hz).

MS (EI^+):

m/z (%) = 299.4 (100) $[C_{14}H_{25}B_2N_6]^+$, 138.2 (40) $[hpp]^+$.

IR (solid CsI):

2964 (m) ν(C-H), 2852 (m) ν(C-H), 2398-2230 (m) ν(B-H), 1565 (s) ν(CN), 1451 (m) δ(C-H), 1217 (s) δ(B-H), 1160 (s) δ(B-H), 799 cm^{-1} (m) ν(B-N).

EA :

calcd. C [%] 55.67, H [%] 9.34, N [%] 27.82.

found C [%] 54.30 , H [%] 9.35, N [%] 25.81.

Melting point:

225 °C

4.4.2 Synthesis of [HB(*μ*-hpp)]$_2$

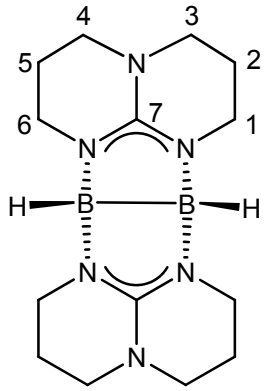

$C_{14}H_{26}B_2N_6$
Mol. Wt: 300.02 g/mol

The compound was synthesized by using two methods:

Method A:

Materials

[H_2B(*μ*-hpp)]$_2$	0.11 g	0.35 mmol
[Rh(1,5-cod)Cl]$_2$	0.0035 g	0.007 mmol
Toluene	25 mL	

Experimental

[H_2B(*μ*-hpp)]$_2$ (0.11 g, 0.35 mmol) was dissolved in toluene (25 mL) and [Rh(1,5-cod)Cl]$_2$ (0.0035 g, 0.007 mmol, ca. 2 mol-% Rh) was added as a solid. The reaction mixture was stirred for 43 h at 114 °C. After filtration, the resulting solution was concentrated and stored for several days at -20°C to afford X-ray quality colourless crystals of [HB(*μ*-hpp)]$_2$.

Yield

0.09 g	0.30 mmol	86 %

Method B:

Materials

hppH	2.51 g	18.03 mmol
$H_3B{\cdot}NMe_3$	1.32 g	18.03 mmol
$[Rh(1,5\text{-cod})Cl]_2$	0.0197 g	0.036 mmol
Toluene	75 mL	

Experimental

A solution of $H_3B{\cdot}NMe_3$ (1.32 g, 18.03 mmol) in toluene (40 mL) was slowly added by syringe to a stirred solution of hppH (2.51 g, 18.03 mmol) in toluene (35 mL). The precatalyst $[Rh(1,5\text{-cod})Cl]_2$ (0.0197 g, 0.036 mmol, ca. 0.2 mol-% Rh) was added as a solid, and the reaction mixture was stirred for 65 h at 114°C. The solution was filtered, and the pale-yellow solution was concentrated and stored for several days at -20°C to give colourless crystals of $[HB(hpp)]_2$.

Yield

2.16 g	7.20 mmol	80 %

^{1}H NMR (400 MHz, C_6D_6):

δ [ppm] = 3.51 (m, H1a, 4H), 3.39 (ddd, H1b, 4H, ^2J(H1b-H1a) = 12.6, ^3J(H1b-H2a) = 7.8, ^3J(H1b-H2b) = 4.8 Hz), 2.42 (m, H3a, 4H), 2.31 (ddd, H3b, 4H, ^2J(H3b-H3a) = 11.0 Hz, ^3J(H3b-H2a) = 5.4 Hz, ^3J(H3b-H2b) = 5.4 Hz), 1.47 ppm (m, H2, 8H).

^{13}C NMR (100.6 MHz, C_6D_6):

δ [ppm] = 156.89 (C7), 47.07 (C3), 45.82 (C1), 23.26 ppm (C2).

^{11}B NMR (128.3 MHz, C_6D_6):

δ [ppm] = - 1.14 ppm (br, *B*H).

MS (EI$^+$):

m/z (%) = 299.5 (100) $[C_{14}H_{25}B_2N_6]^+$.

IR (solid CsI):

2936 (m) ν(C-H), 2843 (m) ν(C-H), 2272 (m) ν(B-H ip), 2249 (m) ν(B-H oop), 1576 (s) ν(CN), 1313 (m) δ(C-H), 1076 (m) δ(B-H), 906 cm^{-1} (m) ν(B-N).

EA :

calcd. C [%] 56.05, H [%] 8.73, N [%] 28.01.

found C [%] 55.70, H [%] 8.80, N [%] 27.57.

4.4.3 Synthesis of $[H_3B_2(\mu\text{-hpp})_2]I$

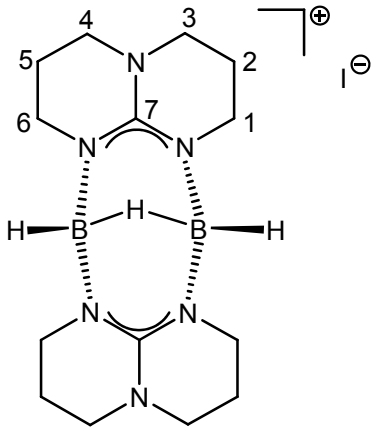

$C_{14}H_{27}B_2IN_6$

Mol. Wt: 427.93 g/mol

Materials

$[HB(\mu\text{-hpp})]_2$	0.09 g	0.28 mmol
I_2	0.035 g	0.14 mmol
Toluene	35 mL	

Experimental

A solution of I_2 (0.035 g, 0.14 mmol) in toluene (10 mL) was slowly added to a stirred solution of $[HB(\mu\text{-hpp})]_2$ (0.09 g, 0.28 mmol) in toluene (25 mL) at 0 °C. After stirring for 20 h, the solution was filtered. Removal of the solvent under reduced pressure led to a white precipitate (together with small traces of $hppH_2I$). Crystals suitable for X-ray diffraction were grown from a hexane/toluene (2:1) mixture at 3°C.

Yield

0.024 g 0.06 mmol 40 %

^{1}H NMR (400 MHz, C_6D_6):

δ [ppm] = 3.65 (ddd, H1a, 4H, ^{2}J(H1a-H1b) = 11.3 Hz, ^{3}J(H1a-H2a) = 9.32 Hz, ^{3}J(H1a-H2b) = 4.71 Hz), 3.42 (ddd, H3a, 4H, ^{2}J(H3a-H3b) = 11.96 Hz, ^{3}J(H3a-H2a) = 9.65 Hz, ^{3}J(H3a-H2b) = 3.92 Hz), 2.78 (m, H3b, 4H), 2.29 (m, H1b, 4H), 1.71 (m, H2a, 4H), 1.33 ppm (m, H2b, 4H).

^{13}C NMR (100.56 MHz, C_6D_6):

δ [ppm] = 47.08 (C1), 43.07 (C3), 21.64 ppm (C2).

^{11}B NMR (128.3 MHz, C_6D_6):

δ [ppm] = – 2.20 ppm (dd ^{1}J(B-$H_{term.}$) = 125 Hz, ^{1}J(B-H_{bridge}) = 40 Hz).

MS (EI^+):

m/z (%) = 299.2 (100) $[C_{14}H_{25}N_6B_2]^+$, 301 (60) $[C_{14}H_{27}N_6B_2]^+$.

IR (solid CsI):

2954 (m) ν(C-H), 2863 (m) ν(C-H), 2425 (m) ν(B-H_t), 1872 (m) ν(B-H_b), 1601 (s) ν(CN), 1571 (s) ν(CN), 1325 (m) δ(C-H), 1235 (m) δ(C-H), 1143 (m) δ(B-H), 1046 cm^{-1} (m) ν(B-N).

EA ($C_{14}H_{27}B_2IN_6$ + $C_7H_{14}IN_3$):

calcd. C [%] 36.29, H [%] 5.95, N [%] 18.14.

found C [%] 37.97, H [%] 6.31, N [%] 17.78.

4.4.4 Synthesis of $[H_3B_2(\mu\text{-hpp})_2]Cl$

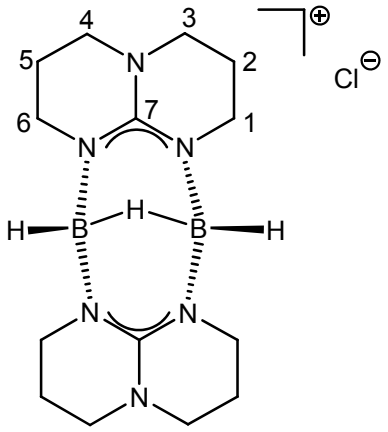

$C_{14}H_{27}B_2ClN_6$

Mol. Wt: 336.48 g/mol

Materials

$[HB(\mu\text{-hpp})]_2$	0.075 g	0.25 mmol
HCl (1M solution in Et_2O)		0.25 mmol
Toluene	30 mL	

Experimental

A solution of $[HB(\mu\text{-hpp})]_2$ in 30 mL toluene was cooled to 30°C and 1 equiv. of HCl (1 M solution in Et_2O) added. The solution was allowed to warm up to room temperature and stirred for 20 h, during which time a white precipitate was observed. Then the precipitate was filtered off and dried under vacuum leading to 0.03 g of $[H_3B_2(\mu\text{-hpp})_2]Cl$ (together with traces of hpp_2Cl).

Yield

0.03 g	0.09 mmol	40 %

^{1}H NMR (400 MHz, $CDCl_3$):

δ [ppm] = 3.59 (ddd, H2a, 4H, ^2J(H2a-H2b) = 12.43 Hz, ^3J(H2a-H3a) = 7.95 Hz, ^3J(H2a-H3b) = 4.86 Hz), 3.38 (ddd, H4a, 4H, ^2J(H4a-H4b) = 12.34 Hz, ^3J(H4a-H3a) = 8.23 Hz, ^3J(H4a-H3b) = 4.06 Hz), 3.31 (m, H4b, 4H), 3.20 (m, H2b, 4H), 2.08 (m, H3a, 4H), 1.96 (m, H3b, 4H).

^{13}C NMR (100.56 MHz, $CDCl_3$):

δ [ppm] = 47.59 (C1), 43.90 (C3), 21.80 (C2).

^{11}B NMR (128.3 MHz, $CDCl_3$):

δ [ppm] = – 1.10 ppm.

IR (solid CsI):

2954 (m) ν(C-H), 2863 (m) ν(C-H), 2425 (m) ν(B-H_t), 1872 (m) ν(B-H_b), 1601 (s) ν(CN), 1571 (s) ν(CN), 1325 (m) δ(C-H), 1235 (m) δ(C-H), 1143 (m) δ(B-H), 1046 cm^{-1} (m) ν(B-N).

4.5 Synthesis and characterization of new binuclear boron monocation containing three bridging guanidinate (hpp) ligands

4.5.1 Synthesis of $[Cl_2B_2(\mu\text{-hpp})_3]BCl_4$

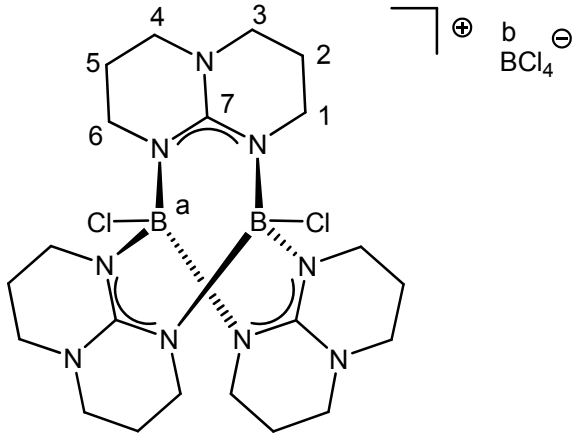

$C_{21}H_{36}B_2Cl_2N_9$

Mol. Wt: 659.72 g/mol

Materials

hppH	0.30 g	2.16 mmol
BCl_3 (1 M in toluene)	2.16 mL	2.16 mmol
Toluene	15 mL	

Experimental

A solution of BCl_3 (2.16 mL, 1M in toluene) was added to a solution of hppH (0.30 g, 2.16 mmol) in toluene (15 mL) by syringe, and the reaction mixture was stirred for 4 h at room temperature, after which the reaction was filtered and the volatiles were removed to afford an oil. The oil was dissolved in CH_2Cl_2 and [hppH$_2$]Cl was removed partial by filtration. Colourless crystals were grown from dichloromethane/hexane (2:1) mixture at 3°C.

^{1}H NMR (400 MHz, CD_2Cl_2):

δ [ppm] = 3.75 (br, H1a, 6H), 2.62 (t, H1b, 6H), 3.34 (br, H3a, 6H), 3.20 (br, H3b, 6H), 2.3 (br, H2a, 6H), 1.90 (br, H2b, 6H).

^{13}C NMR (100.56 MHz, CD_2Cl_2):

δ [ppm] = 47.9 (C-3), 41.8 (C-1), 24.0 (C-2).

^{11}B NMR (128.30 MHz, CD_2Cl_2):

δ [ppm] = 4.5 (s, B-a), 6.9 (s, B-b).

4.6 Synthesis and characterization of new binuclear boron di- and monocations containing two bridging guanidinate (hpp) ligands

4.6.1 Synthesis of starting materials

4.6.1.1 Synthesis of Tris(pentafluorophenyl)borane

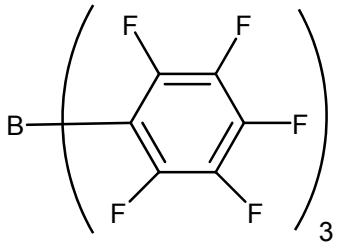

$C_{18}BF_{15}$

Mol. Wt: 511.98 g/mol

Materials

Bromopentafluorobenzene	5.00 g	20.0 mmol
^{n}BuLi (1.6 M in hexane)	12.7 ml	20.2 mmol
BCl_3 (1 M in heptane)	6.7 ml	6.7 mmol
Hexane	45.0 ml	

Experimental

2.5 mL of bromopentafluorobenzene (5.00 g, 20.2 mmol, ρ = 1.98 g/mL) were dissolved in dry hexane (45.0 mL) in a 100 mL three necked flask and then cooled down to -75°C by using an ethanol-liquid nitrogen bath. Subsequently, 12.7 mL of ^{n}BuLi (1.6 M in hexane, 20.2 mmol) were slowly added whereupon the solution turned milky white. Then the mixture was warmed to -55°C over a period of one hour and afterwards was stirred at -25°C for another hour. After cooling again to -78°C the BCl_3 (6.7 mL, 6.7 mmol) was dropped slowly to the mixture, which was then slowly warmed up to room temperature. After leaving over night the precipitate was separated from the solution by decanting. Finally, the solvent was removed under vacuum to yield a white solid. The solid was weighed and kept in the glovebox due to its high sensitivity to water.

Yield

1.48 g	2.9 mmol	40-50 %

^{11}B-NMR (128.3 MHz, C_6D_6):

δ [ppm] = 7.41

4.6.1.2 Synthesis of Lithium tetrakis(pentafluorophenyl)borate

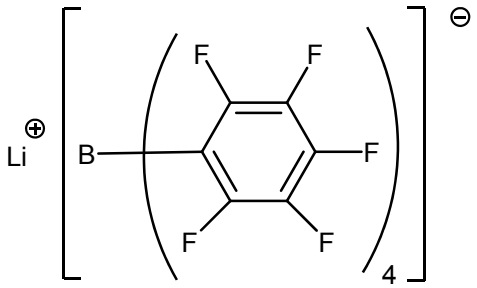

$C_{24}BF_{20}Li$

Mol. Wt: 685.98 g/mol

Materials

Bromopentafluorobenzene	0.86 g	3.5 mmol
^{n}BuLi (1.6 M in hexane)	2.1 ml	3.1 mmol
$B(C_6F_5)_3$	1.48 g	2.9 mmol
Diethylether	10.0 ml	
Hexane	30.0 ml	

Experimental

In a 50 ml schlenk-flask, a solution of 0.44 mL of bromopentafluorobenzene (0.86 g, 3.5 mmol) in 10.0 mL diethylether was cooled (by using EtOH/N_2(l) bath) to -100°C and then the ^{n}BuLi (2.1 mL, 3.1 mmol) was added slowly via syringe. The solution was stirred for 1 h at -50°C and then warmed to -20°C over a period of 1 h. After this, the solution was transferred at room temperature via canula into a suspension of $B(C_6F_5)_3$ (1.48 g, 2.9 mmol) in 30 ml of hexane. After stirring for 2 h at room temperature the white precipitate was filtrated and dried under vacuum.

Yield

1.24 g	1.8 mmol	62 %

^{11}B-NMR (128.3 MHz, CD_2Cl_2):

δ [ppm] = -16.7

4.6.1.3 Synthesis of 1,2-Dichloro-1,2-(bisdimethyldiamino)-diborane

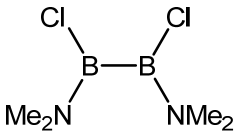

$C_4H_{12}B_2Cl_2N_2$

Mol. Wt: 180.68 g/mol

Materials

$B_2(NMe_2)_4$	4.32 g	21.8 mmol
HCl (1M olution in Et_2O)	87.3 ml	87.3 mmol
Et_2O	40.0 ml	

Experimental

To a rapidly stirred solution of $B_2(NMe_2)_4$ (5.0 mL, ρ = 0.864 g/mL, 4.32 g, 21.8 mmol) in Et_2O (40.0 mL) in a 250 ml schlenk-flask, a solution of HCl in Et_2O (1 M, 87.3 mL, 87.3 mmol) was added over a period of 10 min, during which time a large amount of a white precipitate was formed. The reaction mixture was stirred for 1 h, after which time it was filtrated. The solid filtercake was washed with Et_2O (2 x 10 mL) and all solvent was then carefully removed from the colorless filtrate by vacuum pumping at room temperature affording a yellowish oil. Vacuum distillation of the raw product (28-35°C, 0.4-0.35 mbar) afforded pure 1,2-$B_2Cl_2(NMe_2)_2$ as a colourless liquid.

Yield

2.88 g	15.9 mmol	73 %

^{1}H-NMR ($CDCl_3$, 200 MHz):

δ [ppm] = 2.88 (s, 6H), 2.86 (s, 6H).

^{11}B-NMR ($CDCl_3$, 64 MHz):

δ [ppm] = 40.6.

4.6.2 Synthesis of [{(Me_2(H)N)B(μ-hpp)}$_2$]Cl_2

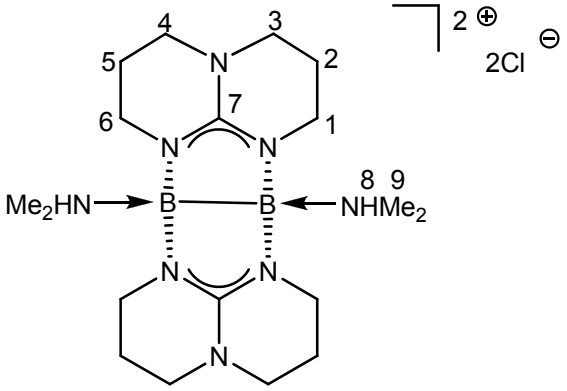

$C_{18}H_{38}B_2Cl_2N_8$

Mol. Wt: 459.08 g/mol

Materials

1,2-$B_2Cl_2(NMe_2)_2$	2.88 g	15.9 mmol
hppH	4.43 g	31.8 mmol
Toluene	200 ml	

Experimental

1,2-$B_2Cl_2(NMe_2)_2$ (2.88 g, 15.9 mmol) was slowly added to a stirred solution of hppH (4.43 g, 31.8 mmol) in toluene (200.0 ml) by syringe, and the reaction mixture was then stirred at room temperature for 14 h. The product was separated by filtration and washed two times with 12.0 ml of toluene to give, after recrystallization from CH_2Cl_2, a colorless solid. X-ray quality crystals were grown from a mixture of dichloromethane/hexane at room temperature.

Yield

4.47 g	9.7 mmol	61 %

^{1}H-NMR (400 MHz, CD_2Cl_2):

δ [ppm] = 8.90 (septet, H8, 2H, ^3J(H8-H9) = 5.5), 3.67 (dt, H1a, 4H, ^2J(H1a-H1b) = 12.8 Hz, ^3J(H1a-H2) = 5.0 Hz), 3.30 (dt, H1b, 4H, ^2J(H1b-H1a) = 12.8 Hz, ^3J(H1b-H2) = 6.5 Hz), 3.19 (dt, H3a, 4H, ^2J(H3a-H3b) = 11.9 Hz, ^3J(H3a-H2) = 5.0 Hz), 3.12 (dt,

H3b, 4H, ^{2}J(H3b-H3a) = 11.9 Hz, ^{3}J(H3b-H2) = 6.5 Hz) 2.42 (d, H9, 12H, ^{3}J(H9-H8) = 5.5 Hz), 1.89 (q, H2, 8H, ^{3}J(H2-H1a) = 5.0 Hz, ^{3}J(H2-H1b) = 6.5 Hz, ^{3}J(H2-H3a) = 5.0 Hz, ^{3}J(H2-H3b) = 6.5 Hz).

^{13}C-NMR (100.56 MHz, CD_2Cl_2):

δ [ppm] = 158.36 (C7), 47.79 (C3), 40.39 (C1), 39.86 (C9), 22.18 (C2).

^{11}B-NMR (128.3 MHz, CD_2Cl_2):

δ [ppm] = 1.43.

IR (CH_2Cl_2):

3945 (w), 3691 (w), 3055 (s) ν(C-H), 2987 (s) ν(C-H), 2686 (w), 2522 (w), 2411 (w), 2306 (m), 1590/1562 (m), 1422 (s), 1326 (w), 1271/1269 cm-1 (s) ν(B-N).

MS (ESI$^+$):

m/z (%)*:* 881.8 $[C_{23}H_{46}B_2Cl_{12}N_8]^+$, 809.7 $[C_{23}H_{45}B_2Cl_{10}N_8]^+$, 423.5 $[C_{18}H_{38}B_2Cl_1N_8]^+$, 387.5 $[C_{18}H_{38}B_2N_8]^+$.

EA ($C_{18}H_{38}B_2Cl_2N_8 \cdot CH_2Cl_2$):

calcd. C [%] 41.95, H [%] 7.41, N [%] 20.60.

found C [%] 41.88, H [%] 7.42, N [%] 20.51.

Melting point:

226°C.

4.6.3 Synthesis of $[(Me_2N)B(\mu\text{-hpp})]_2$ and $[(Me_2N)B_2(\mu\text{-hpp})_2(NHMe_2)]Cl$

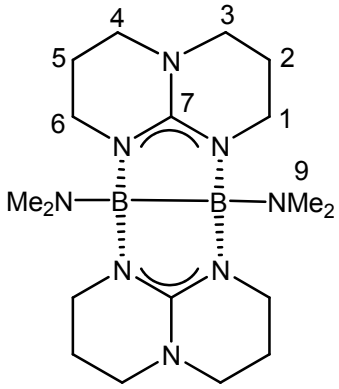

$C_{18}H_{36}B_2N_8$

Mol. Wt: 386.15 g/mol

Materials

hppH	1.86 g	13.4 mmol
^{n}BuLi (1.6 M in hexane)	8.38 mL	13.4 mmol
$B_2Cl_2(NMe_2)_2$	1.21 g	6.7 mmol
Toluene	40 mL	

Experimental

Deprotonation of hppH was accomplished using ^{n}BuLi to form the corresponding hpp$^-$ guanidinate anion. A solution of hppH (1.86 g, 13.4 mmol) in 20 mL of toluene was cooled to 0°C and 1 equiv. of ^{n}BuLi (1.6 M solution in hexane) added. The solution was allowed to warm to room temperature and stirred for 1 h. $B_2Cl_2(NMe_2)_2$ (1.21 g, 6.7 mmol) was slowly added to a stirred solution of Li(hpp) in 20 mL of toluene. The reaction mixture was stirred for 3 h at room temperature, during which time formation of a white precipitate was observed. The LiCl was removed by filtration, and the filtrate was evaporated to afford crude $[(Me_2N)B(\mu\text{-hpp})]_2$. X-ray quality crystals for an intermediate $[(Me_2N)B_2(\mu\text{-hpp})_2(NHMe_2)]Cl{\cdot}CH_2Cl_2$ of this reaction were grown from a mixture of dichloromethane/hexane at room temperature.

^{1}H-NMR (400 MHz, CD_2Cl_2):

δ [ppm] = 3.46 (m, H1, 8H), 3.14 (m, H3, 8H), 2.30 (s, H9, 12H), 1.86 (m, H2, 8H).

^{13}C-NMR (100.56 MHz, CD_2Cl_2):

δ [ppm] = 48.07 (C3), 40.64 (C9), 39.89 (C1), 22.69 (C2).

^{11}B-NMR (128.3 MHz, CD_2Cl_2):

δ [ppm] = 2.25 and 0.17 (the signal most likely belongs to another B containing species which however, does not contain hpp).

4.6.4 Synthesis of $[ClB_2(\mu\text{-hpp})_2(NHMe_2)]Cl$

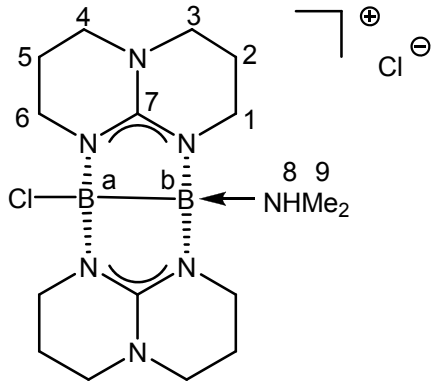

$C_{16}H_{31}B_2Cl_2N_7$

Mol. Wt: 413.99 g/mol

Experimental

Compound $[\{(Me_2(H)N)B(\mu\text{-hpp})\}_2]Cl_2$ undergoes a slow decomposition reaction when is kept for several weeks in a CH_2Cl_2/hexane solution in which one $NHMe_2$ group is eliminated leading to the species $[ClB_2(\mu\text{-hpp})_2(NHMe_2)]Cl$. Similar compound was formed when the dimer $[\{(Me_2(H)N)B(\mu\text{-hpp})\}_2]Cl_2$ was heated in solid state at 210°C for 2 h.

^{1}H-NMR (400 MHz, CD_2Cl_2):

δ [ppm] = 8.72 (m, H8, 1H), 3.76 (dt, H6a, 2H, ^{2}J(H6a-H6b) = 12.9 Hz, ^{3}J(H6a-H5) = 4.7 Hz), 3.43 (m, H1a, 2H), 3.16 (m, H6b, H4, H3, H1b, 12H), 2.43 (d, H9, 6H, ^{3}J(H9-H8) = 5.4 Hz), 1.89 (m, H5, H2, 8H).

^{13}C-NMR (100.56 MHz, CD_2Cl_2):

δ [ppm] = 157.57 (C7), 47.71 (C4), 47.62 (C3), 40.75 (C6), 39.41 (C1), 37.99 (C9), 22.53 (C5), 22.23 (C2).

^{11}B-NMR (128.3 MHz, CD_2Cl_2):

δ [ppm] = 3.11 (B-a), 1.07 (B-b).

MS (ESI^+):

m/z (%)*:* 791.47 $[C_{32}H_{62}B_4Cl_3N_{14}]^+$, 412 $[C_{16}H_{30}B_2Cl_2N_7]^+$, 378.25 $[C_{16}H_{31}B_2Cl_1N_7]^+$, 333,19 $[C_{14}H_{24}B_2Cl_1N_6]^+$.

4.6.5 Synthesis of $[\{Me_2(H)NB(\mu\text{-hpp})\}_2][OTf]_2$

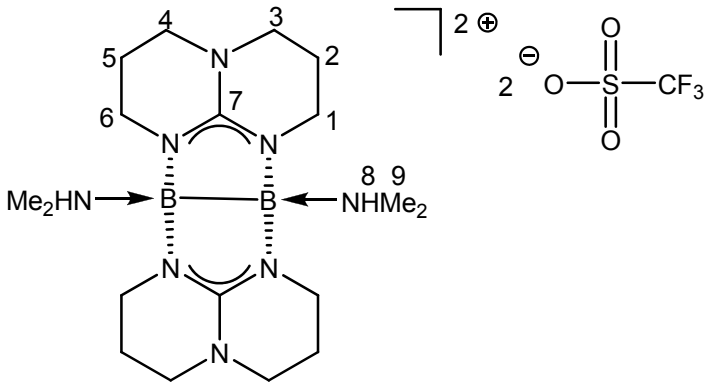

$C_{20}H_{38}B_2F_6N_8O_6S_2$

Mol. Wt: 686.31 g/mol

Materials

$[\{(Me_2(H)N)B(\mu\text{-hpp})\}_2]Cl_2$	0.043 g	0.095 mmol
AgOTf	0.049 g	0.191 mmol
CH_2Cl_2	6.0 ml	

Experimental

To a CH_2Cl_2 solution (3 mL) of compound $[\{(Me_2(H)N)B(\mu\text{-hpp})\}_2]Cl_2$ (0.043 g, 0.095 mmol), a solution of AgOTf (0.049 g, 0.191 mmol), also in 3 mL of CH_2Cl_2, was added at RT and exclusion of light. Soon a milky white precipitate was formed, which slowly turned yellow brown despite the darkened flask. After 15-20 minutes, when the

precipitate starts to turn the colour, the solution was filtrated via canula whereas the precipitate was washed two times with dichlormethane. Finally, the solvent was removed slowly under vacuum affording a white solid. Colourless crystals were obtained from a concentrated solution of CH_2Cl_2 at room temperature.

Yield

0.047 g 0.07 mmol 74 %

^{1}H-NMR (400 MHz, CD_2Cl_2):

δ [ppm] = 6.53 (septet, H8, 2H), 3.28 (dt, H1a, 4H ^{2}J(H1a-H1b) = 10.8 Hz, ^{3}J(H1a-H2) = 5.3 Hz), 3.19 (m, H1b, H3, 12H), 2.55 (d, H9, 12H, ^{3}J(H9-H8) = 5.5 Hz), 1.93 (m, H2, 8H).

^{13}C-NMR (100.56 MHz, CD_2Cl_2):

δ [ppm] = 158.47 (C-7), 47.69 (C-3), 40.25 (C-9), 39.51 (C-1), 21.94 (C-2).

^{11}B-NMR (128.3 MHz, CD_2Cl_2):

δ [ppm] = 1.81.

IR (solid CsI):

3159 (w) ν(N-H), 2965 (w), 2871 (w) ν(C-H), 1616 (m), 1591 (m), 1562 (s) ν(CN), 1328 (m) δ(C-H), 1248/1224 cm^{-1} (s) ν(B-N).

EA ($C_{20}H_{38}B_2F_6N_8O_6S_2$):

calcd. C [%] 35.00, H [%] 5.58, N [%] 16.33.

found C [%] 34.64, H [%] 5.72, N [%] 16.04.

4.6.6 Synthesis of $[\{(Me_2(H)N)B(hpp)\}_2][B(C_6F_5)_4]_2$

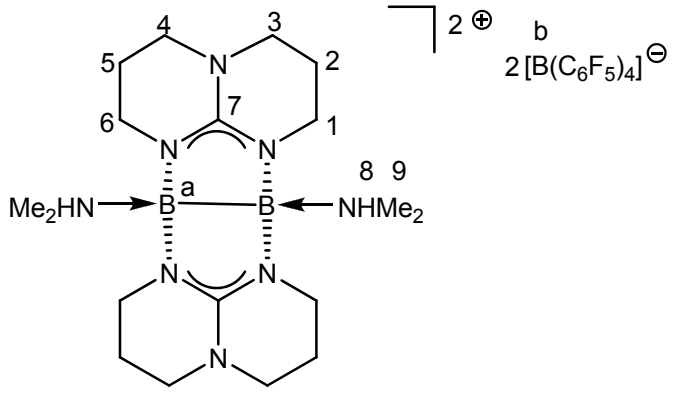

$C_{66}H_{39}B_4F_{40}N_8$

Mol. Wt: 1747.25 g/mol

Materials

$[\{(Me_2(H)N)B(hpp)\}_2]Cl_2$	0.042 g	0.092 mmol
$Li[B(C_6F_5)_4]\cdot Et_2O$	0.161 g	0.185 mmol
CH_2Cl_2	10.0 mL	

Experimental

A solution of $Li[B(C_6F_5)_4]\cdot Et_2O$ (0.161 g, 0.185 mmol) in 5.0 ml CH_2Cl_2 was slowly added to a stirring solution of $[\{Me_2(H)NB(hpp)\}_2][Cl]_2$ (0.042 g, 0.092 mmol) in 5.0 mL CH_2Cl_2. The reaction mixture was stirred at room temperature for 30 min. The product was separated by filtration and washed two times with CH_2Cl_2 (3 mL) to give, after removing the solvent in vacuum, a colourless solid. We were not able to get crystals of compound $[\{(Me_2(H)N)B(hpp)\}_2][B(C_6F_5)_4]_2$.

Yield

0.161 g	0.092 mmol	100%

^{1}H-NMR (400 MHz, CD_2Cl_2):

δ [ppm] = 4.15 (septet, H8, 2H), 3.25 (m, H3, 8H), 3.10 (dt, H1a, 4H, ^2J(H1a-H1b) = 12.3 Hz, ^3J(H1a-H2) = 7.9 Hz), 2.95 (dt, H1b, 4H, ^2J(H1b-H1a) = 11.3 Hz, ^3J(H1b-H2) = 5.7 Hz), 2.63 (d, H9, 12H, ^3J(H9-H8) = 5.8 Hz), 1.96 (m, H2, 8H).

^{13}C-NMR (100.56 MHz, CD_2Cl_2):

δ [ppm] = 158.49 (C-7), 47.41 (C-3), 40.81 (C-9), 39.55 (C-1), 21.44 (C-2).

^{11}B-NMR (128.3 MHz, CD_2Cl_2):

δ [ppm] = 1.2 (B-a), -16.7 (B-b).

^{19}F NMR (376.2 MHz, CD_2Cl_2):

δ [ppm] = -133.18 (d, F_o, ^3J = 9.89 Hz), -163.32 (t, F_p, ^3J = 20.38 Hz), 167.40 (t, F_m, ^3J = 17.95 Hz).

IR (solid CsI):

3275 (w) ν(N-H), 2965 (w), 2879 (w) ν(C-H), 1645 (m), 1604 (m), 1558 (m) ν(CN), 1516 (m), 1466 (s), 1326 (m) δ(C-H), 1275/1224 cm^{-1} (m) ν(B-N).

EA ($C_{66}H_{39}B_4F_{40}N_8$):

calcd. C [%] 45.37, H [%] 2.25, N [%] 6.41.

found C [%] 45.34, H [%] 2.62, N [%] 5.73.

4.7 References

[1] *DENZO-SMN, Data processing software*, Nonius **1998**; http://www.nonius.com.

[2] *SAINT*, Bruker AXS, **2007**.

[3] G. M. Sheldrick, *TWINABS*, Bruker AXS, **2004-2008**.

[4] P. T. Beurskens, in: G. M. Sheldrick, C. Krüger, R. Goddard (eds.), *Crystallographic Computing 3*, Clarendon Press, Oxford, UK, **1985**, p. 216; P. T. Beurskens, G. Beurskens, R. de Gelder, J. M. M. Smits, S. Garcia-Granda, R. O. Gould, *DIRDIF-2008*, Radboud University Nijmegen, The Netherlands, **2008**.

[5] M. C. Burla, R. Caliandro, M. Camalli, B. Carrozzini, G. L. Cascarano, L. De Caro, C. Giacovazzo, G. Polidori, R. Spagna, *SIR2004*, CNR IC, Bari, Italy, **2004**; *J. Appl. Cryst.* **2005**, *38*, 381-388.

[6] (a) G. M. Sheldrick, *SHELXS-97, Program for Crystal Structure Solution*; University of Göttingen: Göttingen, Germany, **1997**; http://shelx.uni-ac.gwdg.de/SHELX/index.html. (b) G. M. Scheldrick, *SHELXL-97, Program for Crystal Structure Refinement*; University of Göttingen: Göttingen, Germany, **1997**; http://shelx.uni-ac.gwdg.de/SHELX/index.html.

[7] *International Tables for X-ray Crystallography*; Kynoch Press: Birmingham, U.K., **1974**; *Vol. 4*.

[8] L. Zsolnai, G. Huttner, *XPMA*; University of Heidelberg: Heidelberg, Germany, **1994**; http://www.uni-heidelberg.de/institute/fak12/AC/huttner/software/software.html.

[9] K. Brandenburg, Diamond Version 3.1e, *Crystal Impact GbR Bonn* **2007**.

[10] POVRay for Windows Version 3.6, *Vision Raytracer* **2007**.

5. Supplementary material

5.1 Crystal data and refinement details

Formula	$C_7H_{16}BN_3$ **2**	$C_5H_{16}BN_3$ **3**
Identification code	b12_2	hi_sl1
M_r [g·mol^{-1}]	153.04	129.02
Crystal size [mm]	0.30 x 0.30 x 0.20	0.20 x 0.10 x 0.08
Crystal system	orthorhombic	monoclinic
Space group	*P* bca	*P* $2_1/n$
a [Å]	8.459(2)	7.9154(10)
b [Å]	13.534(3)	9.2083(11)
c [Å]	15.111(3)	11.6854(15)
α [°]	90	90
β [°]	90	104.279(2)
γ [°]	90	90
V [Å^3]	1730.0(6)	825.41(18)
ρ_{calc} [Mg·m^{-3}]	1.175	1.038
Z	8	4
F(000)	672	288
Range *hkl* (indep.set)	-10 ≤ *h* ≤ 10	-11 ≤ *h* ≤ 11
	-17 ≤ *k* ≤ 17	0 ≤ *k* ≤ 13
	-19 ≤ *l* ≤ 19	0 ≤ *l* ≤ 16
θ range [°]	3.01 to 27.48	2.82 to 31.00
μ [mm^{-1}]	0.072	0.064
T_{max}/T_{min}	0.9900 / 0.9762	0.7460 / 0.5521
Reflections collected	3976	19791
Independent reflections [R_{int}]	1977 [0.0328]	2622 [0.0565]
Observed reflections [$I > 2\sigma(I)$]	1515	1784
Refined parameters/restraints	116/0	146/0
Goodness-of-fit	1.038	1.062
$R(F)$ [$F_o > 4\sigma(F_o)$]	0.0432	0.0470
wR (F^2) (all data)	0.1138	0.1215
Residual electron density [e·Å^{-3}]	0.163	0.249 / -0.264

Formula	$C_{14}H_{28}B_2N_6$ **7**	$C_{14}H_{26}B_2N_6O$ **7A**
Identification code	hi_oc5	hi_oc14
M_r [g·mol^{-1}]	302.04	316.03
Crystal size [mm]	0.25 x 0.13 x 0.10	0.40 x 0.17 x 0.10
Crystal system	monoclinic	monoclinic
Space group	*P* 2_1/c	*P* 2_1/c
a [Å]	8.0912(4)	11.827(7)
b [Å]	12.6485(7)	8.616(4)
c [Å]	15.5315(8)	16.230(9)
α [°]	90	90
β [°]	90.1630(10)	110.899(9)
γ [°]	90	90
V [Å^3]	1589.51(14)	1545.1(14)
ρ_{calc} [Mg·m^{-3}]	1.262	1.359
Z	4	4
F(000)	656	680
Range *hkl* (indep.set)	-11 ≤ *h* ≤ 11	-17 ≤ *h* ≤ 16
	0 ≤ *k* ≤ 18	0 ≤ *k* ≤ 12
	0 ≤ *l* ≤ 22	0 ≤ *l* ≤ 23
θ range [°]	1.3 to 31.5	1.84 to 31.50
μ [mm^{-1}]	0.078	0.088
T_{max}/T_{min}	0.8623 / 0.7974	0.8623 / 0.8112
Reflections collected	39130	38717
Independent reflections [R_{int}]	5255 [0.0398]	5085 [0.0525]
Observed reflections [$I > 2\sigma(I)$]	4092	3608
Refined parameters/restraints	216/2	254/0
Goodness-of-fit	1.08	1.058
$R(F)$ [$F_o > 4\sigma(F_o)$]	0.0559	0.0511
$wR(F^2)$ (all data)	0.1451	0.1472
Residual electron density [e·Å^{-3}]	0.388 / -0.285	0.496 / -0.270

Formula	$C_{21}H_{34}B_2N_6$ **8**	$C_{14}H_{27}B_2IN_6$ **9**
Identification code	hi_oc1	ox123
M_r [g·mol^{-1}]	392.16	427.94
Crystal size [mm]	0.30 x 0.15 x 0.15	0.40 x 0.20 x 0.20
Crystal system	monoclinic	monoclinic
Space group	*P* n	*P* $2_1/c$
a [Å]	8.1843(5)	14.232(3)
b [Å]	8.3965(6)	8.1220(16)
c [Å]	15.5586(10)	15.678(3)
α [°]	90	90
β [°]	100.9340(10)	97.83(3)
γ [°]	90	90
V [Å^3]	1049.77(12)	1795.4(6)
ρ_{calc} [Mg·m^{-3}]	1.241	1.583
Z	2	4
F(000)	426	864
Range *hkl* (indep.set)	-11 ≤ *h* ≤ 11	-18 ≤ *h* ≤ 18
	0 ≤ *k* ≤ 12	-10 ≤ *k* ≤ 10
	0 ≤ *l* ≤ 23	-20 ≤ *l* ≤ 20
θ range [°]	2.43 to 32.07	1.44 to 27.51
μ [mm^{-1}]	0.075	1.791
T_{max}/T_{min}	0.8618/0.7746	0.7159/0.5344
Reflections collected	25932	8232
Independent reflections [R_{int}]	3513 [0.0503]	4128 [0.0250]
Observed reflections [$I > 2\sigma(I)$]	3025	3201
Refined parameters/restraints	388/2	220/0
Goodness-of-fit	1.075	1.038
$R(F)$ [$F_o > 4\sigma(F_o)$]	0.0457	0.0335
$wR(F^2)$ (all data)	0.1248	0.0860
Residual electron density [e·Å^{-3}]	0.374/-0.237	0.897/ -1.163

Formula	$C_{14}H_{28}BClN_6$ **11**	$C_{13}H_{20}IN_3$ **12**
Identification code	ox134	ox119
M_r [g·mol^{-1}]	326.68	345.22
Crystal size [mm]	0.40 x 0.10 x 0.10	0.35 x 0.35 x 0.30
Crystal system	orthorhombic	orthorhombic
Space group	$P\,2_12_1$	P bca
a [Å]	8.1830(16)	11.099(2)
b [Å]	9.3390(19)	9.791(2)
c [Å]	21.781(4)	26.324(5)
α [°]	90	90
β [°]	90	90
γ [°]	90	90
V [Å^3]	1664.5(6)	2860.6(10)
ρ_{calc} [Mg·m^{-3}]	1.304	1.603
Z	4	8
F(000)	704	1376
Range hkl (indep.set)	-10 ≤ h ≤ 10	-14 ≤ h ≤ 14
	-12 ≤ k ≤ 12	-12 ≤ k ≤ 12
	-28 ≤ l ≤ 20	-34 ≤ l ≤ 33
θ range [°]	1.87 to 27.47	2.40 to 27.46
μ [mm^{-1}]	0.236	2.223
T_{max}/T_{min}		
Reflections collected	3839	6576
Independent reflections [R_{int}]	3815 [0.0000]	3260 [0.0171]
Observed reflections [$I > 2\sigma(I)$]	2427	2808
Refined parameters/restraints	215/0	162/2
Goodness-of-fit	1.042	1.058
$R(F)$ [$F_o > 4\sigma(F_o)$]	0.0561	0.0214
$wR(F^2)$ (all data)	0.1132	0.0497
Residual electron density [e·Å^{-3}]	0.267/-0.305	0.473/-0.577

Formula	$C_7H_{14}ClN_3$ **13**	$C_{21}H_{36}B_3Cl_6N_9$ **14**
Identification code	hi_oc9	hi_oc7_5
M_r [g·mol^{-1}]	175.66	659.72
Crystal size [mm]	0.40 x 0.30 x 0.20	0.15 x 0.10 x 0.10
Crystal system	monoclinic	monoclinic
Space group	$P\,2_1/c$	$P\,2_1$
a [Å]	6.7505(6)	8.8661(11)
b [Å]	8.6338(7)	16.0255(19)
c [Å]	14.8649(12)	11.1979(14)
α [°]	90	90
β [°]	100.4840(10)	111.014(2)
γ [°]	90	90
V [Å^3]	851.90(12)	1485.2(3)
ρ_{calc} [Mg·m^{-3}]	1.370	1.475
Z	4	2
F(000)	376	684
Range *hkl* (indep.set)	-10 ≤ h ≤ 9	-13 ≤ h ≤ 13
	0 ≤ k ≤ 12	-23 ≤ k ≤ 23
	0 ≤ l ≤ 22	-16 ≤ l ≤ 16
θ range [°]	2.74 to 32.29	2.0 to 32.1
μ [mm^{-1}]	0.388	0.872
T_{max}/T_{min}	0.8623 / 0.7661	0.746345 / 0.629557
Reflections collected	17745	22590
Independent reflections [R_{int}]	2876 [0.0299]	14311 [0.0843]
Observed reflections [$I > 2\sigma(I)$]	2638	11136
Refined parameters/restraints	142/0	429/6
Goodness-of-fit	1.105	1.156
$R(F)$ [$F_o > 4\sigma(F_o)$]	0.0279	0.0584
$wR(F^2)$ (all data)	0.0803	0.1239
Residual electron density [e·Å^{-3}]	0.512/-0.193	0.695/-0.849

Formula	$C_{23}H_{48}B_2Cl_{12}N_8$ **15**	$C_{19}H_{39}B_2Cl_3N_8$ **16**
Identification code	hi_rd3	neu
M_r [g·mol^{-1}]	883.71	507.55
Crystal size [mm]	0.20 x 0.20 x 0.10	0.50 x 0.50 x 0.40
Crystal system	triclinic	triclinic
Space group	*P*-1	*P*-1
a [Å]	10.0946(8)	9.859(2)
b [Å]	10.7605(8)	10.313(2)
c [Å]	18.2651(14)	14.883(3)
α [°]	93.798(2)	74.73(3)
β [°]	92.7700(10)	83.49(3)
γ [°]	93.593(2)	62.60(3)
V [Å^3]	1973.0(3)	1296.0(5)
ρ_{calc} [Mg·m^{-3}]	1.488	1.301
Z	2	2
F(000)	912	540
Range *hkl* (indep.set)	-12 ≤ *h* ≤ 12	-12 ≤ *h* ≤ 12
	-13 ≤ *k* ≤ 13	-12 ≤ *k* ≤ 13
	0 ≤ *l* ≤ 23	-19 ≤ *l* ≤ 19
θ range [°]	1.9 to 26.78	2.29 to 27.58
μ [mm^{-1}]	0.872	0.378
T_{max}/T_{min}	0.7463/0.6591	
Reflections collected	37 530	48680
Independent reflections [R_{int}]	8381 [0.0698]	5767 [0.0341]
Observed reflections [$I > 2\sigma(I)$]	5619	3957
Refined parameters/restraints	429/6	332/5
Goodness-of-fit	1.053	1.036
$R(F)$ [$F_o > 4\sigma(F_o)$]	0.0454	0.0635
$wR(F^2)$ (all data)	0.1196	0.1965
Residual electron density [e·Å^{-3}]	1.168/-1.014	0.700/-0.784

Formula	$C_{16}H_{31}B_2Cl_{12}N_7 \cdot 1.2\ CH_2Cl_2$	$C_{21}H_{40}B_2Cl_2F_6N_8O_6S_2$
	17 ·1.2 CH_2Cl_2	**19**
Identification code	neuox5	hi_oc11a
M_r [g·mol^{-1}]	257.95	771.25
Crystal size [mm]	0.8 x 0.8 x 0.6	0.14 x 0.06 x 0.06
Crystal system	monoclinic	monoclinic
Space group	*P* $2_1/c$	*P* $2_1/c$
a [Å]	10.579(2)	22.632(12)
b [Å]	29.517(6)	18.960(11)
c [Å]	16.602(3)	15.902(9)
α [°]	90	90
β [°]	96.73(3)	99.814(17)
γ [°]	90	90
V [Å^3]	5148.4(18)	6724(7)
ρ_{calc} [Mg·m^{-3}]	1.331	1.524
Z	8	8
F(000)	2163	3200
Range *hkl* (indep.set)	-13 ≤ *h* ≤ 13	-27 ≤ *h* ≤ 26
	-37 ≤ *k* ≤ 38	0 ≤ *k* ≤ 22
	-21 ≤ *l* ≤ 21	0 ≤ *l* ≤ 18
θ range [°]	1.38 to 27.52	1.80 to 25.12
μ [mm^{-1}]	0.521	0.4
T_{max}/T_{min}		0.861954/0.667208
Reflections collected	22676	116173
Independent reflections [R_{int}]	11789 [0.0666]	11937[0.1984]
Observed reflections [$I > 2\sigma(I)$]	6591	5708
Refined parameters/restraints	580/2	855/117
Goodness-of-fit	1.031	1.010
$R(F)$ [$F_o > 4\sigma(F_o)$]	0.0753	0.0916
$wR(F^2)$ (all data)	0.2507	0.2033
Residual electron density [e·Å^{-3}]	1.082/-0.539	2.314/-1.049

Table 1: Atomic coordinates (x 10^4) and equivalent isotropic displacement parameters (Å^2 x 10^3) for $H_3B{\cdot}$hppH **2**. U_{eq} is defined as one third of the trace of the orthogonalized U_{ij} tensor.

	x	*y*	*z*	U_{eq}
B(1)	1092(2)	5668(1)	-1128(1)	32(1)
N(1)	2300(1)	5612(1)	596(1)	30(1)
N(2)	4639(1)	6432(1)	270(1)	31(1)
N(3)	2731(1)	6109(1)	-831(1)	27(1)
C(1)	2645(2)	5513(1)	1530(1)	34(1)
C(2)	3812(2)	6294(1)	1812(1)	37(1)
C(3)	5190(2)	6306(1)	1177(1)	36(1)
C(4)	3241(1)	6054(1)	-6(1)	25(1)
C(5)	3731(1)	6558(1)	-1509(1)	34(1)
C(6)	4862(2)	7309(1)	-1128(1)	40(1)
C(7)	5750(1)	6865(1)	-358(1)	36(1)

Table 2: Atomic coordinates (x 10^4) and equivalent isotropic displacement parameters (Å^2 x 10^3) for $H_3B{\cdot}N(H)C(NMe_2)_2$ **3**. U_{eq} is defined as one third of the trace of the orthogonalized U_{ij} tensor.

	x	*y*	*z*	U_{eq}
B	-1662(2)	1545(2)	400(1)	22(1)
C(1)	1249(1)	2991(1)	1136(1)	16(1)
C(2)	-513(2)	3642(2)	2511(1)	27(1)
C(3)	919(2)	5549(1)	1627(1)	26(1)
C(4)	3430(2)	2442(1)	34(1)	24(1)
C(5)	4231(2)	3956(1)	1811(1)	25(1)

N(1)	364(1)	1807(1)	744(1)	19(1)
N(2)	595(1)	4012(1)	1730(1)	19(1)
N(3)	2842(1)	3243(1)	935(1)	19(1)

Table 3: Atomic coordinates (x 10^4) and equivalent isotropic displacement parameters (Å^2 x 10^3) for [$H_2B(\mu$-hpp)]$_2$ **7**. U_{eq} is defined as one third of the trace of the orthogonalized U_{ij} tensor.

	x	*y*	*z*	U_{eq}
B(1)	5852(4)	510(2)	4224(2)	16(1)
B(51)	9152(5)	-517(2)	-782(2)	22(1)
C(1)	2981(3)	872(2)	4796(2)	14(1)
C(2)	3179(4)	688(2)	3276(2)	21(1)
C(3)	2459(4)	1800(2)	3174(2)	23(1)
C(4)	1121(4)	1943(2)	3860(2)	22(1)
C(5)	247(3)	1504(2)	5328(2)	22(1)
C(6)	739(4)	996(2)	6158(2)	26(1)
C(7)	2563(4)	1178(2)	6280(2)	24(1)
C(51)	7969(4)	880(2)	218(2)	18(1)
C(52)	7602(3)	1183(2)	-1277(2)	19(1)
C(53)	5755(4)	994(2)	-1175(2)	22(1)
C(54)	5246(4)	1509(2)	-315(2)	26(1)
C(55)	6119(4)	1936(2)	1150(2)	28(1)
C(56)	7435(4)	1791(2)	1824(2)	28(1)
C(57)	8171(4)	699(2)	1729(2)	22(1)
N(1)	3937(3)	598(2)	4118(2)	18(1)
N(2)	3470(3)	625(2)	5588(2)	17(1)
N(3)	1543(3)	1401(2)	4656(2)	21(1)
N(51)	8440(3)	621(2)	-597(2)	19(1)
N(52)	8927(3)	600(2)	867(2)	19(1)

N(53)	6528(3)	1402(2)	333(2)	19(1)

Table 4: Atomic coordinates (x 10^4) and equivalent isotropic displacement parameters (Å^2 x 10^3) for [$H_2OB_2(\mu$-hpp$)_2$] **7A**. U_{eq} is defined as one third of the trace of the orthogonalized U_{ij} tensor.

	x	*y*	*z*	U_{eq}
B(1)	2452(1)	6406(2)	1146(1)	19(1)
B(2)	2470(2)	4927(2)	2335(1)	21(1)
C(1)	3542(2)	9138(2)	1458(1)	24(1)
C(2)	3450(2)	10560(2)	1982(1)	26(1)
C(3)	4259(1)	10289(2)	2931(1)	26(1)
C(4)	4668(1)	8510(2)	4178(1)	27(1)
C(5)	4621(1)	6840(2)	4453(1)	27(1)
C(6)	3385(1)	6180(2)	3920(1)	25(1)
C(7)	3473(1)	7583(2)	2670(1)	18(1)
C(10)	-1508(1)	7121(2)	334(1)	22(1)
C(11)	-1512(1)	5361(2)	1514(1)	25(1)
C(14)	436(1)	6028(2)	1345(1)	16(1)
C(8A)	360(2)	7385(2)	24(1)	19(1)
C(9A)	-708(2)	8276(2)	93(1)	21(1)
C(12A)	-811(2)	4102(2)	2124(1)	25(1)
C(13A)	431(2)	4724(3)	2655(2)	22(1)
C(8B)	437(11)	8087(16)	354(8)	28(3)
C(9B)	-753(11)	7529(16)	-247(8)	29(3)
C(12B)	-631(11)	4913(15)	2492(8)	30(3)
C(13B)	457(15)	4110(20)	2423(10)	36(3)
N(1)	3142(1)	7755(1)	1795(1)	19(1)
N(2)	3181(1)	6262(2)	2983(1)	20(1)
N(3)	4078(1)	8732(2)	3228(1)	22(1)
N(4)	1043(1)	6659(2)	871(1)	19(1)

N(5)	1065(1)	5227(1)	2072(1)	19(1)
N(6)	-789(1)	6186(1)	1091(1)	18(1)
O	2775(1)	4940(1)	1566(1)	23(1)

Table 5: Atomic coordinates (x 10^4) and equivalent isotropic displacement parameters (Å^2 x 10^3) for [HB(μ-hpp)]$_2$ **8**. U_{eq} is defined as one third of the trace of the orthogonalized U_{ij} tensor.

	x	*y*	*z*	U_{eq}
B(1)	9044(2)	3404(3)	3142(1)	13(1)
B(2)	8806(3)	5426(3)	3422(1)	15(1)
C(1)	6576(2)	1264(2)	2768(1)	16(1)
C(2)	4724(2)	1235(2)	2387(1)	19(1)
C(3)	3814(2)	2163(2)	2989(1)	19(1)
C(4)	3494(2)	4961(3)	3464(2)	21(1)
C(5)	4083(3)	6609(3)	3273(2)	24(1)
C(6)	5932(2)	6762(2)	3641(1)	18(1)
C(7)	6154(2)	4013(2)	3184(1)	13(1)
C(8)	10517(2)	1168(2)	4260(1)	16(1)
C(9)	11883(3)	1032(2)	5070(1)	19(1)
C(10)	11432(2)	2061(2)	5791(1)	18(1)
C(11)	11493(3)	4980(2)	6115(1)	18(1)
C(12)	11700(3)	6532(3)	5657(1)	19(1)
C(13)	10181(3)	6803(2)	4947(1)	19(1)
C(14)	10364(2)	3971(2)	4652(1)	13(1)
C(15)	1366(2)	7190(3)	923(1)	20(1)
C(16)	780(3)	7939(3)	1611(2)	23(1)
C(17)	586(3)	9570(3)	1622(2)	27(1)
C(18)	978(3)	10499(3)	962(2)	30(1)
C(19)	1573(3)	9781(3)	278(2)	26(1)
C(20)	1765(2)	8139(3)	261(1)	21(1)

C(21)	1570(3)	5406(3)	898(2)	33(1)
N(1)	7175(2)	2864(2)	2998(1)	13(1)
N(2)	6873(2)	5407(2)	3421(1)	14(1)
N(3)	4482(2)	3775(2)	3105(1)	16(1)
N(4)	10034(2)	2816(2)	4052(1)	13(1)
N(5)	9827(2)	5419(2)	4379(1)	13(1)
N(6)	11222(2)	3694(2)	5474(1)	17(1)

Table 6: Atomic coordinates (x 10^4) and equivalent isotropic displacement parameters (Å^2 x 10^3) for $[H_3B_2(\mu\text{-hpp})_2]$I **9**. U_{eq} is defined as one third of the trace of the orthogonalized U_{ij} tensor.

	x	*y*	*z*	U_{eq}
I(1)	2358(1)	1007(1)	4214(1)	40(1)
N(1)	1533(2)	-754(3)	6662(1)	18(1)
N(2)	3129(2)	-288(3)	6842(1)	20(1)
N(3)	2091(2)	1973(3)	6734(1)	20(1)
N(4)	1854(2)	-3086(3)	5628(1)	18(1)
N(5)	3457(2)	-2849(3)	5948(1)	20(1)
N(6)	2814(2)	-3630(3)	4558(1)	22(1)
B(1)	1742(2)	-2544(4)	6539(2)	20(1)
B(2)	3303(2)	-2132(4)	6804(2)	21(1)
C(1)	2247(2)	340(3)	6727(2)	18(1)
C(2)	543(2)	-197(4)	6544(2)	25(1)
C(3)	458(2)	1456(4)	6956(2)	25(1)
C(4)	1131(2)	2642(4)	6618(2)	27(1)
C(5)	2863(2)	3153(4)	6708(2)	30(1)
C(6)	3779(2)	2461(4)	7160(2)	37(1)
C(7)	3957(2)	775(4)	6825(2)	33(1)
C(8)	2706(2)	-3164(3)	5358(2)	19(1)
C(9)	995(2)	-3245(4)	5001(2)	22(1)

C(10)	1159(2)	-4542(4)	4337(2)	26(1)
C(11)	2010(2)	-4065(4)	3912(2)	25(1)
C(12)	3714(2)	-3448(5)	4215(2)	40(1)
C(13)	4451(2)	-2566(4)	4827(2)	34(1)
C(14)	4404(2)	-3159(4)	5727(2)	29(1)

Table 7: Atomic coordinates (x 10^4) and equivalent isotropic displacement parameters (Å^2 x 10^3) for $[H_2B(hppH)_2]Cl$ **11**. U_{eq} is defined as one third of the trace of the orthogonalized U_{ij} tensor.

	x	*y*	*z*	U_{eq}
Cl(1)	7160(1)	1685(1)	1348(1)	31(1)
N(1)	5251(3)	1114(3)	3366(1)	18(1)
N(2)	2703(3)	39(3)	3439(1)	21(1)
N(3)	2943(3)	2166(3)	2894(1)	19(1)
N(4)	5866(3)	478(3)	4490(1)	19(1)
N(5)	4154(3)	-1378(3)	4787(1)	23(1)
N(6)	4829(3)	364(3)	5496(1)	20(1)
B(1)	6069(4)	3(4)	3809(2)	20(1)
C(1)	3648(3)	1112(3)	3227(1)	17(1)
C(2)	6234(3)	2242(3)	3069(2)	22(1)
C(3)	5340(3)	3660(3)	3105(2)	24(1)
C(4)	3763(3)	3511(3)	2747(1)	24(1)
C(5)	1298(3)	2048(3)	2635(2)	25(1)
C(6)	623(4)	546(3)	2678(2)	26(1)
C(7)	966(3)	-21(3)	3312(2)	26(1)
C(8)	4962(3)	-171(3)	4922(1)	20(1)
C(9)	6725(4)	1793(4)	4669(1)	27(1)
C(10)	7371(3)	1674(4)	5319(1)	28(1)
C(11)	5973(3)	1417(3)	5745(1)	26(1)
C(12)	3767(4)	-271(3)	5959(1)	27(1)

C(13)	2407(4)	-1140(4)	5672(2)	34(1)
C(14)	3179(4)	-2178(4)	5230(2)	33(1)

Table 8: Atomic coordinates (x 10^4) and equivalent isotropic displacement parameters (Å^2 x 10^3) for hppH$_2$I **12**. U_{eq} is defined as one third of the trace of the orthogonalized U_{ij} tensor.

	x	*y*	*z*	U_{eq}
I(1)	5116(1)	929(1)	4188(1)	18(1)
N(1)	4155(2)	-2679(2)	4634(1)	21(1)
N(2)	5803(2)	-2633(2)	4106(1)	22(1)
N(3)	4525(2)	-4524(2)	4103(1)	18(1)
C(1)	4821(2)	-3283(2)	4275(1)	18(1)
C(2)	3099(2)	-3299(2)	4872(1)	21(1)
C(3)	3178(2)	-4839(2)	4831(1)	20(1)
C(4)	3437(2)	-5219(2)	4284(1)	20(1)
C(5)	5161(2)	-5104(2)	3665(1)	22(1)
C(6)	6476(2)	-4691(2)	3681(1)	23(1)
C(7)	6574(2)	-3152(2)	3699(1)	24(1)
C(8)	8800(3)	-3309(3)	2672(1)	41(1)
C(9)	7862(3)	-3777(3)	2381(1)	46(1)
C(10)	7606(2)	-3184(3)	1926(1)	48(1)
C(11)	8292(3)	-2122(3)	1755(1)	49(1)
C(12)	9232(3)	-1644(3)	2040(1)	47(1)
C(13)	9488(2)	-2232(3)	2499(1)	42(1)

Table 9: Atomic coordinates (x 10^4) and equivalent isotropic displacement parameters (Å^2 x 10^3) for hppH$_2$Cl **13**. U_{eq} is defined as one third of the trace of the orthogonalized U_{ij} tensor.

	x	*y*	*z*	U_{eq}
N(1)	7147(1)	3227(1)	1720(1)	12(1)
N(2)	3863(1)	3974(1)	1095(1)	15(1)
N(3)	5582(1)	2350(1)	288(1)	16(1)
C(1)	5568(1)	3209(1)	1034(1)	12(1)
C(2)	3824(1)	5154(1)	1794(1)	16(1)
C(3)	5089(1)	4586(1)	2681(1)	16(1)
C(4)	7201(1)	4222(1)	2524(1)	14(1)
C(5)	7343(1)	1512(1)	99(1)	17(1)
C(6)	8824(1)	1208(1)	977(1)	16(1)
C(7)	9102(1)	2674(1)	1550(1)	15(1)
Cl(1)	1404(1)	1857(1)	4077(1)	17(1)
N(1)	7147(1)	3227(1)	1720(1)	12(1)
N(2)	3863(1)	3974(1)	1095(1)	15(1)
N(3)	5582(1)	2350(1)	288(1)	16(1)
C(1)	5568(1)	3209(1)	1034(1)	12(1)
C(2)	3824(1)	5154(1)	1794(1)	16(1)
C(3)	5089(1)	4586(1)	2681(1)	16(1)

Table 10: Atomic coordinates (x 10^4) and equivalent isotropic displacement parameters (Å^2 x 10^3) for $[(Cl_2B_2(\mu\text{-hpp})_3]BCl_4$ **14**. U_{eq} is defined as one third of the trace of the orthogonalized U_{ij} tensor.

	x	*y*	*z*	U_{eq}

B(1)	5948(6)	8679(3)	9700(5)	13(1)
B(2)	8958(6)	9462(3)	9843(5)	13(1)
B(3)	2393(5)	6440(3)	5007(5)	19(1)
C(1)	6200(5)	10103(3)	8822(5)	13(1)
C(2)	3740(6)	10780(3)	7371(5)	20(1)
C(3)	2920(5)	9946(3)	7359(5)	19(1)
C(4)	4117(6)	9259(3)	7420(5)	16(1)
C(5)	6254(6)	11571(3)	8203(5)	19(1)
C(6)	7978(6)	11603(3)	9150(5)	18(1)
C(7)	8145(6)	10997(3)	10225(5)	16(1)
C(8)	7850(5)	8127(3)	8691(5)	14(1)
C(9)	7167(6)	6708(3)	7761(6)	21(1)
C(10)	6150(6)	6621(3)	8594(6)	23(1)
C(11)	6939(6)	7111(3)	9812(5)	18(1)
C(12)	9040(6)	7590(3)	7152(5)	24(1)
C(13)	9878(6)	8426(3)	7304(5)	20(1)
C(14)	8775(6)	9086(3)	7500(5)	16(1)
C(15)	8270(6)	9016(3)	11735(5)	14(1)
C(16)	7743(6)	8832(3)	13746(5)	21(1)
C(17)	5963(6)	8809(3)	12907(5)	22(1)
C(18)	5700(6)	9366(3)	11759(5)	18(1)
C(19)	10483(6)	9131(4)	13832(5)	21(1)
C(20)	11600(6)	9220(3)	13082(5)	21(1)
C(21)	10944(5)	8692(3)	11898(5)	17(1)
Cl(1)	3967(1)	8146(1)	9612(1)	18(1)
Cl(2)	10953(1)	10002(1)	9927(1)	17(1)
Cl(3)	3454(2)	7454(1)	5226(2)	33(1)
Cl(4)	1826(2)	6205(1)	6410(1)	31(1)
Cl(5)	3780(2)	5614(1)	4849(1)	28(1)
Cl(6)	546(2)	6477(1)	3561(1)	35(1)
N(1)	5482(4)	9344(2)	8641(4)	13(1)
N(2)	7723(4)	10169(2)	9667(4)	14(1)
N(3)	5432(5)	10779(3)	8211(4)	16(1)

N(4)	7019(4)	7995(2)	9464(4)	14(1)
N(5)	8501(5)	8881(2)	8688(4)	14(1)
N(6)	8037(5)	7509(3)	7940(4)	17(1)
N(7)	6678(4)	9042(2)	11049(4)	15(1)
N(8)	9335(4)	9014(2)	11124(4)	12(1)
N(9)	8798(5)	8982(3)	13009(4)	17(1)

Table 11: Atomic coordinates (x 10^4) and equivalent isotropic displacement parameters (Å^2 x 10^3) for [{$(Me_2(H)N)B(\mu$-hpp)$\}_2$]Cl_2 **15**. U_{eq} is defined as one third of the trace of the orthogonalized U_{ij} tensor.

	x	*y*	*z*	U_{eq}
B(1)	9011(3)	7283(3)	2737(2)	11(1)
B(2)	9853(3)	6426(3)	2083(2)	11(1)
C(1)	7925(3)	9478(3)	2528(2)	14(1)
C(2)	6894(3)	9731(3)	1936(2)	16(1)
C(3)	7561(3)	9915(3)	1225(2)	18(1)
C(4)	8902(3)	8195(3)	1577(2)	11(1)
C(5)	9783(3)	6801(3)	652(2)	15(1)
C(6)	9928(3)	7927(3)	196(2)	17(1)
C(7)	8720(3)	8686(3)	285(2)	17(1)
C(8)	6520(3)	6655(3)	3105(2)	15(1)
C(9)	5749(3)	5458(3)	3276(2)	17(1)
C(10)	5551(3)	4600(3)	2584(2)	16(1)
C(11)	7832(3)	5308(3)	2350(1)	11(1)
C(12)	9140(3)	4059(3)	1542(2)	16(1)
C(13)	7833(3)	3665(3)	1116(2)	17(1)
C(14)	6774(3)	3444(3)	1656(2)	19(1)
C(15)	10628(3)	8762(3)	3599(2)	22(1)
C(16)	9691(3)	6842(3)	4077(2)	20(1)
C(17)	12341(3)	7163(3)	2023(2)	20(1)

C(18)	11794(3)	5363(3)	2716(2)	20(1)
C(41)	4891(3)	6684(3)	269(2)	17(1)
C(42)	8168(3)	2259(3)	4116(2)	28(1)
C(43)	3511(4)	3437(3)	4570(2)	30(1)
C(51)	5642(3)	495(3)	5942(2)	20(1)
Cl(1)	9335(1)	3111(2)	3663(1)	96(1)
Cl(2)	6602(1)	2132(1)	3642(1)	33(1)
Cl(3)	4270(1)	8194(1)	303(1)	30(1)
Cl(4)	5973(1)	6521(1)	1042(1)	22(1)
Cl(5)	5816(1)	357(1)	6903(1)	22(1)
Cl(6)	6020(1)	2064(1)	5729(1)	24(1)
C(44A)	2589(3)	1663(3)	1798(2)	26(1)
Cl(7A)	1059(6)	738(6)	1678(3)	32(1)
Cl(8A)	3816(5)	1028(5)	1286(3)	32(1)
C(44B)	2589(3)	1663(3)	1798(2)	26(1)
Cl(7B)	1039(12)	890(20)	1825(16)	64(3)
Cl(8B)	3670(20)	710(30)	1299(6)	57(4)
Cl(9)	2608(1)	4406(1)	882(1)	18(1)
Cl(10)	2284(1)	764(1)	5380(1)	19(1)
Cl(11)	3033(1)	2793(1)	3692(1)	38(1)
Cl(12)	2897(1)	4931(1)	4738(1)	36(1)
N(1)	8662(2)	8406(2)	2290(1)	12(1)
N(2)	9607(2)	7206(2)	1420(1)	10(1)
N(3)	8478(2)	8938(2)	1063(1)	13(1)

Table 12: Atomic coordinates (x 10^4) and equivalent isotropic displacement parameters (Å^2 x 10^3) for [$(Me_2N)(Me_2HN)B_2(\mu$-hpp$)_2$]Cl **16**. U_{eq} is defined as one third of the trace of the orthogonalized U_{ij} tensor.

	x	*y*	*z*	U_{eq}
Cl(1)	3330(1)	8997(1)	3938(1)	42(1)

N(1)	-3273(3)	13796(3)	1772(2)	40(1)
N(2)	-1609(3)	12595(3)	2984(2)	32(1)
N(3)	-3866(3)	14773(3)	3101(2)	45(1)
N(4)	-2565(3)	11286(3)	1369(2)	35(1)
N(5)	-957(3)	10071(3)	2610(2)	33(1)
N(6)	-2405(3)	8980(3)	2254(2)	48(1)
N(7)	-1843(4)	13183(4)	315(2)	57(1)
N(8)	977(3)	11122(3)	2317(2)	31(1)
B(1)	-2033(4)	12508(4)	1344(2)	32(1)
B(2)	-807(4)	11554(4)	2316(2)	29(1)
C(1)	-2950(3)	13738(3)	2635(2)	35(1)
C(2)	-4763(5)	14868(4)	1344(3)	66(1)
C(3)	-5411(6)	16282(4)	1704(3)	78(2)
C(4)	-5408(5)	15877(4)	2744(3)	68(1)
C(5)	-3591(4)	14534(4)	4088(2)	51(1)
C(6)	-1919(4)	13696(4)	4312(2)	48(1)
C(7)	-1232(4)	12257(3)	3972(2)	41(1)
C(8)	-1992(3)	10096(3)	2082(2)	34(1)
C(9)	-3723(5)	11451(4)	759(4)	75(2)
C(10)	-4671(7)	10839(8)	1140(4)	38(2)
C(10B)	-3795(12)	9977(12)	921(6)	55(3)
C(11)	-3681(5)	9117(5)	1749(3)	63(1)
C(12)	-1833(5)	7715(4)	3049(4)	71(1)
C(13)	-336(5)	7477(5)	3309(4)	42(1)
C(13B)	-1043(19)	7954(19)	3872(10)	106(8
C(14)	-395(5)	8881(4)	3458(2)	55(1)
C(15)	-862(15)	12574(17)	-268(9)	86(6)
C(16)	-1972(11)	14843(12)	216(7)	61(3)
C(15B)	-979(12)	11965(13)	-245(6)	46(2)
C(16B)	-1337(12)	14220(12)	-3(7)	56(2)
C(17)	1266(4)	12451(4)	2123(2)	44(1)
C(18)	1837(4)	10173(4)	1661(2)	41(1)
C(100)	6122(4)	8136(4)	5610(2)	44(1)
Cl(2)	4880(1)	8170(1)	6558(1)	54(1)

Cl(3)	7772(1)	6394(1)	5749(1)	72(1)

Table 13: Atomic coordinates (x 10^4) and equivalent isotropic displacement parameters (Å^2 x 10^3) for [Cl(Me$_2$HN)B$_2$(μ-hpp)$_2$]Cl **17**. U_{eq} is defined as one third of the trace of the orthogonalized U_{ij} tensor.

	x	*y*	*z*	U_{eq}
Cl(1)	6457(1)	2365(1)	6108(1)	33(1)
Cl(2)	1238(1)	2357(1)	1068(1)	32(1)
Cl(3)	-2306(1)	426(1)	970(1)	34(1)
Cl(4)	2621(1)	515(1)	6064(1)	36(1)
N(1)	5748(3)	2089(1)	4483(2)	29(1)
N(2)	4374(3)	1498(1)	4534(2)	26(1)
N(3)	4252(4)	1939(1)	3341(2)	33(1)
N(4)	7530(3)	1640(1)	5339(2)	28(1)
N(5)	6171(3)	1041(1)	5360(2)	27(1)
N(6)	8363(3)	900(1)	5355(2)	33(1)
N(7)	4338(3)	1371(1)	6057(2)	26(1)
N(8)	766(3)	2032(1)	-548(2)	29(1)
N(9)	-461(3)	1402(1)	-500(2)	28(1)
N(10)	-597(4)	1826(1)	-1713(2)	37(1)
N(11)	2565(3)	1648(1)	425(2)	29(1)
N(12)	1346(3)	1010(1)	439(2)	26(1)
N(13)	3575(3)	938(1)	551(2)	32(1)
N(14)	-663(3)	1304(1)	1008(2)	28(1)
B(1)	6253(5)	1884(2)	5322(3)	28(1)
B(2)	5236(4)	1437(2)	5348(3)	25(1)
B(3)	1225(4)	1856(2)	322(3)	26(1)
B(4)	302(5)	1380(2)	345(3)	26(1)
C(1)	4787(4)	1838(1)	4102(2)	27(1)
C(2)	6380(5)	2434(2)	4048(3)	41(1)

C(3)	5476(6)	2637(2)	3370(3)	54(2)
C(4)	4856(5)	2266(2)	2842(3)	44(1)
C(5)	3360(5)	1618(2)	2905(3)	40(1)
C(6)	2554(4)	1392(2)	3483(3)	38(1)
C(7)	3430(4)	1176(2)	4174(3)	33(1)
C(8)	7377(4)	1186(1)	5349(2)	26(1)
C(9)	8780(4)	1844(2)	5361(3)	40(1)
C(10)	9702(5)	1527(2)	5036(5)	76(2)
C(11)	9657(5)	1073(2)	5345(4)	50(1)
C(12)	8189(4)	405(2)	5346(3)	41(1)
C(13)	6982(4)	275(2)	5685(3)	43(1)
C(14)	5885(4)	557(1)	5277(3)	31(1)
C(15)	3422(4)	1746(2)	6088(3)	37(1)
C(16)	5101(4)	1310(2)	6859(3)	37(1)
C(17)	-107(4)	1755(1)	-939(3)	29(1)
C(18)	1316(5)	2398(2)	-972(3)	36(1)
C(19)	425(5)	2566(2)	-1673(3)	50(1)
C(20)	-49(5)	2172(2)	-2201(3)	46(1)
C(21)	-1389(5)	1480(2)	-2165(3)	45(1)
C(22)	-2178(5)	1231(2)	-1597(3)	44(1)
C(23)	-1288(4)	1048(2)	-876(3)	36(1)
C(24)	2519(4)	1193(1)	474(2)	26(1)
C(25)	3769(4)	1887(2)	479(3)	33(1)
C(26)	4790(4)	1593(2)	172(3)	38(1)
C(27)	4844(4)	1146(2)	609(3)	38(1)
C(28)	3520(4)	440(1)	604(3)	34(1)
C(29)	2299(4)	289(2)	900(3)	38(1)
C(30)	1174(4)	522(1)	401(3)	36(1)
C(31)	-1655(4)	1660(2)	965(3)	39(1)
C(32)	9(4)	1278(2)	1841(3)	36(1)
C(100)	3129(6)	630(2)	8214(3)	40(2)
C(101)	-539(5)	75(2)	2813(3)	37(1)
C(102)	-3693(6)	500(2)	2830(4)	49(2)
Cl(5)	2331(2)	1152(1)	8361(1)	50(1)

Cl(6)	4728(2)	645(1)	8630(1)	39(1)
Cl(7)	77(2)	498(1)	3480(1)	59(1)
Cl(8)	669(2)	-244(1)	2454(1)	71(1)
Cl(9)	-3374(2)	1059(1)	3172(1)	52(1)
Cl(10)	-5312(2)	362(1)	2764(1)	52(1)

Table 14: Atomic coordinates (x 10^4) and equivalent isotropic displacement parameters (Å^2 x 10^3) for [{(Me_2HN)B(μ-hpp)}$_2$]OTf_2 **19**. U_{eq} is defined as one third of the trace of the orthogonalized U_{ij} tensor.

	x	*y*	*z*	U_{eq}
B(1)	1013(4)	4583(4)	2437(5)	21(2)
B(2)	1006(4)	5060(4)	3361(5)	20(2)
B(3)	4050(4)	-426(4)	2531(5)	19(2)
B(4)	3957(4)	104(4)	1624(5)	18(2)
C(1)	1708(3)	4928(4)	1277(4)	24(2)
C(2)	2358(3)	5118(4)	1348(5)	31(2)
C(3)	2448(4)	5853(4)	1684(5)	37(2)
C(4)	2337(3)	6601(4)	2945(5)	33(2)
C(5)	1865(4)	6779(4)	3458(5)	35(2)
C(6)	1741(3)	6132(4)	3959(4)	26(2)
C(7)	1755(3)	5511(3)	2623(4)	20(2)
C(8)	124(3)	4505(4)	1082(4)	21(2)
C(9)	-547(3)	4558(4)	950(5)	26(2)
C(10)	-726(3)	5299(4)	1133(4)	23(2)
C(11)	-663(3)	6133(4)	2351(4)	25(2)
C(12)	-476(3)	6140(4)	3286(5)	30(2)
C(13)	188(3)	6052(4)	3525(4)	22(2)
C(14)	107(3)	5249(3)	2326(4)	19(2)
C(15)	1760(3)	3523(4)	2663(5)	30(2)
C(16)	697(3)	3260(4)	2575(5)	29(2)
C(17)	1580(3)	4388(4)	4667(5)	30(2)

C(18)	486(3)	4375(4)	4435(5)	26(2)
C(19)	4935(3)	-282(4)	3876(4)	20(2)
C(20)	5599(3)	-212(4)	3928(4)	25(2)
C(21)	5739(3)	538(4)	3704(5)	27(2)
C(22)	5540(3)	1386(4)	2501(5)	25(2)
C(23)	5024(3)	1696(4)	1885(5)	26(2)
C(24)	4729(3)	1127(3)	1316(4)	22(2)
C(25)	4860(3)	408(3)	2595(4)	15(2)
C(26)	3388(3)	-334(4)	3770(4)	24(2)
C(27)	2722(3)	-257(4)	3787(5)	29(2)
C(28)	2536(3)	493(4)	3516(5)	25(2)
C(29)	2531(3)	1370(4)	2373(5)	30(2)
C(30)	2946(3)	1680(4)	1814(5)	28(2)
C(31)	3103(3)	1102(3)	1237(4)	24(2)
C(32)	3206(3)	360(3)	2482(4)	20(2)
C(33)	4673(3)	-1549(4)	2359(5)	26(2)
C(34)	3579(3)	-1668(4)	2202(5)	29(2)
C(35)	4393(3)	-521(4)	405(5)	27(2)
C(36)	3303(3)	-477(4)	310(4)	27(2)
N(1)	1523(2)	4985(3)	2111(3)	19(1)
N(2)	1539(3)	5558(3)	3363(4)	23(1)
N(3)	2166(3)	5964(3)	2426(4)	28(2)
N(4)	386(2)	4732(3)	1944(3)	18(1)
N(5)	400(2)	5441(3)	3089(3)	20(1)
N(6)	-411(2)	5531(3)	1959(3)	19(1)
N(7)	1145(2)	3749(3)	2305(4)	19(1)
N(8)	1029(2)	4789(3)	4321(3)	22(1)
N(9)	4640(2)	-123(3)	3005(3)	16(1)
N(10)	4528(2)	555(3)	1821(3)	18(1)
N(11)	5345(2)	764(3)	2926(4)	20(1)
N(12)	3498(3)	-196(3)	2909(3)	20(1)
N(13)	3388(2)	516(3)	1743(3)	18(1)
N(14)	2778(2)	712(3)	2772(4)	21(1)
N(15)	4109(2)	-1275(3)	2622(4)	21(1)

N(16)	3880(2)	-109(3)	639(3)	19(1)
C(501)	400(4)	7245(4)	657(5)	49(2)
Cl(1)	608(1)	7302(1)	-342(2)	62(1)
Cl(2)	741(1)	6532(1)	1258(1)	42(1)
C(601)	4316(4)	2193(4)	4707(5)	36(2)
Cl(3)	3941(1)	2083(1)	5576(1)	50(1)
Cl(4)	4135(1)	1513(1)	3947(1)	48(1)
S(1)	1311(1)	2648(1)	346(1)	22(1)
C(101)	1978(3)	2893(4)	-87(4)	32(2)
F(11)	1831(2)	3221(3)	-818(3)	53(1)
F(12)	2289(2)	2318(2)	-237(3)	43(1)
F(13)	2344(2)	3295(2)	442(3)	45(1)
O(11)	1062(2)	3324(2)	504(3)	31(1)
O(12)	1543(2)	2253(3)	1100(3)	34(1)
O(13)	966(2)	2262(3)	-338(3)	34(1)
S(2)	3620(1)	4292(1)	3508(1)	28(1)
C(201)	3500(3)	3472(3)	2904(4)	25(2)
F(21)	3241(2)	3587(2)	2090(3)	44(1)
F(22)	3140(2)	3039(2)	3239(3)	40(1)
F(23)	4011(2)	3131(2)	2886(3)	37(1)
O(21)	4036(3)	4668(3)	3093(4)	57(2)
O(22)	3876(2)	4039(3)	4347(3)	33(1)
O(23)	3033(2)	4578(3)	3444(3)	44(2)
S(3)	6068(1)	2535(1)	315(1)	23(1)
C(301)	6790(3)	2853(3)	146(4)	27(2)
F(31)	6747(2)	3400(2)	-387(3)	45(1)
F(32)	7098(2)	2347(2)	-194(3)	37(1)
F(33)	7133(2)	3053(2)	866(3)	39(1)
O(31)	5777(2)	2352(3)	-521(3)	32(1)
O(32)	5815(2)	3141(2)	670(3)	25(1)
O(33)	6219(2)	1964(3)	901(3)	39(1)
S(4)	1196(1)	5851(1)	6616(2)	55(1)
C(401)	1824(4)	6410(4)	6597(5)	47(2)
F(41)	2245(2)	6027(4)	6263(4)	86(2)

F(42)	1692(2)	6977(3)	6125(4)	65(2)
F(43)	2065(2)	6629(2)	7379(3)	55(1)
O(41)	993(2)	5689(3)	5745(3)	44(2)
O(42)	1422(3)	5275(3)	7151(4)	54(2)
O(43)	798(3)	6356(4)	6996(4)	63(2)

5.2 Quantum chemical calculations

Table A: Structural parameters for the transition states and minima of the 1,2- and 1,4- dehydrogenation of $H_3B{\cdot}N(H)C(NH_2)_2$

structure	electronic energy	N-H1	B-H2	N-B			Ti-H1	Ti-H2	Ti-N	Ti-B
1-2 dehydrogenation (mechanism 1)										
BCH8N3										
Gua-BH3	-232.0717304	101.3	226.6	159.9						
M1_TS	-231.9978102	131.7	135.2	156.1						
M1_Gua-BH2	-230.8761581			136.5						
BC11H18N3Ti		101.3	226.6	159.9						
Gua-BH3	-232.0717304	101.6	123.2	158.1			305.7	199.2	352.8	313.8
M1_S_1	-677.2410079	117.2	126.8	156.5			180.1	192.5	232.0	256.7
M1_TS_1-2	-677,2360823	233.6	196.2	151.3			166.4	196.2	209.7	258.2
M1_S_2	-677,2885313	411.6	175.9	141.2			167.8	171.9	419.9	337.5
M1_TS_2-3	-677,2376713			136.3			168.1	167.5		
M1_S_3	-677,2420045			136.5			167.6	167.6		
M1_Gua-BH2	-230,8761581			136.5						
M1_Gua-BH2	-230,8761581									
				N-C	C-N	N-B				
1-4 dehydrogenation (mechanism 2)										
BCH8N3										
Gua-BH3	-232.0717304	101.3	226.6	136.1	130.3	159.9				
M2_TS	-232,0333758	161.7	147.5	130.0	136.7	149.9				
M2_Gua-BH2	-230,874364			127.7	141.2	141.1				
BC11H18N3Ti										
Gua-BH3	-232.0717304	101.3	226.6	136.1	130.3	159.9				
M2_S_1	-677,2426138	103.1	124.5	134.6	131.4	157.9	277.6	193.8	377.0	315.5
M2_TS_1-2	-677,2243482	146.7	130.0	131.9	134.5	153.1	185.3	184.9	327.7	304.4
M2_S_2	-677,2789455	222.5	125.8	132.4	133.1	154.6	165.8	191.2	218.0	310.2
M2_TS_2-3	-677,2380069	228.2	242.9	129.0	141.3	142.1	169.5	171.2	232.7	400.9
M2_S_3	-677,2426864			127.9	141.7	140.8	167.6	168.4		
M2_Gua-BH2	-230,874364			127.7	141.2	141.1	167.6	167.6		
M2_Gua-BH2	-20,874364			127.7	141.2	141.1				

Table B: Structures as calculated for **2** and several possible products of its dehydrogenation reactions. The energy-minimum structures and the δ(^{11}B) values were calculated at the DFT-GIAO//B3LYP/6-311+G* level.

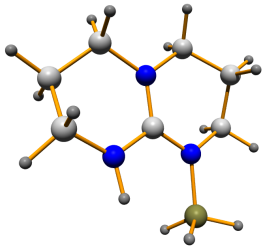

E = -465.60725813 a.u.

δ = -24.2 ppm

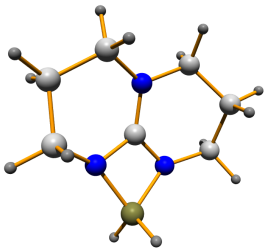

E = -464.40394513 a.u.

δ = -2.6 ppm

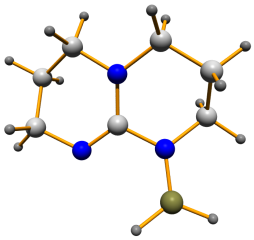

E = -464.40543443 a.u.

δ = 39.4 ppm

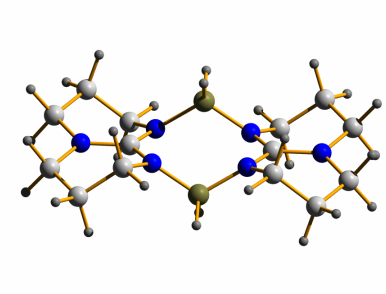

E = -928.87655104 a.u.

δ = - 3.4 ppm

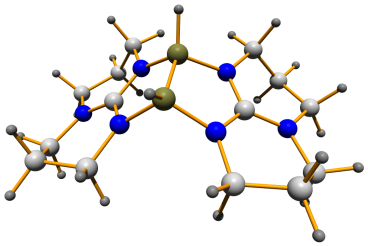

E = -927.68451187 a.u.

δ = -3.0 ppm

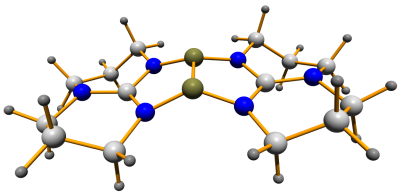

E = -926.39618105 a.u.

δ = 27.6 ppm

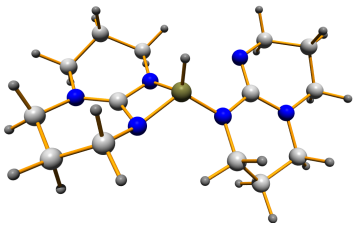

E = -902.16099881 a.u.

δ = -1.51 ppm

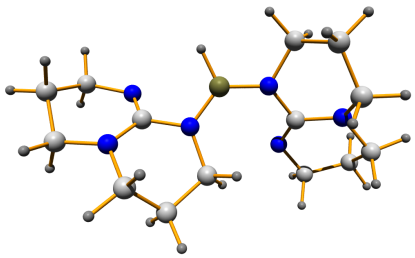

E = -902.16488508 a.u.

δ = 28.40 ppm

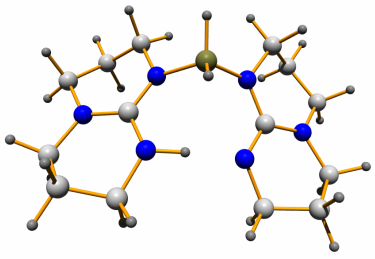

E = -903.37055263 a.u.

δ = -7.9 ppm

Table C: Structures as calculated for **3** and several possible products of its dehydrogenation reactions. The energy-minimum structures and the δ(^{11}B) values were calculated at the DFT-GIAO//B3LYP/6-311+G* level.

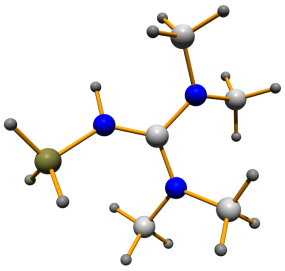

E = - 389.35112180 a.u.

δ = -23.60 ppm

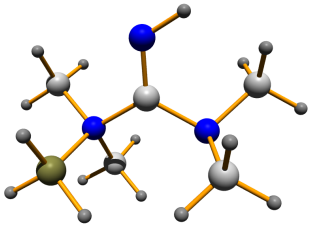

E = - 389.32488601 a.u.

δ = -7.58 ppm

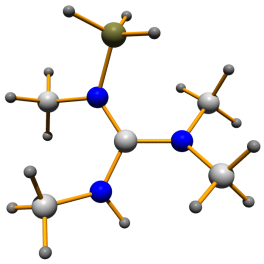

E = -389.34859748 a.u.

δ = -21.32 ppm

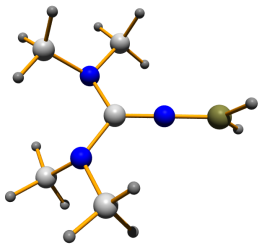

E = -388.16449635 a.u.

δ = 23.16 ppm

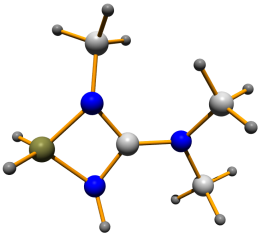

E = -348.85043300 a.u.

δ = -4.62 ppm

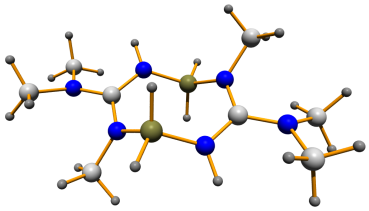

E = -697.76300670 a.u.

δ = -11.12 ppm

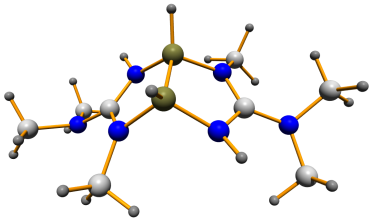

E = - 696.55302760 a.u.

δ = -6.16 ppm

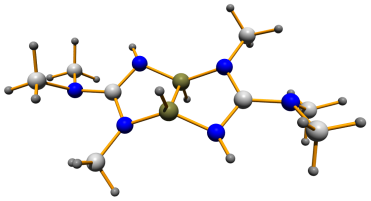

E = -696.47986980 a.u.

δ = 0.34 ppm

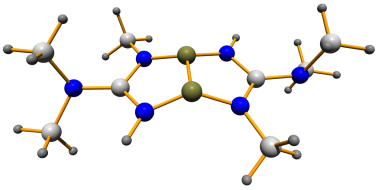

E = -695.28076788 a.u.

δ = 24.76 ppm

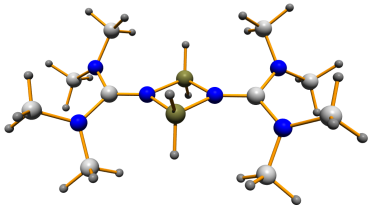

E = -776.35504027 a.u.

δ = -9.20 ppm

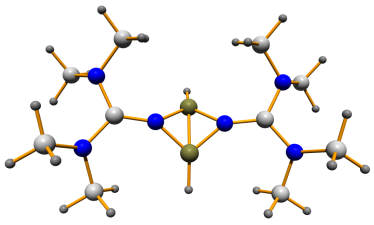

E = -775.08215304 a.u.

δ = -12.09 ppm

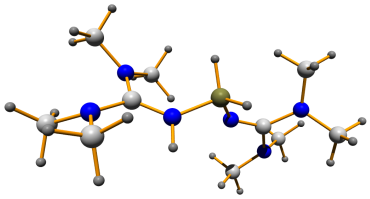

E = -750.8526606 a.u.

δ = -11.88 ppm

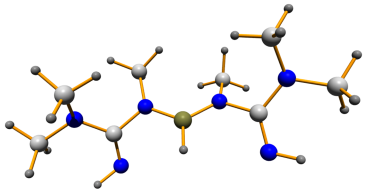

E = -671.04415809 a.u.

δ = 29.48 ppm

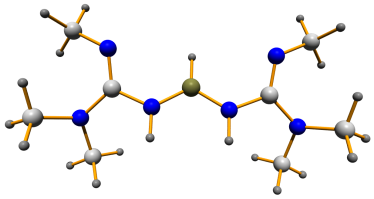

E = -671.05157383 a.u.

δ = 25.97 ppm

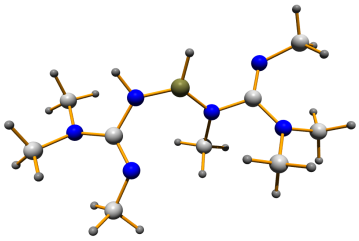

E = -710.35852747 a.u.

δ = 28.42 ppm

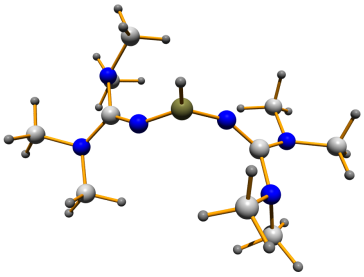

E = -749.68231527 a.u.

δ = 21.55 ppm

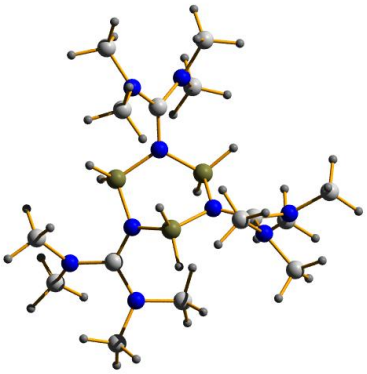

E = -1164.5460388 a.u.

6. Publications

1. "Repeated Dihydrogen Elimination from Boranes and Gallanes Stabilized by Guanidine-Type Bases: A Quantum Chemical Study Motivated by Recent Experimental Results", O. Ciobanu, H.-J. Himmel, *Eur. J. Inorg. Chem.* **2007**, 3565-3572.

2. "Synthesis and Characterization of a New Guanidine-Borane Complex and a Dinuclear Boron (II) Hydride with Bridging Guanidinate Ligands", O. Ciobanu, P. Roquette, S. Leingang, H. Wadepohl, J. Mautz, H.-J. Himmel, *Eur. J. Inorg. Chem.* **2007**, 4530-4534.

3. "Synthesis and Structural Characterization of a Dimeric Boron(II) Cation", R. Dinda, O. Ciobanu, H. Wadepohl, O. Hübner, R. Acharyya, H.-J. Himmel, *Angew. Chem.* **2007**, *119*, 9270-9273; *Angew. Chem. Int. Ed.* **2007**, *46*, 9110-9113.

4. "The 1,1,3,3-Tetramethylguanidine-Borane Adduct: Theoretical Comparison of the Bonding Properties in Amine- and Guanidine-Borane Adducts", O. Ciobanu, S. Leingang, H. Wadepohl, H.-J. Himmel, *Eur. J. Inorg. Chem.* **2008**, 322-329.

5. "The First Dinuclear B(II) Monocations with Bridging Guanidinate Ligands: Synthesis and Properties", O. Ciobanu, D. Emeljanenko, E. Kaifer, H.-J. Himmel, *Inorg. Chem.* **2008**, *47*, 4774-4778.

6. "Thermal and Catalytic Dehydrogenation of the Guanidine-Borane Adducts $H_3B{\cdot}$hppH (hppH = 1,2,4,6,7,8-hexahydro-2H-pyrimido[1,2-a]pyrimidine) and $H_3B{\cdot}N(H)C(NMe_2)_2$: A Combined Experimental and Quantum Chemical Study", O. Ciobanu, F. Allouti, P. Roquette, S. Leingang, M. Enders, H. Wadepohl, H.-J. Himmel, *Eur. J. Inorg. Chem.* **2008**, 5482-5493.

7. "Synthesis of a Stable $B_2H_5^+$ Analogue by Protonation of a Double Base-Stabilized Diborane(4)", O. Ciobanu, E. Kaifer, M. Enders, H.-J. Himmel, *Angew. Chem.* **2009**, *121*, 5646-5649; *Angew. Chem. Int. Ed.* **2009**, *48*, 5538-5541.

8. "Reactions between Boron and Magnesium Halides and the Bicyclic Guanidine hppH (1,3,4,6,7,8-hexahydro-2H-pyrimido[1,2-a]pyrimidine): Guanidinates with New Strucutural Motifs)", O. Ciobanu, A. Fuchs, M. Reinmuth, A. Lebkücher, E. Kaifer, H. Wadepohl, H.-J. Himmel, *Z. Anorg. Allg. Chem.* **2009**, in press.

7. Acknowledgements

It is a great pleasure to thank the many people who made this thesis possible. First of all, I would like to express my gratitude to my supervisor Prof. Dr. Dr. Hans-Jörg Himmel. This thesis would not have been possible without Prof. Himmel's accepting me as a Ph.D student in his group and his intellectual guidance, kind support and many constructive discussions.

In particular many thanks go to Mrs. Karin Gissmann and Dr. Elisabeth Kaifer for their encouragement and help during my research.

I would like to express my thanks to all my colleagues from Himmel and Heinze groups, who have helped me directly and indirectly in accomplishing this thesis and for creating me a stimulating and pleasant working environment to grow me personally as well as professionally. Particularly, I want to thank Nikola Schulenberg and Pascal Roquette for pleasant working conditions in lab and cooperation. I thank Simone Leingang, Ute Wild, Viktoriia Vitske, and Anastasia Peters for their encouragement and help during my thesis. I am also grateful to Drs. Fayçal Alluoti, Julio Lloret-Fillol and Olaf Hübner for helpful discussions regarding computational chemistry.

I wish to thank Prof. Dr. Markus Enders and Mrs. Beate Termin for excellent NMR services and for their helpful discussions, Mr. Thomas Jannack, and Dr. Jürgen Gross for mass spectra, Mrs. Vetter, and Mr. Liebscher for carrying out elemental analyses. Many thanks go also to Prof. Dr. H. Wadelpohl, Dr. Elisabeth Kaifer, Dr. Jürgen Mautz, and Mrs. Heidrun Haungs for crystal structure analyses and very helpful discussions. I wish to thanks Prof. Dr. W. Siebert for valuable discussions.

I would like to express my thanks to Prof. Dr. Cristian Silvestru from Babeş-Bolyai University, Romania for encouraging me to come to Germany and Dr. Mona Bogza for her friendship and continuous support during my thesis.

Special thanks go to all my friend*s* from Moldavia, Romania, Ukraine and Germany for providing support and healthy distractions.

My deepest gratitude goes to my family, my boyfriend Martin and his family for their love, support, warm encouragement and huge patience. Multumesc lui Dimnezeu!

Finally, I wish to acknowledge the Deutsche Forschungsgemeinschaft (DFG) for the financial support.

„Hiermit erkläre ich an Eides statt, dass ich die vorliegende Arbeit selbständig und ohne unerlaubte Hilfsmittel durchgeführt habe.“

Oxana Ciobanu